TECHNISCHE UNIVERSITÄT MÜNCHEN
TUM School of Engineering and Design

Dynamic Analysis of Composite Plates in Thermal Environments:

Numerical and Experimental Studies

Sourav Chandra

Vollständiger Abdruck der von der TUM School of Engineering and Design der Technischen Universität München zur Erlangung des akademischen Grades eines

Doktors der Ingenieurwissenschaften (Dr.-Ing.)

genehmigten Dissertation.

Vorsitz: Prof. Dr.-Ing. Klaus Drechsler

Prüfer der Dissertation: 1. Prof. Dr.-Ing. Steffen Marburg
2. Prof. Dr. Santosh Kapuria

Die Dissertation wurde am 07.11.2022 bei der Technischen Universität München eingereicht und durch die TUM School of Engineering and Design am 06.06.2023 angenommen.

"Take up one idea. Make that one idea your life — think of it, dream of it, live on that idea. Let the brain, muscles, nerves, every part of your body, be full of that idea, and just leave every other idea alone."

The Complete Works of Swami Vivekandanda (Volume I)

I dedicated this thesis to

My mother Sumitra Chandra, my father Ananda Kishore Chandra, and my uncle Barun Kr. Datta for their unconditional love and support

and

the Almighty God

Acknowledgment

While walking down memory lane at the end moment of my journey as a doctoral researcher, I must confess that the lane I left behind was defined by those who surrounded me. This journey was overwhelmed with the mixed experience of struggle, challenges, happiness, and blessing. However, this kaleidoscopic journey would never have been so adventurous and enjoyable without the strong support from my well-wishers. Now, I take this opportunity to pay my homage to those well-wishers.

I convey my deepest gratitude to Prof. Dr.-Ing. Steffen Marburg, my supervisor and professor of the Chair of Vibroacoustics of Vehicles and Machines. Your guidance approach allows me to grow as an independent researcher. Furthermore, your valuable guidance and suggestions helped me to achieve my research goal, and encouraged me to learn from you. As an ideal doctor father (Doktorvater in German), you have always supported me in the difficult spell of the research. Thank you Steffen, for showing untiring patience and faith in me, and giving me the freedom to explore my research.

I wanted to thank my mentor, Dr.-Ing. Kheirollah Sepahvand for his valuable suggestions while developing the German Academic Exchange Services (DAAD) research proposal. The discussions with you during the initial days of my doctoral research helped me understand the stochastic finite element methods.

I sincerely thank Prof. Dr. Vasant Matsagar, Dogra Chair Professor in the Department of Civil Engineering, Indian Institute of Technology (IIT) Delhi, who inspired me while conducting this research. The discussion with you during your stay in Munich and Berlin has helped me to formulate the research objectives. You also motivated me to break my inertia and subsequently expand the research domain. Furthermore, you have given me the opportunity to work in the Multi-Hazard Protective Structures (MHPS) laboratory at IIT Delhi during the final period of my doctoral research.

I also pay my gratefulness to Dr. Marcus Maeder, the Academic Adviser of our chair, for navigating me with novel ideas while conducting experiments at Weimar. I could remember our countless meetings, which finally brought our experimental article to its present form. Dear Marcus, your suggestions and discussions have helped me a lot to shape this dissertation.

I was grateful to Prof. Dr. Arup Guha Nioygi (Professor, Jadavpur University, Kolkata, India) and Prof. Dr. Sreyashi Das (Associate Professor, Jadavpur University, Kolkata, India), who introduced me to the research field of composite structures and finite elements; and inspired me to conduct the research. I am always thankful to both of you for igniting my research aspiration.

I would like to express my thanks to Elke Reichardt, Sabine Crnjanowic, and Martina Sommer for helping me with administrative tasks at the Chair- especially Elke's cooperation deserves much acknowledgment. I also wanted to thank all the colleagues in our chair, and special thanks go to Bettina Chocholaty, Martin Eser, Karl-Alexander Hoppe, Christopher Jelich, Felix Kronowetter, Simone Preuss, Christian Kronowetter, Magdalena Scholz, Xiaodong Sun, Yuanyuan Liu, Dr. Patrick Langer, Zhe Liu, Johannes Schmid and Jonas Schmid. I should offer my gratitude to Zhe for taking the pain to read the first draft of my manuscripts. My present colleagues at the MHPS laboratory at IIT Delhi also deserve the heartfelt gratitude, and the gratitude goes to Kusum Saini, Rudroneel Manna, Sarranya Banerjee, Yash Chordiya, Sreenitya Singamsetty, Daniel H. Zelleke, Akshay Baheti, Harshada Sharma, and Dr. Pravin S. Jagtap. You, the noble minds of TUM and IIT Delhi, have always surrounded me and made my journey more exciting and enjoyable.

My journey in the TUM would never been started without the inspiration and support of Dr. Atanu Sahu, Assistant Professor, National Institute of Technology (NIT) Silchar, and his wife, Dr. Anuja Roy. You are the persons who have motivated me to apply to the DAAD-PhD Scholarship program, and held me strongly during all the difficult spells of my doctoral research.

This homage remains incomplete without mentioning the friends whom I met in Germany, and become my closest friends. I wish to convey my gratitude to Nikhil Ghodichore (IIT Delhi, India), Debdeep Sarkar (Ruhr-Universität Bochum, Germany), Komal Jhala (TUM, Germany), Anoop Kodakkal (TUM, Germany), Dr. Somdatta Goswami (Assistant Professor, Brown University, USA), Dr. Trinetra Mukherjee (Université de Bretagne Occidentale, France) for their continual encouragement and valuable suggestions. Dear Dr. Ajay Singh (University of Luxembourg, Luxembourg), my days in Munich would be more complicated without your support and encouragement. Thanks for your continuous motivation.

I would like to express my deepest thanks to the DAAD for financially supporting this doctoral research work. Additionally, the last semester of this doctoral research work is supported by the Industrial Research & Development (IRD) Unit of IIT Delhi, I am also indebted to IIT Delhi.

When it comes to extending gratitude towards family, at the first opportunity, I convey my gratitude to Frau Houshyar-Frazin Elfriede, I used to call her Oma, with whom I stayed during the entire period of Munich. It is due to her love and affection, I never felt that I was away from home for such a long time. During the alarming period of Corona breakout, we have tried to support each other in our own way. Oma, thank you for your unconditional love and untiring attitude. I pray for your good health and happiness. I also express my gratitude to her daughter Frau Carreta and her family, who have considered me like their family member.

Expressing gratitude towards my mother, Sumitra Chandra, and my father, Ananda Kishor Chan-

dra, would not be enough to convey my homage towards them; rather, I am honored to be their child. Without the support from my parent, this journey would remain as an untold story. They have strengthened my wings with their love and affection so that I can dare to fly. Dear Mam and Baba, I can hardly understand the austerity you have sustained during these days; however, your blessings are always with me. My family remains incomplete without mentioning my cousin-sister, Ishita Pal, and her two daughters. It is due to them, my parents never felt lonely, even though I was away from them for such a long duration. The silent prayer of my grandmother Kananbala Datta, needs to be acknowledged in my upbringing and my entire education. Now, it is the time to express my love and gratitude to my uncle (Chotomamau), Barun Kr. Datta, the best gift to my life. He always remains on my side as a friend, philosopher, and guide. He inspired me to believe in my own strength and extract positivity in every life spell. Chotomamu, I am incredibly grateful to have you by my side.

The last but by no means the least, I am thankful to the Almighty for His countless blessing and giving me the strength to accept the life gracefully.

"I do not pray to protect me from perils, let me be fearless.
Amidst sorrow and pain, I may not be consoled, let me overcome."
– Rabindranath Tagore (collected from the Geetanjali).

Munich, 09 November 2023

Kurzfassung

In der vorliegenden Arbeit werden numerische und experimentelle Studien zu dynamischen Analysen von laminierten Verbundstrukturen in unterschiedlichen thermischen Umgebungen vorgestellt. Die numerischen Studien zielen darauf ab, die deterministischen und stochastischen dynamischen Reaktionen von unversteiften und versteiften laminierten Verbundplatten bei unterschiedlichen Temperaturen zu untersuchen. In der experimentellen Studie wird eine innovative, auf der operationellen Modalanalyse (OMA) basierenden Messstrategie vorgestellt, um die experimentellen Modalantworten von laminierten Verbundplatten bei verschiedenen Temperaturen zu bewerten und anschließend die temperaturabhängigen elastischen und dämpfenden Eigenschaften zu ermitteln. Verbundwerkstoffe werden zunehmend in der Automobil, und Luft- und Raumfahrtindustrie eingesetzt, wo die aus Verbundwerkstoffen hergestellten Strukturen thermisch variierenden Umgebungen und dynamischen Belastungen ausgesetzt sind. In Anbetracht der umfangreichen Anwendung von Verbundwerkstoffstrukturen in der Automobil- und Luft- und Raumfahrtindustrie soll in dieser Forschungsarbeit das deterministische und stochastische Verhalten der dynamischen Reaktion von Verbundwerkstoffplatten in unterschiedlichen thermischen Umgebungen untersucht werden.

Die deterministische numerische Analyse beinhaltet eine verallgemeinerte Finite-Elemente (FE) Formulierung, um das dynamische Verhalten von einfachen und versteiften laminierten Verbundplatten in thermischer Umgebung zu analysieren. Die detaillierte Analyse der ungedämpften und gedämpften dynamischen Antworten führt zur Erkenntnis, die versteiften Platten gegenüber den einfachen Platten in thermischer Umgebung zu berücksichtigen. Im Allgemeinen verschlechtern sich die elastischen Eigenschaften der Verbundplatten mit zunehmender Temperatur, während die viskoelastischen Dämpfungseigenschaften mit zunehmender Temperatur bis zur Glasübergangstemperatur ansteigen. Für die numerische Analyse werden die temperaturabhängigen Materialeigenschaften aus den in der Literatur verfügbaren statischen und quasistatischen Versuchen abgeleitet. Die Dämpfungseigenschaften der Platten werden mithilfe von verschiebungsbasierten und energiebasierten Ansätzen bewertet, wobei versteifte Platten bei höheren Temperaturen bessere Dämpfungseigenschaften aufweisen. Für die stochastische dynamische Analyse wird die verallgemeinerte polynomiale Chaosmethode (gPC) als Metamodell verwendet, um die Unsicherheit in der dynamischen Durchbiegung für einfache Platten aufgrund eines zufälligen mittleren Temperaturanstiegs zu bewerten.

In der experimentellen Analyse werden die modalen Eigenschaften mehrerer antisymmetrischer Kreuzlagen- und Winkellagenlaminate unter Verwendung der OMA bei verschiedenen Temperaturen bewertet. Die berührungslosen Anregungs- und Messstrategien werden eingesetzt, um die

Herausforderungen bei der Durchführung des Experiments in einer geschlossenen Wärmekammer zu bewältigen. Dieses Verfahren kann eingesetzt werden, um die in-situ Modaldaten einer Struktur zu schätzen, ohne die Eingangsdaten zu erfassen. Darüber hinaus werden diese Modaldaten verwendet, um die deterministischen temperaturabhängigen Materialeigenschaften von Verbundwerkstofflamellen zu ermitteln. Für die Ermittlung der Materialeigenschaften wird ein zweistufiger Optimierungsalgorithmus verwendet. Der ermittelte Schermodul verschlechtert sich mit zunehmender Temperatur; dies deutet auf eine starke Temperaturabhängigkeit des Schermoduls hin.

Diese Dissertation dient als Grundlage für die Entwicklung einer leiseren und sichereren Verbundwerkstoffstruktur in thermischer Umgebung. Die ersten beiden Veröffentlichungen ebneten den Weg zur Kontrolle der dynamischen Reaktion von Verbundwerkstoffstrukturen und damit zur Schaffung einer ruhigeren Umgebung. Die dritte Veröffentlichung befasste sich mit dem experimentellen Verfahren zur Abschätzung der deterministischen temperaturabhängigen Materialeigenschaften von Verbundwerkstofflamellen in situ. Diese Arbeit kann erweitert werden, um die Unsicherheit in den Materialeigenschaften abzuschätzen. Die auf einem Metamodell basierende stochastische dynamische Analyse wird in der vierten Veröffentlichung vorgestellt und kann erweitert werden, um die Zuverlässigkeit einer Verbundwerkstoffstruktur in thermischer Umgebung zu untersuchen.

Abstract

In the present thesis, numerical and experimental studies on dynamic analyses of laminated composite structures in varying thermal environment are presented. The numerical studies aimed to investigate deterministic and stochastic dynamic responses of both unstiffened and stiffened laminated composite plates at different temperatures. The experimental study presented an innovative measurement strategy, based on operational modal analysis (OMA), in order to evaluate experimental modal responses of laminated composite plates at different temperatures and to subsequently identify the temperature-dependent elastic and damping properties. The composite materials are increasingly used in the automobile and aerospace industries, where the structures made of composite materials are exposed to thermal environment together with dynamic loads. Considering the extensive application of composite structures in the automobile and aerospace industries, this research work intended to study the deterministic and stochastic behaviors of dynamic response of composite plates in varying thermal environment.

The deterministic numerical analysis includes a generalized finite element (FE) formulation to analyze dynamic response of unstiffened and stiffened laminated composite plates in thermal environment. The detailed analysis of undamped and damped dynamic responses has suggested to consider the stiffened plates rather than the unstiffened plates in varying thermal environments. Generally, elastic properties of composite lamina degrade with the increment of temperature, whereas the viscoelastic damping properties increase with the increment of temperature until the glass transition temperature is reached. For the numerical analysis, the temperature-dependent material properties are derived from the static and quasi-static tests as available in research literature. The damping performance of the plates is evaluated by using the displacement-based and energy-based approaches, where stiffened plates show better damping performance at higher temperatures. For stochastic dynamic analysis, the generalized polynomial chaos (gPC) expansion method is used as a metamodel to evaluate stochasticity in dynamic deflection for unstiffened plates due to random mean temperature increment.

In the experimental analysis, modal characteristics of several antisymmetric cross-ply and angle-ply laminates are evaluated by using OMA at different temperatures. The noncontact-based excitation and measurement strategies are used to address the challenges in conducting the experiment within an enclosed thermal chamber. This procedure can be implemented to estimate the in situ modal data of a structure without recording the input data. Furthermore, this modal data is used to identify the deterministic temperature-dependent material properties of composite lamina. A two-stage optimization algorithm is used for the material properties identification. The identified

shear modulus degrades subsequently with the increment of temperature; this indicates a strong temperature dependency for the shear modulus.

This thesis serves as a groundwork towards designing quieter and safer composite structures in thermal environment. The first two publications have paved the way to control the dynamic response of composite structures in order to create a quieter environment. The third publication has dealt with the experimental procedure to estimate the deterministic in situ temperature-dependent material properties of composite lamina. This work can be extended to estimate the uncertainty in the material properties. The metamodel-based stochastic dynamic analysis is presented in the fourth publication and can be extended to investigate the reliability of a composite structure in thermal environment.

List of Publications

Appended publications

- S. Chandra, K. Sepahvand, V.A. Matsagar, S. Marburg, Stochastic dynamic analysis of composite plate with random temperature increment. *Composite Structures*, 226, 111159, 2019.
  Author contribution statement:
  S. Chandra: Conceptualization (90%), Methodology (90%), Programming, Software, Validation, Investigation, Result analysis (80%), Data curation, Writing - original draft (85%), Visualization, Writing - review & editing (70%). **K. Sepahvand:** Conceptualization (5%), Methodology (10%), Result analysis (10%), Writing - original draft (15%), Writing - review & editing (15%). **V.A. Matsagar:** Conceptualization (5%), Result analysis (10%), Writing - review & editing (10%), Supervision (15%). **S. Marburg:** Resource, Writing - review & editing (5%), Supervision (85%).

- S. Chandra, K. Sepahvand, V.A. Matsagar, S. Marburg, Dynamic response of stiffened laminated composite plate in thermal environment. *Composite Structures*, 300, 116049, 2022.
  Author contribution statement:
  S. Chandra: Conceptualization (90%), Methodology (90%), Programming, Software, Validation, Investigation, Result analysis (80%), Data curation, Writing - original draft, Visualization, Writing - review & editing (70%). **K. Sepahvand:** Methodology (10%), Writing - review & editing (5%). **V.A. Matsagar:** Conceptualization (10%), Result analysis (20%), Writing - review & editing (15%), Supervision (15%). **S. Marburg:** Resource, Writing - review & editing (10%), Supervision (85%).

- S. Chandra, M. Maeder, K. Sepahvand, V.A. Matsagar, S. Marburg, Damping analysis of stiffened laminated composite plates in thermal environment. *Composite Structures*, 300, 116163, 2022.

  Author contribution statement:

  S. Chandra: Conceptualization (80%), Methodology (85%), Programming, Software, Validation, Investigation, Result analysis (85%), Data curation, Writing - original draft, Visualization, Writing - review & editing (70%). **M. Maeder:** Conceptualization (10%), Methodology (10%), Investigation, Result analysis (10%), Writing - review & editing (5%). **K. Sepahvand:** Methodology (5%), Writing - review & editing (5%). **V.A. Matsagar:** Conceptualization (10%), Result analysis (5%), Writing - review & editing (10%), Supervision (20%). **S. Marburg:** Resource, Writing - review & editing (10%), Supervision (80%).

- S. Chandra, M. Maeder, J. Bienert, H. Beinersdorf, W. Jiang, V.A. Matsagar, S. Marburg, Identification of temperature-dependent elastic and damping Parameters of carbon-epoxy composite plates based on experimental modal data. *Mechanical Systems and Signal Processing*, 187, 109945, 2022.

  Author contribution statement:

  S. Chandra: Conceptualization (60%), Methodology (55%), Conducting experiment (55%), Programming (65%), Software (55%), Validation (70%), Investigation (75%), Result analysis (70%), Data curation (85%), Writing - original draft (70%), Visualization (90%), Writing - review & editing (55%), Project administration (60%). **M. Maeder:** Conceptualization (35%), Methodology (35%), Conducting experiment (40%), Programming (25%), Software (35%), Validation (30%), Investigation (25%), Result analysis (20%), Data curation (15%), Writing - original draft (30%), Visualization (10%) Writing - review & editing (10%), Project administration (40%). **J. Bienert:** Methodology (5%), Programming (10%), Software (10%), Writing - review & editing (5%). **H. Beinersdorf:** Conducting Experiment (5%), Writing - review & editing (5%). **W. Jiang:** Methodology (5%), Writing - review & editing (5%). **V.A. Matsagar:** Conceptualization (5%), Result analysis (5%), Writing - review & editing (10%), Supervision (5%). **S. Marburg:** Resource, Result analysis (5%), Writing - review & editing (15%), Supervision (95%).

Unappended publications

Book chapters

- S. Chandra, M. Maeder, S. Marburg, Identification of Temperature Dependent Material Properties in Composite Plates Utilizing Experimental Vibration Data. *Material Modeling and Structural Mechanics*, 115-134, 2022.

Conference publications/ presentations

- S. Chandra, K. Sepahvand, S. Marburg, Bayesian Inference Method to Identify Random Parameters. In *DAGA: 44. Jahrestagung der Deutschen Arbeitsgemeinschaft für Akustik*, 19–22 March 2018, Technical Unicaversity of Munich (TUM), Germany, pages 1460–1463, 2018.
- S. Chandra, K. Sepahvand, S. Marburg, Stochastic Vibro-acoustic Analysis in the Uncertain Thermal Environment. In *DAGA: 45. Jahrestagung der Deutschen Arbeitsgemeinschaft für Akustik*, 18–21 March 2019, Rostock, Germany, pages 117–120, 2019.
- S. Chandra, K. Sepahvand, C. Geweth, F.S. Khosroshahi, S. Marburg, Stochastic non-parametric identification in composite structures using experimental modal data. In *Proceedings of 3rd International Conference on Uncertainty Quantification in Computational Science and Engineering (UNCECOMP)*, 24–26 June 2019, Crete, Greece, pages 543–554, 2019.
- S. Chandra, K. Sepahvand, C. Geweth, F.S. Khosroshahi, S. Marburg, Bayesian Inference to Damping Identification of Fiber-Reinforced Composites from Experimental Modal Data. In *Proceedings of the 23rd International Congress on Acoustics*, 9–13 September, 2019, Aachen, Germany, pages 6312–6319, 2019.
- S. Chandra, K. Sepahvand, S. Marburg, Uncertainty analysis in dynamic response of composite structures in thermal environment. In *DAGA: 46. Jahrestagung der Deutschen Arbeitsgemeinschaft für Akustik*, 16–19 March 2020, Hannover, Germany, 2020, pages 896–899, 2020.
- S. Chandra, K. Sepahvand, V. Matsagar, S. Marburg, Stochastic Modal damping analysis of stiffened laminated composite plate. In *Recent Advances in Computational Mechanics and Simulations, Springer Singapore*, 7th International Congress on Computational Mechanics and Simulation (ICCMS 2019), 11-13 December 2019, Indian Institute of Technology (IIT) Mandi, Mandi, India, pages 635-650, 2021.

- S. Chandra, K. Saini, V. Matsagar, S. Marburg, Reliability Assessment of Laminated Composite Plates under Impulsive Loads. In *Book of Abstracts-5th National Conference on Reliability and Safety (NCRS-2022)*, Virtual Conference, 10–12 March 2022, page 74, 2022.

List of Acronyms

CLPT classical laminated plate theory

DMA dynamic mechanical analysis

dNDF damped non-dimensional frequency

DOF degree of freedom

EFDD Enhanced Frequency Domain Decomposition

EMA experimental modal analysis

FE finite element

FEM finite element method

FOPT first-order perturbation technique

FSDT first-order shear deformation theory

gPC generalized polynomial chaos

HSDT higher-order shear deformation theory

MC Monte Carlo

NDF non-dimensional frequency

OMA operational modal analysis

PC polynomial chaos

PDF probability density function

PZA piezoelectric alloy

PZM piezoelectric material

SDC specific damping coefficient

SMA shape memory alloy

SSFEM spectral stochastic finite element method

SSI Stochastic Subspace Iteration

List of Figures

List of Tables

Contents

Part I

Thesis Overview

Chapter 1

Introduction

The idea of potential usage of composite materials in aerospace industries as the principal structural materials was first perceived by N. A. de Bruyne [20], and he presented his idea at the Royal Aeronautical Society, UK, in 1937. Since the late 1930s, the application of composite materials in aerospace and automobile industries has increased in a broad range of areas. Essentially, different socio-economic factors such as cost of energy, consequence of pollution, and quality of life are the key drivers towards the movement of composite technology in the transportation sector. Furthermore, scarcity of cheap source of energy stimulates the new technological development in the transportation sector with aims of weight reduction and minimum energy usage without compromising comfort, reliability, and safety of passengers. In this scenario, composite materials draw significant attention to engineers and researchers. Apart from these benefits, composite materials impart excellent mechanical properties in terms of strength, fatigue resistance, corrosion resistance, fire resistance, and stability while subjected to varying kind of environmental exposures. Furthermore, composite materials present superior mechanical properties and strength to weight ratio. In recent years, technological development in aerospace and lightweight structural engineering is focusing to replace conventional structural materials with composite and/or hybrid materials by blending metallic and nonmetallic fibers and polymers.

Initial large-scale application of composite materials in commercial aircraft was observed in 1985. Thereupon the Airbus A320 reduced 15% of the air-frame weight by introducing composite materials in vertical and horizontal stabilizers. Furthermore, the new age commercial aircraft such as the Boeing B787 and the Airbus A380 comprise composite materials in about 50% of their total empty mass of the structure [52]. In addition to aerospace industry, composite materials are used extensively in automobile industry to manufacture high-speed trains, sports-cars, etc. To develop quiet and safe composite structures for aerospace and automobile vehicles, the corresponding re-

search and development are much needed.

Composite plate-/shell-like structures are used in the fuselage and wing box of an aircraft. These structures are integrated with stiffeners to improve the structural efficiency in terms of load-carrying capacity, dynamic response, buckling, stress concentration, etc. Furthermore, stiffened composite plates/shells contribute to weight reduction by reducing plate thickness without showing any buckling tendency. Therefore, the advantages of plate-/shell-like composite structures can exploited efficiently by attaching appropriate stiffeners.

A composite materials is a two-phase system. On the one hand, the phase which is stiffer and stronger, and usually discontinuous, is termed as "reinforcement" (dispersed phase). On the other hand, the less stiff and weaker phase is continuous and is called "matrix" (continuous phase) [139]. A generalized classification of composite materials based on the constituent phases is shown in Figure 1. Among the different composites, the graphite-epoxy, carbon-epoxy, and IM7-(intermediate modulus carbon fibers)PEEK (polyetheretherketone) composites are extensively used in various components of aircraft and unmanned aerial vehicles. For example, the carbon-epoxy and carbon-PEEK composites are used in the fuselage and wing-box of the Airbus A350 [116]. It is also found that the application of composite materials reduces the inspection and maintenance costs of the structure. During the high-speed maneuvering of a vehicle, the ambient temperature of the vehicle skin increases due to aerodynamic heating. The variation in temperature ultimately modifies the material properties of the composite structure, thereby vibrational characteristics of the structure also modified due to thermal variation. Generally, the matrix phase influences the temperature-dependent behavior of elastic and damping properties of a composite lamina. A subsonic flight (i.e., cruising speed less than 1 Mach) of an aircraft may encounter a temperature variation between -55 °C and 60 °C. The skin temperature of a supersonic flight cruising at 2.4 Mach could reach up to 150 °C due to aerodynamic heating [120]. It is noted that thermosetting resin such as epoxy is widely used in composite materials of aircraft structures. Generally, the glass transition temperature, T_g, of epoxy increases with the increment of the temperature of cure. For example, epoxy-based composites which are cured at 120 °C and 150 °C temperatures, have a upper limit of the glass transition temperature of $100-130$ °C and 150 °C, respectively [40]. Thereby, the glass transition temperature of a composite material is dominated by the glass transition temperature of the corresponding matrix base. Furthermore, the PEEK, a thermoplastic resin-based composite, is a preferable choice where temperature of a structure is potentially high. The PEEK-based resin has the high glass transition temperature, i.e., around 390 °C. A list of operating temperatures for different resin types are given in [41]. Moreover, the graphite-epoxy and IM7-PEEK composite materials are characterized by a very low coefficient of thermal expansion. Therefore, these

composite materials are extensively used in aerospace structures.

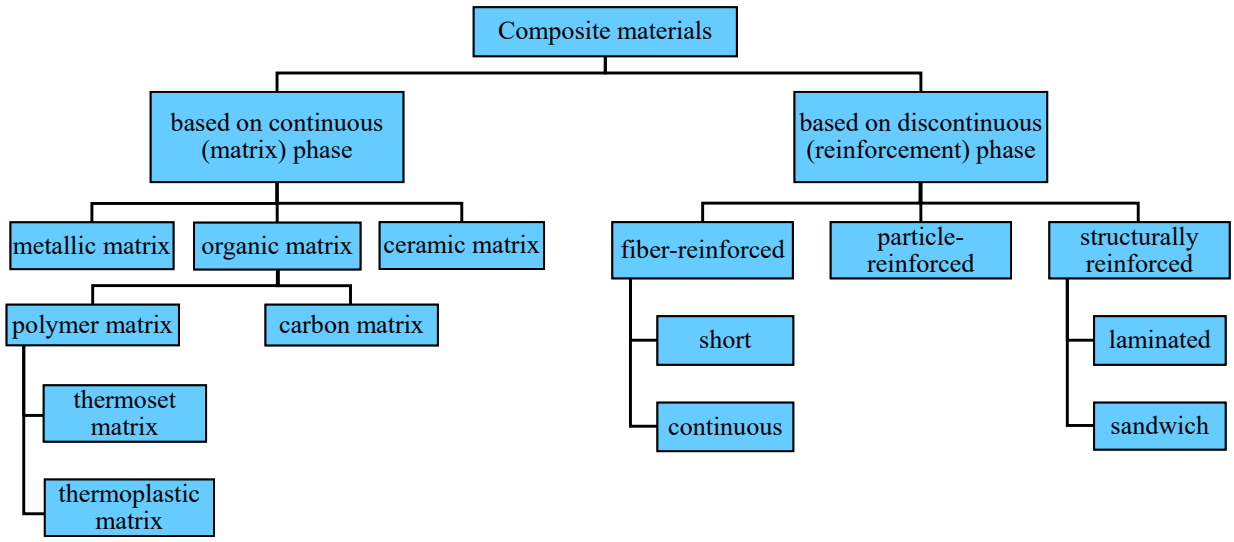

Figure 1: Classification of composite materials based on constituent phases

As highlighted earlier, laminated composite plates made of graphite-epoxy and IM7-PEEK composites are extensively used in important structural components of aircraft and automobiles. During maneuvering, these structures are exposed to varying thermal environments and dynamic loads. To ensure a safe design of these composite structures along with maintaining a quieter environment, numerical and experimental studies on dynamic analyses of composite plates in thermal environment are essential.

Outline of the dissertation

This dissertation is presented in two parts. In the first part, contributions are discussed chapter-wise, and the appended publications are included in the second part. The present discussion is the part of Chapter 1, where the state of the art for dynamic analysis of composite plates/shells is summarized, followed by a discussion of the research contributions. In Chapter 2, applied numerical and experimental methodologies are discussed. The summary of individual appended publications is given in Chapter 3. Afterwards, the results and novelty of the present work are discussed in Chapter 4 with reference to the available research literature. Finally, this dissertation is concluded by discussing its research outcomes and future research outlooks in Chapter 5. Additionally, validation studies related to Publication 2 are given in Appendix A.

1.1 State of the art

1.1.1 Plate theories

In 1959, Pister and Dong [131] presented the classical laminated plate theory (CLPT) for the analysis of laminated composite plates. This study is considered as the most fundamental study for the development of laminated composite plate theory. In the following years, Reissner and Stavsky [142] and Dong et al. [38] have analyzed laminated composite plates subjected to static load using the CLPT. In the CLPT, the shear deformation along the thickness has been ignored, which is posed as one of the limitations of the CLPT. Since then, extensive research has been carried out to address the limitation of the CLPT in various stages. The limitation of the CLPT has been addressed with the introduction of first-order shear deformation theory (FSDT) [107, 141, 191, 197]. In the FSDT, the shear strain is assumed to be constant throughout the thickness. A shear correction factor is introduced in this theory to account for the nonlinearity of the shear strain along the thickness. The shear correction factor is a dimensionless quantity which accounts for the discrepancy between the constant variation of the shear strain according to the CLPT and the actual nonlinear variation of the shear strain. Typically, the finite element (FE) method [9, 12, 43] is considered as a widely accepted structural analysis tool within the scientific community. The analysis of composite plates is carried out using the CLPT or the FSDT within the finite element (FE) framework. To overcome limitations of the FSDT, FE formulations based on various higher-order shear deformation theories (HSDTs) [69, 74, 79, 100] and zigzag theory [39, 76] have been developed. These theories are extended to estimate the thermoelastic stress distribution [39, 72, 76, 111, 132, 168] of laminated composite and sandwich plates subjected to quasi-static load. Moreover, the transient response of laminated composite plates and shells has been studied in [71, 82] using the HSDTs.

A few review articles have been appeared which summarize the historical development of the mechanics of composites [64] and various shear deformation theories [73, 74, 98, 101, 138]. Since the early development and application of laminated composite plates, large-scale studies were conducted based on different plate theories. Many state of the art surveys are conducted in bending, vibration, and buckling of laminated composite plates, and a few selected studies [75, 149, 150, 202] are suggested here for reading. Furthermore, with the increasing usage of composite plates for research and industrial applications, several text books [7, 33, 139, 185] are available to works related to mechanics of composites.

While using composite plates as a principal structural member in spacecraft, aircraft, automobiles, etc., the dynamic behavior of laminated composite plates in varying thermal environments need to

be studied. Notwithstanding the inevitability, the vibration amplitude of a composite structure in varying thermal environments should be minimized by implementing a suitable damping evaluation strategy and devising appropriate design features so that structural performance and reliability can be improved. It was mentioned earlier that stiffened panels made of laminated composite plates are efficiently used to reduce the magnitude of vibration. A brief review of the past studies on the vibration of laminated composite plates subjected to external loads in varying thermal environments is presented in what follows.

1.1.2 Vibration of composite plates in thermal environment

Theoretical and experimental studies on thermal effects in composite materials were initiated by Halpin [58]. Later, Halpin and Pagano [59] and Whitney and Ashton [190] studied the bending, buckling, and vibration of laminated composite plates in thermal environment. They used the generalized Duhamel-Neumann form of Hooke's law to develop the governing equations of laminated composite plates. The decrease in the dimensionless natural frequencies of graphite-epoxy laminated composite plates due to the increase in the temperature and moisture content has been shown by Ram and Sinha [134]. They used the FSDT to conduct the dynamic analysis by considering the effect of the temperature and moisture content related residual stress. The decrement of the dimensionless natural frequencies is mainly caused due to the degradation in the elastic properties of the graphite-epoxy composite lamina with the increase in temperature and moisture content. Furthermore, free vibration behavior of thick composite plates [127] and shells [102, 103] in hygrothermal environment has been studied by implementing various HSDTs. Shen and Yang [163] and Shen et al. [162] have carried out a nonlinear flexural vibration analysis of functionally graded shear-deformable fiber-reinforced laminated composite cylindrical shells in hygrothermal condition.

Transient response of composite plates and shells in thermal environment has been assessed by various researchers. Huang et al. [67] studied the dynamic response of shear-deformable laminated composite plates in hygrothermal environment using the HSDT. Later, Shen et al. [164, 165] have examined the transient response in terms of the central deflection and bending moment for the elastically supported shear-deformable laminated composite plates using the HSDT as proposed by Reddy [139]. Naidu and Sinha [110] described variations in the nonlinear transient response of thick doubly-curved graphite-epoxy laminated composite shells with the changing hygrothermal environments. Researchers also examined the free and forced vibration responses of the graphite-epoxy composite shells with multiple delaminations [125] and initial imperfection [112] in varying hygrothermal environments. Recently, Garg and Chalak [51] have presented a state-of-the-art

review article on the application of various FE formulations for analyzing laminated composite and sandwich plates and shells in hygrothermal environment.

1.1.3 Damping in composite plates

Different types of damping

Controlling the dynamic response in lightweight structures made of laminated composite plates or shells is a challenging task, although essential to ensure structural safety and passengers' comfort. Additionally, structural vibration control ensures a better fatigue life and a quieter operational environment. The vibration control of a structure is achieved by implementing a suitable damping strategy. Based on the mechanism, structural damping is classified into two broad categories: passive damping and active damping. The passive damping in composite plates refers to energy dissipation due to the interaction between fibers and matrix [62, 63]. Since passive damping is an inherent property of a composite material, this damping is known as the intrinsic or inherent damping of composite structures [183]. Often, single or multiple viscoelastic layer(s) are embedded into a host composite laminate to improve the efficiency of passive vibration control [44, 135]. On the other hand, different active vibration control strategies are implemented by attaching smart materials, e.g., piezoelectric materials (PZMs) [77] and shape memory alloys (SMAs), with the host composite plates. These smart materials require external power supply while being operational. Generally, piezoelectric alloy (PZA) patches or PZA layers are embedded in a composite laminate to improve the damping performance of the plate. Furthermore, SMA materials are available in different forms, such as SMA particles, SMA fibers, SMA wires, SMA sheets, etc. [25, 48, 152, 201], and embedded in the laminated composite plates according to the functional requirements. Two primary damping mechanisms and the associated damping materials are illustrated in Figure 2. Other than these two damping mechanisms, semi-active damping mechanism is also used in vibration control, however not included in this discussion.

This dissertation is mainly concerns with temperature-dependent inherent damping behavior of laminated composite plates. Therefore, upcoming discussions focus on viscoelastic damping behavior of composite materials in varying thermal environments.

Viscoelastic behavior of composites in thermal environment

Active damping imparts better vibration control at the expense of the efficient control algorithm and external power supply, and these extra costs often render the system economically nonviable.

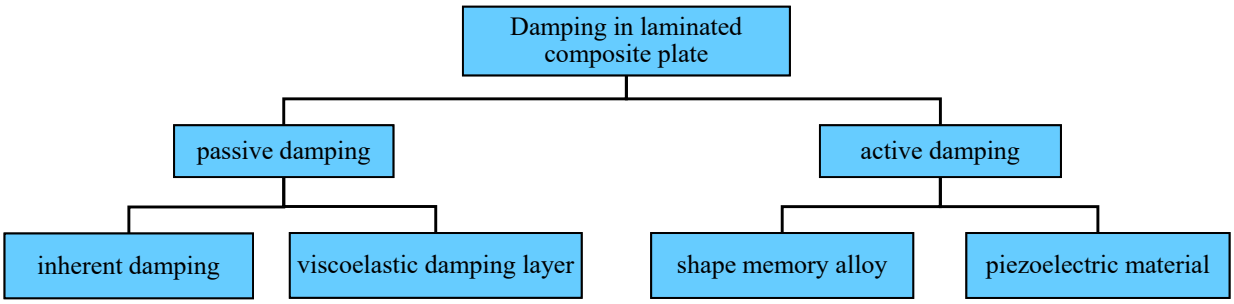

Figure 2: Classification of damping for laminated composite plates

Acknowledging these facts, passive damping is considered as the most cost-effective vibration control strategy along with lower maintenance effort. Moreover, the passive damping mechanism is more sensitive to temperature and is specifically influenced by the viscoelastic behavior of the matrix part of the composites. In various temperature regimes of interest, the viscoelastic behavior of composite materials is described by the glassy (near-room temperature), transition, and rubbery regions [114]. The temperature-dependent variation in storage moduli and damping loss factor of a typical viscoelastic material is shown in Figure 3. It indicates that the damping loss factor increases with the increment of temperature from the glassy region and reaches its maximum value at the glass transition temperature, T_g. The damping loss factor decreases with further increment of the temperature beyond the glass transition temperature (T_g). The glass transition temperature lies within the transition region. Notably, higher magnitude of damping properties at the elevated temperature can be advantageously used for passive vibration control at higher temperature region. In contrast to the damping behavior, storage modulus decreases with the increment of temperature. In the glassy region, the degradation in the storage modulus is at a slower rate, whereas in the transition region, a rapid degradation in the elastic moduli is observed. Essentially, beyond the glass transition temperature, composite materials behave like a rubbery material, and its load-carrying capacity becomes almost negligible [41]. Hence, the knowledge of the glass transition temperature is essential for the efficient application of a composite material for a given operative temperature range.

Traditionally, the application of an individual control technique in the form of either passive damping or active damping is preferred by researchers in the field of structural vibration control or acoustic control. However, in few studies [10, 55, 91, 184] it is found that active vibration control supported by passive vibration control has shown distinct advantages of robustness and stability over the individual vibration control mechanism. Furthermore, this combined control strategy

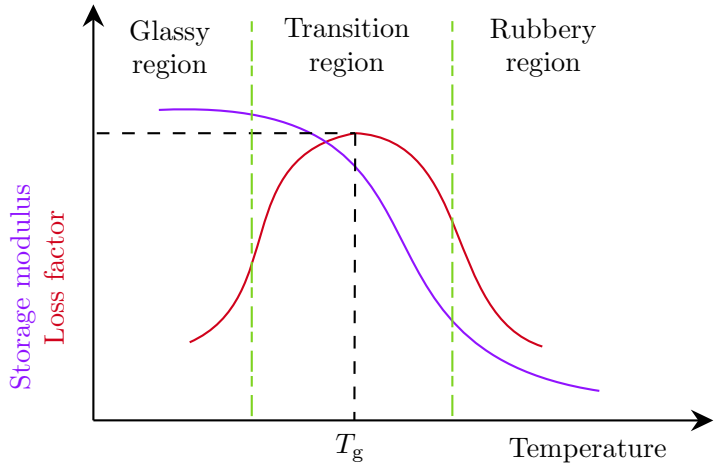

Figure 3: A representative diagram describing the temperature effect on storage modulus and loss factor of a typical isotropic viscoelastic material

leads to an overall weight reduction as a result of smaller actuator size and lesser power requirement. The high bandwidth control of lightweight structures is greatly improved by adapting the combined control strategy in order to improve the damping performance. Furthermore, the first stage implementation of passive damping reduces the vibration suppression effort of the smart controller when the structure is subjected to impulse loading and equipped with the combined control strategy [57]. Therefore, studying the inherent damping performance of laminated composite plates in thermal environment has emerged as a potential research opportunities pertaining to its easy and cost-effective applications as well as higher damping capacity at elevated temperatures. The past studies on inherent damping analysis of laminated composite plates are described in the following.

Inherent damping in composite plates

The energy dissipation through the surface of a vibrating plate is due to the contribution of the inherent damping characteristics of composite plates. Furthermore, the inherent damping in a composite plate is contributed by the viscoelastic behavior of the matrix part and the interaction between fibers and matrix. The mathematical representation of passive damping of a vibrating structure is not very straightforward, hence various damping models have been developed to represent passive damping mathematically. A detailed description of different damping models is found in [2]. Damping models such as Maxwell, Voigt, and standard viscoelastic models are used to predict the passive damping capacity [177] of a structure and were subsequently incorporated into the FE formulation. The complex modulus method and the strain energy method are widely

implemented procedures to estimate the passive damping in laminated composite plates within the FE framework; see references [22, 183] for more details. A brief discussion on numerical and experimental damping analysis of composite plates is presented in the subsequent paragraphs.

Damping model: complex modulus method

In 1962, Neumark [113] introduced the concept of complex moduli to evaluate viscoelastic damping in a dynamic system. Neumark has acknowledged that the stress-strain relationship of viscoelastic materials is harmonically time-dependent in a steady state condition. Even before publishing this article [113], Kerwin [78] had mentioned that the damping loss factor for a constrained viscoelastic damping layer is dependent on frequency and temperature. Note that the frequency dependent loss factor, $\eta(\omega)$, for a viscoelastic material is presented by the ratio between the loss modulus, $E'(\omega)$, and the storage modulus, $E(\omega)$, such that $\eta(\omega) = \frac{E'(\omega)}{E(\omega)}$. Here, the loss modulus accounts for the energy dissipation, and the storage modulus is a representation of the energy which is recoverable. Moreover, the complex elastic modulus, E^*, of an isotropic viscoelastic material is expressed as: $E^* = E(1+i\eta)$. Later, Hashin [61] has presented a microscopic viscoelastic analysis for fiber-reinforced composites by using the composite cylinder assemblage model. In his subsequent articles, Hashin has also studied dynamic behavior of particulate composites [62] and fiber-reinforced composites [63] in the framework of microscopic complex modulus method.

Damping model: strain energy method

The idea of energy dissipation from a dynamic system originated from the work of Ungar and Kerwin [186]. They described that the specific damping coefficient (SDC) of a structure, which is under a steady-state of vibration, is a ratio between the energy dissipated per circle and the total energy associated with the vibration. Adams and Bacon [1] extended the work of Ungar and Kerwin [186] for laminated composite plates, insofar as the authors decomposed the dissipated energy of the composite plate in the direction of the principal stress components of the constituent lamina and subsequently discussed the contribution of the dissipated energy with respect to the total dissipated energy along the principal stress direction. In further works, Saravanos and Chemis [145] described that during vibration of a composite plate a part of the dissipated energy transforms into heat, which leads to increasing the temperature of the plate. They reported that the increment of the ambient temperature influences matrix dominated damping components, e.g., shear SDC and transverse SDC of the associated lamina. The continual research of Saravanos and Chemis [146] contributed to development of a micromechanical damping theory based on the individual energy

dissipation characteristics of fibers and matrix. Moreover, this micromechanical theory considers the effect of the variation of temperature and moisture concentration on the damping parameters. However, the accuracy of this method depends on the prior knowledge of the elastic and damping properties of fibers and matrix as well as on the application of a suitable micromechanical model.

Influence of temperature

The magnitudes of the damping parameters along the principal stress directions of a lamina differ at varying temperature states. For viscoelastic materials such as lamina, increasing tendencies of the damping values are observed with the increment of temperature. To obtain better damping performance at higher temperature by utilizing higher damping values, researchers investigated increase in the damping capacity of composite laminates at different elevated temperatures [19, 21, 37]. Additionally, the damping capacity of composite laminates can be improved further by incorporating layers of polymer having viscoelastic characteristics [8, 13, 14, 135].

Generally, dynamic mechanical analysis (DMA) of a composite laminate is carried out to evaluate the variation in the elastic and damping properties with respect to temperature and frequency. A detailed investigation using DMA of the IM7-PEEK composite lamina has been carried out by Melo and Radford [105] and evaluated the corresponding frequency- and temperature-dependent elastic and damping parameters. Later, Sefrani and Berthelot [153] conducted a combined experimental-numerical analysis to estimate the temperature-dependent bending modulus and loss factors of unidirectional glass fiber composite lamina. In recent times, inverse methods [66, 94, 204] have been used to estimate the temperature-dependent elastic and damping properties of the composite lamina by using experimental modal data. The literature review indicates that the researchers and scientists typically used two experiment-based procedures to estimate modal damping values of composite plates, namely: (1) DMA and (2) inverse methods. Thermal environment has significant influence on the damping parameters of composite lamina, however, their impacts on dynamic response are yet to be studied in details. The few studies available in research literature, which have studied the damped dynamic response of composite plates due to inherent damping, are described in the following subsection.

Inherently damped vibration of composite plates

The damped dynamic response of composite structures was studied to investigate the controlling efficacy of the inherent damping properties. The transient response of laminated composite plates, having inherent damping properties, was studied by Zabaras and Perveze [130, 200]. Besides these

studies, Yi et al. [198] discussed the influence of temperature on the damped dynamic response of cross-ply and angle-ply composite cylindrical shells by considering the temperature-independent elastic and damping properties. In addition to these time domain analyses, frequency domain analysis of the IM7-PEEK composite plates has been carried out by Jeyaraj et al. [68] in varying thermal environments by considering the temperature-dependent elastic and damping properties of the associated lamina. The contrasting temperature-dependent behavior of elastic and damping properties of such composite lamina has mandated for a detailed investigation to evaluate the damping performance of the composite laminate at different temperatures. Note that Jeyaraj et al. [68] did not quantitatively evaluate the damping performance of the IM7-PEEK composite laminate in varying temperatures, even though the quantitative assessment of damping is absolutely necessary to identify a suitable laminae configurations for providing the best damping performance.

1.1.4 Vibration of stiffened plates

To exploit the full potential of plate-like structures, plates can be reinforced by attaching stiffeners. Furthermore, the addition of stiffeners offers an overall reduction in the amplitude of dynamic response with the cost of minimum weight penalty. Different forms of stiffeners are used in several components of aircraft, car bodies, and hulls of ships to avoid large deflection and buckling phenomenon. For example, a large number of cross stiffeners and a few number of longitudinal stiffeners offer rigidity to the fuselage, which is a thin-walled shell-like structure, of a pressurized aircraft [4]. Additionally, the wing, torsional box, and rib of an aircraft benefit in term of better stability and stiffness through an attached optimized form of stiffener(s). Over the years, these parts of an aircraft are replaced with composite materials. Thereby stiffened composite structures need a detailed investigation for the purpose of extensive application in the aircraft structure for better performance and accurately predicting their thermo-mechanical dynamic response.

Various FE strategies are developed to study the bending and dynamic behavior of isotropic [34, 108, 121] and orthotropic [34, 108, 109, 182] stiffened plates. The increased application of stiffened composite structure suggests to conduct dynamic analyses of stiffened laminated composite plates [26, 92, 124]. In order to analyze stiffened plates, researchers have proposed different modeling techniques. Chattopadhyay et al. [26] idealized a stiffener as the Timoshenko beam element while analyzing a blade-stiffened composite plate. Qing et al. [133] studied free vibration behavior of stiffened laminated composite plates considering the compatibility of displacement and stress between the plate, modeled with plate element, and the stiffener, modeled with the refined beam and torsional element. Ray and Satsangi [137] developed a scheme to analyze arbitrarily oriented hat-stiffeners, where the initially determined stiffness matrix of the stiffener has been transferred

to the plate depending on the position of the stiffener. They idealized the stiffener as a three-node beam element. Unlike the previous studies, Pal and Niyogi [124] and Yu et al. [199] modeled the stiffener(s) as plate elements. While analyzing the dynamic response of stiffened laminated and sandwich folded plates, Pal and Niyogi [124] modeled both stiffened and folded plates using plate elements by introducing suitable transformation. The modeling of folded and stiffened composite plates is based on the original work of Niyogi et al. [117]. The formulation proposed by Yu et al. [199] is based on the absolute nodal coordinate formulation. This formulation is more efficient to describe large deformation problems, but these are not within the scope of the present study. It is noteworthy that the plate-plate element model offers better interface compatibility than the plate-beam model while analyzing a stiffened structure.

Significant numbers of research articles have discussed free vibration behavior of stiffened laminated composite plates [26, 124, 133, 137, 167], however, transient analysis of these plates is rarely available. Based on the analysis framework presented in references [26, 137], Kumar and Mukhopadhyay [87] studied dynamic deflection of stiffened laminated composite plates for different kinds of stiffeners. Furthermore, Pal and Niyogi [124] present a limited discussion on the dynamic deflection of stiffened folded plates. In recent times, Thakur et al. [181] thoroughly discussed the dynamic behavior of laminated composite folded plates in hygrothermal environment by applying the nonpolynomial shear deformation theory.

The recent developments in the aerospace and automobile industries deal with replacing conventional structural materials with composite materials, whereby stiffened composite plates are used extensively in various forms to ensure structural stability and safety. In operating condition, these structures are exposed to thermal environment. Considering these facts, understanding dynamic behavior of stiffened laminated composite plates in varying thermal environments is an essential to conduct research on; however, research work reported in this domain are less. Moreover, the damping performance of these stiffened plates due to the temperature-dependent elastic and damping properties has never been explored.

1.1.5 Parameter identification of composites

Since the considerable upsurge in application of composite materials in critical structural components of aerospace and high-speed vehicles, the knowledge on the temperature-dependent properties of these materials is essential for the simulation engineer. Furthermore, there has been a constant need to develop a user-friendly experimental procedure for dynamic analysis of composite plates in varying thermal environments in order to determine the in situ temperature-dependent

elastic and damping properties of composite materials. Unlike conventional structural materials, composite materials are not isotropic material but rather transversely anisotropic. The material properties characterization of composite materials was based on suitable assumptions of homogenization. For the practical application, the estimation of macro-mechanical properties of composite plates at the lamina level serves the purpose. The macro-mechanical properties are expressed along the principal stress direction of the lamina.

Over the last three decades, significant research has been dedicated to estimate the material properties of composites. This research is mainly devoted to improve the experimental procedure and the associated numerical strategy. For material properties identification of composite lamina, two broad approaches are chosen: (1) experimental approach and (2) numerical approach. Under the category of the experimental material properties identification scheme, static and dynamic measurements are conducted. The static destructive tests involve tensile tests, compression tests, bending tests, torsion tests, etc. to acquire stresses and strains of a specimen, and directly evaluate elastic properties by applying the fundamental stress-strain theory. Many of these test procedures have been standardized by the International Organization for Standardization and the American Society for Testing and Materials [31, 32]. To evaluate elastic parameters of a composite laminate, separate tests need to be conducted, therefore the identification of all elastic parameters by using separate test procedures is time-consuming. Under the category of numerical approach, two methods, i.e., forward methods and inverse methods are used. In these methods, experimental data are used to derive the material properties of composite lamina, numerically. In forward methods [145, 146], the lamina properties are estimated by solving the stress and strain fields based on closed-form solutions or by applying the FE method using the underlying mechanics virtual work principle. Within the category of forward methods, the properties of lamina are estimated by knowing the properties of constituent parameters, i.e., fibers and matrix, geometry of the specimen, and well-posed sets of the boundary conditions. Note that, the properties of constituents parameters are evaluate experimentally beforehand. In contrast to forward methods, macro-mechanical properties of composite lamina can be identified based on the given knowledge of the boundary conditions and measurement of the displacement (or strain) fields, which are known as inverse methods [6, 70, 180].

The development of different micro-mechanical theories [1, 115, 145, 147] endeavors to predict the elastic and damping properties of composite lamina. Additionally, the contribution of hygrothermal environments has an influence on the elastic and damping properties of a composite lamina, which was thoroughly studied by Saravanos and Chemis [146] with reference to the previously developed micro-mechanical theory [145]. Basically, these studies fall under the category of forward

methods. The accuracy of the estimated properties depends on the knowledge of the constituents materials, e.g., elastic and damping properties of fibers and matrix, ratio between fibers and matrix, and behavior of the fibers-matrix interface. Essentially, both the direct experimental approach and numerically assisted forward approach often do not provide the in situ material properties while the composite plates are subjected to the dynamic loading in operating condition.

In this context, inverse methods have appeared with the most realistic solution, according to which elastic and damping properties of composite lamina can be determined by using the in situ dynamic test data of composite plates [172, 187]. The primary idea of the implementation of inverse methods is to minimize the error function, which is a difference between measured and simulated modal values, using an appropriate optimization technique. The elastic properties of composite lamina are predicted by Soares et al. [170] and Bledzki et al. [18, 143] utilizing experimentally derived modal frequencies of composite plates. In these studies, the computational efficiency of the optimization scheme was improved by employing the response surface method as a metamodel. For a deeper insight into inverse methods, several books [6, 70, 180] can be referred. Furthermore, Sol et al. [173, 174] and Visscher et al. [188, 189] evaluated damping properties of composite lamina using inverse methods. In these studies, modal data of composite plates are derived by using experimental modal analysis (EMA). Following the principle of the EMA, both input signal and output response are recorded to evaluate frequency response functions and thereby enable estimating modal characteristics of the vibrating plates. Review articles by Tam et al. [178, 179] can be referred to get an overall idea of the recent development (e.g., optimization algorithm, optimization function, etc.) of inverse methods for parameter identification of composite lamina.

Temperature-dependent properties

Since composite materials are viscoelastic in nature, the corresponding elastic and damping properties are frequency- and temperature-dependent. To simulate the realistic dynamic behavior of a composite structure in thermal environment, it is crucial to consider temperature-dependent material properties. Hence, simulation engineers essentially require the detailed knowledge of the temperature-dependent elastic and damping properties of the real structure in operating condition. In such a situation, inverse methods can be used appropriately to evaluate the temperature-dependent elastic and damping properties of composite lamina. The temperature-dependent modal data are collected by conducting experiments within the thermal enclosure. Nevertheless, continual development of the experimental procedure and identification strategy is under process. Frederiksen [45] and his co-workers [128] conducted the EMA using unidirectional glass-epoxy and carbon-epoxy laminated composite plates within a thermal enclosure, and they determined the

associated temperature-dependent elastic properties. Later, Sefrani and Berthelot [153] have estimated temperature-dependent damping properties of the unidirectional glass-fiber composite beam utilizing the experimental data. In these studies [45, 128, 153], the corresponding composite plate, which is placed inside the thermal chamber, is excited by an impulse hammer by implementing suitable modification in the excitation strategy. Additionally, both the input signal and output response are recorded to estimate the modal data of the plate, which increase complexity in the experimental procedure and data storage efficiency. Li et al. [93, 94] identified the temperature-dependent elastic and damping properties of composite lamina by using inverse methods for conducting the experiment within a thermal chamber. Instead of using the impulse hammer method, aerodynamic impulse was used to excite the plate, and a laser Doppler vibrometer was used to measure the nodal response of the vibrating plate.

In addition to inverse methods, the DMA is also used to measure the elastic and damping properties at different temperatures. In the DMA, an oscillating force is applied to a small unidirectional (or multidirectional) laminated composite beam type sample. The analysis of the response to that force determines the material properties; see the textbook by Menard [106] for more detailed discussions on the DMA. This quasi-static experimental procedure can predict five elastic parameters and three damping parameters at different temperatures and frequencies [104]. However, the frequency range of the DMA is limited between $0-100$ Hz. Applying the DMA, Melo et al. [105] thoroughly studied the temperature- and frequency-dependent elastic and damping properties of the IM7-PEEK composite lamina. The composite properties identified at the low frequency range using a small test sample is questioned for its applicability to real structures operating at a higher frequency regimes.

Upon reviewing the background research work, further improvement in the experimental procedure for inverse methods is felt necessary to make the procedure more user-friendly and realistic. In this way, the in situ experimental data can be recorded and subsequently the temperature-dependent modal parameters of the composite plate, and the temperature-dependent material properties of the corresponding lamina can be estimated. Nevertheless, the DMA evaluates temperature- and frequency-dependent elastic and damping properties of a lamina, however in quasi-static conditions. The implementation of the DMA-estimated elastic and damping properties for dynamic analysis of a composite structure in a higher frequency range has raised the concern of its applicability. Therefore, an inverse method is used to evaluate the in situ temperature-dependent material properties of composite lamina by utilizing dynamic test data.

1.1.6 Uncertainty quantification of dynamic response

In the engineering sector, computer simulations are widely used to reproduce and predict the behavior of complex physical systems. Despite of the drastic growth in computational power and the continual improvement of the computer modeling of dynamic systems, two salient challenges still existing: firstly, inevitable modeling-related errors, and secondly, lack of precise knowledge of input parameters, since it is hardly possible to obtain exact material properties due to their inherent variabilities and the paucity of information. Therefore, the effect of uncertainties needs to be considered during the computer simulation of a physical system. In this dissertation, modeling-related uncertainties are assumed to be negligible while the influence of the uncertainties in input parameters are considered. Hence, to ensure a safe design for a composite structure in thermal environment, the associated uncertainty quantification of the dynamic response of a composite structure is essential by implementing a computationally efficient numerical procedure.

Uncertainty quantification of dynamic response in an engineering system is a much needed and challenging area of research in recent times. Primarily two methods, namely the intrusive method and the nonintrusive method, are used for uncertainty quantification [175]. The numerical modeling of a structural system is assumed to interpret the relationship between input and output parameters. Generally, the dynamic analysis of composite structures is conducted by using the FE-based numerical modeling. The intrusive method, which adopted the governing equations of a structure as the deterministic model, has limited application. The application of the intrusive method for uncertainty quantification of a FE-based structural system is a computationally challenging task. The nonintrusive method, which realizes the deterministic model for a set of input parameters, can be used instead of the intrusive method. The so-called MC simulation is the well-known nonintrusive scheme. Nevertheless, the low convergence rate has limited the applicability of the MC simulation. In contrast, metamodels are extensively used for uncertainty quantification of engineering systems [175, 176]. In the metamodel setup, major computational cost is utilized to train the metamodel. Overall, metamodels offer sufficient accuracy in uncertainty quantification with minimum computational cost. The spectral methods are polynomial metamodels based on functional analysis. The polynomial chaos (PC) expansion method is widely used as a spectral method, and it is based on the pioneering work by Ghanem and Spanos [54]. In the context of the spectral finite element method, the spectral representation of the PC has been done by using the Hermite polynomial functions. Since then, this method has been generalized and popularized in the field of stochastic structural mechanics [171]. An extensive research work has been dedicated to generalize this spectral method for different random spaces by adopting suitable basis functions from the Askey family of hypergeometric polynomials [160, 193–196]. This generalized setup of the

PC expansion is referred as "generalized polynomial chaos (gPC) expansion". Additionally, the perturbation method, a non-sampling based approach, is also used for uncertainty quantification of composite plates. According to the perturbation method, random parameters are expanded by the Taylor series expansion. The Taylor series expansion up to first-order is used to develop the first-order perturbation technique (FOPT), which is implemented to estimate the response uncertainty in engineering systems [3, 29, 50, 65] with lower level of randomness in input parameters. Studies by Sepahvand et al. [155–157] are dedicated to evaluate uncertainty in eigenfrequencies and mode shapes due to random elastic parameters and randomness in fiber orientations using the gPC expansion method. Furthermore, different variants of this method are explored to assess uncertainty in lamination parameters [151], frequency response function [35], eigenfrequencies [129], and static deflection [27, 148] of laminated composite plates. Limited applications of the FOPT are also found in the literature [56, 90, 166] on uncertainty quantification of different response parameters of composite plates.

Effect of uncertainty in thermal environment

A few studies on uncertainty quantification of the time-independent dynamic response of composite plates without considering any thermal effect are available in research literature. However, the contribution of the temperature variation in uncertainty quantification of dynamic response is an essential area of research to ensure structural safety of composite plates in varying thermal environments. Uncertainty in the first eigenfrequency, arising due to the randomness in the individual system parameters at varying temperature states, is documented in literature, e.g., by Lal and Singh [89] and Kumar [84, 85]. Stochastic free vibration response of elastically supported laminated composite plate in hygrothermal environment was studied by Kumar et al. [86] using micro-mechanical theory. Their studies implemented the FOPT to model the uncertainty propagation where the level of uncertainty remains within a smaller range. Unlike the earlier studies which assumed a uniform temperature distribution, Lal and Singh [88] studied stochasticity in the thermal buckling temperature due to nonuniform distribution of temperature for a laminated composite plate resting on an elastic foundation with random system properties. Applying generalized high-dimensional model representation, Dey et al. [36] discussed the propagation of ply-level and material uncertainties to the first three eigenfrequencies at the temperature range of $125 - 375$ K. This discussion reveals that stochastic dynamic analysis of displacement parameters of composite plates in varying thermal environments has never been studied, although it is a very important research field to ensure the structural safety of a composite structure which is subjected to dynamic loading in varying thermal environments. The present dissertation contributes to fill this

research gap by conducting stochastic dynamic analysis of composite plates in random thermal environments.

1.2 Research contributions

This dissertation contributes to the domain of dynamic analysis of composite structures with complex geometry in varying thermal environments by developing a generalized FE framework. The literature review pointed out that the elastic properties of carbon- or graphite-based lamina degrade with the increment of temperature, thus contributing to the loss of stiffness to the associated composite plate. The addition of stiffener(s) improves stiffness of the plate and can be advantageously used to reduce the amplitude of the dynamic response of the composite plates at elevated temperatures. Furthermore, the inherent damping capacity of composite lamina increases with the increment of temperature up to glass transition temperature of the composite lamina. In this connection, the damping behavior of these stiffened plates also needs to be understood prior to their realistic application in varying thermal environments. Furthermore, knowledge on the in situ temperature-dependent elastic and damping properties of composite lamina level is essential for deterministic and stochastic analysis of composite plates in varying thermal environments.

While composite structures have numerous applications in aerospace and transportation industries, the detailed dynamic analyses of composite plates, specifically for the stiffened plates in varying thermal environments, are severely limited. As a part of this research work, the following research gaps are addressed:

- Study both the undamped and damped dynamic behavior of unstiffened and stiffened laminated composite plates in varying thermal environment. Moreover, there is a need to develop a generalized FE framework to analyze the complex geometry, e.g., of stiffened plates.
- Develop an efficient numerical strategy to quantify the damping performance of composite plates for different combinations of stiffener, lamina sequences, etc. at different temperatures, and thereby identify the configuration which imparts the best damping performance in varying thermal environments.
- Develop a combined experimental and numerical mechanism to evaluate in situ dynamic characteristics of a composite plate at different temperatures, and thereby estimate deterministic in situ temperature-dependent material properties by using inverse methods.
- Uncertainty in temperature and material properties propagates into dynamic response, and the corresponding stochastic dynamic behavior needs to be analyzed for further designing

these structures in thermal environment.

The four publications are appended to this dissertation to address the stated research gaps. Publications 1 and 2 contribute to fill the initial two research gaps. The third research gap is discussed in Publication 3. Additionally, stochastic dynamic analysis of composite plates is carried out in connection with random temperature increment in Publication 4, which is intended to address the fourth research gap.

Publications 1 and 2 are sequentially dedicated to undamped and damped dynamic analyses of unstiffened and stiffened laminated composite plates in varying thermal environments. These publications are furnished with a detailed literature review to understand the background of the conducted investigations. Herein, a generalized FE formulation is developed to analyze unstiffened and stiffened laminated composite plates in varying thermal environments. The FE formulation is developed with reference to the Hamilton's variational principle. Moreover, in Publication 2 an innovative energy-based strategy is developed to assess the damping performance of composite structures. This energy-based approach has outperformed the conventional displacement-based approach in assessing the damping performance. Notably, the conventional displacement-based approach exploits the idea of the logarithmic decrement to estimate the damping performance. Detailed parametric studies are carried out to identify the best configuration of a stiffened plate in order to obtain the highest damping performance at different temperatures.

Furthermore, the temperature-dependent material properties of carbon-epoxy lamina are estimated by applying an inverse method, and presented in Publication 3. It deals with a combined experimental-numerical procedure. In this work, a novel noncontact-based operational modal analysis (OMA) of a composite plate is presented within a thermal enclosure by addressing previously counted limitations. Furthermore, the experimentally evaluated modal data are utilized to estimate the deterministic temperature-dependent elastic and damping properties of composite lamina implementing a two-stage genetic algorithm. The FE framework, which is developed in Publication 2, is incorporated in the optimization algorithm.

The stochastic dynamic analysis of composite plates due to random temperature increment is presented in Publication 4 by using the gPC-based metamodel. The previously developed deterministic model is used to generate training data set to train the gPC-based metamodel. The gPC expansion method is used to evaluate the statistical properties of eigenfrequencies and transient response at different random temperatures. This publication can be viewed as an initial stepping stone to assess the reliability of carbon- or graphite-based laminated composite structures in varying thermal environments. Detailed summaries of these publications are given in Chapter 3.

This dissertation chronologically addresses the identified research gaps. The initial two publica-

tions are the building blocks for the remaining two publications. In a nutshell, the present dissertation presents detailed numerical and experimental investigations in the field of dynamic analysis of composite plates in varying thermal environments.

Chapter 2

Theory and Applied Methods

This chapter is dedicated to describe the theoretical background of the numerical and experimental procedures which are adopted in this dissertation. Herein, a brief overview of the relevant theories is given, whereas detailed descriptions of the adopted methodologies are presented in the respective publication.

2.1 Laminated composite plates

A laminate is a plate-like structure which consists of two or more unidirectional laminae or plies staking together in unidirectional or multidirectional orientations. A lamina (or ply) is a plane layer of unidirectional fibers suspended in a matrix. A lamina is considered as an orthotropic material with the principal material axis in the direction of fibers, i.e., the in-plane longitudinal direction, normal to the direction of fibers in the plane of lamina, i.e., the in-plane transverse direction, and normal to the plane of the lamina. These principal axes of a lamina are designated as 1, 2, and 3, respectively, and form the basis of the lamina coordinate (1, 2, 3) system. Analysis of laminates has been done by adopting an unified laminate coordinate (x, y, z) system, because the principal lamina axes of a lamina can vary layer-wise. The coordinate systems are shown in Figure 4 with reference to the composite lamina and the associated laminate. The angle between the laminate axis x and the lamina axis 1 is designated by θ. When laminae stacking sequences are symmetric about the mid-plane of the laminate, the laminate is referred to as a "symmetric laminate"; whereas if a lamination scheme becomes antisymmetric about the mid-plane of the laminate, the laminate is denoted as an "antisymmetric laminate". Lamina sequences of typical symmetric and antisymmetric laminates are shown in Figure 4. Conventionally, lamina sequence is designated from bottom layer to the top layer by the symbol θ.

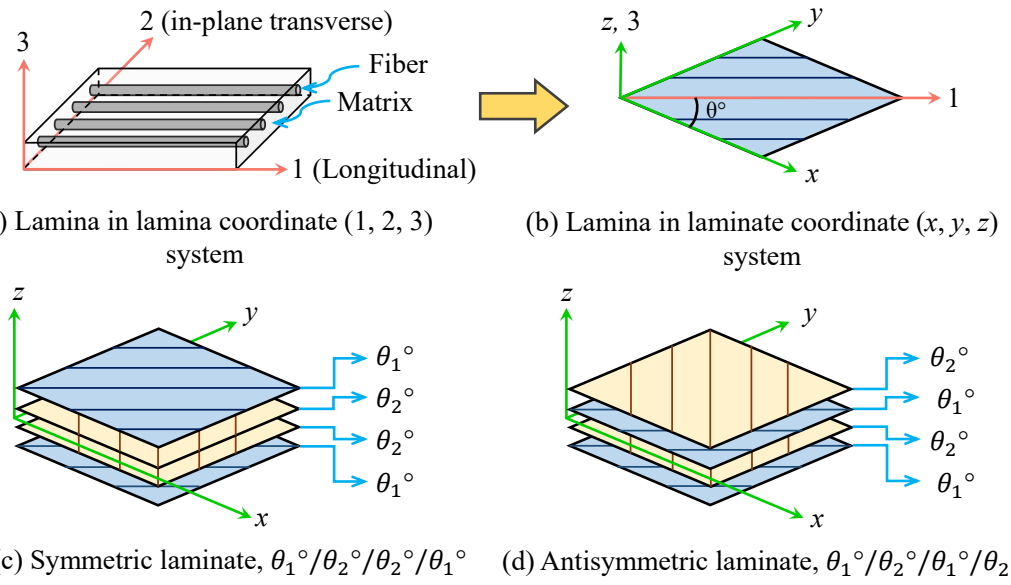

(a) Lamina in lamina coordinate (1, 2, 3) system

(b) Lamina in laminate coordinate (x, y, z) system

(c) Symmetric laminate, $\theta_1°/\theta_2°/\theta_2°/\theta_1°$

(d) Antisymmetric laminate, $\theta_1°/\theta_2°/\theta_1°/\theta_2°$

Figure 4: Typical representation of the lamina coordinate (1, 2, 3) system, the laminate coordinate (x, y, z) system, and symmetric and antisymmetric laminates

The modeling of a composite structure for static and dynamic analyses has been done on macroscopic level, where the influence of the material discontinuity at the microscopic level of a lamina is neglected. In the case of a fiber-reinforced composite lamina, the heterogeneity at the lamina level, due to the existence of two constituent materials, i.e., fibers and matrix, has been avoided by determining homogeneous properties of the lamina on the macroscopic scale. The homogenized material properties of a lamina are derived by applying the concept of representative volume elements. The reference [139] can be referred for a detailed discussions on the representative volume elements to obtain the homogenized material properties of a lamina. However, homogenization to obtain the lamina properties is not within the scope of the present investigation; instead, lamina properties are taken from the literature or derived from the experimental measurement.

In order to describe the macromechanical behavior of a lamina, the state of the three-dimensional stress and strain is represented by the generalized Hooke's law. The three-dimensional state of stress or strain in a continuum is described by the stress or strain tensor, respectively. In general, tensor components on an infinitely small cube are described in such a way that the first component of the subscript denotes the direction of the force and the second component of the subscript denotes the plane on which the force is acting. To illustrate this description, a three-dimensional stress tensor, σ_{ij} ($i,\ j = 1,2,\text{and } 3$), for an infinitely small cube is shown in Figure 5. Upon this basic notation and the coordinate systems, constitutive relationships of a composite plate are developed by using the basic frameworks of the continuum mechanics.

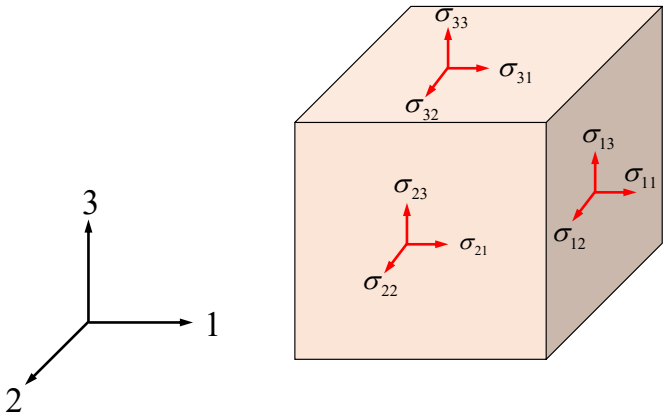

Figure 5: Three-dimensional stress tensor (σ_{ij}) in the Cartesian coordinate (1, 2, 3) system

2.2 Modeling of laminated composite plates

In this section, the modeling of laminated composite plates within the framework of the finite element method (FEM) is described. To this end, constitutive relationships of lamina and laminates are discussed and, finally, incorporated into the FE framework for dynamic analysis.

2.2.1 Constitutive relationship of a lamina

A Cartesian coordinate system is used to describe the stress-strain relationship of a composite lamina. For linear anisotropic materials, the constitutive relationship is presented as

$$\sigma_{ij} = C_{ijkl}\varepsilon_{kl}, \tag{2.1}$$

in which σ_{ij} is the three-dimensional stress tensor and the associated strain tensor is ε_{ij} in accordance with the tensorial notation. Furthermore, C_{ijkl} are material coefficients which contain 81 elastic constants for anisotropic materials. Due to the symmetry of $\sigma_{ij} = \sigma_{ji}$ and $\varepsilon_{ij} = \varepsilon_{ji}$, the material coefficients follow a symmetric relationship, such that

$$C_{ijkl} = C_{jikl}, \qquad C_{ijkl} = C_{ijlk}. \tag{2.2}$$

Moreover, the strain energy per unit volume, i.e., strain energy density function, W, is defined as

$$W = \frac{1}{2}C_{ijkl}\varepsilon_{ij}\varepsilon_{kl}. \tag{2.3}$$

Using mathematical identity, the following relationship is obtained

$$\frac{\partial^2 W}{\partial \varepsilon_{ij} \partial \varepsilon_{kl}} = \frac{\partial^2 W}{\partial \varepsilon_{kl} \partial \varepsilon_{ij}}, \tag{2.4}$$

that conforms to the relationship of $C_{ijkl} = C_{klij}$. Finally, elastic constants for anisotropic materials are related as

$$C_{ijkl} = C_{klij} = C_{jikl} = C_{ijlk}, \tag{2.5}$$

and thus, the number of independent elastic coefficients is reduced to 21. Instead of writing in the tensorial form, the constitutive relationship for anisotropic materials can be written in a contracted single subscript notation for the stress and strain components as well as in a double subscript notation for the elastic constants. The constitutive relationship for anisotropic materials with 21 elastic constants is presented as

$$\begin{Bmatrix} \sigma_1 = \sigma_{11} \\ \sigma_2 = \sigma_{22} \\ \sigma_3 = \sigma_{33} \\ \sigma_4 = \tau_{13} \\ \sigma_5 = \tau_{23} \\ \sigma_6 = \tau_{12} \end{Bmatrix} = \begin{bmatrix} C_{11} & C_{12} & C_{13} & C_{14} & C_{15} & C_{16} \\ C_{12} & C_{22} & C_{23} & C_{24} & C_{25} & C_{26} \\ C_{13} & C_{23} & C_{33} & C_{34} & C_{35} & C_{36} \\ C_{14} & C_{24} & C_{34} & C_{44} & C_{45} & C_{46} \\ C_{15} & C_{52} & C_{53} & C_{45} & C_{55} & C_{56} \\ C_{16} & C_{26} & C_{36} & C_{46} & C_{56} & C_{66} \end{bmatrix} \begin{Bmatrix} \varepsilon_1 = \varepsilon_{11} \\ \varepsilon_2 = \varepsilon_{22} \\ \varepsilon_3 = \varepsilon_{33} \\ \varepsilon_4 = 2\varepsilon_{13} = \gamma_{13} \\ \varepsilon_5 = 2\varepsilon_{23} = \gamma_{23} \\ \varepsilon_6 = 2\varepsilon_{12} = \gamma_{12} \end{Bmatrix}, \tag{2.6}$$

where in, $C_{21} = C_{12}$, $C_{31} = C_{13}$, $C_{32} = C_{23}$, $C_{41} = C_{14}$, $C_{42} = C_{24}$, $C_{43} = C_{34}$, $C_{51} = C_{15}$, $C_{52} = C_{25}$, $C_{53} = C_{35}$, $C_{54} = C_{45}$. Furthermore, σ_1, σ_2 denote the inplane normal stresses, σ_3 denotes the out-of-plane normal stress, σ_4, σ_5 denote the out-of-plane shear stress, and σ_6 denotes the inplane shear stress. Additionally, ε_1, ε_2, ε_3, ε_4, ε_5, and ε_6 are the corresponding strain components. This constitutive relationship is expressed in a compact form as

$$\boldsymbol{\sigma} = \boldsymbol{C}\boldsymbol{\varepsilon}. \tag{2.7}$$

Here $\boldsymbol{C}$ denotes the compliance matrix, and $\boldsymbol{\sigma}$ and $\boldsymbol{\varepsilon}$ denote the stress and strain vectors, respectively. Furthermore, an orthotropic material is characterized by the three planes of symmetry that are mutually orthogonal. In this case, only 9 independent elastic constants, i.e., C_{11}, C_{12}, C_{13}, C_{22}, C_{23}, C_{33}, C_{44}, C_{55}, and C_{66}, are used to describe the material adequately. A unidirectional lamina which is subjected to an on-axis loading can be modeled by the orthotropic material behavior. Moreover, the behavior of fiber-reinforced materials is defined by transversely isotropic materials' behavior. In this type of materials, the major coordinate axis is aligned along the fiber

direction, and the isotropic behavior is assumed in the cross-sectional direction of the fiber axis. The compliance matrix, $\boldsymbol{C}$, for transversely isotropic materials takes the following form

$$\boldsymbol{C} = \begin{bmatrix} C_{11} & C_{12} & C_{12} & 0 & 0 & 0 \\ C_{12} & C_{22} & C_{23} & 0 & 0 & 0 \\ C_{12} & C_{23} & C_{22} & 0 & 0 & 0 \\ 0 & 0 & 0 & C_{44} & 0 & 0 \\ 0 & 0 & 0 & 0 & \frac{1}{2}(C_{22}-C_{23}) & 0 \\ 0 & 0 & 0 & 0 & 0 & C_{44} \end{bmatrix}, \tag{2.8}$$

and the corresponding independent elastic constants are only 5. A fiber-reinforced composite lamina having fibers parallel to the lamina axis 1 (cf. Figure 4) is assumed to be a thin plate, hence plane stress condition can be applied quite adequately. Due to the application of this condition, the stress normal to the plate surface, i.e., σ_3, is neglected. Considering the principal lamina axes 1 and 2, the relation between elements of the compliance matrix and the engineering constants, i.e., E_{11}, E_{22}, G_{12}, G_{23}, ν_{12}, and ν_{21}, of a lamina is given by

$$\begin{aligned} &C_{11} = \frac{E_{11}}{1-\nu_{12}\nu_{21}}, \qquad C_{12} = \frac{\nu_{12}E_{11}}{1-\nu_{12}\nu_{21}}, \qquad C_{22} = \frac{E_{22}}{1-\nu_{12}\nu_{21}}, \\ &C_{44} = G_{12}, C_{55} = G_{23}, \qquad C_{66} = G_{12}. \end{aligned} \tag{2.9}$$

In the above relationships, fibers are oriented in the direction of the lamina axis 1, and the flat surface of the lamina lies on the 1-2 plane. These relationships are termed as the "on-axis relations". By ignoring the normal stress component (σ_3), the constitutive relationship of a composite lamina is obtained after implementing a necessary row-wise rearrangement and written as

$$\begin{Bmatrix} \sigma_1 \\ \sigma_2 \\ \sigma_6 \\ \sigma_4 \\ \sigma_5 \end{Bmatrix} = \begin{bmatrix} C_{11} & C_{12} & 0 & 0 & 0 \\ C_{12} & C_{22} & 0 & 0 & 0 \\ 0 & 0 & C_{66} & 0 & 0 \\ 0 & 0 & 0 & C_{44} & 0 \\ 0 & 0 & 0 & 0 & C_{55} \end{bmatrix} \begin{Bmatrix} \varepsilon_1 \\ \varepsilon_2 \\ \varepsilon_6 \\ \varepsilon_4 \\ \varepsilon_5 \end{Bmatrix}. \tag{2.10}$$

To develop the constitutive relationship of composite laminate, the constitutive relationship of lamina, cf. Eq. (2.10), requires to be expressed in the laminate coordinate (x, y, z) system by employing suitable transformation, and this relationship is known as the "off-axis relations"; see Figure 4. In the laminate coordinate (x, y, z) system, the stress-strain relationship of a specific lamina, say the k^{th} lamina, is expressed in the following form by accounting for the thermal effect:

$$\begin{Bmatrix} \sigma_{\mathrm{x}} \\ \sigma_{\mathrm{y}} \\ \tau_{\mathrm{xy}} \\ \tau_{\mathrm{xz}} \\ \tau_{\mathrm{yz}} \end{Bmatrix}_{\mathrm{k}} = \begin{bmatrix} Q_{11} & Q_{12} & Q_{16} & 0 & 0 \\ Q_{12} & Q_{22} & Q_{26} & 0 & 0 \\ Q_{16} & Q_{26} & Q_{66} & 0 & 0 \\ 0 & 0 & 0 & Q_{44} & Q_{45} \\ 0 & 0 & 0 & Q_{45} & Q_{55} \end{bmatrix}_{\mathrm{k}} \begin{Bmatrix} \varepsilon_{\mathrm{x}} - e_{\mathrm{x}} \\ \varepsilon_{\mathrm{y}} - e_{\mathrm{y}} \\ \gamma_{xy} - e_{\mathrm{xy}} \\ \gamma_{xz} \\ \gamma_{yz} \end{Bmatrix}_{\mathrm{k}}. \tag{2.11}$$

Herein, the principal thermal strain components are presented in the laminate coordinate (x, y, z) system as

$$e_{\mathrm{x}} = e_1 \cos^2\theta + e_2 \sin^2\theta, \qquad e_{\mathrm{y}} = e_1 \sin^2\theta + e_2 \cos^2\theta, \quad e_{\mathrm{xy}} = (e_1 - e_2)\cos 2\theta, \tag{2.12}$$

where the thermal strains, e_1 and e_2, are expressed with reference to the lamina coordinate (1, 2, 3) system and are given by

$$e_1 = \alpha_1 \Delta T, \qquad e_2 = \alpha_2 \Delta T, \tag{2.13}$$

in which α_1 and α_2 are the coefficients of thermal expansion along the axes 1 and 2, respectively, and ΔT denotes the uniform variation of the temperature with reference to the room temperature. The compact representation of Eq. (2.11) for the k^{th} lamina is given by

$$\boldsymbol{\sigma}_{\mathrm{k}} = \boldsymbol{Q}_{\mathrm{k}} \left\{ \boldsymbol{\varepsilon}_{\mathrm{k}} - \boldsymbol{\alpha}_{\mathrm{k}} \Delta T \right\}. \tag{2.14}$$

The elements of the off-axis constitutive relationship matrix, $\boldsymbol{Q}$, of a lamina are defined as

$$\begin{aligned}
Q_{11} &= C_{11}\cos^4\theta + 2(C_{12} + 2C_{66})\sin^2\theta\cos^2\theta + C_{22}\sin^4\theta, \\
Q_{12} &= (C_{11} + C_{22} - 4C_{66})\sin^2\theta\cos^2\theta + C_{12}(\sin^4\theta + \cos^4\theta), \\
Q_{22} &= C_{11}\sin^4\theta + 2(C_{12} + 2C_{66})\sin^2\theta\cos^2\theta + C_{22}\cos^4\theta, \\
Q_{16} &= (C_{11} - C_{12} - 2C_{66})\sin\theta\cos^3\theta + (C_{12} - C_{22} + 2C_{66})\sin^3\theta\cos\theta, \\
Q_{26} &= (C_{11} - C_{12} - 2C_{66})\sin^3\theta\cos\theta + (C_{12} - C_{22} + 2C_{66})\sin\theta\cos^3\theta, \\
Q_{66} &= (C_{11} + C_{22} - 2C_{12} - 2C_{66})\sin^2\theta\cos^2\theta + C_{66}(\sin^4\theta + \cos^4\theta), \\
Q_{44} &= C_{44}\cos^2\theta + C_{55}\sin^2\theta, \\
Q_{45} &= (C_{55} - C_{44})\sin\theta\cos\theta, \\
Q_{55} &= C_{55}\cos^2\theta + C_{44}\sin^2\theta.
\end{aligned} \tag{2.15}$$

Thus, the stress-strain relationship for an arbitrarily oriented lamina is derived by considering the

effect of temperature variation in the laminate coordinate (x, y, z) system. Based on this stress-strain relationship, the resultant forces and moments of the associated laminate are derived, which is described in the next subsection.

2.2.2 Constitutive relationship of a laminate

A laminated composite plate of thickness h consists of n numbers of unidirectional laminae bonded together to act as an integral continuum. Laminae in a laminate may have the same or different thickness and may have unidirectional or multidirectional lamina sequences. The geometry of an undeformed laminated composite plate is shown in Figure 6.

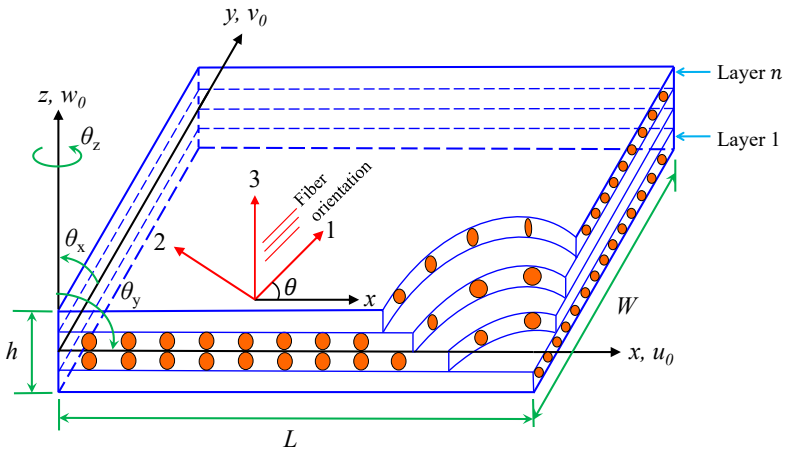

Figure 6: Geometry of a laminated composite plate showing positive direction of displacements and rotations

Herein, plates are assumed to be thin, therefore, the first-order shear deformation theory (FSDT) is employed for analysis. The FSDT is applied here with suitable modification for laminated composite plates as proposed by Yang, Norris, and Stavasky (YNS) [197]. The assumptions for the application of the FSDT are:

- the material is linear and elastic;
- the thickness of the plate is small compared to the other two dimensions;
- the deflection of the laminated composite plate is very small;
- the normal to the mid-plane remains straight before deformation but are not necessarily normal to the mid-plane after deformation; and
- the transverse normal stress is negligibly small and has not been considered.

The undeformed and deformed geometries of a thin composite plate along the x-z and y-z planes are shown in Figure 7. The components of the generalized displacement vector, $\bar{\boldsymbol{d}}$, at a distance z from the mid-plane are described in terms of the in-plane displacements, u_0 and v_0, at the mid-plane, the out-of-plane displacements, w_0, of the mid-plane. Furthermore, θ_x and θ_y are the rotations about the x-axis and y-axis, respectively. The generalized displacement components are given as

$$\left\{ \begin{array}{c} u \\ v \\ w \end{array} \right\} = \left\{ \begin{array}{c} u_0 + z\theta_\mathrm{y} \\ v_0 - z\theta_\mathrm{x} \\ w_0 \end{array} \right\}, \qquad \left\{ \begin{array}{c} \theta_\mathrm{x} \\ \theta_\mathrm{y} \end{array} \right\} = \left\{ \begin{array}{c} \frac{\partial w}{\partial y} - \varphi_\mathrm{y} \\ -\frac{\partial w}{\partial x} + \varphi_\mathrm{x} \end{array} \right\}, \tag{2.16}$$

where φ_x and φ_y are the shear rotations in the x-z and y-z planes. The generalized displacement vector is presented by $\bar{\boldsymbol{d}} = \{u \quad v \quad w \quad \theta_\mathrm{x} \quad \theta_\mathrm{y}\}^\mathrm{T}$. The assumption of small deflection is implemented to evaluate the linear strain vector, $\boldsymbol{\varepsilon} = \{\varepsilon_\mathrm{x} \quad \varepsilon_\mathrm{y} \quad \gamma_\mathrm{xy} \quad \gamma_\mathrm{xz} \quad \gamma_\mathrm{yz}\}^\mathrm{T}$, at a distance z from the mid-plane; thereby, the first-order terms are considered to evaluate the linear strain vector ($\boldsymbol{\varepsilon}$). The kinematic relation to evaluate the components of the linear strain vector ($\boldsymbol{\varepsilon}$) is expressed by

$$\begin{aligned}
&\varepsilon_\mathrm{x} = \frac{\partial u_0}{\partial x} + z\frac{\partial \theta_\mathrm{y}}{\partial x} = \varepsilon_{0\mathrm{x}} + z\kappa_\mathrm{x}, && \varepsilon_\mathrm{y} = \frac{\partial v_0}{\partial y} - z\frac{\partial \theta_\mathrm{x}}{\partial y} = \varepsilon_{0\mathrm{y}} + z\kappa_\mathrm{y}, \\
&\gamma_\mathrm{xy} = \frac{\partial u_0}{\partial y} + \frac{\partial v_0}{\partial x} + z\left(\frac{\partial \theta_\mathrm{y}}{\partial y} - \frac{\partial \theta_\mathrm{x}}{\partial x}\right) = \gamma_{0\mathrm{xy}} + z\kappa_\mathrm{xy}, && \\
&\gamma_\mathrm{xz} = \varphi_\mathrm{x} = \frac{\partial w}{\partial x} + \theta_\mathrm{y} = \gamma_{0\mathrm{xz}}, && \gamma_\mathrm{yz} = \varphi_\mathrm{y} = \frac{\partial w}{\partial y} - \theta_\mathrm{x} = \gamma_{0\mathrm{yz}}.
\end{aligned} \tag{2.17}$$

Herein, $\varepsilon_{0\mathrm{x}}$, $\varepsilon_{0\mathrm{y}}$, $\gamma_{0\mathrm{xy}}$, κ_x, κ_y, κ_xy, γ_xz, and γ_yz are the mid-plane strain terms, and the corresponding vector representation is

$$\{\varepsilon^*\} = \{\varepsilon_{0\mathrm{x}} \quad \varepsilon_{0\mathrm{y}} \quad \gamma_{0\mathrm{xy}} \quad \kappa_\mathrm{x} \quad \kappa_\mathrm{y} \quad \kappa_\mathrm{xy} \quad \gamma_\mathrm{xz} \quad \gamma_\mathrm{yz}\}^\mathrm{T}. \tag{2.18}$$

The constitutive relationship of a laminate is established in two steps. Initially, the constitutive relationship of a lamina, cf. Eq. (2.11), is expressed in terms of the linear strain, cf. Eq. (2.17). Finally, the lamina stress vector is integrated over the laminate thickness (h) to obtained the stress-resultants vector, $\boldsymbol{F}_\mathrm{r}$, and the mid-plane strain vectors of the laminate. The constitutive relationship for the k^{th} lamina in the laminate coordinate (x, y, z) system is presented as

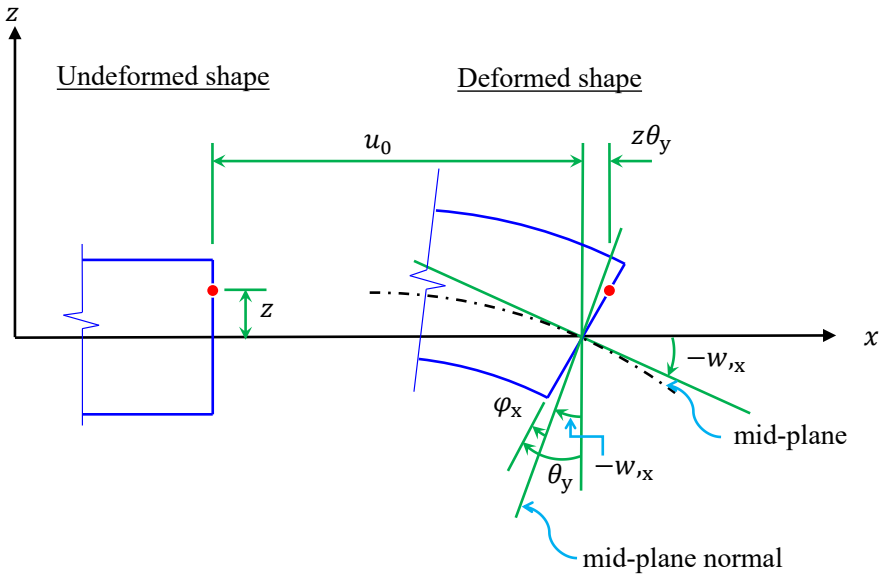

(a) Cross-section along the *x*-*z* plane

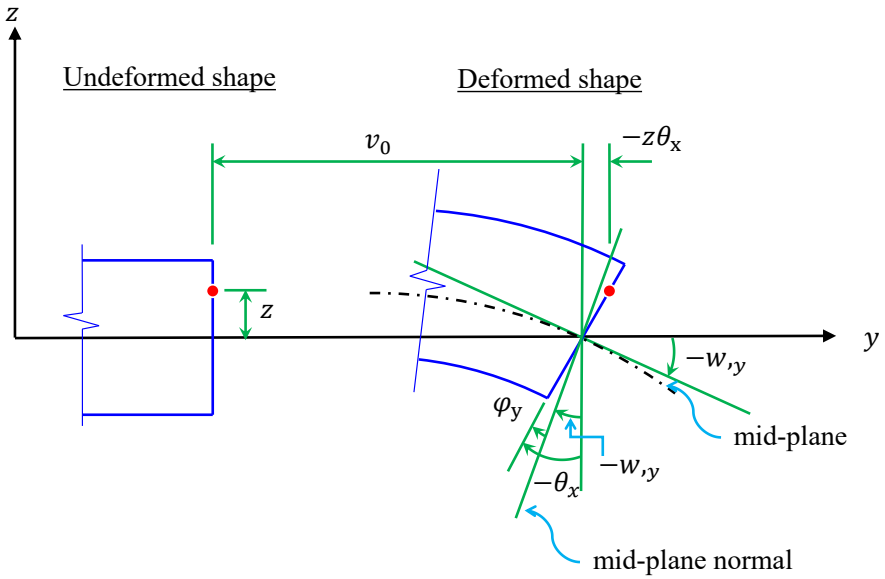

(b) Cross-section along the *y*-*z* plane

Figure 7: Deformation of a laminated composite plate in the *x*-*z* and *y*-*z* planes

$$\left\{\begin{array}{c}\sigma_{\mathrm{x}}\\ \sigma_{\mathrm{y}}\\ \tau_{\mathrm{xy}}\end{array}\right\}_{\mathrm{k}} = \left[Q_{\mathrm{ij}}\right]_{\mathrm{k}} \left\{\begin{array}{c}\varepsilon_{0\mathrm{x}}+z\kappa_{\mathrm{x}}\\ \varepsilon_{0\mathrm{y}}+z\kappa_{\mathrm{y}}\\ \gamma_{0\mathrm{xy}}+z\kappa_{\mathrm{xy}}\end{array}\right\}_{\mathrm{k}} - \left[Q_{\mathrm{ij}}\right]_{\mathrm{k}} \left\{\begin{array}{c}e_{\mathrm{x}}\\ e_{\mathrm{y}}\\ e_{\mathrm{xy}}\end{array}\right\}_{\mathrm{k}}, \text{ for } i,\ j=1,\ 2, \text{ and } 6 \tag{2.19}$$

and

$$\left\{\begin{array}{c}\tau_{\mathrm{xz}}\\ \tau_{\mathrm{yz}}\end{array}\right\}_{\mathrm{k}} = \varkappa\left[Q_{\mathrm{ij}}\right]_{\mathrm{k}} \left\{\begin{array}{c}\varphi_{\mathrm{x}}\\ \varphi_{\mathrm{y}}\end{array}\right\}_{\mathrm{k}}, \text{ for } i,\ j=4 \text{ and } 5. \tag{2.20}$$

Herein, the shear correction factor, $\varkappa = 5/6$, is considered to account for nonlinear distribution of the transverse shear strains along the laminate thickness. The laminae stresses are integrated over the thickness of the laminate to account for the thickness-wise laminate property. Due to integration, the stress terms lead to the stress-resultant terms, whereas the strain terms lead to the mid-plane strain terms. Accordingly, the in-plane forces of the laminate are obtained as

$$\begin{aligned}\left\{\begin{array}{c}N_{\mathrm{x}}\\ N_{\mathrm{y}}\\ N_{\mathrm{xy}}\end{array}\right\}_{\mathrm{k}} &= \int_{-h/2}^{h/2} \left\{\begin{array}{c}\sigma_{\mathrm{x}}\\ \sigma_{\mathrm{y}}\\ \tau_{\mathrm{xy}}\end{array}\right\}_{\mathrm{k}} \mathrm{d}z = \sum_{k=1}^{n} \int_{z_{\mathrm{k}-1}}^{z_{\mathrm{k}}} \left\{\begin{array}{c}\sigma_{\mathrm{x}}\\ \sigma_{\mathrm{y}}\\ \tau_{\mathrm{xy}}\end{array}\right\}_{\mathrm{k}} \mathrm{d}z\\ &= \sum_{k=1}^{n} \int_{z_{\mathrm{k}-1}}^{z_{\mathrm{k}}} \left[Q_{\mathrm{ij}}\right]_{\mathrm{k}} \left\{\begin{array}{c}\varepsilon_{0\mathrm{x}}+z\kappa_{\mathrm{x}}\\ \varepsilon_{0\mathrm{y}}+z\kappa_{\mathrm{y}}\\ \gamma_{0\mathrm{xy}}+z\kappa_{\mathrm{xy}}\end{array}\right\}_{\mathrm{k}} \mathrm{d}z - \sum_{k=1}^{n} \int_{z_{\mathrm{k}-1}}^{z_{\mathrm{k}}} \left[Q_{\mathrm{ij}}\right]_{\mathrm{k}} \left\{\begin{array}{c}e_{\mathrm{x}}\\ e_{\mathrm{y}}\\ e_{\mathrm{xy}}\end{array}\right\}_{\mathrm{k}} \mathrm{d}z\\ &= \mathscr{A}_{\mathrm{ij}} \left\{\begin{array}{c}\varepsilon_{0\mathrm{x}}\\ \varepsilon_{0\mathrm{y}}\\ \gamma_{0\mathrm{xy}}\end{array}\right\} + \mathscr{B}_{\mathrm{ij}} \left\{\begin{array}{c}\kappa_{0\mathrm{x}}\\ \kappa_{0\mathrm{y}}\\ \kappa_{0\mathrm{xy}}\end{array}\right\} - \mathscr{A}_{\mathrm{ij}} \left\{\begin{array}{c}e_{\mathrm{x}}\\ e_{\mathrm{y}}\\ e_{\mathrm{xy}}\end{array}\right\} \quad \text{for } i,\ j=1,\ 2, \text{ and } 6.\end{aligned} \tag{2.21}$$

Similarly, the corresponding moments and shear forces are computed as

$$\begin{aligned}\left\{\begin{array}{c}M_{\mathrm{x}}\\ M_{\mathrm{y}}\\ M_{\mathrm{xy}}\end{array}\right\}_{\mathrm{k}} &= \int_{-h/2}^{h/2} \left\{\begin{array}{c}\sigma_{\mathrm{x}}\\ \sigma_{\mathrm{y}}\\ \tau_{\mathrm{xy}}\end{array}\right\}_{\mathrm{k}} z\mathrm{d}z = \sum_{k=1}^{n} \int_{z_{\mathrm{k}-1}}^{z_{\mathrm{k}}} \left\{\begin{array}{c}\sigma_{\mathrm{x}}\\ \sigma_{\mathrm{y}}\\ \tau_{\mathrm{xy}}\end{array}\right\}_{\mathrm{k}} z\mathrm{d}z\\ &= \sum_{k=1}^{n} \int_{z_{\mathrm{k}-1}}^{z_{\mathrm{k}}} \left[Q_{\mathrm{ij}}\right]_{\mathrm{k}} \left\{\begin{array}{c}z\varepsilon_{0\mathrm{x}}+z^2\kappa_{\mathrm{x}}\\ z\varepsilon_{0\mathrm{y}}+z^2\kappa_{\mathrm{y}}\\ z\gamma_{0\mathrm{xy}}+z^2\kappa_{\mathrm{xy}}\end{array}\right\}_{\mathrm{k}} \mathrm{d}z - \sum_{k=1}^{n} \int_{z_{\mathrm{k}-1}}^{z_{\mathrm{k}}} \left[Q_{\mathrm{ij}}\right]_{\mathrm{k}} \left\{\begin{array}{c}ze_{\mathrm{x}}\\ ze_{\mathrm{y}}\\ ze_{\mathrm{xy}}\end{array}\right\}_{\mathrm{k}} \mathrm{d}z,\\ &= \mathscr{B}_{\mathrm{ij}} \left\{\begin{array}{c}\varepsilon_{0\mathrm{x}}\\ \varepsilon_{0\mathrm{y}}\\ \gamma_{0\mathrm{xy}}\end{array}\right\} + \mathscr{D}_{\mathrm{ij}} \left\{\begin{array}{c}\kappa_{0\mathrm{x}}\\ \kappa_{0\mathrm{y}}\\ \kappa_{0\mathrm{xy}}\end{array}\right\} - \mathscr{B}_{\mathrm{ij}} \left\{\begin{array}{c}e_{\mathrm{x}}\\ e_{\mathrm{y}}\\ e_{\mathrm{xy}}\end{array}\right\}, \quad \text{for } i,\ j=1,\ 2, \text{ and } 6,\end{aligned} \tag{2.22}$$

and

$$\begin{aligned}\left\{\begin{array}{c} Q_{\mathrm{x}} \\ Q_{\mathrm{y}} \end{array}\right\}_{\mathrm{k}} &= \int_{-h/2}^{h/2} \left\{\begin{array}{c} \tau_{\mathrm{xz}} \\ \tau_{\mathrm{yz}} \end{array}\right\}_{\mathrm{k}} \mathrm{d}z = \sum_{k=1}^{n} \int_{z_{\mathrm{k}-1}}^{z_{\mathrm{k}}} \left\{\begin{array}{c} \tau_{\mathrm{xz}} \\ \tau_{\mathrm{yz}} \end{array}\right\}_{\mathrm{k}} \mathrm{d}z \\ &= \sum_{k=1}^{n} \int_{z_{\mathrm{k}-1}}^{z_{\mathrm{k}}} \varkappa \left[Q_{\mathrm{ij}}\right]_{\mathrm{k}} \left\{\begin{array}{c} \varphi_{\mathrm{x}} \\ \varphi_{\mathrm{y}} \end{array}\right\}_{\mathrm{k}} \mathrm{d}z \\ &= \bar{\mathscr{A}}_{\mathrm{ij}} \left\{\begin{array}{c} \gamma_{\mathrm{xz}} \\ \gamma_{\mathrm{yz}} \end{array}\right\}, \quad \text{for } i,\ j = 4 \text{ and } 5. \end{aligned} \tag{2.23}$$

Finally, the stress-resultant vector, $\boldsymbol{F}_{\mathrm{r}} = \{N_{\mathrm{x}} \quad N_{\mathrm{y}} \quad N_{\mathrm{xy}} \quad M_{\mathrm{x}} \quad M_{\mathrm{y}} \quad M_{\mathrm{xy}} \quad Q_{\mathrm{x}} \quad Q_{\mathrm{y}}\}^{\mathrm{T}}$, is developed with reference to Eqs. (2.21), (2.22), and (2.23). Now, the constitutive relationship of the laminate is expressed as

$$\boldsymbol{F}_{\mathrm{r}} = \boldsymbol{D}\boldsymbol{\varepsilon}^{*} - \boldsymbol{D}\boldsymbol{e}^{*}, \tag{2.24}$$

in which $\boldsymbol{e}^{*} = \{e_{\mathrm{x}} \quad e_{\mathrm{y}} \quad e_{\mathrm{xy}} \quad 0 \quad 0 \quad 0 \quad 0 \quad 0\}^{\mathrm{T}}$ is the mid-plane thermal strain vector, and $\boldsymbol{D}$ indicates the stress-resultant and mid-plane strain relationship matrix in the form of

$$\boldsymbol{D} = \left[\begin{array}{c|c|c} \mathscr{A} & \mathscr{B} & 0 \\ \hline \mathscr{B} & \mathscr{D} & 0 \\ \hline 0 & 0 & \bar{\mathscr{A}} \end{array}\right]. \tag{2.25}$$

The elements of the $\boldsymbol{D}$ matrix, i.e., $\mathscr{A}$, $\mathscr{B}$, $\mathscr{D}$, and $\bar{\mathscr{A}}$, are shown in Publication 1.

Thermal strain

Components of the initial strain vector, $\boldsymbol{\varepsilon}_{\mathrm{nt}} = \{\varepsilon_{x_{\mathrm{nt}}} \quad \varepsilon_{y_{\mathrm{nt}}} \quad \gamma_{xy_{\mathrm{nt}}} \quad \gamma_{xz_{\mathrm{nt}}} \quad \gamma_{yz_{\mathrm{nt}}}\}^{\mathrm{T}}$, which are described by the nonlinear portion of the overall stress [119], due to thermal load are given as

$$\begin{aligned} &\varepsilon_{x_{\mathrm{nt}}} = \frac{1}{2}(u_{,\mathrm{x}}^2 + v_{,\mathrm{x}}^2 + w_{,\mathrm{x}}^2), && \varepsilon_{y_{\mathrm{nt}}} = \frac{1}{2}(u_{,\mathrm{y}}^2 + v_{,\mathrm{y}}^2 + w_{,\mathrm{y}}^2), \\ &\gamma_{xy_{\mathrm{nt}}} = (u_{,\mathrm{x}}u_{,\mathrm{y}} + v_{,\mathrm{x}}v_{,\mathrm{y}} + w_{,\mathrm{x}}w_{,\mathrm{y}}), \\ &\gamma_{xz_{\mathrm{nt}}} = (u_{,\mathrm{x}}u_{,\mathrm{z}} + v_{,\mathrm{x}}v_{,\mathrm{z}}), && \gamma_{yz_{\mathrm{nt}}} = (u_{,\mathrm{y}}u_{,\mathrm{z}} + v_{,\mathrm{y}}v_{,\mathrm{z}}). \end{aligned} \tag{2.26}$$

The generalized displacement terms in Eq. (2.26) are expressed in terms of the mid-plane displacement, cf. Eq. (2.16), and subsequently, the initial strain vector ($\boldsymbol{\varepsilon}_{\mathrm{nt}}$) is presented in a compact form as

$$\boldsymbol{\varepsilon}_{\mathrm{nt}} = \frac{1}{2}\boldsymbol{R}\boldsymbol{d}^{*}, \tag{2.27}$$

in which the $\boldsymbol{R}$ matrix relates the initial strain vector ($\boldsymbol{\varepsilon}_{\mathrm{nt}}$) and the vector of partial derivative of mid-plane displacement, $\boldsymbol{d}^*$; for the $\boldsymbol{R}$ matrix, see Publication 1. Moreover, the partial derivative of mid-plane displacement ($\boldsymbol{d}^*$) is given by

$$\boldsymbol{d}^* = \{u_{0,\mathrm{x}} \quad u_{0,\mathrm{y}} \quad v_{0,\mathrm{x}} \quad v_{0,\mathrm{y}} \quad w_{0,\mathrm{x}} \quad w_{0,\mathrm{y}} \quad \theta_{\mathrm{x,x}} \quad \theta_{\mathrm{x,y}} \quad \theta_{\mathrm{y,x}} \quad \theta_{\mathrm{y,y}} \quad \theta_{\mathrm{x}} \quad \theta_{\mathrm{y}}\}^{\mathrm{T}}, \tag{2.28}$$

with reference to the mid-plane displacement vector, $\boldsymbol{d} = \{u_0 \quad v_0 \quad w_0 \quad \theta_{\mathrm{x}} \quad \theta_{\mathrm{y}}\}^{\mathrm{T}}$.

Equations of motion

For a three-dimensional elastic body, the conservation of momentum is stated as

$$\nabla \cdot \boldsymbol{\sigma} + B = \rho \frac{\partial \dot{\boldsymbol{d}}}{\partial t} \tag{2.29}$$

where $\boldsymbol{\sigma}$ is the stress tensor, the symbol ∇ denotes the classical differential operator, B indicates the body force, ρ denotes density of the elastic material, and $\dot{\boldsymbol{d}}$ is the velocity field in relation to the displacement field $\boldsymbol{d}$, which is described as the mid-plane displacement in this work. The governing equation of motion for a solid body is obtained by summing up the forces and moment acting on the representative volume of the body. In the absence of the body force (B), the equations of motion for the three-dimensional elastic body is given as [139]

$$\begin{aligned} &\sigma_{\mathrm{x,x}} + \tau_{\mathrm{yx,y}} + \tau_{zx,z} = \rho \ddot{u}, \quad \sigma_{\mathrm{xy,x}} + \tau_{\mathrm{y,y}} + \tau_{zy,z} = \rho \ddot{v}, \\ &\tau_{\mathrm{xz,x}} + \tau_{\mathrm{yz,y}} + \sigma_{z,z} = \rho \ddot{w}. \end{aligned} \tag{2.30}$$

For application in a composite plate, the expanded representations of u, v, and w, cf. Eq. (2.16), are incorporated into Eq. (2.30) and finally render the equations of motion for the k^{th} lamina. To consider the contribution of all laminae, an integration over the thickness of the laminate is carried out, which yields the following relationship

$$\begin{aligned} &N_{\mathrm{x,x}} + N_{\mathrm{yx,y}} = \bar{p}\ddot{u}_0 + \bar{r}\ddot{\theta}_{\mathrm{x}}, && N_{\mathrm{xy,x}} + N_{\mathrm{y,y}} = \bar{p}\ddot{v}_0 - \bar{r}\ddot{\theta}_{\mathrm{y}}, \\ &Q_{\mathrm{x,x}} + Q_{\mathrm{y,y}} + q = \bar{p}\ddot{w}_0, && \\ &M_{\mathrm{x,x}} + M_{\mathrm{yx,y}} - Q_{\mathrm{x}} = \bar{r}\ddot{u}_0 + \bar{q}\ddot{\theta}_{\mathrm{x}}, && M_{\mathrm{xy,x}} + M_{\mathrm{y,y}} - Q_{\mathrm{y}} = \bar{r}\ddot{v}_0 - \bar{q}\ddot{\theta}_{\mathrm{y}}, \end{aligned} \tag{2.31}$$

in which $(\bar{p},\bar{r},\bar{q}) = \int_{-h/2}^{h/2}\rho(1,z,z^2)\mathrm{d}z$. The equations of motion for the composite plates can be written in a matrix form after applying suitable rearrangement and presented as

$$\begin{Bmatrix} N_{\mathrm{x,x}}+N_{\mathrm{yx,y}} \\ N_{\mathrm{xy,x}}+N_{\mathrm{y,y}} \\ Q_{\mathrm{x,x}}+Q_{\mathrm{y,y}}+q \\ -M_{\mathrm{xy,x}}-M_{\mathrm{y,y}}+Q_{\mathrm{y}} \\ M_{\mathrm{x,x}}+M_{\mathrm{yx,y}}-Q_{\mathrm{x}} \end{Bmatrix} = \begin{bmatrix} \bar{p} & 0 & 0 & \bar{r} & 0 \\ 0 & \bar{p} & 0 & 0 & \bar{r} \\ 0 & 0 & \bar{p} & 0 & 0 \\ \bar{r} & 0 & 0 & \bar{q} & 0 \\ 0 & \bar{r} & 0 & 0 & \bar{q} \end{bmatrix} \begin{Bmatrix} \ddot{u}_0 \\ \ddot{v}_0 \\ \ddot{w}_0 \\ \ddot{\theta}_{\mathrm{x}} \\ \ddot{\theta}_{\mathrm{y}} \end{Bmatrix}, \tag{2.32}$$

wherein, $\bar{r}$ is calculated as zero. Above equation can be written in compact form as

$$\boldsymbol{F} = \bar{\boldsymbol{M}}\ddot{\boldsymbol{d}}, \tag{2.33}$$

where $\boldsymbol{F}$ denotes the force vector, $\bar{\boldsymbol{M}}$ is the inertia matrix, and $\ddot{\boldsymbol{d}}$ represents the acceleration vector.

2.2.3 Finite element (FE) formulation

Numerical implementation of the mathematical modeling of vibrating composite plates in thermal environment has been done by using the finite element (FE) approach. In the FE idealization, the plate domain, Ω, is visualized and modelled as an ensemble of finite numbers of user-defined elements, Ω_{e}, of simple geometry. These elements are connected at finite number of joints, which are known as "node"s [118]. These nodes serve as data points for polynomial interpolation on an element, Ω_{e}, of the underlying physical quantities. For further explanation, the in-plane displacement in longitudinal direction (u) is assumed to be a physical quantity. This physical quantity within an element, say an 8-node plate plate element, can be represented in terms of nodal values of the element by identifying appropriate polynomial functions, and can be written as

$$u \approx \hat{u} = \sum_{i=1}^{nn} N_{\mathrm{i}}\boldsymbol{u}_{\mathrm{e,i}}, \tag{2.34}$$

in which $\boldsymbol{u}_{\mathrm{e}} = \{u_1 \quad u_2 \quad u_3 \quad u_4 \quad u_5 \quad u_6 \quad u_7 \quad u_8\}^{\mathrm{T}}$ indicates the corresponding i^{th} nodal displacement for the element Ω_{e}, and polynomial-based interpolation function is denoted by N_{i}, which is often known as "shape function" [9, 118]. These interpolation functions are chosen in such a way that the solution is continuous over the entire domain. The total number of nodes in each element is given by nn. Generally, two types of interpolation functions are used in the FE analysis: firstly, the Lagrange interpolation function, in which only the physical quantity of interest is continuous and interpolated, and the element based on this function is known as "C^0 element", where higher

derivatives of the quantity are not continuous; secondly, the Hermite polynomial, in which the physical quantity of interest and its higher derivatives are continuous [9]. The corresponding element is known as "C^{m} element", where m $(1,\ 2,\ \ldots\ )$ indicates the order of the derivative, which needs to be continuous.

In the present analysis, an 8-node C^0 isoparametric plate element is chosen to discretize the composite plate domain. The use of the isoparametric element facilitates applicability of the same shape function for the geometry and the physical quantity of interest as well. With reference to

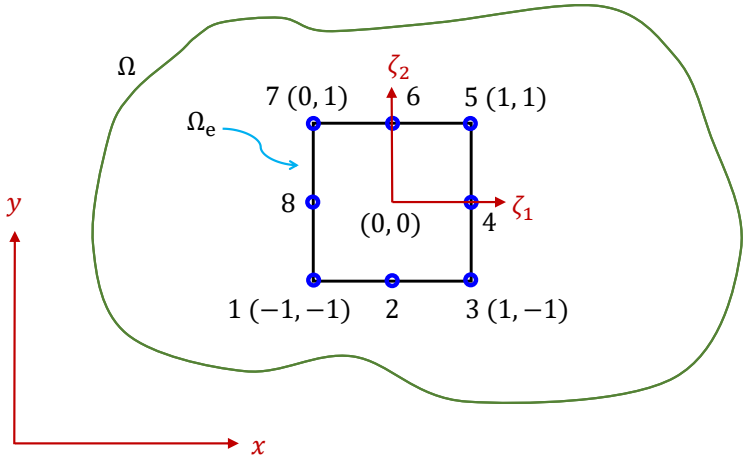

Figure 8: Arbitrary plate geometry (Ω) along with representation of an 8-node isoparametric element (Ω_{e}) in the natural coordinate ($\zeta_1,\ \zeta_2$) system

Figure 8, the interpolation functions for the 8-node serendipity element is expressed as [30, 117]

$$\begin{aligned} N_{\mathrm{i}}(\zeta_1,\zeta_2) &= (1+\zeta_1\zeta_{1,\mathrm{i}})(1+\zeta_2\zeta_{2,\mathrm{i}})(\zeta_1\zeta_{1,\mathrm{i}}+\zeta_2\zeta_{2,\mathrm{i}}-1)/4, \quad \text{for } i=1,\ 3,\ 5,\ \text{and } 7 \\ N_{\mathrm{i}}(\zeta_1,\zeta_2) &= (1-\zeta_1^2)(1+\zeta_2\zeta_{2,\mathrm{i}})/2, \quad \text{for } i=2 \text{ and } 6 \\ N_{\mathrm{i}}(\zeta_1,\zeta_2) &= (1-\zeta_2^2)(1+\zeta_1\zeta_{1,\mathrm{i}})/2, \quad \text{for } i=4 \text{ and } 8 \end{aligned} \tag{2.35}$$

where ζ_1 and ζ_2 are the natural coordinates of the element, and $\zeta_{1,\mathrm{i}}$ and $\zeta_{2,\mathrm{i}}$ denote the magnitudes at the i^{th} node.

The FSDT-based analysis of a composite plate is governed by the five degrees of freedom (DOFs), i.e., u_0, v_0, w_0, θ_{x}, and θ_{y}, and the plane area of the plate geometry is depicted with reference to the x and y coordinates. Thus, coordinates (x_{e} and y_{e}) inside an element are interpolated by the shape functions, N_{i}, and the associated nodal values, $x_{\mathrm{e,i}}$ and $y_{\mathrm{e,i}}$, as

$$x \approx \hat{x} = \sum_{i=1}^{nn=8} N_{\mathrm{i}}(\zeta_1,\zeta_2)x_{\mathrm{e,i}}, \qquad y \approx \hat{y} = \sum_{i=1}^{nn=8} N_{\mathrm{i}}(\zeta_1,\zeta_2)y_{\mathrm{e,i}}. \tag{2.36}$$

Additionally, the DOFs in terms of mid-plane displacement ($\boldsymbol{d}$) are expressed by the same shape function [30, 140], as

$$\boldsymbol{d} \approx \hat{\boldsymbol{d}} = \boldsymbol{N}\boldsymbol{d}_{\mathrm{e}}, \tag{2.37}$$

in which $\boldsymbol{d}_{\mathrm{e}} = \{u_{01} \;\; v_{01} \;\; w_{01} \;\; \theta_{\mathrm{x}1} \;\; \theta_{\mathrm{y}1} \;\; \ldots \;\; u_{08} \;\; v_{08} \;\; w_{08} \;\; \theta_{\mathrm{x}8} \;\; \theta_{\mathrm{y}8}\}^{\mathrm{T}}$ is the nodal mid-plane displacement vector, and $\boldsymbol{N} = \sum_{i=1}^{8} N_{\mathrm{i}}(\zeta_1, \zeta_2)\boldsymbol{I}_5$ is the shape function matrix with $\boldsymbol{I}_5$ as the 5×5 identity matrix. Finally, the strain displacement relationship of a laminate is developed in terms of nodal displacements, as will be discussed in the next subsection.

Strain and displacement relationship

The mid-plane strain vector ($\boldsymbol{\varepsilon}^*$) relates with the nodal mid-plane displacement vector, $\boldsymbol{d}_{\mathrm{e}}$, as

$$\boldsymbol{\varepsilon}^* = \boldsymbol{B}\boldsymbol{d}_{\mathrm{e}}, \tag{2.38}$$

where the strain-displacement matrix, $\boldsymbol{B}$, is expressed as

$$\boldsymbol{B} = \sum_{i=1}^{8} \begin{bmatrix} N_{\mathrm{i,x}} & 0 & 0 & 0 & 0 \\ 0 & N_{\mathrm{i,y}} & 0 & 0 & 0 \\ N_{\mathrm{i,y}} & N_{\mathrm{i,x}} & 0 & 0 & 0 \\ 0 & 0 & 0 & 0 & N_{\mathrm{i,x}} \\ 0 & 0 & 0 & -N_{\mathrm{i,y}} & 0 \\ 0 & 0 & 0 & -N_{\mathrm{i,x}} & N_{\mathrm{i,y}} \\ 0 & 0 & N_{\mathrm{i,x}} & 0 & N_{\mathrm{i}} \\ 0 & 0 & N_{\mathrm{i,y}} & -N_{\mathrm{i}} & 0 \end{bmatrix}, \quad \text{for } i = 1 \text{ to } 8. \tag{2.39}$$

Subsequently, the initial thermal strain ($\boldsymbol{\varepsilon}_{\mathrm{nt}}$), which is derived in Eq. (2.27), is presented in terms of the nodal mid-plane displacement vector ($\boldsymbol{d}_{\mathrm{e}}$), as

$$\boldsymbol{\varepsilon}_{\mathrm{nt}} = \frac{1}{2}\boldsymbol{R}\boldsymbol{G}\boldsymbol{d}_{\mathrm{e}}, \tag{2.40}$$

where $\boldsymbol{G}$ is the shape function matrix corresponding to $\boldsymbol{d}^*$; see Publication 1 for details of the $\boldsymbol{R}$ and $\boldsymbol{G}$ matrices.

2.2.4 Governing equation

The governing equation of a structural system, which is subjected to dynamic loading, is derived from the constitutive relationship of the material model following the equations of energy conservation in continuum mechanics. The constitutive relationship and the equation of motion of a laminate are discussed in the previous subsections. The FE formulation is used to derive the governing equation of composite plates following the laws of the conservation of energy. Herein, a brief discussion on the development of the FE-based governing equation of laminated composite plates is given, however for deeper understanding, readers may refer [7, 12, 30, 43, 140, 203].

The governing equation of laminated composite plates in thermal environment has been derived by obtaining equations of motion using the Hamilton's variational principle. It states that the motion of a system from time instant t_1 to t_2 is such that the time integral of the difference between the potential energy, $\mathbb{E}$, and the kinetic energy, $\mathbb{K}$, remains stationary for the true path, however vanishes at the end of the interval. The energy dissipation, $\mathbb{Q}$, due to the dissipative force vector, $\boldsymbol{f}_{\text{diss}}$, is also considered while developing the equations of motion. Notationally, it is presented as

$$\int_{t_1}^{t_2} \delta(\mathbb{E} - \mathbb{K} + \mathbb{Q}) \mathrm{d}t = 0. \tag{2.41}$$

The potential energy consists of the combination of the strain energy, $\mathbb{U}$, and work done by the external load, $\mathbb{W}$, which are related as: $\mathbb{E} = \mathbb{U} - \mathbb{W}$. Moreover, the total elemental potential energy is due to the contribution of elemental mechanical strain energy, $\mathbb{U}_{\text{me}}$, and elemental thermal strain energy, $\mathbb{U}_{\text{te}}$. They are given as

$$\mathbb{U}_{\text{me}} = \frac{1}{2} \int_{A_{\text{e}}} \boldsymbol{\varepsilon}^{*\text{T}} \boldsymbol{F}_{\text{r}} \mathrm{d}A_{\text{e}}, \qquad \mathbb{U}_{\text{te}} = \int_{V_{\text{e}}} \boldsymbol{\varepsilon}_{\text{nt}}^{\text{T}} \boldsymbol{\sigma}_{\text{r}} \mathrm{d}V_{\text{e}}, \tag{2.42}$$

where $\boldsymbol{\sigma}_{\text{r}}$ denotes the residual stress matrix. The elemental work done, $\mathbb{W}_{\text{e}}$, due to the external load vector, $\boldsymbol{q}$, is written as

$$\mathbb{W}_{\text{e}}(t) = \int_{A_{\text{e}}} \boldsymbol{d}^{\text{T}} \boldsymbol{q} \mathrm{d}A_{\text{e}}. \tag{2.43}$$

Additionally, the elemental kinetic energy ($\mathbb{K}_{\text{e}}$) and the elemental damping energy ($\mathbb{Q}$) are presented in the following manner

$$\mathbb{K} = \frac{1}{2} \int_{A_{\text{e}}} \dot{\boldsymbol{d}}^{\text{T}} \bar{\boldsymbol{M}} \dot{\boldsymbol{d}} \mathrm{d}A_{\text{e}}, \qquad \mathbb{Q} = \int_{\text{A}} \boldsymbol{d}^{\text{T}} \bar{\boldsymbol{C}} \dot{\boldsymbol{d}} \mathrm{d}A_{\text{e}}, \tag{2.44}$$

in which $\bar{\boldsymbol{C}}$ is the proportional matrix which accounts for the energy dissipation characteristics of the structure and relates to the dissipative force vector ($\boldsymbol{f}_{\text{diss}}$) such that $\boldsymbol{f}_{\text{diss}} = \bar{\boldsymbol{C}} \dot{\boldsymbol{d}}$. The elemental

matrices are obtained from the energy equations, so that

$$\begin{aligned}
\boldsymbol{K}_{\mathrm{e}} &= \int_{-1}^{1}\int_{-1}^{1} \boldsymbol{B}^{\mathrm{T}}\boldsymbol{D}\boldsymbol{B}|\boldsymbol{J}|\mathrm{d}\zeta_1\mathrm{d}\zeta_2, \qquad \boldsymbol{K}_{\mathrm{Ge}} = \int_{-1}^{1}\int_{-1}^{1} \boldsymbol{G}^{\mathrm{T}}\boldsymbol{S}_{\mathrm{r}}\boldsymbol{G}|\boldsymbol{J}|\mathrm{d}\zeta_1\mathrm{d}\zeta_2, \\
\boldsymbol{M}_{\mathrm{e}} &= \int_{-1}^{1}\int_{-1}^{1} \boldsymbol{N}^{\mathrm{T}}\bar{\boldsymbol{M}}\boldsymbol{N}|\boldsymbol{J}|\mathrm{d}\zeta_1\mathrm{d}\zeta_2, \qquad \boldsymbol{C}_{\mathrm{e}} = \int_{-1}^{1}\int_{-1}^{1} \boldsymbol{N}^{\mathrm{T}}\bar{C}\boldsymbol{N}|\boldsymbol{J}|\mathrm{d}\zeta_1\mathrm{d}\zeta_2, \\
\boldsymbol{P}_{\mathrm{e}} &= \int_{-1}^{1}\int_{-1}^{1} \boldsymbol{N}^{\mathrm{T}}\boldsymbol{q}|\boldsymbol{J}|\mathrm{d}\zeta_1\mathrm{d}\zeta_2.
\end{aligned} \tag{2.45}$$

Here, elemental matrices, i.e., $\boldsymbol{K}_{\mathrm{e}}$, $\boldsymbol{K}_{\mathrm{Ge}}$, $\boldsymbol{M}_{\mathrm{e}}$, and $\boldsymbol{C}_{\mathrm{e}}$ denote the elemental stiffness matrix, the elemental geometric stiffness matrix, the elemental mass matrix, the elemental damping matrix, respectively; whearas, $\boldsymbol{P}_{\mathrm{e}}$ denotes the elemental external load vector. In Eq. (2.45), $\boldsymbol{S}_{\mathrm{r}}$ indicates the initial-stress resultant matrix [134]. Furthermore, $|\boldsymbol{J}|$ is the determinant of the Jacobian matrix, $\boldsymbol{J}$. These elemental matrices, as obtained by using the FE formulation, are assembled to obtain global matrices of the composite structure.

This dissertation studies the influence of the addition of the stiffener(s) to reduce the dynamic responses in thermal environment. Further, the stiffener is oriented in a coordinate system which is different from the coordinate system of the plate. To consider the influence of different parts in a particular coordinate system, i.e., the global coordinate system, a necessary transformation has been performed prior to the assembling operation. During transformation θ_{z} drilling DOF has been incorporated in the mid-plane displacement vector ($\boldsymbol{d}$). A detailed discussion on the transformation procedure is available in Publication 1.

It is noteworthy that the Jcaobian matrix, $\boldsymbol{J}$, facilitates the coordinate mapping between the physical coordinate (x, y) system and the natural coordinate (ζ_1, ζ_2) system [9, 140]. The inverse of the Jacobian matrix, a function of the natural coordinates, can be evaluated easily by applying the Gaussian quadrature rule of specific order. The elemental area, d_{e}, in the physical space can thus be obtained by numerical integration in the natural coordinates within the ranges of -1 and 1 and further multiplied with the determinant of the Jacobian matrix ($|\boldsymbol{J}|$), as: $\mathrm{d}A_{\mathrm{e}} = |\boldsymbol{J}|\mathrm{d}\zeta_1\mathrm{d}\zeta_2$.

To evaluate the governing equation, only necessary fundamentals are provided here without giving mathematically complete and rigorous derivations, which is otherwise available in Publications 1 and 2. Following this strategy, energy equations are incorporated into the Hamilton's variational principle to obtain the damped governing equation of composite plates in thermal environments. The governing equation is written as

$$\left[\boldsymbol{K}' + \boldsymbol{K}'_{\mathrm{G}}\right]\boldsymbol{d}'(t) + \boldsymbol{C}'\dot{\boldsymbol{d}}'(t) + \boldsymbol{M}'\ddot{\boldsymbol{d}}'(t) = \boldsymbol{P}'(t), \tag{2.46}$$

in which the matrices with prime represents the related global matrices in the global coordinate system after applying necessary transformation due to the stiffener(s). The global matrices, i.e., $\boldsymbol{K}'$, $\boldsymbol{K}'_{\mathrm{G}}$, $\boldsymbol{C}'$, and $\boldsymbol{M}'$, and the global load vector, i.e., $\boldsymbol{P}'$, are derived from the associated elemental matrices and vector, respectively. Here, the mid-plane displacement of stiffened plates is expressed in the global coordinate system, and is denoted by $\boldsymbol{d}'$. The global damping matrix ($\boldsymbol{C}'$) is derived indirectly considering definitions of the Rayleigh damping or the modal expansion damping; see Publication 2 and references [53, 130] for further details. The detailed discussion and step-by-step derivation of the governing equation are given in Publications 1 and 2.

The homogeneous solution of the governing equation, cf. Eq. (2.46), by ignoring damping matrix, provides undamped eigenfrequencies, f_{m}, at different temperatures. The damped modal frequencies, f_{dm}, and modal damping values, η_{m}, are obtained at different temperatures after conducting damped free vibration analysis by taking damping matrix into consideration. Additionally, transient responses of displacement and stresses are studied to understand the effect of adding stiffeners in thermal environments by implementing the Newmark's integration technique. Notably, the constant average acceleration scheme of numerical integration is implemented by considering the necessary assessment of consistency and accuracy of the algorithm. Overall, undamped or damped frequencies, modal damping values, and time histories of displacement and stresses are considered to be the quantities of interest within the purview of this investigation.

2.3 Viscoelastic modeling

The application of polymeric materials such as epoxy in laminated composite plates or sandwich plates, makes the plate viscoelastic. Thus, the behavior of these plates can not be explained by the theory of elasticity or viscosity alone. During the deformation of such materials, a part of the total energy is dissipated as heat through viscous loss and the remaining energy is stored elastically. Therefore, the theory of viscoelasticity is used to describe dynamic behavior of composite plates.

Various classical mathematical models such as the Maxwell, Kelvin-Voigt, and Poynting-Thomson models, which were used to describe the dynamics of viscoelastic materials as a combination of damper and elastic spring. The elastic spring simulates the elastic behavior, whereas the damper captures the viscous behavior. However, these classical models have some merits and demerits [11]. Some improved models, e.g. the Laplace transformation approach, are nowadays implemented to explain the viscoelastic behavior. The time-dependent behavior of these materials is primarily characterized by creep and relaxation. A detailed description of various damping models

can be found in numerous textbooks [11, 28, 99] and report [2]. The basic idea and derivation of the viscoelastic model for a composite lamina are briefly outlined below.

Viscoelastic damping model of composite materials

The viscoelastic properties of a lamina follow the transversely isotropic material behavior. Initially, viscoelastic behavior of isotropic materials is described and thereafter implemented in composite lamina. The Boltzmann superposition principle is used to explain the viscoelastic behavior of isotropic materials by considering the effect of time-varying relaxation strain on the time history of the relaxation stress. This principle is based on the following two key ideas:

- response to any event is linear; and
- all separate events lead to independent responses.

While developing the model for an isotropic material, it is assumed that stress, σ, and strain, ε, are harmonically time-dependent at a frequency ω (rad/s) and described as

$$\sigma(t) = \sigma_0 e^{i\omega t}, \qquad \varepsilon(t) = \varepsilon_0 e^{i\omega t}. \tag{2.47}$$

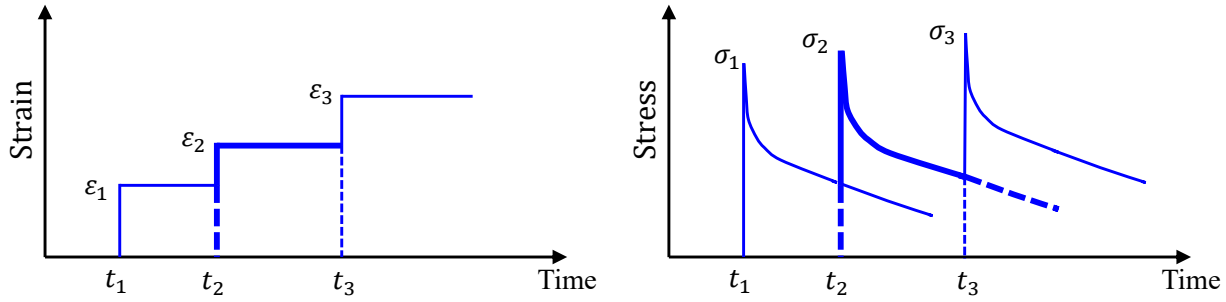

(a) Input: strain relaxation profile

(b) Output: stress relaxation profile

Figure 9: Superposition of relaxation stresses resulted from stepped relaxation strains. Numerically, for example, the time-dependent relaxation stress, $\sigma_2(t)$, due to the stepped relaxation strain, $\varepsilon_2(t)$, is expressed by: $\sigma_2(t) = \int_{-\infty}^{t_2} h(t_2 - \tau)\, d\varepsilon_2(\tau)$.

The linear viscoelastic constitutive relationship is developed with consideration that the stress state at a time, t, is a superposition of stress steps from all the strain changes at all time, τ, before t, and

is mathematically presented with reference to Figure 9, as

$$\sigma(t) = \int_{-\infty}^{t} h(t-\tau)\,\mathrm{d}\varepsilon(\tau), \tag{2.48}$$

where τ is a time variable describing history before time, t, and $h(t)$ is the relaxation modulus. The relaxation modulus is the ratio between the stress and amplitude of the relaxation strain. The above equation is rewritten by involving the strain rate, $\dot{\varepsilon}(\tau)$, as

$$\sigma(t) = \int_{-\infty}^{t} h(t-\tau)\dot{\varepsilon}(\tau)\,\mathrm{d}\tau. \tag{2.49}$$

As the strain, $\varepsilon(\tau)$, is time-dependent, the strain rate, $\dot{\varepsilon}(\tau)$, can be written as

$$\dot{\varepsilon}(\tau) = i\omega\varepsilon_0 e^{\mathrm{i}\omega\tau}, \tag{2.50}$$

and is substituted in Eq. (2.49) by following the principle of superposition, and thus leads to

$$\sigma(t) = i\omega\varepsilon_0 \int_{-\infty}^{t} h(t-\tau)e^{\mathrm{i}\omega\tau}\,\mathrm{d}\tau. \tag{2.51}$$

Applying the change of variable $t' = t - \tau$ in Eq. (2.51) leads to

$$\sigma(t) = i\omega\varepsilon_0 \int_{0}^{\infty} h(t')e^{\mathrm{i}\omega(\mathrm{t}-\mathrm{t}')}\,\mathrm{d}t'. \tag{2.52}$$

Since $e^{-i\omega t'} = \cos\omega t' - i\sin\omega t'$, Eq. (2.52) can be restated as

$$\sigma(t) = \varepsilon_0\big(E(\omega) + iE'(\omega)\big)e^{\mathrm{i}\omega\mathrm{t}}, \tag{2.53}$$

with the definitions of

$$E(\omega) = \omega\int_{0}^{\infty} h(t')\sin wt'\,\mathrm{d}t', \qquad E'(\omega) = \omega\int_{0}^{\infty} h(t')\cos wt'\,\mathrm{d}t'. \tag{2.54}$$

Now the constitutive relationship of an isotropic linear viscoelastic material is presented as

$$\sigma(\omega) = E^*(\omega)\varepsilon(\omega), \tag{2.55}$$

where $E^*(\omega)$ is the complex elastic modulus which accounts for the energy dissipation under

harmonic vibration, and is written as

$$E^*(\omega) = E(\omega) + iE'(\omega), \tag{2.56}$$

in which the real part, $E(\omega)$, is termed as the "storage modulus", and the imaginary part, $E'(\omega)$, is termed as the "loss modulus". The ratio between the loss modulus and storage modulus is defined as the loss factor, η. Accordingly, the complex elastic modulus, $E^*(\omega)$, is shown as

$$E^*(\omega) = E(\omega)\big(1 + i\eta(\omega)\big). \tag{2.57}$$

Hence, frequency-independent complex elastic moduli of a composite lamina can be presented in the lamina coordinate (1, 2, 3) system, as

$$E_{11}^* = E_{11}(1 + i\eta_{11}), \quad E_{22}^* = E_{22}(1 + i\eta_{22}), \quad G_{12}^* = G_{12}(1 + i\eta_{12}), \tag{2.58}$$

where η_{11}, η_{22}, and η_{12} are the damping loss factors along the longitudinal, transverse, and shear directions, respectively. The loss factors are determined by adopting various approaches: (1) conducting micro-mechanical analysis by knowing the properties of the constituent materials [145, 146], (2) applying quasi-static measurement technique, i.e., DMA [105], and (3) applying a combined experimental-numerical procedure [94, 153, 204] which is based on the idea of inverse methods. In this dissertation, Publication 3 presents an innovative inverse method to identify the deterministic temperature-dependent elastic and damping properties of the composite lamina.

The consideration of the energy dissipation due to viscoelastic behavior of composites has been made by incorporating the global damping matrix ($\boldsymbol{C'}$) in the governing equation, cf. Eq. (2.46). For the purpose of damped dynamic analysis of stiffened laminated composite plates in thermal environment, the damping matrix is developed based on the Rayleigh damping or the modal expansion damping procedures. In Publication 2, a detailed comparative study of these two damping procedures is given to identify the best damping evaluation approach. The best approach is used to evaluate the global damping matrix for conducting further damped dynamic analysis of composite plates in varying thermal environments.

2.4 Material properties identification

In Section 2.2, the FE-based modeling of laminated composite plates in thermal environment has been discussed in order to evaluate response quantities of interest, i.e., eigenfrequencies, modal

damping values, and time history of displacement and stress. In this forward modeling approach, physical laws, i.e., constitutive relationships of lamina and laminate, are integrated into the FE modeling to calculate the quantities of interest. However, the accuracy in the calculations depends on the assumed values of the material properties. Therefore, sound knowledge of the material properties in terms of elastic moduli and damping loss factors is essential to simulate the dynamic response of a composite structure at different temperatures. Based on the actually measured modal parameters, the in situ material properties, often known as "model parameters", can be inferred, and this procedure is known as "inverse methods".

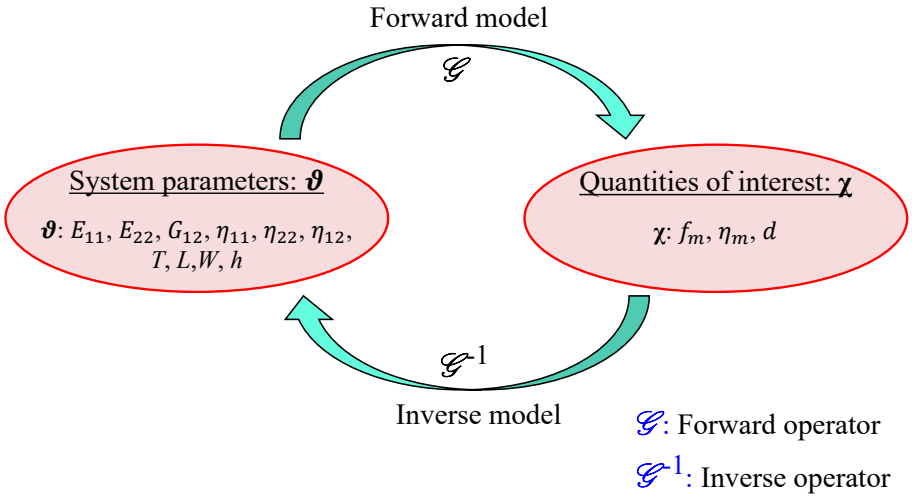

Figure 10: A representative diagram of forward methods and inverse methods

Assuming from a naive viewpoint that a forward model can predict error-free values of a quantity of interest, $\boldsymbol{\chi}$, by knowing the model parameters $\boldsymbol{\vartheta}$. The forward model is mathematically represented as

$$\boldsymbol{\chi} = \mathscr{G}(\boldsymbol{\vartheta}), \tag{2.59}$$

in which $\mathscr{G}$ is regarded as the forward operator. On the other hand, the identification of model parameters ($\boldsymbol{\vartheta}$) by using inverse method is mathematically presented as

$$\boldsymbol{\vartheta} = \mathscr{G}^{-1}(\boldsymbol{\chi}), \tag{2.60}$$

where $\mathscr{G}^{-1}$ is regarded as the inverse operator. In Figure 10, the basic idea of the forward methods and the inverse methods is illustrated. This setup of the forward and inverse methods remains under the purview of deterministic analysis, where errors related to the measurement and inherent randomness in the system parameters are neglected. However in a real-case scenario, the inherent uncertainties in the identified model properties introduce uncertainties to the system response,

and the stochastic inverse methods can be used to evaluate stochastic model parameters of the system. For additional information regarding the application of the stochastic inverse methods, where propagation of uncertainties is considered to estimate uncertainties in the elastic and damping properties of composite plates, see research literature [23, 24, 158, 159] for more detailed discussions. Nevertheless, this dissertation intends to identify the temperature-dependent elastic and damping properties of composite lamina by neglecting influence of the uncertainties.

The implementation of an inverse method to estimate the temperature-dependent elastic and damping properties is carried out in two phases: firstly, the modal parameters of a laminated composite plate are evaluated experimentally at different temperatures, and secondly, the temperature-dependent model parameters are estimated by minimizing the error between experimental and numerical modal responses at each temperature state. Ideally, an inverse method leads to solving an optimization algorithm which intends to minimize the error between measured modal response and simulated modal response as derived from a forward model. A brief description of the experimental procedure and the optimization algorithm is given in the following subsections.

2.4.1 Experimental procedures

In order to estimate the temperature-dependent modal parameters, e.g., eigenfrequencies, modal damping values, and modeshapes, composite plates are tested within an enclosed thermal chamber where a specific control of temperature and moisture states is possible. Based on the adopted measurement strategy and system identification technique, the experimental procedures can be broadly classified in two ways: experimental modal analysis (EMA) and operational modal analysis (OMA).

The EMA has been used for decades to extract modal parameters of a structure. According to the EMA, the structure is excited by a single or several known dynamic forces, and the associated responses are recorded at nodal points. Finally, modal parameters in the frequency range of interest are extracted from the measured input and output data. The input-output-based procedure such as the EMA is considered as a reliable system identifier, which allows to validate the accuracy of the frequency response function by observing the coherence function. However, in reality, measuring input forces is often unfeasible and thus limits applicability of the EMA.

Even though the EMA is a well-established approach, it is often not suitable for large structures, e.g., bridge, building, etc., where the vibration level is very low and the measurement of excitation forces, i.e., earthquake induced loads, wind loads, etc., is not a very easy task. Therefore, the OMA techniques have been developed, where modal parameters are extracted by using the

measured output response only. The unmeasured input forces are modeled as stochastic quantities with unknown parameters with known behavior, such as a white noise excitation. In mechanical engineering, the OMA is used to evaluate the modal properties of a car body and aeroplane structure in operating condition. Different analysis algorithms, such as Stochastic Subspace Iteration (SSI), Enhanced Frequency Domain Decomposition (EFDD) techniques, etc., are used to estimate modal properties. Since, this dissertation is not claiming any contribution regarding improvement of these algorithms, the available algorithms in the commercial OMA software are used for the modal properties estimation; see [5, 15, 60, 96, 123, 161] for the SSI and the EFDD algorithms.

In this dissertation, a laminated composite plate, which is tested at a specific temperature within a thermal chamber, is excited by an acoustic white noise signal, and subsequently nodal velocities are recorded in time domain. Instead of using the EMA, the OMA is preferred in such a case, since collecting input forces acting on the plate surface due to white noise excitation is a challenging task. Additionally, the SSI or the EFDD algorithm is used to estimate the experimental modal frequencies and modal damping values at different temperatures.

2.4.2 Material properties identification

The identification of the temperature-dependent model parameters, i.e., elastic moduli and damping loss factors, of a composite lamina is presented as a solution of the assigned optimization problems after knowing the measured and simulated eigenfrequencies and modal damping values. The optimization problems for the applied inverse method is sequentially stated as follows

- For the identification of elastic moduli:

$$\begin{aligned} \bar{r}_1^* &= \underset{\bar{\boldsymbol{r}}_1}{\operatorname{argmin}}\ \mathscr{C}(\bar{\boldsymbol{r}}_1), \\ \text{subject to}\ \ \bar{\boldsymbol{r}}_{1_{\min}} &< \bar{\boldsymbol{r}}_1 < \bar{\boldsymbol{r}}_{1_{\max}}, \end{aligned} \tag{2.61}$$

  in which $\mathscr{C}(\bar{\boldsymbol{r}}_1)$ is the objective function where $\bar{r}_1 = \left\{ E_{11} \quad \frac{E_{11}}{E_{22}} \quad \frac{E_{11}}{G_{12}} \right\}^{\mathrm{T}}$ is evaluated to estimate the elastic moduli, i.e., E_{11}, E_{22}, and G_{12}, of the composite lamina.

- For the identification of damping loss factors:

$$\begin{aligned} \bar{r}_2^* &= \underset{\bar{\boldsymbol{r}}_2}{\operatorname{argmin}}\ \mathscr{C}(\bar{\boldsymbol{r}}_2), \\ \text{subject to}\ \ \bar{\boldsymbol{r}}_{2_{\min}} &< \bar{\boldsymbol{r}}_2 < \bar{\boldsymbol{r}}_{2_{\max}}, \end{aligned} \tag{2.62}$$

in which $\mathscr{C}(\bar{\boldsymbol{r}}_2)$ is the objective function with $\bar{r}_2 = \begin{Bmatrix} \eta_{11} & \eta_{22} & \eta_{12} \end{Bmatrix}^{\mathrm{T}}$ containing the vector of damping loss factors of the composite lamina.

A brief description of the inverse method for the deterministic identification of the temperature-dependent elastic and damping properties of a composite lamina has been presented. The detailed discussions of the experimental procedure and the implemented optimization algorithms are available in Publication 3.

2.5 Uncertainty quantification

In the earlier sections, numerical schemes for deterministic forward and inverse models for dynamic analysis and material properties identification, respectively, of composite plates in thermal environment have been discussed. The forward operator ($\mathscr{G}$) of the dynamic model describes the deterministic mapping from $\mathbb{R}^{\mathrm{P}}$ to $\mathbb{R}^{\mathrm{Q}}$, where $P,\ Q \geq 1$. In the deterministic analysis, for a set of input vector, $\boldsymbol{\vartheta} = \{\vartheta_1 \quad \vartheta_2 \quad \ldots \quad \vartheta_{\mathrm{P}}\} \in \mathbb{R}^{\mathrm{P}}$, the model evaluation $\mathscr{G}(\boldsymbol{\vartheta})$ renders a set of output vector, $\boldsymbol{\chi} = \{\chi_1 \quad \chi_2 \quad \ldots \quad \chi_{\mathrm{Q}}\} \in \mathbb{R}^{\mathrm{Q}}$. Here, the numbers of input and output variables are denoted by P and Q, respectively. Within the present scope of study, the input vector involves a set of elastic properties, damping properties, temperature, dimensions, external loading, etc., and the corresponding output variables result in a set of modal frequencies and modal damping values of the composite plate as well as displacement and stresses at a specific node of the adopted FE mesh. By recalling the forward model, cf. Eq. (2.59), the deterministic analysis is represented by

$$\boldsymbol{\chi} = \mathscr{G}(\boldsymbol{\vartheta}). \tag{2.63}$$

With the existence of the uncertainty in the input parameters ($\boldsymbol{\vartheta}$), the probabilistic framework is needed to be introduced in the numerical analysis. Consider a probability space $(\Omega, \mathscr{F}, \mathscr{P})$ where Ω is a probability space with σ-algebra $\mathscr{F}$, and $\mathscr{P}$ indicates the probability measure of the random field. Furthermore, consider K sets of input random variables, which are represented by $\boldsymbol{\Theta} \in \mathbb{R}^{\mathrm{K}\times\mathrm{P}}$, for uncertainty analysis. Without loss of generality, the input random variables are assumed to be independent. The realization of the random input variables ($\boldsymbol{\Theta}$) generates a random response matrix, $\boldsymbol{X} \in \mathbb{R}^{\mathrm{K}\times\mathrm{Q}}$, as

$$\boldsymbol{X} = \mathscr{G}(\boldsymbol{\Theta}). \tag{2.64}$$

For the sake of simplicity, the single random response $X \in \mathbb{R}^{\mathrm{K}\times 1}$ is considered for further discussion. The random response quantity X is characterized with a finite variance, i.e., $\mathbb{E}[X^2] < +\infty$.

The probabilistic response of X is characterized by the mean, μ_X, and standard deviation, σ_X. Primarily, various sampling-based techniques are used to evaluate these statistical quantities of interest (μ_X and σ_X) by repetitive realization of the function $\mathscr{G}(\boldsymbol{\Theta})$.

Well-known methods for uncertainty quantification of structural systems are reviewed in Section 1.1.6. Accordingly, the Monte Carlo (MC) simulation is used to evaluate statistical quantities of interest by realizing a large numbers of the functions, i.e., $\mathscr{G}(\boldsymbol{\Theta})$. However, this method is computationally demanding and suffers to meet the required convergence criteria. In such circumstances, different metamodeling techniques are implemented to overcome these limitations. The generalized polynomial chaos (gPC) expansion method has appeared as one of the most popular metamodeling techniques with extensive application in the engineering sector. In this modeling technique, the spectral representation of the random fields using appropriate orthogonal polynomials contributes to achieve a rapid convergence.

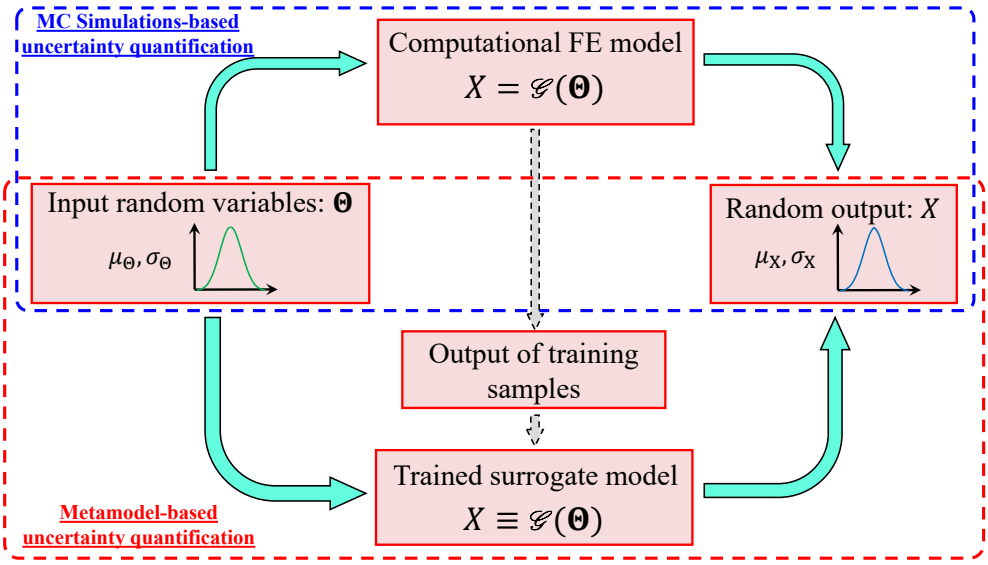

Figure 11: A representative diagram of uncertainty quantification of a dynamic system using MC simulation and surrogate model

Overall, the aim of these two stochastic methods is to evaluate the stochastic parameters of interest, i.e., mean and standard deviation. A schematic diagram of MC simulation-based and metamodel-based uncertainty quantification techniques is illustrated in Figure 11. A brief outline of these two methods is given below.

Monte Carlo (MC) simulation

In the Monte Carlo (MC) approach, the direct evaluation of a large numbers of response quantity $X(=\mathscr{G}(\boldsymbol{\Theta}))$ is used in order to estimate the mean and standard deviation. A sufficiently large random input sample $\boldsymbol{\Theta} = \{\boldsymbol{\vartheta}^{(1)}\ \boldsymbol{\vartheta}^{(2)}\ ...\ \boldsymbol{\vartheta}^{(\mathrm{K})}\}^{\mathrm{T}}$ is drawn from the joint probability density function $f_{\boldsymbol{\Theta}}$. The statistical parameters, i.e., mean, $\mu_{\mathrm{X,mc}}$, and standard deviation, $\sigma_{\mathrm{X,mc}}$, of random response are obtained as

$$\mu_{\mathrm{X,mc}} = \frac{1}{K}\sum_{i=1}^{K}\mathscr{G}(\boldsymbol{\vartheta}^{(\mathrm{i})}), \qquad \sigma_{\mathrm{X,mc}} = \left(\frac{\sum_{i=1}^{K}\left(\mathscr{G}(\boldsymbol{\vartheta}^{(\mathrm{i})}) - \mu_{\mathrm{X,mc}}\right)^{2}}{K-1}\right)^{\frac{1}{2}}. \tag{2.65}$$

From the statistical view point, these parameters are also random in nature due to the randomness of selecting $\boldsymbol{\vartheta}^{(\mathrm{i})}$. Nonetheless, the convergence rate of the MC estimator is quite slow ($\propto \frac{1}{\sqrt{K}}$), thus it is computationally demanding based on the required accuracy.

Generalized polynomial chaos (gPC) expansion method

The polynomial chaos (PC) expansion is presented as an approximation of the random response by using multivariate orthogonal polynomials, Ψ_{j}, in the finite basis up to terms S and is expressed as

$$X = \mathscr{G}(\boldsymbol{\Theta}) \approx \sum_{j=0}^{S} a_{\mathrm{j}}\Psi_{\mathrm{j}}(\bar{\boldsymbol{\xi}}). \tag{2.66}$$

Under this setup, the Hermite polynomial is used as an orthonormal polynomial in conjunction with the deterministic coefficients, a_{j} with multi-index j [16, 154, 160]. The orthogonal polynomial basis function is expressed in terms of multidimensional random variable, $\bar{\boldsymbol{\xi}} \in \mathbb{R}^{K\times \mathrm{P}}$. Moreover, the total number of terms in p^{th} order truncated polynomial is $S+1$, where $S+1 = \frac{(p!+P!)}{p!P!}$. Generally, the selection of orthogonal polynomial basis functions is made with respect to the joint probability density function (PDF) of the input random variable $\boldsymbol{\Theta}$. In other words, the PDF of the input random variables and the orthogonal polynomials belong to the same random space, otherwise necessary space transformation needs to be carried out [160]. The PDFs of random input variables and the corresponding optimal orthogonal polynomials are illustrated in Table 1. Since the method can handle frequently used random space by using the corresponding optimal polynomials, term "generalized" has been introduced, and the process is known as the "generalized polynomial chaos (gPC) expansion method".

Table 1: The random variables and the corresponding optimal orthogonal polynomials

Random variables	Optimal orthogonal polynomials
Gaussian	Hermite
Gamma	Laguerre
Beta	Jacobi
Uniform	Legendre

The orthogonality relation for multidimensional univariate polynomials is satisfied as

$$\mathbb{E}[\psi_s, \psi_t] = r^2 \delta_{\mathrm{st}}, \tag{2.67}$$

in which $r^2 = \mathbb{E}[\psi_s^2]$ and δ_{st} denote the norm of the polynomials and the Kronecker delta, respectively.

The estimation of the model response by using the gPC expansion method turns into the determination of the unknown deterministic coefficients (a_{j}). To determine these coefficients, there are two distinct methodologies available:

- Intrusive method: By this method, the selected expansions are inserted into the governing partial differential equations, and coefficients are obtained by the Galerkin's projection technique. The approximation with respect to Eq. (2.66) is regarded as discritization in stochastic dimension, which is then combined with spatial FE discritization, hence it is named spectral stochastic finite element method (SSFEM). Detailed discussions of this technique are available in [54, 160]. Nevertheless, the intrusive method leads to solve a huge matrix system, hence high computational cost arises in terms of time and memory.
- Nonintrusive method: Alternative to the previous method, the nonintrusive method has emerged in the domain of the SSFEM. In this setup, deterministic model evaluation has been done at some preselected collocation points. It is noteworthy that the deterministic model is either in the form of the governing partial differential equations or the FE model of the system, and this deterministic model is often known as "black-box" [97, 160]. Finally, the stochastic error minimization is carried out by using the least-square minimization technique to obtain the unknown deterministic coefficients, a_{j}. Moreover, the selection of the order of the orthogonal polynomials and choice of the collocation points are the key factor for achieving rapid convergence. The collocation points (or experimental design) are derived from: the roots of higher order orthogonal polynomials, the Latin Hypercube Sampling, and the Sobol sequence sampling, etc. Readers may refer to [16, 17, 49, 80, 95, 176] for detailed discussions on the application of different sampling schemes.

Once the unknown deterministic coefficients are evaluated, the statistical parameters ($\mu_{\mathrm{X,gPC}}$ and $\sigma_{\mathrm{X,gPC}}$) of quantity of interest are obtained, as

$$\mu_{X,\mathrm{gPC}} = a_0 \qquad \sigma_{X,\mathrm{gPC}} = \left(\sum_{j=1}^{S} a_{\mathrm{j}}^2 r^2 \right)^{\frac{1}{2}}. \tag{2.68}$$

In this dissertation, the nonintrusive approach of determination of the unknown coefficients is implemented where collocation points are selected based on the roots of the higher order polynomials. In Publication 4, uncertainties in time-independent parameters, i.e., eigenfrequencies and time-dependent parameters, i.e., time history of displacement are investigated due to randomness in the temperature variation. The application of the gPC expansion method in time domain involves the evaluation of the unknown deterministic coefficients at each time instance, and finally, random responses are evaluated at each time instance; see [80, 83, 144] for the application of the gPC expansion method for stochastic time domain analysis. The modified representation of the gPC expansion method for stochastic time domain analysis of a dynamic system is

$$X(\boldsymbol{\Theta},t) = \mathscr{G}(\boldsymbol{\Theta},\, t) \approx \sum_{j=0}^{S} a_{\mathrm{j}}(t)\Psi_{\mathrm{j}}(\boldsymbol{\Theta}). \tag{2.69}$$

Knowing the influence of the random variation of temperature at different mean temperature states for laminated composite plates has been of a great interest to the research community, and the subsequent effect on the quantities of interest, i.e., eigenfrequencies and transient response, are discussed in Publication 4.

2.6 Material properties

In order to conduct numerical simulation, material properties of the considered composite material needs to be known beforehand. To assess the dynamic behavior of composite plates in a considerably large temperature range, the composite material should be selected in such a way that the material remains stable within the given temperature range. Considering stability aspect of composite plates, the temperature range remains below the glass transition temperature. This dissertation aims to investigate the dynamic behavior of composite plates at the temperature range of $0^\circ - 125^\circ$ C. To this end, carbon- or graphite-based composites with high glass transition temperature are adopted in this investigation. The carbon- or graphite-based composites are widely used in different high-performance composite structures for the purpose of application in commer-

cial aircraft and high-speed trains. Generally, two types of polymer matrices, i.e., thermoset and thermoplastic, are used in these composites. The epoxy is a type of thermoset resin and widely utilized to manufacture carbon- or graphite-based composites. The epoxy resin demonstrates a tendency of moisture absorption in both the cured and uncured stages. This limitation of thermoset resins resulted in the development of thermoplastic resins, such as Polyether ether ketone (PEEK) and Polyether ketone ketone (PEKK). The carbon- or graphite-based composites having thermoplastic and thermoset matrices are considered in this dissertation as a natural choice in view of their realistic applications in the aerospace and transportation industries. For the numerical analysis using the FE-based forward operator, the composite materials are selected based on the availability of the temperature-dependent material properties in the literature/report. Herein, the graphite-epoxy and the IM7-PEEK composites are selected for the numerical analysis by considering availability of the temperature-dependent material properties in the given temperature range. The temperature-dependent elastic properties of graphite-epoxy lamina are shown in Table 2 and is adopted from [134]. The temperature-dependent elastic properties of the graphite-epoxy composite lamina are used for conducting stochastic dynamic analysis of the composite plates in Publication 4. The temperature-dependent elastic properties of the IM7-PEEK composite lamina are presented in Table 3 and adopted after suitable interpolation in the experimental data as available in [136]. The detailed interpolation procedure of elastic properties is stated in Publication 1. Similar interpolation strategy was implemented to evaluate the temperature-dependent damping loss factors of IM7-PEEK composite lamina using the available experimental data in [105]. The temperature-dependent material properties of the IM7-PEEK composite lamina are used for numerical analysis in Publications 1 and 2. Additionally, the experiment was conducted by using the T700 carbon-epoxy laminated composite plates, where the availability of the composite materials along with necessary lamina sequences was the decisive factors. The experimental investigation using the T700 carbon-epoxy composite plate and the identified material properties are presented in Publication 3.

Table 2: Elastic moduli of graphite-epoxy lamina at different temperatures, cf. [134]

	Temperature					
Elastic moduli	300 K	325 K	350 K	375 K	400 K	425 K
E_{11} (GPa)	130	130	130	130	130	130
E_{22} (GPa)	9.5	8.5	8.0	7.5	7.0	6.75
G_{12} (GPa)	6.0	6.0	5.5	5.0	4.75	4.5
ν_{12} (-)	0.3	0.3	0.3	0.3	0.3	0.3

$G_{13} = G_{12}, \quad G_{23} = 0.5G_{12}, \quad \nu_{21} = \nu_{12}\frac{E_{22}}{E_{11}}.$

Table 3: Material properties of IM7-PEEK lamina at different temperatures, cf. [105, 136]

	Temperature					
Material properties	0 °C	25 °C	50 °C	75 °C	100 °C	125 °C
E_{11} (GPa)	159.4	160.9	160.3	159.7	159.1	158.6
E_{22} (GPa)	9.7	9.7	9.3	8.9	8.6	8.2
G_{12} (GPa)	7.7	7.7	7.1	6.6	6.0	5.4
ν_{12} (-)	0.290	0.289	0.286	0.282	0.279	0.275
η_{11} (%)	0.45	0.51	0.55	0.65	0.72	0.70
η_{22} (%)	0.75	0.73	0.81	0.91	1.01	1.26
η_{22} (%)	1.05	1.01	1.09	1.43	1.48	1.49

$G_{13} = G_{12}, \quad G_{23} = 0.5 G_{12}, \quad \nu_{21} = \nu_{12} \frac{E_{22}}{E_{11}}.$

This dissertation intends to investigate the dynamic behavior of carbon- or graphite-based composite structures in thermal environment. To this end, suitable numerical and experimental procedures are developed and presented. Therefore, the consideration of three different types of composite materials does not influence the overall research aim.

Chapter 3

Summary of Appended Publications

In the preceding chapter, short summaries of the enclosed four publications along with the salient results are presented. The salient contributions of this dissertation are subdivided into two parts; the first part is devoted to develop the FE formulation to conduct deterministic and stochastic dynamic analyses of unstiffened and stiffened laminated composite plates in varying thermal environments, and in the second part, a novel OMA-based experimental procedure is presented to study the modal characteristics of composite plates in varying thermal environments and subsequently identify the temperature-dependent elastic and damping properties using an inverse method. This dissertation contributed in different research fields of dynamic analysis of composite structures as highlighted in Figure 12. However, the primary contributions are oriented towards the central theme, i.e., numerical and experimental studies deals with dynamic analysis of laminated composite plates in thermal environments, reported in the dissertation. The publication-wise contributions of the appended publications with respect to numerical and experimental investigations is illustrated in Figure 12.

The contributions of the individual publication in terms of deterministic and stochastic analyses are shown in Figure 12. It is observed that Publications 1 and 2 presented a detailed discussion on undamped and damped dynamic analyses of unstiffened and stiffened laminated composite plates in varying thermal environments. These deterministic analyses are aimed to study the influence of the stiffener as well as lamina sequences at different temperatures. Furthermore, in Publication 3, a novel experimental procedure has been presented by conducting an OMA-based modal analysis of composite plates in varying thermal environments in order to deterministic identification of the temperature-dependent elastic and damping properties of composite lamina. For material properties identification, a mixed experimental-numerical procedure is implemented by minimizing the difference between the experimentally and numerically derived modal responses. This procedure

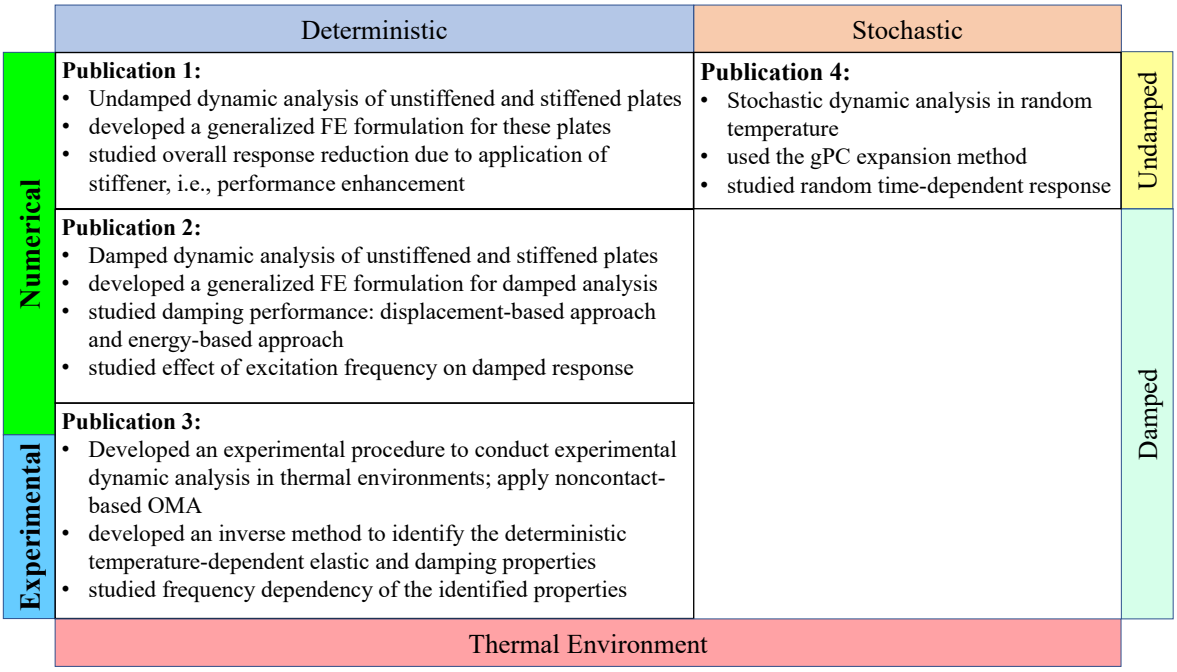

Figure 12: Schematic diagram of the dissertation structure in terms of research publications and the associated contributions

is known as the inverse method. Finally, uncertainty in dynamic response due to the random variation in temperature has been discussed in Publication 4. While using optimization algorithms to minimize the deviation of the experimental and numerical modal responses in Publication 3 and generating training data for the gPC-based metamodel in Publication 4, the FE-based numerical procedures developed in Publications 1 and 2 are implemented. The key results and the novel contributions of the attached four publications are summarized in the following sections.

3.1 Publication 1

Dynamic Response of Stiffened Laminated Composite Plate in Thermal Environment

Submission status: This article has been published in the journal of *Composite Structures*.

Novelty and key results: Over the last few decades, composite materials are increasingly used in aircraft and high-speed vehicles as primary structural materials. To understand the dynamic characteristics of these composite structures in thermal environment, conducting a detailed dynamic analysis is essential. Typically, the elastic properties of composite materials degrade with increasing temperature, accordingly, the amplitude of dynamic response of composite plates is higher at elevated temperatures. In such a situation, stiffened plates can be used to suppress the amplitude of the dynamic response.

To analyze the undamped dynamic response of unstiffened and stiffened laminated composite plates in thermal environment, a generalized FE formulation using the FSDT is developed. The development of the FE formulation is inferred from the Hamilton's variational principle by implementing appropriate coordinate transformation for the stiffener. A detailed dynamic analysis of the IM7-PEEK unstiffened and stiffened composite plates was conducted by using different plate geometries and lamina sequences. The stiffened plate with stiffener oriented parallel to the longer edge made-up of antisymmetric cross-ply laminates (i.e., $0°/90°/0°/90°$) presented the highest first non-dimensional frequencies (NDFs) within the considered temperature range of $0-125\ ^\circ$ C and thus indicated the highest stiffness compared to other plate geometries and the lamina configurations. Moreover, the occurrence of dynamic instability in unstiffened plates at elevated temperature can be avoided by adding stiffener. Stiffened plates offered overall suppression of dynamic deflection and normal stress. In the given temperature range, the stiffened plate which imparted the highest stiffness showed also the maximum response reduction. This stiffened plate also presented a higher rate of response reduction with the increment of stiffener depths; furthermore, the rate of response reduction is the highest at 100 °C.

Such outcomes indicate the advantage of the application of the stiffened plates at elevated temperature. Various parameters, e.g., lamina sequences, depths and orientations of stiffeners, etc. need to be selected optimally to maximize the dynamic response reduction at different temperatures. The generalized FE formulation can be further applied to analyze the composite structures with complex geometry, e.g., folded plates or box-like structures, etc. in varying thermal environments.

Specific contribution to the publication: Chandra proposed the analysis framework and implemented it through MATLAB. After developing the appropriate numerical model, Chandra was

responsible for conducting validation studies and subsequent parametric studies. Furthermore, Chandra wrote the original draft of the manuscript and coordinated with all the other coauthors.

3.2 Publication 2

Damping Analysis of Stiffened Laminated Composite Plates in Thermal Environment

Submission status: This article has been published in the journal of *Composite Structures*.

Novelty and key results: Generally, viscoelastic damping properties of composite materials increase with the increment in temperature up to glass transition temperature, whereas elastic properties degrade with increasing temperature. Beside the increment in the amplitude of dynamic response, higher viscoelastic properties can contribute to control the dynamic response at elevated temperatures. Considering this contrasting behavior of the elastic and damping properties with respect to the temperature increment, the damping performance of the unstiffened and stiffened IM7-PEEK laminated composite plate is studied for the sake of the various application of composite structures in varying thermal environments.

The damping performance of the unstiffened and stiffened laminated composite plates is studied for various geometries and lamina sequences in varying thermal environments, i.e., $0-125$ °C by using the displacement-based and the energy-based approaches. In FE method, the modal expansion damping is used to derive the damping matrix, and the proposed numerical model was validated by published results; cf. Appendix A. Based on the detailed parametric studies conducted, it is observed that the energy-based approach is the most robust one to evaluate the damping performance over the displacement-based approach. Furthermore, studies showed that the stiffened antisymmetric cross-ply (i.e., $0°/90°/0°/90°$) laminated composite plate with stiffener oriented parallel to the longer edge imparts the best damping performance at 100 °C. Overall, stiffened plates presented a better damping performance and improved response reduction efficiency near the resonance frequency at elevated temperatures.

The detailed parametric study explained the underlying relations between plate geometries, lamina sequences, and temperature-dependent material properties to achieve the best damping performance. The detailed analysis revealed that the stiffened plates can better utilize the higher damping properties to improve the damping performance at elevated temperatures than unstiffened plates.

Specific contribution to the publication: Chandra developed the analysis framework and implemented it through MATLAB. In addition, Chandra was responsible for conducting all simulations, data visualizations, and the corresponding interpretations. Furthermore, Chandra wrote the original draft and coordinated with all the other coauthors.

3.3 Publication 3

Identification of Temperature-Dependent Elastic and Damping Parameters of Carbon-Epoxy Composite Plates Based on Experimental Modal Data

Submission status: The article has been published in the journal of *Mechanical Systems and Signal Processing*.

Novelty and key results: To simulate a realistic dynamic response of composite plates in varying thermal environments, knowledge of the in situ temperature-dependent elastic and damping properties is essential. Several limitations in the experimental procedure need to be addressed regarding the evaluation of the in situ temperature-dependent materials properties of composite lamina using inverse methods. To overcome these limitations, an innovative OMA-based experimental procedure is presented, and the in situ temperature-dependent material properties of the T700 carbon-epoxy composite plates are evaluated by using experimental modal data.

The output-only OMA of the carbon-epoxy composite plate was conducted within an enclosed thermal chamber where the freely suspended plate was excited by a white noise acoustic excitation, and the associated nodal responses were measured by laser Doppler vibrometers. The output responses are used to derive the temperature-dependent modal characteristics of the plate. To identify the deterministic temperature-dependent elastic and damping properties of the composite lamina, a two-stage optimization strategy was implemented under the framework of an inverse method. The identified temperature-dependent material parameters indicated that the transverse modulus and shear modulus degrade rapidly with the increment in temperature. Additionally, inherent uncertainties in the composite plates play a major role in the identification of material properties, therefore the implementation of the stochastic identification technique is recommended.

This work presented a novel noncontact-based experimental strategy to estimate modal properties of the composite plates in thermal environment where only output responses are measured on real-time basis. The temperature-dependent elastic properties of the composite lamina are evaluated by conducting experiment with several samples of two types of laminates, i.e., symmetric cross-ply and angle-ply laminates and showed a nominal variation in the identified elastic properties; however, the corresponding trend of the temperature dependency can be assessed with sufficient accuracy. Furthermore, critical assessment of the error between experimentally and numerically simulated modal frequencies suggests the necessity to derive the in situ elastic properties of composite lamina while mimicking the actual operating conditions instead of adapting static or quasi-static test procedures.

Specific contribution to the publication: Chandra conducted the experiments and post-processing

of the experimental data in cooperation with Maeder. Chandra also involved in developing the numerical setup for inverse method in consultation with Maeder and Marburg. Chandra wrote the original draft of the manuscript while considering suggestions of all the other coauthors.

3.4 Publication 4

Stochastic dynamic analysis of composite plate with random temperature increment

Submission status: This publication has been published in the journal of *Composite Structures*.

Novelty and key results: The material properties of composite materials and surrounding thermal environment are uncertain in nature. Hence, dynamic response of composite plates become also uncertain. The estimation of uncertainties in dynamic response is essential for the safe design of a structure. This publication deals with the uncertainty quantification of dynamic response due to randomness in the ambient temperature, and this randomness is propagating to the temperature-dependent elastic properties. The nonintrusive gPC expansion method is used for the uncertainty quantification of dynamic response at different mean temperatures of increasing order.

The nonintrusive one-dimensional gPC expansion method is used to evaluate uncertainty in eigenfrequencies and the dynamic deflection of the graphite-epoxy laminated composite plates due to randomness in the mean temperature in increasing order ranging from 325 K to 400 K with a step size of 25 K. The parametric studies showed that uncertainty in the eigenfrequencies increases with the increment of the mean temperature. Furthermore, the amplitude of the mean central deflection decreased in delayed time domain due to the increment in the mean temperature; however, the pattern of the associated dispersion in the time domain is altered with the types of loading, e.g., pulse and impulse loads, and lamina sequences. Furthermore, it is also seen that the PDFs of the peak dynamic deflection became non-Gaussian and unsymmetric with the increment in the mean temperature.

This publication studied the influence of the randomness in temperature on the dynamic response of graphite epoxy composite plates. The study describes efficiency of the application of the gPC expansion method for stochastic dynamic analysis of composite plates due to randomness in the mean temperature. On the basis of the presented numerical examples, the stochastic behavior of dynamic deflection is investigated, and the uncertainty in the dynamic deflection evidently plays a significant role in the reliability analysis of composite plates in varying thermal environments.

Specific contribution to the publication: Chandra developed the analysis framework and was responsible for conducting all simulations, data visualizations, and corresponding interpretations. Furthermore, Chandra wrote the original draft and coordinated with all coauthors to accommodate their suggestions.

Chapter 4

Discussion of Results

In this chapter, the scientific contributions of this dissertation with regards to the existing literature in the domain of numerical and experimental investigations of dynamic behavior of carbon- and graphite-based composite structures in varying thermal environments are discussed. In Chapter 3, the novelty and the key contributions of each publication surpassing the existing research are described. The initial two publications are assumed as the primary bedrock for this dissertation, which presents generalized FE formulations for dynamic analysis of unstiffened and stiffened laminated composite plates in thermal environments. These publications initially presented a detailed literature review to explain the state-of-the-art research status, and finally numerical analyses are presented to address the identified research gaps. Perceiving the requirement to estimate the in situ temperature-dependent material properties of composite lamina, an efficient inverse method is presented in Publication 3. Using this inverse method, the temperature-dependent elastic and damping properties of composite lamina are evaluated. The last publication is considered an initiative for quantifying the uncertainties in dynamic response of laminated composite plates in varying thermal environments.

Within the scope of Publication 1, a generalized FE formulation has been developed with reference to the Hamilton's variational principle to analyze unstiffened and stiffened composite plates in varying thermal environment. So far, different researchers [112, 125, 164, 165] have studied dynamic response of unstiffened plates and shells in varying thermal environments. Additionally, few studies on the free-vibration analysis of unstiffened and stiffened plates in thermal environment are available, cf. [134, 167, 169]. However, the influence of the addition of stiffener to laminated composite plates in varying thermal environment has not been studied in detail. This publication aims to fill this gap by conducting a detailed dynamic analysis of unstiffened and stiffened laminated composite plates to quantify responses in terms of deflection and normal stress.

Furthermore, a sequential development of the generalized FE formulation for analysis of these plates is presented herein. In this generalized FE framework, a suitable coordinate transformation is incorporated to accommodate the stiffener geometry. The geometric stiffness matrix, which is developed due to the temperature variation related prestressing effect in the composite laminates, is also incorporated in the governing equation. Since engineers commonly consider the FSDT to analyze the thin composite structures using commercial software, this study adopts the FSDT to develop the required FE framework for analysis of stiffened plates. Additionally, the FSDT can predict the static and dynamic responses for thin composite plates with sufficient accuracy. Detailed validation studies are included in the publication to ensure the correctness of the developed FE framework, and the results obtained subsequently. Four different laminates, namely symmetric and antisymmetric cross-ply laminates, i.e., $0°/90°/90°/0°$ and $0°/90°/0°/90°$, and symmetric and antisymmetric angle-ply laminates, i.e., $45°/-45°/-45°/45°$ and $45°/-45°/45°/-45°$, are used for the numerical analysis. The dynamic analysis of these plates was carried out at six different temperatures, i.e., 0 °C, 25 °C, 50 °C, 75 °C, 100 °C, and 125 °C, to investigate the influence of the stiffener(s) on reducing the magnitude of the transient response of deflection and normal stress. The stiffener oriented parallel to the longer or shorter edge is considered for this analysis.

Furthermore, the literature review given in Publication 2 has pointed out the necessity of conducting dynamic analysis to assess the inherent damping performance of unstiffened and stiffened laminated composites plates in varying thermal environment. The damped dynamic response of unstiffened laminated composite plates due to inherent damping was studied by Zabaras and Pervez [200], where they used the definition of Rayleigh damping to obtain the damping matrix. Furthermore, Yi et al. [198] discussed the time-dependent behavior of the viscoelastic composite shells at two different temperatures without considering temperature-dependent material properties and the geometric stiffness matrix. To utilize the inherent damping capacity of composite lamina for controlling the dynamic response of composite plates in varying thermal environments, a comparative assessment of the damping performance at different temperatures is necessary; however, related studies are not available. In this respect, Publication 2 is the first attempt to investigate the damped dynamic response of unstiffened and stiffened laminated composite plates at different temperatures. The governing equation developed in Publication 1 is modified accordingly to conduct damped dynamic analysis in Publication 2, and it subsequently enables to explore the effect of the addition of the stiffener in order to mitigate the dynamic response at different temperatures.

For numerical analysis, the temperature-dependent elastic and damping properties of the IM7-PEEK composite lamina were used. These temperature-dependent material properties are adopted from the existing research literature, where elastic properties are evaluated from static tests [136],

and damping properties are evaluated from quasi-static DMA procedure [105]. The temperature-dependent properties for these publications are derived from the test data using piecewise linear interpolation and extrapolation techniques; see Publication 1 for detailed discussions. A generalized observation on these temperature-dependent properties indicates that the elastic properties degrade with the increment of temperature with reference to the room temperature (25 °C), whereas the magnitude of the damping parameters increases with the increment of temperature.

Even though the inherent damping capacity of laminated composite plates is less in comparison to the active damping capacity, it is absolutely necessary to understand the inherent damping performance of a composite plate prior to consider for the active damping. There is no such study available where damping performance of composite plates due to inherent damping is evaluated. In their study, Zabaras and Pervez [200] and Yi et al. [198] rely on the visual observation to understand the damping performance. In the domain of the earthquake engineering, different displacement-based performance criteria are used to assess the control performance of passive and active dampers; see Elias et al. [42]. Publication 2 proposed the displacement-based and the energy-based mechanisms to assess the inherent damping performance of unstiffened and stiffened laminated composite plates in varying thermal environments. The displacement-based criterion relies on the definition of the logarithmic decrement of damped response as obtained at a given nodal point. Since the energy-based approach considers all nodal displacements in order to evaluate damping performance, this approach has appeared as the best suited approach to evaluate the inherent damping performance.

For damped dynamic analysis reported in Publication 2, the damping matrix was developed by using the Rayleigh damping approach and the modal expansion damping approach, wherein the modal expansion damping approach was identified as the best approach to simulate the damped response of stiffened laminated composite plates at elevated temperatures. The successful implementation of the Rayleigh damping is based on some assumptions (see [53]), and the unfullfillment of these criteria often leads to develop a damping matrix that is not positive semi-definite. Thereby, the time domain response becomes unbounded. The occurrence of the unbounded dynamic response has been noticed for $45°/-45°/-45°/45°$ stiffened laminated composite plates with stiffener oriented parallel to the longer edge at 75 °C temperature. This numerical response-related instability has been addressed by implementing the concept of the modal expansion damping to develop the damping matrix. Henceforth, for further analysis in this article the modal expansion damping is used to develop the damping matrix.

It is found that, due to having only a very nominal contribution of inherent damping, the difference between the NDFs and the damped non-dimensional frequencies (dNDFs) is almost negligible.

However, the modal damping values are deemed to mitigate the dynamic response. Among the considered laminates, $45°/-45°/45°/-45°$ unstiffened plate presents the highest first NDF and the lowest peak undamped dynamic deflection at all temperatures. Therefore, this unstiffened plate provides the highest stiffness and also shows the best damping performance at 0 °C according to the energy-based approach; cf. Publication 2. Note that, according to the displacement-based approach, the best damping performance was given by $0°/90°/90°/0°$ unstiffened plate at 0 °C. However, the reliability of the energy-based approach is significantly better than that of the displacement-based approach, as the former approach considers the dynamic behavior of the entire composite structure to estimate the damping performance, whereas the latter approach is based on a particular nodal displacement. The $0°/90°/0°/90°$ stiffened plate with a stiffener oriented parallel to the longer edge imparts the highest first NDF and the lowest peak undamped dynamic deflection at all temperatures, which indicates that this configuration imparts the best stiffness among the considered plates in this study. Furthermore, this plate shows the best damping performance at 100 °C, as derived using the energy-based approach, whereas the displacement-based approach recommends this stiffened plate geometry with $45°/-45°/45°/-45°$ laminate to offer the best damping performance. Finally, the detailed investigation ensured the reliability of the energy-based approach to evaluate the damping performance of composite plates.

The undamped dynamic analysis in Publication 1 showed that the addition of stiffener improves the stiffness of a composite plate to a sufficient extent; accordingly, the amplitude of dynamic deflection and normal stress is also reduced, even at elevated temperatures. The increment of the stiffener depth has reduced the amplitude of dynamic deflection; however, the rate of reduction of the amplitude has reduced with the increment of stiffener depth. The numerical analysis in Publication 2 suggested that the damping performance of the stiffened plates is better than that of the unstiffened plates. Moreover, stiffened plates show a better damping performance at higher temperature, i.e., 100 °C, whereas the damping performance of unstiffened plates is better at lower temperature, i.e., 0 °C. It is recommended to use the energy-based approach to estimate damping performance. At the higher temperature range, i.e. $75-100$ °C, the effect of the inherent damping capacity for stiffened laminated composite plates is better to reduce the peak dynamic deflection near the resonance frequency.

Publications 1 and 2 are independent research articles; however it is conveneint to discuss their scientific contributions together due to having a similarity in material properties and the considered plate geometries. Firstly, these publications have presented a sequential development of a generalized FE formulation for dynamic analysis of unstiffened and stiffened laminated composite plates in varying thermal environments. This FE framework can be further extended to analyze differ-

ent complex geometries, i.e., folded plates, stiffened folded plates, rectangular box-like structures, shell structures, etc. Secondly, an efficient mechanism to assess damping performance of a composite structure has been presented in Publications 2. Thirdly, presented numerical examples show that stiffened plates offer a better damping performance at higher temperatures by using higher inherent damping properties of composite lamina at elevated temperatures. Based on this idea, the damping performance of composite plates can be improved further at elevated temperatures by incorporating interleaved damping layers.

Earlier it has been mentioned that in Publications 1 and 2, the temperature-dependent elastic and damping properties of IM7-PEEK composite plates are taken from published research data [105, 136], where static and quasi-static test procedures are used to derive the material properties. It is noteworthy that Kodur et el. [81] has aptly summarized different standard and nonstandard static and quasi-static test protocols to estimate strength and elastic properties of composite lamina along the principal lamina directions at varying temperatures. Therefore, to evaluate material properties of lamina using static and quasi-static test procedures, several tests are needed to be carried out. Furthermore, these tests are a time-consuming process and involve various modeling- and sampling-related uncertainties. In this scenario, a unified test procedure is necessary to evaluate the temperature-dependent elastic and damping properties of a lamina. Furthermore, the conventional static and quasi-static measurement techniques do not accounts for the frequency-dependent characteristics of composite lamina in a higher frequency range, although the consideration of the frequency-dependent material properties is important to predict the in situ dynamic response in the given frequency range. To address these limitations of static and quasi-static direct methods, inverse methods can be used to evaluate the in situ temperature-specific material properties using dynamic test data, where only a single experiment needs to be performed at a particular temperature. In Publication 3, an innovative test protocol using the operational modal analysis (OMA) is presented to derive the temperature-dependent modal characteristics, and then the temperature-dependent material properties of a composite lamina are evaluated by utilizing the experimentally derived modal data.

Publication 3 contributes to the experimental aspect of this dissertation. In operating condition, it is very challenging to accumulate the input load data on a vehicle structure, whereas the output response can be recorded without much difficulty. Considering necessity for the ease of practical application of an experimental procedure, a novel experimental strategy has been presented in this publication, and subsequently evaluated the temperature-dependent material properties. To ensure the objective of practical applicability of the test procedure, the OMA is adopted, in which only the time domain data of the output response is recorded, and it is utilized to evaluate the modal

properties of a composite structure. Importantly, for the classical experimental modal analysis (EMA) both input load data and output response data are required. This publication intends to present an innovative OMA to evaluate modal characteristics of a composite plate at different temperatures.

Several experimental analyses [18, 46, 47, 143, 170] were conducted by researchers to estimate material properties of composite lamina at ambient temperature using inverse methods. However, conducting dynamic analysis within an enclosed thermal chamber to evaluate the temperature-dependent material properties of a composite lamina is obviously a challenging task. Frederiksen [45] and Pedersen and Frederiksen [128] described the EMA-based experimental strategy to measure the modal data at different temperatures. They used temperature-resistant impact hammer to excite the composite plate inside the thermal enclosure, and lightweight accelerometers were attached to the plate to detect the dynamic response. They simulated free-free boundary conditions while experimenting with the plate. Recently, Li et al. [93, 94] presented an experimental strategy which used acoustic pressure to excite the composite plate. The plate is fixed at one end and placed inside the thermal chamber. The laser Doppler vibrometer is used to measure the dynamic response of the plate. In the present study, T700 carbon-epoxy laminated composite plates were considered to estimate the temperature-dependent material properties. To this end, the composite plate with free-free boundary conditions is excited by acoustic white noise signal inside the thermal chamber, and the nodal dynamic response of the plate was measured by two laser Doppler vibrometers. The measured data were post-processed to extract modal parameters for the T700 carbon-epoxy antisymmetric cross-ply and angle-ply laminated composite plates following the guideline of the OMA. The nature of variation of the temperature-dependent eigenfrequencies and eigen modes for the cross-ply and angle-ply laminates are discussed in detail. In the adopted inverse method, a two-stage optimization strategy is implemented to identify the temperature-dependent elastic and damping properties. The two-stage optimization strategy is based on the idea of the associated sensitivity of the identified properties. Generally, the elastic properties are more sensitive than the inherent damping properties while evaluating eigenfrequencies. The consistency in the identified elastic properties indicates the reliability of the adopted inverse strategy and the associated experimental protocol. The experimentally evaluate temperature-dependent behavior of eigenfrequencies for antisymmetric angle-ply and cross-ply laminates has been discussed with reference to the fiber angle and the corresponding mode shapes. This study also confirms the frequency-dependent behavior of the identified elastic properties and indicates the importance of conducting dynamic tests and measurements to identify the material properties of composite lamina instead of merely considering static and quasi-static test procedures.

The experiment was conducted with two sets of cross-ply and angle-ply laminates. The deterministic material properties of 8 numbers of plate samples are estimated separately by using the proposed inverse method; however, the identified properties of eight plate samples indicate the existence of uncertainties in the material properties. Therefore, it was suggested to evaluate uncertainties in the material properties by using stochastic inverse methods. Sephavand et al. [154, 158] and Chandra et al. [23, 24] used the gPC-based inverse method and the Bayesian inference technique to estimate stochasticity in the material properties of composite lamina at the room temperature. These inverse methods can be implemented to identify the stochastic temperature-dependent material properties of composite lamina, and considered as a future research outlook. Hence, it is absolutely necessary to study the uncertainties in the dynamic response of composite plates in varying thermal environments. However, due to the absence of the in situ statistical data of the material properties for carbon-based composite lamina at different temperatures, in Publication 4 an assumed statistical parameters are utilized for stochastic dynamic analysis of composite plates in varying thermal environments.

Publication 4 is devoted to study stochastic dynamic behavior of composite plates in thermal environment. In fact, stochastic dynamic behavior of graphite-epoxy composite plates due to random temperature increment is presented in this publication. The stochastic analysis is conducted by using the gPC expansion method. The gPC expansion method is a well-established computationally efficient metamodel to derive the stochastic dynamic response of an engineering system. However, the applicability of this metamodel to evaluate the stochastic dynamic response of composite plates is very limited. The first-order perturbation technique (FOPT) is used quite extensively [122, 126] to quantify uncertainties in static response and eigenfrequencies. Lal and Singh [89], Kumar et al. [84, 85], and Dey et al. [36] studied uncertainty in static response and eigenfrequencies at different temperatures due to random material and geometric properties. In this respect, this publication studied for the first time uncertainty in dynamic response due to randomness in temperature by using the gPC expansion method. The graphite-epoxy laminated composite plate is used for this analysis. The elastic properties of the graphite-epoxy composite lamina are temperature-dependent, therefore uncertainty in temperature propagate into the material properties. For numerical analysis, mean temperatures are considered in the order of 325 K, 350 K, 375 K, and 400 K. The uncertainty in time domain deflection for symmetric cross-ply and angle-ply laminates subjected to pulse and impulse loadings is presented as well. The gPC method is successfully applied to estimate stochastic time domain deflection due to single random parameter, i.e., temperature. With the increment of mean temperature, the mean eigenfrequencies have decreased, whereas the associated standard deviations have increased. Furthermore, consideration of impulse loading shows a higher level of uncertainty in the delayed time domain, whereas in the

case of the pulse loading, the level of uncertainty decreases in the delayed time domain. The PDF of the peak dynamic deflection shows a larger dispersion at higher temperature. The level of uncertainties varies in time and temperature domains, which suggests to conduct detailed stochastic dynamic analysis of composite plates in varying thermal environment by considering uncertainty in the material and geometric properties. In this respect, the sparse gPC expansion method can be utilized to accommodate a large number of random parameters; see [16, 17] for further readings. Overall, this publication will pave the way towards a reliable design of composite structures in thermal environment.

To summarize these discussion, it can be mentioned that the stated research gaps are addressed in this dissertation through the four publications. This work partially contributes to the broad field of numerical and experimental analyses of composite structures in thermal environments. A generalized FE formulation is developed to analyze unstiffened and stiffened laminated composite plates in varying thermal environments. The displacement-based and energy-based mechanisms to evaluate inherent damping performance of composite structures in varying thermal environment are developed. Furthermore, the detailed parametric studies indicate the best possible configuration of stiffener orientation, stiffener depth, lamina sequence, and temperature state to obtain the best damping performance. The experimental procedure to measure the in situ dynamic characteristics of composite plates in thermal environment is presented; it subsequently enable to identify the deterministic in situ temperature-dependent elastic and damping properties by exploiting the previously developed FE formulation. Finally, the stochastic dynamic analysis of composite plates due to random temperature increment is presented.

Chapter 5

Conclusions

5.1 Summary of major outcomes

To conclude this research work, the major outcomes and their implication in the scientific field are summarized. Nowadays, composite materials are used to develop different structural parts of aircraft, high-speed vehicles, etc., and these structures are exposed to thermal environment and also subjected to dynamic loads. While developing prototypes of these types of composite structures, the associated research involves knowledge of the state-of-the-art literature, development of a suitable structural system, numerical analysis of the structural system and subsequently performance evaluation of the structure to identify the best configuration of the structural system. The first two papers contributed to the development of this research field. Furthermore, knowledge of the in situ material properties of the composite lamina is essential to simulate the dynamic response of the prototype structure considering the influence of the operating frequencies and temperature. This requirement has been discussed in Publication 3 with reference to the experimental procedure to identify the in situ material properties. To ensure structural safety, probabilistic analysis of the structure is necessary by quantifying uncertainty in dynamic response due to randomness in material properties and thermal environment. In Publication 4, uncertainty in the dynamic response has been evaluated due to randomness in the varying temperatures. Overall, this dissertation partially contributed at different stages to the development of a prototype composite structure for application in thermal environment.

The outcomes are illustrated in accordance with the two broad fields of contributions, i.e. numerical analysis and experimental analysis of composite plates. The major contributions regarding the numerical analysis are the following:

- FE-based numerical tool has been developed using the FSDT for conducting dynamic analysis of thin unstiffened and stiffened laminated composite plates in thermal environment. This generalized FE formulation is derived with reference to the Hamilton's variational principle for undamped and damped dynamic analyses.
- The modal expansion damping appeared as the best suited approach to develop the damping matrix for conducting damping analysis of a composite structure with complex geometry in varying thermal environments than that of the Rayleigh damping.
- In general, elastic properties of composite lamina degrade with the increment of temperature, whereas the associated inherent damping values increase with the increment of temperature until the glass transition temperature is reached. To quantify the inherent damping performance of composite plates at different temperatures, the displacement-based and energy-based mechanisms are proposed. Among these two, the energy-based mechanism appeared as the most reliable approach for the damping performance assessment.
- It is observed that the lamina sequences and stiffener orientation govern the overall stiffness of a composite plat. Among the considered unstiffened and stiffened laminated composite plates, the best damping performance is obtained for the configuration which offered the highest stiffness. Thereby, the unstiffened composite plate with antisymmetric angle-ply laminate and the stiffened composite plate with a stiffener oriented parallel to the longer edge with antisymmetric cross-ply laminate are identified as the best configuration to offer the best damping performance for unstiffened and stiffened plates, respectively.
- The stiffened plate configuration imparted highest damping performance at 100 °C by utilizing higher stiffness property as obtained by attaching a stiffener, whereas the unstiffened plates presented the best damping performance at 0 °C.
- Near the resonance frequency, stiffened plates presented a better response reduction performance due to inherent damping capacity of the composite lamina at elevated temperatures, i.e., $75 - 100$ °C.
- The gPC expansion method is efficiently used for the stochastic dynamic analysis of composite plates due to the random temperature increment.
- The stochastic dynamic analysis of laminated composite plates showed a significant amount of uncertainty in the dynamic deflection in time and temperature domains. The dispersion of the PDFs of the peak dynamic deflection increased with the increment of the mean temperature. Furthermore, the nature of the PDFs became non-Gaussian at elevated mean temperatures.

With respect to the experimental procedure with composite plates and the corresponding identification of the in situ temperature-dependent elastic and damping properties of composite lamina, the following main contributions are identified:

- A novel noncontact-based experimental strategy is proposed for the experimental dynamic analysis of a composite plate within a thermal enclosure. The output-only OMA is implemented to extract the temperature-dependent modal characteristics of the composite plate in varying thermal environments. Furthermore, the consistency in the extracted eigenfrequencies ensured reliability of the presented experimental protocol.
- The experimental data showed that the temperature dependency of the eigenfrequencies is governed by the fiber angle and the temperature-dependent elastic properties of the associated composite lamina and mode shapes of the plate.
- The proposed two-stage optimization algorithm efficiently identified the deterministic temperature-dependent elastic properties of the composite lamina and subsequently evaluates the trends of temperature-dependent behavior of the elastic properties. Additionally, uncertainties in the identified material properties were also observed.
- The identified elastic properties of the composite lamina are frequency-dependent, which suggested to consider the dynamic modal analysis to evaluate the in situ material properties in operating frequency range. Therefore, the present experimental procedure is preferred over the traditional static tests and quasi-static DMA, in which the material properties are not estimated by acknowledging the operational frequency range of higher magnitude.

5.2 Future research outlooks

The numerous potential research avenues can be explored as a direct consequence of this research work. In this regard, the blank space in Fig. 12 can be refereed to identify the future research scopes. Few future scopes of development are listed below:

- The damping performance of the unstiffened and stiffened laminated composite plates at different temperatures is studied in this work. The developed FE formulation can be directly utilized to investigate the damping performance of unstiffened and stiffened laminated folded plates. Furthermore, the damping performance of these structures can be studied under different dynamic loads, e.g., impulse load, step load, sinusoidal load, etc.
- The current work is focused on the composite plates. Different forms of shell structure can be studied to evaluate their damping performance and stochastic behavior.

- To achieve higher damping performance, viscoelastic damping layers can be inserted within the host composite plate, and the corresponding damping performance in thermal environment can be evaluated before considering for an industrial application.
- The inherent damping properties of a composite structure also contribute to control the interior and exterior acoustic responses. The inherent damping properties of composite structures influence the acoustic control in thermal environment and this research field needs further investigation.
- The efficiency of passive damping for structural and acoustic controls is limited. A passive-active hybrid control mechanism can be exploited to improve the individual control performance.
- The current work investigates stochastic dynamic response of composite plates due to uncertainties in temperature. Additionally, material and geometric properties of composite plates are also random in nature. The existing gPC-based metamodelling framework can be improved to accommodate a large number of random variables to evaluated the uncertainties in dynamic response in varying thermal environments.
- The present work considers the FSDT to analyze composite plates. This work can be extended to consider various higher-order plate theories to analyze thick plates and shells and subsequently evaluate their damping performance and uncertainties in dynamic response at different temperatures.
- The proposed experimental protocol can be improved further to minimize the model-related uncertainties, as having appeared in the identified damping properties. Furthermore, stochastic inverse methods can be implemented to estimate uncertainties in the material properties of composite lamina at different temperatures.

Appendix A

Validation Studies

The validation studies are conducted to ensure correctness and reproducibility of a numerical model-generated output. In Publication 1, the FE-based numerical model for an undamped dynamic analysis of unstiffened and stiffened laminated composite plates has been validated sequentially. However, detailed validation studies for damping analysis of unstiffened and stiffened laminated composite plates were not included in Publication 2 due to brevity. In this chapter, validation examples for the FE-based numerical model for damping analysis of composite plates at the room temperature are presented. Herein, the modal damping values and damped dynamic responses of laminated composite plates are compared with the published results. The validation of the present FE model to analyze undamped dynamic response of unstiffened and stiffened laminated composite plates in thermal environment has been presented in Publication 1.

Modal damping values for unstiffened plates

The modal damping values in terms of SDCs, Ψ_{m}, of an unstiffened plate are calculated by using the viscoelastic damping formulation at the room temperature (i.e., 25 °C), and the present results are compared with the results that are published by Hu and Dokainish [66]. An 8-layered laminated composite plate, Plate 734 as denoted in [66], with lamina sequence $(0^\circ/90^\circ)_{2\mathrm{s}}$ with free-free boundary conditions is taken for the analysis. The dimension of the plate is $(227 \times 227 \times 2.05)$ mm^3. The plate is discretized into 4×4 mesh. The elastic and damping properties of this plate is given in Table 4. The damped eigenfrequencies, f_{dm}, and the modal SDCs, Ψ_{m}, are calculated by using the present FE formulation and presented in Table 5. The results obtained by using the present FE formulation are in close agreement with the results that reported by Hu and Dokainish [66].

Table 4: Properties of the composite lamina of the unstiffened laminated composite Plate 734, cf. [66], at room temperature, i.e. 25 °C, to validate the damped eigenfrequencies and modal damping values

Parameters	Properties		
Elastic moduli* (GPa)	$E_{11}=34.49$	$E_{22}=9.40$	$G_{12}=G_{13}=4.49$
Poisson's ratio (-)	$\nu_{12}=0.30$	-	-
Damping (%)	$\Psi_{11}=0.87$	$\Psi_{22}=4.75$	$\Psi_{12}=6.13$
Density (kg/m^3)	$\rho=1813.9$	-	-

* $G_{23}=0.5G_{12}$, $\nu_{21}=\nu_{12}\frac{E_{22}}{E_{11}}$.

Table 5: Comparison of the damped eigenfrequencies, f_{dm}, and the modal SDCs, Ψ_{m}, as calculated using the present FE formulation, and that reported by Hu and Dokainish [66] for $(0^\circ/90^\circ)_{2\mathrm{s}}$ unstiffened laminated composite Plate 734

Mode, m	Present study		Hu and Dokainish [66]	
	f_{dm} (Hz)	Ψ_{m} (%)	f_{dm} (Hz)	Ψ_{m} (%)
1	66.37	5.91	66.43	5.93
2	126.42	2.34	126.30	2.22
3	160.14	1.33	160.00	1.49
4	184.17	4.17	184.00	4.21
5	206.37	3.20	206.10	3.22

Damped response for unstiffened plates

The damped dynamic response of an unstiffened laminated composite plate is evaluated at the room temperature and compared with the published results given in [200]. The elastic and damping parameters as well as the density of the considered composite lamina, which is designated as Material III in [200], are given in Table 6. The damped eigenfrequencies, f_{dm}, and the modal SDCs, Ψ_{m}, of $(0^\circ/90^\circ/0/90)_{\mathrm{s}}$ unstiffened laminated composite plate with free-free boundary conditions are calculated by using the present formulation and compared with those given by Zabaras and Pervez [200]. The dimension of the composite plate is $(227\times227\times2.05)$ mm^3, and the plate is discretized into 6×6 mesh. A good agreement between the results as obtained by using the present FE formulation and those reported in [200] is observed in Table 7. The initial six rigid modes are ignored in the modal analysis.

The damped dynamic response of a 2-layered $(0^\circ/90^\circ)$ composite plate, using the composite material as described in Table 6, is calculated by implementing the present formulation. The plan

Table 6: Properties of the composite lamina (Material III) at room temperature, i.e., 25 °C, to validate the modal damping values for the unstiffened laminated composite plate, cf. [192, 200].

Parameters	Properties		
Elastic moduli* (GPa)	$E_{11}=37.78$	$E_{22}=10.91$	$G_{12}=G_{13}=4.91$
Poisson's ratio (-)	$\nu_{12}=0.30$	-	-
Damping (%)	$\Psi_{11}=0.87$	$\Psi_{22}=5.05$	$\Psi_{12}=6.91$
Density (kg/m^3)	$\rho=1813.9$	-	-

* $G_{23}=G_{12}$, $\nu_{21}=\nu_{12}\frac{E_{22}}{E_{11}}$.

Table 7: Comparison between the damped eigenfrequencies, f_{dm}, and the modal SDCs, Ψ_{m}, calculated by using the present FE formulation, and as reported by Zabaras and Pervez [200] for $(0°/90°/0°/90°)_{\mathrm{s}}$ unstiffened laminated composite plate.

Mode, m	Present study		Zabras et al. [200]		Lin et al. [200]	
	f_{dm} (Hz)	Ψ_{m} (%)	f_{dm} (Hz)	Ψ_{m} (%)	f_{dm} (Hz)	Ψ_{m} (%)
1	69.48	6.66	59.4	6.26	66.3	7.12
2	133.56	2.52	132.13	2.75	129.28	2.51
3	168.23	1.40	170.28	2.1	167.1	1.57
4	193.80	4.63	187.34	4.54	187.76	4.91
5	216.37	3.54	239.74	2.99	211.15	3.67

area of the considered plate is (227×227) mm^2, and the plate thickness is derived from the given aspect ratio of $L/h=5$. The plate is with simply-supported boundary conditions in all sides and is subjected to the pulse loading of $q(t)=100$ N/m^2 over the entire plan area of the plate. The damped dynamic deflection, w, as calculated by using the Rayleigh damping and the modal expansion damping (considering first 20 modes) are plotted along with that given by Zabaras and Pervez [200] in Figure 13. The damped dynamic deflection obtained from the ANSYS® simulation is also shown in this figure. The figure shows that the mitigation of the deflection amplitude in the time domain as derived by using the present formulation follows the similar trend as obtained from the ANSYS® simulation and Zabaras and Pervez [200]. However, periodicity of the calculated responses are not matching exactly with the reference response plot as obtained from the ANSYS® simulation and Zabaras and Pervez [200]. The nonmatching of the response periodicity is due to the discrepancy between the calculated damped eigenfrequencies and that evaluated by the ANSYS® simulation and in [200]. The first eigenfrequency obtained from the present FE formulation, ANSYS® simulation, and Zabaras and Pervez [200] are 2193 Hz, 2122 Hz, and 2391 Hz (approximately), respectively, and all three are within an allowable limit. This validation study confirms that present FE formulation can evaluate damped dynamic response of unstiffened lami-

nated composite plates with sufficient accuracy, and thereby used in Publication 2.

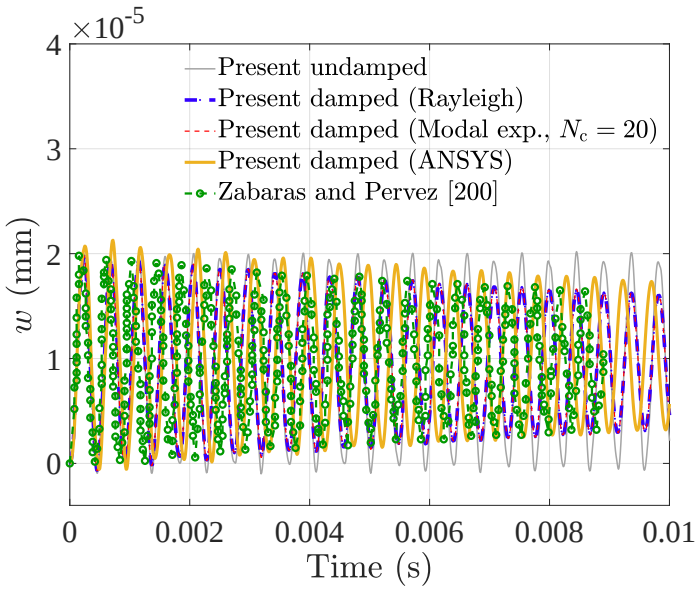

Figure 13: Comparison between the damped transient response of the deflection, w, as obtained by using the present FE formulation, and that reported by Zabaras and Pervez [200] for $(0^\circ/90^\circ)$ unstiffened laminated composite plate with all four edges simply-supported subjected to pulse loading, $q(t) = 100$ N/m^2, over the entire plan area

In these validation examples, the damped eigenfrequencies, modal damping values, and the damped dynamic response of unstiffened laminated composite plates at the room temperature are calculated using the present FE formulation. The results are matched well with the corresponding results as obtained in the literature and the ANSYS® simulation. In Publication 1, this numerical model has been validated for undamped dynamic analysis of both unstiffened and stiffened laminated composite plates in thermal environment. Therefore, the presented FE formulation can be used to evaluate the modal damping values and damped dynamic response of unstiffened and stiffened laminated composite plates in thermal environments, as used in Publication 2.

Bibliography

[1] R.D. Adams and D.G.C. Bacon. Effect of fibre orientation and laminate geometry on the dynamic properties of CFRP. *Journal of Composite Materials*, 7(4):402–428, 1973.

[2] S. Adhikari. *Damping Models for Structural Vibration*. PhD thesis, Cambridge University, Cambridge, U.K., 2000.

[3] S. Adhikari. Random eigenvalue problems revisited. *Sadhana*, 31(4):293–314, 2006.

[4] R.C. Alderliesten. *Introduction to Aerospace Structures and Materials*. Delft University of Technology, Delft, The Netherlands, 2018.

[5] M. Aoki. *State Space Modeling of Time Series*. Springer Berlin Heidelberg, 1990.

[6] R.C. Aster, B. Borchers, and C.H. Thurber, editors. *Parameter Estimation and Inverse Problems*. Elsevier, Third edition, 2019.

[7] E.J. Barbero. *Finite Element Analysis of Composite Materials*. CRC Press, New York, First edition, 2008.

[8] D. Barpanda and P.R. Mantena. Dynamic mechanical analysis of pultruded glass-graphite/epoxy hybrid composites at elevated temperatures. *Journal of Reinforced Plastics and Composites*, 15(5):497–532, 1996.

[9] K.J. Bathe. *Finite Element Procedures in Engineering Analysis*. Prentice Hall, Upper Saddle River, New Jersy, Updated edition, 1982.

[10] A. Baz and J. Ro. Vibration control of plates with active constrained layer damping. *Smart Materials and Structures*, 5(3):272–280, 1996.

[11] A.M. Baz. *Active and Passive Vibration Damping*. John Wiley & Sons Inc., New York, 2019.

[12] T. Belytschko, L.W. Kam, B. Moran, and K. Elkhodary. *Nonlinear Finite Elements for Continua and Structures*. John Wiley & Sons Inc., New York, Second edition, 2013.

[13] B. Benchekchou, M. Coni, H.V.C. Howarth, and R.G. White. Some aspects of vibration damping improvement in composite materials. *Composites Part B: Engineering*, 29(6):809–817, 1998.

[14] B. Benchekchou and R.G. White. Acoustic fatigue and damping technology in FRP composites. *Composite Structures*, 37(3-4):299–309, 1997.

[15] J.S. Bendat and A.G. Piersol. *Random Data - Analysis and Measurement Procedures*. John Wiley & Sons, New York, 2011.

[16] G. Blatman and B. Sudret. An adaptive algorithm to build up sparse polynomial chaos expansions for stochastic finite element analysis. *Probabilistic Engineering Mechanics*, 25(2):183–197, 2010.

[17] G. Blatman and B. Sudret. Adaptive sparse polynomial chaos expansion based on least angle regression. *Journal of Computational Physics*, 230(6):2345–2367, 2011.

[18] A.K. Bledzki, A. Kessler, R. Rikards, and A. Chate. Determination of elastic constants of glass/epoxy unidirectional laminates by the vibration testing of plates. *Composites Science and Technology*, 59(13):2015–2024, 1999.

[19] H. Bouadi and C.T. Sun. Hygrothermal effects on structural stiffness and structural damping of laminated composites. *Journal of Materials Science*, 25(1):499–505, 1990.

[20] N.A.D. Bruyne. Plastic materials for aircraft construction. *Journal of the Royal Aeronautical Socity*, 41:523–590, 1937.

[21] G. Cederbaum. Random vibrations of viscoelastic laminated plates. *Journal of Applied Mechanics*, 57(3):688–693, 1990.

[22] R. Chandra, S.P Singh, and K. Gupta. Damping studies in fiber-reinforced composites – A review. *Composite Structures*, 46(1):41–51, 1999.

[23] S. Chandra, K. Sepahvand, C.A. Geweth, F. Saati, and S. Marburg. Bayesian inference to damping identification of fiber-reinforced composites from experimental modal data. In M. Ochmann, editor, *Proceedings of the 23rd International Congress on Acoustics, integrating 4th EAA Euroregio*. DEGA, 2019.

[24] S. Chandra, K. Sepahvand, C.A. Geweth, F. Saati, and S. Marburg. Stochastic non-parametric identification in composite structures using experimental modal data. In *Proceedings of the 3rd International Conference on Uncertainty Quantification in Computational Sciences and Engineering (UNCECOMP 2019)*, pages 543–554. Institute of Structural Analysis and Antiseismic Research School of Civil Engineering National Technical University of Athens (NTUA) Greece, 2019.

[25] S.-H. Chang and C.-Y. Lee. Damping characteristics of TiNi shape memory alloy wires reinforced epoxy resin. *Journal of Reinforced Plastics and Composites*, 30(23):1931–1938, 2011.

[26] B. Chattopadhyay, P.K. Sinha, and M. Mukhopadhyay. Finite element analysis of blade-stiffened composite plates under transverse loads. *Journal of Reinforced Plastics and Composites*, 12(1):76–100, 1993.

[27] N.-Z. Chen and C.G. Soares. Spectral stochastic finite element analysis for laminated composite plates. *Computer Methods in Applied Mechanics and Engineering*, 197(51):4830–4839, 2008.

[28] R.M. Christensen. *Theory of Viscoelasticity: An Introduction*. Academic Press, New York, Second edition, 1982.

[29] J.D. Collins and W.T. Thomson. The eigenvalue problem for structural systems with statistical properties. *AIAA Journal*, 7(4):642–648, 1969.

[30] R.D. Cook, D.S. Malkus, M.E. Plesha, and R.J. Witt. *Concepts and Applications of Finite Element Analysis*. John Wiley & Sons Inc., New York, Fourth edition, 2001.

[31] D3039/D3039M. Standard test method for tensile properties of polymer matrix composite materials. Technical report, ASTM International, West Conshohocken, PA 19428-2959, U.S., 2017.

[32] D4255/D4255M. Standard test method for in-plane shear properties of polymer matrix composite materials by the rail shear method. Technical report, ASTM International, West Conshohocken, PA 19428-2959, U.S., 2020.

[33] I.M. Daniel and O. Ishai. *Engineering Mechaincs of Composite Materials*. Oxford University Press, New York, 1994.

[34] A. Deb and M. Booton. Finite element models for stiffened plates under transverse loading. *Computers and Structures*, 28:361–372, 1988.

[35] S. Dey, T. Mukhopadhyay, H.H. Khodaparast, and S. Adhikari. Fuzzy uncertainty propagation in composites using gram–schmidt polynomial chaos expansion. *Applied Mathematical Modelling*, 40(7):4412–4428, 2016.

[36] S. Dey, T. Mukhopadhyay, S.K. Sahu, G. Li, H. Rabitz, and S. Adhikari. Thermal uncertainty quantification in frequency responses of laminated composite plates. *Composites Part B: Engineering*, 80:186–197, 2015.

[37] B.J. Dobson and R. Drew. Experimental investigation of the effects of temperature on the dynamic properties of a carbon fibre-reinforced plate. *Composites*, 22(3):199–203, 1991.

[38] S.B. Dong, K.S. Pister, and R.L. Taylor. On the theory of laminated anisotropic shells and plates. *Journal of the Aerospace Sciences*, 29(8):969–975, 1962.

[39] P.C. Dumir, J.K. Nath, P. Kumari, and S. Kapuria. Improved efficient zigzag and third order theories for circular cylindrical shells under thermal loading. *Journal of Thermal Stresses*, 31(4):343–367, 2008.

[40] S. Dutton, D. Kelly, and A. Baker. *Composite Materials for Aircraft Structures*. American Institute of Aeronautics and Astronautics, Inc., Reston, Virginia, U.S.A., Second edition, 2004.

[41] S. Ebnesajjad. Introduction to plastics. In E. Baur, K. Ruhrberg, and W. Woishnis, editors, *Chemical Resistance of Engineering Thermoplastics*, Plastics Design Library, pages xiii–xxv. William Andrew Publishing, 2016.

[42] S. Elias, V. Matsagar, and T.K. Datta. Distributed tuned mass dampers for multi-mode control of benchmark building under seismic excitations. *Journal of Earthquake Engineering*, 23(7):1137–1172, 2019.

[43] A. Ferreira and N. Fantuzzi. *MATLAB codes for finite element analysis. Solids and structures*. Springer Nature, Switzerland, Second edition, 2020.

[44] I.C. Finegan and R.F. Gibson. Improvement of damping at the micromechanical level in polymer composite materials under transverse normal loading by the use of special fiber coatings. *Journal of Vibration and Acoustics, Transactions of the ASME*, 120(2):623–627, 1998.

[45] P.S. Frederiksen. Identification of temperature dependence for orthotropic material moduli. *Mechanics of Materials*, 13(1):79–90, 1992.

[46] P.S. Frederiksen. Application of an imroved model for the identification of material parameters. *Mechanics of Composite Materials and Structures*, 4(4):297–316, 1997.

[47] P.S. Frederiksen. Experimental procedure and results for the identification of elastic constants of thick orthotropic plates. *Journal of Composite Materials*, 31(4):360–382, 1997.

[48] T. Fukuda, N. Ohshima, and K. Hourai. Use of shape memory polymer for damping control of fiber composite materials. *Proceedings of the 9th International Conference on Composite Materials: Composites Design CADCOMP*, pages 323–328, 1993.

[49] B. Ganapathysubramanian and N. Zabaras. Sparse grid collocation schemes for stochastic natural convection problems. *Journal of Computational Physics*, 225(1):652–685, 2007.

[50] R. Ganesan and V.K. Kowda. Free-vibration of composite beam-columns with stochastic material and geometric properties subjected to random axial loads. *Journal of Reinforced Plastics and Composites*, 24(1):69–91, 2005.

[51] A. Garg and H.D. Chalak. A review on analysis of laminated composite and sandwich structures under hygrothermal conditions. *Thin-Wall Structures*, 142:205–226, 2019.

[52] D. Gay. *Composite Materials: Design and Applications*. CRC Press, New York, Third edition, 2014.

[53] M. Geradin and D.J. Rixen. *Mechanical Vibrations: Theory and Application to Structural Dynamics*. Wiley, West Sussex, U.K., 2015.

[54] R.G. Ghanem and P.D. Spanos. *Stochastic Finite Elements: A Spectral Approach*. Springer, New York, 1991.

[55] T.C. Godoy and M.T. Areias. Modeling and analysis of laminate composite plates with embedded active–passive piezoelectric networks. *Journal of Sound and Vibration*, 330(2):194–216, 2011.

[56] N. Grover, R. Sahoo, B.N. Singh, and D.K. Maiti. Influence of parametric uncertainties on the deflection statistics of general laminated composite and sandwich plates. *Composite Structures*, 171:158–169, 2017.

[57] R. Gueler. The virtues of passive damping for feedback controlled flexible structures. Master's thesis, Department of Aeronautics and Astronautics, Massachusetts Institute of Technology, U.S.A., 1991.

[58] J.C. Halpin. Effect of environmental factors on composite materials. *Techinal Report AFML-TR-67-423*, pages 1–61, 1969.

[59] J.C. Halpin and N.J. Pagano. Consequences of environmentally induced dilation in solids. *Techinal Report AFML-TR-68-395*, pages 1–32, 12 1969.

[60] M. Danial A. Hasan, Z.A.B. Ahmad, M. Salman Leong, and L.M. Hee. Enhanced frequency domain decomposition algorithm: a review of a recent development for unbiased damping ratio estimates. *Journal of Vibroengineering*, 20(5):1919–1936, 2018.

[61] Z. Hashin. Viscoelastic fiber reinforced materials. *AIAA Journal*, 4(8):1411–1417, 1966.

[62] Z. Hashin. Complex moduli of viscoelastic composites-I. general theory and application to particulate composites. *International Journal of Solids and Structures*, 6(5):539–552, 1970.

[63] Z. Hashin. Complex moduli of viscoelastic composites-II. fiber reinforced materials. *International Journal of Solids and Structures*, 6(6):797–807, 1970.

[64] C.T. Herakovich. Mechanics of composites: A historical review. *Mechanics Research Communications*, 41:1–20, 2012.

[65] M. Hoshiya and H.C. Shah. Free vibration of stochastic beam-column. *Journal of the Engineering Mechanics Division*, 97(4):1239–1255, 1971.

[66] B.-G. Hu and M.A. Dokainish. Damped vibration of laminated composite plates-modeling and finite element analysis. *Finite Elements in Analysis and Design*, 15(2):103–124, 1993.

[67] X.-L. Huang, H.-S. Shen, and J.-J. Zheng. Nonlinear vibration and dynamic response of shear deformable laminated plates in hygrothermal environments. *Composites Science and Technology*, 64(10-11):1419–1435, 2004.

[68] P. Jeyaraj, N. Ganesan, and C. Padmanabhan. Vibration and acoustic response of a composite plate with inherent material damping in a thermal environment. *Journal of Sound and Vibration*, 320(1):322–338, 2009.

[69] K.D. Jonnalagadda, T.R. Tauchert, and G.E. Blandford. High-order thermoelastic composite plate theories: An analytic comparison. *Journal of Thermal Stresses*, 16(3):265–284, 1993.

[70] J. Kaipio and E. Somersalo. *Statistical and Computational Inverse Problems*. Springer, New York, U.S.A., 2005.

[71] T. Kant, C.P. Arora, and J.H. Varaiya. Finite element transient analysis of composite and sandwich plates based on a refined theory and a mode superposition method. *Composite Structures*, 22(2):109–120, 1992.

[72] T. Kant and R.K. Khare. Finite element thermal stress analysis of composite laminates using a higher-order theory. *Journal of Thermal Stresses*, 17(2):229–255, 1994.

[73] T. Kant, D.R.J. Owen, and O.C. Zienkiewicz. A refined higher-order C^0 plate bending element. *Computers & Structures*, 15(2):177–183, 1982.

[74] T. Kant, J.H. Varaiya, and C.P. Arora. Finite element transient analysis of composite and sandwiched plates based on a refined theory and implicit time integration schemes. *Computerss and Structures*, 36(3):401–420, 1990.

[75] R.K. Kapania and S. Raciti. Recent advances in analysis of laminated beams and plates. Part I - shear effects and buckling. *AIAA Journal*, 27(7):923–935, 1989.

[76] S. Kapuria and G.G.S. Achary. An efficient higher order zigzag theory for laminated plates subjected to thermal loading. *International Journal of Solids and Structures*, 41(16):4661–4684, 2004.

[77] S. Kapuria, P. Kumari, and J.K. Nath. Efficient modeling of smart piezoelectric composite laminates: A review. *Acta Mechanica*, 214(1):31–48, Oct 2010.

[78] E.M. Kerwin. Damping of flexural waves by a constrained viscoelastic layer. *Journal of the Acoustical Society of America*, 31(7):952–962, 1959.

[79] R.K. Khare, T. Kant, and A.K. Garg. Closed-form thermo-mechanical solutions of higher-order theories of cross-ply laminated shallow shells. *Composite Structures*, 59(3):313–340, 2003.

[80] A. Kodakkal, S.K. Saha, K. Sepahvand, V.A. Matsagar, F. Duddeck, and S. Marburg. Uncertainties in dynamic response of buildings with non-linear base-isolators. *Engineering Structures*, 197:109423, 2019.

[81] V. Kodur, S. Venkatachari, V.A. Matsagar, and S.B. Singh. Test methods for characterizing the properties of fiber-reinforced polymer composites at elevated temperatures. *Polymers*, 14(9), 2022.

[82] J.R. Kommineni and T. Kant. Large deflection elastic and inelastic transient analyses of composite and sandwich plates with a refined theory. *Journal of Reinforced Plastics and Composites*, 12(11):1150–1170, 1993.

[83] A. Kumar, S.K. Saha, and V.A. Matsagar. Stochastic response analysis of elastic and inelastic systems with uncertain parameters under random impulse loading. *Journal of Sound and Vibration*, 461:114899, 2019.

[84] R. Kumar. Effects of hygrothermomechanical loading and uncertain system environments on flexural and free vibration response of shear deformable laminated plates: Stochastic finite element method micromechanical model investigation. *Journal of Frontiers of Aerospace Engineering*, 6(1):39–69, 2017.

[85] R. Kumar. Hygrothermally induced nonlinear free vibration response of laminated composite plates with random system properties: Stochastic finite element micromechanical model investigation. *Journal of Frontiers of Aerospace Engineering*, 6(2):116–145, 2017.

[86] R. Kumar, H.S. Patil, and A. Lal. Hygrothermoelastic free vibration response of laminated composite plates resting on elastic foundations with random system properties: Micromechanical model. *Journal of Thermoplastic Composite Materials*, 26(5):573–604, 2013.

[87] Y.V.S. Kumar and M. Mukhopadhyay. Transient response analysis of laminated stiffened plates. *Composite Structures*, 58(1):97–107, 2002.

[88] A. Lal and B.N. Singh. Effect of uncertain system properties on thermo-elastic stability of laminated composite plates under nonuniform temperature distribution. *International Journal of Applied Mechanics*, 02(02):399–420, 2010.

[89] A. Lal and B.N. Singh. Stochastic free vibration of laminated composite plates in thermal environments. *Journal of Thermoplastic Composite Materials*, 23(1):57–77, 2010.

[90] A. Lal, B.N. Singh, and R. Kumar. Static response of laminated composite plates resting on elastic foundation with uncertain system properties. *Journal of Reinforced Plastics and Composites*, 26(8):807–829, 2007.

[91] M.J. Lam, W.R. Saunders, and D.J. Inman. Modeling active constrained-layer damping using golla-hughes-mctavish approach. In C.D. Johnson, editor, *Smart Structures and Materials 1995: Passive Damping*, volume 2445, pages 86–97. International Society for Optics and Photonics, SPIE, 1995.

[92] D.-M. Lee and I. Lee. Vibration analysis of anisotropic plates with eccentric stiffeners. *Computers & Structures*, 57(1):99–105, 1995.

[93] H. Li, H. Wu, T. Zhang, B. Wen, and Z. Guan. A nonlinear dynamic model of fiber-reinforced composite thin plate with temperature dependence in thermal environment. *Composites Part B: Engineering*, 162:206–218, 2019.

[94] H. Li, T. Wu, Z. Gao, X. Wang, H. Ma, Q. Han, and Z. Qin. An iterative method for identification of temperature and amplitude dependent material parameters of fiber-reinforced polymer composites. *International Journal of Mechanical Sciences*, 184:105818, 2020.

[95] W. Li, Z. Lu, and D. Zhang. Stochastic analysis of unsaturated flow with probabilistic collocation method. *Water Resources research*, 45(2):183–197, 2009.

[96] L. Ljung. *System Identification - Theory for the User*. Prentice Hall PTR, New Jersey, 1999.

[97] N. Lüthen, S. Marelli, and B. Sudret. Sparse polynomial chaos expansions: Literature survey and benchmark. *SIAM/ASA Journal on Uncertainty Quantification*, 9(2):593–649, 2021.

[98] A. Maji and P.K. Mahato. Development and applications of shear deformation theories for laminated composite plates: An overview. *Journal of Thermoplastic Composite Materials*, 0(0):0892705720930765, 2020.

[99] A.Y. Malkin and A.I. Isayev. *Rheology: Concepts, Methods, and Applications*. ChemTec Publishing, Toronto, Second edition, 2012.

[100] Mallikarjuna and T. Kant. Free vibration of symmetrically laminated plates using a higher-order theory with finite element technique. *International Journal for Numerical Methods in Engineering*, 28(8):1875–1889, 1989.

[101] Mallikarjuna and T. Kant. A critical review and some results of recently developed refined theories of fiber-reinforced laminated composites and sandwiches. *Composite Structures*, 23(4):293–312, 1993.

[102] A. Mangala, M. Jayasuriya, S.N. Dwivedi, L. Louisiana, N.T. Sivaneri, and D.W. Lyons. Doubly curved laminated composite shells with hygrothermal conditioning and dynamic loads, Part 2: FEA and numerical results of shells of revolution. *Mechanics of Advanced Materials and Structures*, 9(1):69–97, 2002.

[103] A. Mangala, M. Jayasuriya, S.N. Dwivedi, N.T. Sivaneri, and D.W. Lyons. Doubly curved laminated composite shells with hygrothermal conditioning and dynamic loads, Part 1: A theoretical development and semielastic solution using a higher-order displacement field. *Mechanics of Advanced Materials and Structures*, 9(1):53–68, 2002.

[104] J.D.D. Melo and D.W. Radford. Viscoelastic characterization of transversely isotropic composite laminae. *Journal of Composite Materials*, 37(2):129–145, 2003.

[105] J.D.D. Melo and D.W. Radford. Time and temperature dependence of the viscoelastic properties of CFRP by dynamic mechanical analysis. *Composite Structures*, 70(2):240–253, 2005.

[106] K.P. Menard. *Dynamic Mechanical Analysis: A Practical Introduction*. CRC Press, New York, 1999.

[107] R.D. Mindlin. Influence of rotatory inertia and shear on flexural motions of isotropic, elastic plates. *Journal of Applied Mechanics*, 18(1):31–38, 1951.

[108] A. Mukherjee and M. Mukhopadhyay. Review of dynamic behaviour of stiffened plates. *The Shock and Vibration Digest*, 338(18):3–8, 1986.

[109] M. Mukhopadhyay and A. Mukherjee. Recent advances on the dynamic behaviour of stiffened plates. *The Shock and Vibration Digest*, 69(21):6–9, 1989.

[110] N.V.S. Naidu and P.K. Sinha. Nonlinear transient analysis of laminated composite shells in hygrothermal environments. *Composite Structures*, 72(3):280–288, 2006.

[111] N.S. Naik and A.S. Sayyad. An accurate computational model for thermal analysis of laminated composite and sandwich plates. *Journal of Thermal Stresses*, 42(5):559–579, 2019.

[112] N. Nanda and S. Pradyumna. Nonlinear dynamic response of laminated shells with imperfections in hygrothermal environments. *Journal of Composite Materials*, 45(20):2103–2112, 2011.

[113] S. Neumark. Concept of complex stiffness applied to problems of oscillations with viscous and hysteretic damping. Technical report, Aeronautical Research Council, London, 1962.

[114] T.D. Nguyen, H.Q. Jerry, F. Castro, and K.N. Long. A thermoviscoelastic model for amorphous shape memory polymers: Incorporating structural and stress relaxation. *Journal of the Mechanics and Physics of Solids*, 56(9):2792–2814, 2008.

[115] R.G. Ni and R.D. Adams. The damping and dynamic moduli of symmetric laminated composite beams - theoretical and experimental results. *Journal of Composite Materials*, 18(2):104–121, 1984.

[116] L. Nicolais, M. Meo, and E. Milella. *Composite Materials: A Vision for the Future*. Springer-Verlag, London, 2011.

[117] A.G. Niyogi, M.K. Laha, and P.K. Sinha. Finite element vibration analysis of laminated composite folded plate structures. *Shock and Vibration*, 6(5-6):273–283, 1999.

[118] O.O. Ochoa and J.N. Reddy. *Finite Eleemnt Analysis of Composite Laminates*. Kluwer Academic Publishers, London, UK, Second edition, 1992.

[119] J.T. Oden and E.A. Ripperger. *Mechanics of Elastic Structures*. McGraw-Hill, New York, U.S.A., 1984.

[120] National Academy of Sciences. Accelerated aging of materials and structures: The effects of long-term elevated-temperature exposure. Technical report, Washington, DC, 1996.

[121] M.D. Olson and C.R. Hazell. Vibration studies on some integral rib-stiffened plates. *Journal of Sound and Vibration*, 50(1):43–61, 1977.

[122] A.K. Onkar and D. Yadav. Non-linear free vibration of laminated composite plate with random material properties. *Journal of Sound and Vibration*, 272(3):627–641, 2004.

[123] P.V. Overschee and B.D. Moor. *Subspace Identification for Linear Systems*. Springer US, 1996.

[124] S. Pal and A.G. Niyogi. Application of folded plate formulation in analyzing stiffened laminated composite and sandwich folded plate vibration. *Journal of Reinforced Plastics and Composites*, 27(7):693–710, 2008.

[125] P.K. Parhi, S.K. Bhattacharyya, and P.K. Sinha. Hygrothermal effects on the dynamic behavior of multiple delaminated composite plates and shells. *Journal of Sound and Vibration*, 248(2):195–214, 2001.

[126] J.S. Park, C.G. Kim, and C.S. Hong. Stochastic finite element method for laminated composite structures. *Journal of Reinforced Plastics and Composites*, 14(7):675–693, 1995.

[127] B.P. Patel, M. Ganapathi, and D.P. Makhecha. Hygrothermal effects on the structural behaviour of thick composite laminates using higher-order theory. *Composite Structures*, 56(1):25–34, 2002.

[128] P. Pedersen and P.S. Frederiksen. Identification of orthotropic material moduli by a combined experimental/numerical method. *Measurement*, 10(3):113–118, 1992.

[129] X. Peng, D. Li, H. Wu, Z. Liu, J. Li, S. Jiang, and J. Tan. Uncertainty analysis of composite laminated plate with data-driven polynomial chaos expansion method under insufficient input data of uncertain parameters. *Composite Structures*, 209:625–633, 2019.

[130] T. Pervez and N. Zabaras. Transient dynamic and damping analysis of laminated anisotropic plates using a refined plate theory. *International Journal for Numerical Methods in Engineering*, 33(5):1059–1080, 1992.

[131] K.S. Pister and S.B. Dong. Elastic bending of layered plates. *Journal of the Engineering Mechanics Division*, 85(4):1–10, 1959.

[132] D. Punera, T. Kant, and Y.M. Desai. Thermoelastic analysis of laminated and functionally graded sandwich cylindrical shells with two refined higher order models. *Journal of Thermal Stresses*, 41(1):54–79, 2018.

[133] G. Qing, J. Qiu, and Y. Liu. Free vibration analysis of stiffened laminted plates. *International Journal of Solids and Structures*, 43:1357–1371, 2006.

[134] K.S. Ram and P.K. Sinha. Hygrothermal effects on the free vibration of laminated composite plates. *Journal of Sound and Vibration*, 158(1):133–148, 1992.

[135] M.D. Rao and S. He. Dynamic analysis and design of laminated composite beams with multiple damping layers. *AIAA Journal*, 31(4):736–745, 1993.

[136] S.P. Rawal and M.S. Misra. Measurement of mechanical and thermophysical properties of dimensionally stable materials for space applications. *NASA Contractor Report 18552*, pages 1–159, 1992.

[137] C. Ray and S.K. Satsangi. Finite element analysis of laminated hat-stiffened plates. *Journal of Reinforced Plastics and Composites*, 15(12):1174–1193, 1996.

[138] J.N. Reddy. A simple higher-order theory for laminated composite plates. *Journal of Applied Mechanics*, 51(4):745–752, 1984.

[139] J.N. Reddy. *Mechanics of Laminated Composite Plates and Shells: Theory and Analysis*. CRC Press, London, UK, Second edition, 2001.

[140] J.N. Reddy, R.A. Arciniega, and F. Moleiro. *Finite Element Analysis of Composite Plates and Shells*. John Wiley & Sons, Ltd., 2010.

[141] E. Reissner. The effect of transverse shear deformation on the bending of elastic plates. *Journal of Applied Mechanics*, 12(2):A69–A77, 1945.

[142] E. Reissner and Y. Stavsky. Bending and stretching of certain types of heterogeneous aeolotropic elastic plates. *Journal of Applied Mechanics*, 28(3):402–408, 09 1961.

[143] R. Rikards, A. Chate, W. Steinchen, A. Kessler, and A.K. Bledzki. Method for identification of elastic properties of laminates based on experiment design. *Composites Part B: Engineering*, 30(3):279–289, 1999.

[144] S.K. Saha, K. Sepahvand, V.A. Matsagar, A.K. Jain, and S. Marburg. Stochastic analysis of base-isolated liquid storage tanks with uncertain isolator parameters under random excitation. *Engineering Structures*, 57:465–474, 2013.

[145] D.A. Saravanos and C.C. Chamis. Unified micromechanics of damping for unidirectional fiber reinforced composites. Technical report, NASA, 1989.

[146] D.A. Saravanos and C.C. Chamis. Mechanics of damping for fiber composite laminates including hygro-thermal effects. *AIAA Journal*, 28(10):1813–1819, 1990.

[147] D.A. Saravanos and J.M. Pereira. Dynamic characteristics of specialty composite structures with embedded damping layers. *Journal of Vibration and Acoustics*, 117(1):62–69, 01 1995.

[148] P. Sasikumar, A. Venketeswaran, R. Suresh, and S. Gupta. A data driven polynomial chaos based approach for stochastic analysis of CFRP laminated composite plates. *Composite Structures*, 125:212–227, 2015.

[149] A.S. Sayyad and Y.M. Ghugal. On the free vibration analysis of laminated composite and sandwich plates: A review of recent literature with some numerical results. *Composite Structures*, 129:177–201, 2015.

[150] A.S. Sayyad and Y.M. Ghugal. Bending, buckling and free vibration of laminated composite and sandwich beams: A critical review of literature. *Composite Structures*, 171:486–504, 2017.

[151] C. Scarth and S. Adhikari. Modeling spatially varying uncertainty in composite structures using lamination parameters. *AIAA Journal*, 55(11):3951–3965, 2017.

[152] S. Seelecke and I. Müller. Shape memory alloy actuators in smart structures: Modeling and simulation. *Applied Mechanics Reviews*, 57(1-6):23–46, 2004.

[153] Y. Sefrani and J.-M. Berthelot. Temperature effect on the damping properties of unidirectional glass fibre composites. *Composites Part B: Engineering*, 37(4):346–355, 2006.

[154] K. Sepahvand. *Uncertainty Quantification in Stochastic Forward and Inverse Vibration Problems Using Generalized Chaos Expansion*. PhD thesis, Technische Universität Dresden, Dresden, Germany, 2008.

[155] K. Sepahvand. Spectral stochastic finite element vibration analysis of fiber-reinforced composites with random fiber orientation. *Composite Structures*, 145:119–128, 2016.

[156] K. Sepahvand. Stochastic finite element method for random harmonic analysis of composite plates with uncertain modal damping parameters. *Journal of Sound and Vibration*, 400:1–12, 2017.

[157] K. Sepahvand, F.S. Khosroshahi, C.A. Geweth, and S. Marburg. Stochastic structural dynamic analysis with random damping parameters. In *Proceedings of the 46th International Congress and Exposition on Noise Control Engineering*, 2017.

[158] K. Sepahvand and S. Marburg. Identification of composite uncertain material parameters from experimental modal data. *Probabilistic Engineering Mechanics*, 37:148–153, 07 2014.

[159] K. Sepahvand and S. Marburg. Non-sampling inverse stochastic numerical–experimental identification of random elastic material parameters in composite plates. *Mechanical Systems and Signal Processing*, 54-55:172–181, 2015.

[160] K. Sepahvand, S. Marburg, and H.-J. Hardtke. Uncertainty quantification in stochastic system using polynomial chaos expansion. *International Journal of Applied Mechanics*, 02(02):305–353, 2010.

[161] B. Sevim, A. Bayraktar, A.C. Altunişik, S. Adanur, and M. Akköse. Modal parameter identification of a prototype arch dam using enhanced frequency domain decomposition and stochastic subspace identification techniques. *Journal of Testing and Evaluation*, 38(5):1, 2010.

[162] H.-S. Shen, Y. Xiang, and Y. Fan. Nonlinear vibration of functionally graded graphene-reinforced composite laminated cylindrical shells in thermal environments. *Composite Structures*, 182:447–456, 2017.

[163] H.-S. Shen and D.-Q. Yang. Nonlinear vibration of functionally graded fiber-reinforced composite laminated cylindrical shells in hygrothermal environments. *Applied Mathematical Modelling*, 39(5-6):1480–1499, 2015.

[164] H.-S. Shen, J.-J. Zheng, and X.-L. Huang. Dynamic response of shear deformable laminated plates under thermomechanical loading and resting on elastic foundations. *Composite Structures*, 60(1):57–66, 2003.

[165] H.-S. Shen, J.-J. Zheng, and X.-L. Huang. The effects of hygrothermal conditions on the dynamic response of shear deformable laminated plates resting on elastic foundations. *Journal of Reinforced Plastics and Composites*, 23(10):1095–1113, 2004.

[166] B.N. Singh, D. Yadav, and N.G.R. Iyengar. A C^0 element for free vibration of composite plates with uncertain material properties. *Advanced Composite Materials*, 11(4):331–350, 2002.

[167] M. Sit and C. Ray. Temperature induced nonlinear effect on free vibration characteristics of fibre reinforced polymer bridge deck. *Journal of The Institution of Engineers (India): Series A*, 100(1):147–155, 2019.

[168] M. Sit, C. Ray, and D. Biswas. *Thermal stress analysis of laminated composite plates using third order shear deformation theory*. Advances in Structural Engineering: Mechanics, Volume One, 2015.

[169] Moumita Sit and Chaitali Ray. A third order nonlinear model to study the dynamic behaviour of composite laminated structures under thermal effect with experimental verification. *Composite Structures*, 212:106–117, 2019.

[170] C.M.M. Soares, M.M.D. Freitas, A.L. Araújo, and P. Pedersen. Identification of material properties of composite plate specimens. *Composite Structures*, 25(1):277–285, 1993.

[171] C. Soize and R.G. Ghanem. Physical systems with random uncertainties: Chaos representations with arbitrary probability measure. *SIAM Journal of Scientific Computing*, 26:395–410, 2004.

[172] H. Sol. *Identification of Anisotropic Plate Rigidities Using Free Vibration Data*. PhD thesis, Vrije Universiteit, Brussels, 1986.

[173] H. Sol, H. Rahier, and J. Gu. Prediction and measurement of the damping ratios of laminated polymer composite plates. *Materials*, 13(15), 2020.

[174] H. Sol, J.D. Visscher, and W.P. Wild. Identification of the viscoelastic material properties of orthotropic plates using a mixed numerical/experimental technique. *WIT Transactions on Modelling and Simulation*, 5:131–142, 1993.

[175] B. Sudret. *Polynomial chaos expansions and stochastic finite element methods*, page 624. 12 2014.

[176] B. Sudret and A.D. Kiureghian. Stochastic finite element methods and reliability: A state-of-the-art report. Technical report, Department of Civil & Environmental Engineering, University of California, Berkeley, 2000.

[177] C.T. Sun and Y.P. Lu. *Vibration Damping of Structural Elements*. Englewood Cliffs. Prentice Hall PTR, New Jersey, 1995.

[178] J.H. Tam. Identification of elastic properties utilizing non-destructive vibrational evaluation methods with emphasis on definition of objective functions: A review. *Structural and Multidisciplinary Optimization*, 61(4):1677–1710, 2020.

[179] J.H. Tam, Z.C. Ong, Z. Ismail, B.C. Ang, and S.Y. Khoo. Identification of material properties of composite materials using nondestructive vibrational evaluation approaches: A review. *Mechanics of Advanced Materials and Structures*, 24(12):971–986, 2017.

[180] M. Tanaka and G.S. Dulikravich, editors. *Inverse Problems in Engineering Mechanics*. Elsevier Science Ltd., Oxford, U.K., 1998.

[181] B.R. Thakur, S. Verma, B.N. Singh, and D.K. Maiti. Dynamic analysis of folded laminated composite plate using nonpolynomial shear deformation theory. *Aerospace Science and Technology*, 106:106083, 2020.

[182] P.A. Thompson, P. Bettess, and J.B. Caldwell. An isoparametric eccentrically stiffened plate bending element. *Engineering Computations*, 5:110–116, 1989.

[183] A. Treviso, B. Van Genechten, D. Mundo, and M. Tournour. Damping in composite materials: Properties and models. *Composites Part B: Engineering*, 78:144–152, 2015.

[184] M.A. Trindade, T.C. Godoy, C.C. Pagani Jr., and H.F.L. Santos. Passive, active and active-passive vibration control of plate structures using distributed piezoelectric patches. *11th World Congress on Computational Mechanics, WCCM 2014, 5th European Conference on Computational Mechanics, ECCM 2014 and 6th European Conference on Computational Fluid Dynamics, ECFD 2014*, pages 1505–1516, 2014.

[185] S.W. Tsai and H.T. Hahn. *Introduction to Composite Materials*. Technomic Publishing Company, Pennsylvania, U.S.A., 1980.

[186] E.E. Ungar and E.M. Kerwin. Loss factors of viscoelastic systems in terms of energy concepts. *Journal of The Acoustical Society of America*, 34:954–957, 1962.

[187] J.D. Visscher. *Identification of the Complex Stiffness Matrix of Orthotropic Materials by a Mixed Numerical Experimental Method*. PhD thesis, Vrije Universiteit, Brussels, 1995.

[188] J.D. Visscher, H. Sol, W.P.D. Wilde, and J. Vantomme. Identification of the complex moduli of thin fibre reinforced polymer plates using measured modal parameters. In *Proceedings of the EUROMECH Colloquium held in Kerkrade, The Netherlands, 7-9 April 1997*, pages 1–10. Kluwer Academic Publishers, 1997.

[189] J.D. Visscher, H. Sol, W.P.D. Wilde, and J. Vantomme. Identification of the damping properties of orthotropic composite materials using a mixed numerical experimental method. *Applied Composite Materials*, 4:13–33, 1997.

[190] J.M. Whitney and J.E. Ashton. Effect of environment on the elastic response of layered composite plates. *AIAA Journal*, 9:1708–1713, 08 1971.

[191] J.M. Whitney and N.J. Pagano. Shear deformation in heterogeneous anisotropic plates. *Journal of Applied Mechanics*, 37(4):1031–1036, 1970.

[192] C.Z. Xiao, D.X. Lin, and F. Ju. Finite Element Analysis on Modal Parameters of Anisotropic Laminated Plates. *Journal of Vibration, Acoustics, Stress, and Reliability in Design*, 110(4):473–477, 10 1988.

[193] D. Xiu and J.S. Hesthaven. High-order collocation methods for differential equations with random inputs. *SIAM Journal on Scientific Computing*, 27(3):1118–1139, 2006.

[194] D. Xiu and G.E. Karniadakis. The Wiener–Askey polynomial chaos for stochastic differential equations. *SIAM Journal on Scientific Computing*, 24(2):619–644, 2002.

[195] D. Xiu, D. Lucor, C.-H. Su, and G.E. Karniadakis. Stochastic modeling of flow-structure interactions using generalized polynomial chaos. *Journal of Fluids Engineering, Transactions of the ASME*, 124(1):51–59, 2002.

[196] D. Xiu, D. Lucor, C.-H. Su, and G.E. Karniadakis. Performance evaluation of generalized polynomial chaos. *Lecture Notes in Computer Science (including subseries Lecture Notes in Artificial Intelligence and Lecture Notes in Bioinformatics)*, 2660:346–354, 2003.

[197] P.C. Yang, C.H. Norris, and Y. Stavsky. Elastic wave propagation in heterogeneous plates. *International Journal of Solids and Structures*, 2(4):665–684, 1966.

[198] S. Yi, G.D. Pollock, M.F. Ahmad, and H.H. Hilton. Time-dependent analysis of anisotropic viscoelastic composite shell structures. *Computing Systems in Engineering*, 3(1-4):457–467, 1992.

[199] H. Yu, Z. Zhao, D.Y., and Chang Gao. A new composite plate/plate element for stiffened plate structures via absolute nodal coordinate formulation. *Composite Structures*, 247:112431, 2020.

[200] N. Zabaras and T. Pervez. Viscous damping approximation of laminated anisotropic composite plates using the finite element method. *Computer Methods in Applied Mechanics and Engineering*, 81(3):291–316, 1990.

[201] R.-X. Zhang, Q.-Q. Ni, A. Masuda, T. Yamamura, and M. Iwamoto. Vibration characteristics of laminated composite plates with embedded shape memory alloys. *Composite Structures*, 74(4):389–398, 2006.

[202] Y.X. Zhang and C.H. Yang. Recent developments in finite element analysis for laminated composite plates. *Composite Structures*, 88(1):147–157, 2009.

[203] O. C. Zienkiewicz, R. L. Taylor, and J. Z. Zhu. *The Finite Element Method: Its Basis and Fundamentals*. Butterworth-Heinemann, Oxford, U.K., Sixth edition, 2005.

[204] X. Zu, H. Wu, H. Lv, Y. Zheng, and H. Li. An amplitude- and temperature-dependent vibration model of fiber-reinforced composite thin plates in a thermal environment. *Materials (Basel)*, 13(7):1590, 2020.

Part II

Appended Publications

Publication 1

Reference: S. Chandra, K. Sepahvand, V.A. Matsagar, S. Marburg, Dynamic response of stiffened laminated composite plate in thermal environment. *Composite Structures*, 300, 116049, 2022.

Composite Structures 300 (2022) 116049

Contents lists available at ScienceDirect

Composite Structures

journal homepage: www.elsevier.com/locate/compstruct

Dynamic response of stiffened laminated composite plate in thermal environment

S. Chandra [a,*], K. Sepahvand [a], V.A. Matsagar [b], S. Marburg [a]

[a] Chair of Vibroacoustics of Vehicles and Machines, Department of Mechanical Engineering, Technical University of Munich (TUM), 85748 Garching b. Munich, Germany

[b] Department of Civil Engineering, Indian Institute of Technology (IIT) Delhi, Hauz Khas, New Delhi 110 016, India

ARTICLE INFO

Keywords:
Dynamic response
First-order shear deformation theory
Finite element
IM7-PEEK
Normal stress
Stiffened laminated composite plate
Thermal
Transformation

ABSTRACT

Composite materials are increasingly used in aerospace and automobile sectors. These materials are characterized by high stiffness and light-weight in comparison to conventional structural materials. During high-speed maneuvering of these vehicles, associated composite structures are subjected to dynamic loadings and are often exposed to varying thermal environments. To ensure high load carrying capacity and to avoid thermal buckling, stiffened laminated composite plates are preferred in some important structural components, e.g., aircraft's fuselages, wings etc., than unstiffened laminated composite plates. For safe designing of these structures, it is thus necessary to investigate the dynamic behavior of stiffened laminated composite plates in thermal environment. In this paper, the dynamic response of stiffened laminated composite plates made of polyetheretherketone (PEEK) with intermediate modulus (IM7) carbon fibers in thermal environment has been investigated. Furthermore, development of a generalized finite element (FE) formulation using an 8-node isoparametric plate element employing first-order shear deformation theory (FSDT) has also been presented to analyze unstiffened and stiffened laminated composite plates in thermal environment. Detailed parametric study reveals that the dynamic deflection and the corresponding normal stress decrease with adding stiffener, and decreases further with increasing depth of the stiffener in thermal environment.

1. Introduction

Laminated composite structures have enormous potential to be used in various engineering disciplines such as aerospace, transport, and naval industries, and construction of specialized civil engineering structures owing to inherent advantages in their material properties. Due to their superior elastic properties, such laminated composite plates offer higher load-carrying capacity than plates made of conventional structural materials. During high-speed maneuvering, specific parts of an aircraft and automobile structures often experience a rise in temperature while being subjected to a dynamic excitation. Further, dynamic response of composite structures varies significantly due to degradation in the elastic properties of the composite materials with changing temperature. Hence, accurately evaluating the dynamic response of unstiffened and stiffened laminated composite plates in thermal environment is crucial.

Theoretical and experimental studies on thermal effects in composite materials were initiated by Halpin [1]. Later, Halpin and Pagano [2], and Whitney and Ashton [3] have studied the bending, buckling, and vibration of laminated composite plates in thermal environment. Whitney and Ashton [3] used a generalized Duhamel–Neumann form of Hooke's law to develop governing equations of laminated composite plates using a semi-analytical method, e.g., the Ritz method. Later, the Ritz method [4] has been used to analyze different static [5] and dynamic [6,7] problems of composite plates with regular geometry. However, the difficulty of finding suitable basis functions limited the application of the Ritz method for complicated geometry and boundary conditions. Instead, the finite element (FE) method has been developed, where the plate domain is discretized into small finite elements applying simple basis functions, to overcome the limitation of the Ritz Method.

Nowadays, high-strength composites such as graphite–epoxy, carbon–epoxy, carbon–carbon, and intermediate modulus carbon fibers-polyetheretherketone (IM7-PEEK) are used to manufacture important structural components of aircraft and high-speed automobile vehicles, because they offer high elastic strength, high glass transition temperature, and low coefficient of thermal expansion. Ram and Sinha [8] showed that dimensionless natural frequencies of the graphite–epoxy laminated composite plate decrease with the increment in temperature

* Corresponding author.
E-mail address: sourav.chandra@tum.de (S. Chandra).

https://doi.org/10.1016/j.compstruct.2022.116049
Received 3 May 2021; Received in revised form 12 June 2022; Accepted 4 August 2022
Available online 9 August 2022
0263-8223/© 2022 Elsevier Ltd. All rights reserved.

and moisture concentration. They used the FE method for conducting dynamic analysis by incorporating the first-order shear deformation theory (FSDT) which includes residual stress developed due to variation in temperature and moisture concentration. Patel et al. [9] presented static, buckling, and free vibration analyses of thick composite plates using an 8-node element with thirteen degrees of freedom (DOFs) per node in hygrothermal environment. They derived the associated governing equations based on the Lagrangian equations of motion for static, buckling, and free vibration analyses. Furthermore, various stochastic analyses [10–12] of laminated composite plates using the FSDT are found in the literature. Mangala et al. [13,14] developed a hierarchical higher-order shear deformation theory (HSDT) to analyze doubly-curved laminated composite shells in hygrothermal environment. They studied free vibration response of laminated composite shells in different hygrothermal environments. Naidu and Sinha [15,16] presented non-linear static and free vibration analyses for thick doubly-curved graphite–epoxy laminated composite shells based on the Green–Lagrange strains in hygrothermal environment. Shen and Yang [17] and Shen et al. [18] carried out a non-linear flexural vibration analysis of functionally graded shear deformable fiber-reinforced laminated composite cylindrical shells in hygrothermal condition. Several studies [16,19–21] related to buckling analysis of laminated composite plates in thermal environment were also conducted, which are not under the scope of the present study.

Recently, the differential quadrature method (DQM) has appeared as an alternative numerical approach to analyze thick, moderately thick, and thin laminated skew plates and laminated composite plates [22,23]. In these studies the large amplitude free vibration response for the associated composite plates are evaluated based on the modified DQM after implementing suitable modification to the conventional DQM. Because of easier estimation of higher-order derivatives, application of the DQM is most suitable for non-linear free vibration analysis of thick plates, even though, the DQM can deal with regular geometry only, e.g., rectangular plates, and cylindrical and spherical shells [24]. The DQM was used [25] to study bending, buckling, and free vibration behavior of microcomposite plates reinforced by functionally graded single-walled carbon nanotube (FG-SWCNT) in hygrothermal environment. However, the FE method with the low-order (C^0) continuity has been widely used by research community to analyze thin laminated composite plates with regular and complicated geometries.

Transient response of unstiffened composite plates and shells in thermal environment had been assessed by some researchers. Parhi et al. [26] studied free and forced vibration response in terms of central deflection and normal stress, due to multiple delaminations in carbon–epoxy laminated composite shells using the FSDT at varying temperatures and moisture concentrations. Huang et al. [27] studied non-linear free vibration and dynamic response of the shear deformable laminated composite plates using the HSDT including hygrothermal effects. General von Kármán-type equation of motion was used in this study to incorporate the hygrothermal effect. Shen et al. [28,29] examined transient response in terms of central deflection and bending moment of the shear deformable laminated composite plates resting on an elastic foundation, based on the HSDT as proposed by Reddy [30]. Makhecha et al. [31] presented dynamic analysis of laminated composite plates subjected to thermal and mechanical loadings using a new higher order theory. Based on the formulation had proposed in [15], Naidu and Sinha [32] extended their investigation to study the non-linear transient response of thick doubly-curved graphite–epoxy laminated composite shells in thermal environment. However, in these successive studies [15,16,32], a comprehensive discussion related to the derivation of the governing equations is not readily available, particularly unavailable for stiffened structures. In an another study, Nanda and Pradyumna [33] investigated free vibration and transient response of graphite–epoxy laminated composite cylindrical and spherical shells with imperfection in hygrothermal environment. They used the FSDT with von Kármán-type non-linear kinematics without explicitly presenting development of the associated governing equations, and they also did not consider the effect of adding the stiffeners.

To extend the horizon of the research, some related studies of composite plates in thermal environment are included herein. Bandyopadhyay et al. [34] investigated transient response of the delaminated pretwisted conical composite shells due to multiple low-velocity impacts in a hygrothermal environment. Malekzadeh and Monajjemzadeh [35] studied dynamic response of elastically supported functionally graded (FG) plates subjected to a concentrated moving load in thermal environment. Non-linear thermal flutter analysis of supersonic symmetric laminated composite plates was presented by Niu et al. [36], employing the DQM. Non-linear dynamic analysis of composite plates, subjected to a harmonic excitation, with initial geometric imperfection was studied in [37]. A stochastic dynamic response analysis for graphite–epoxy laminated composite plates due to random temperature increment was presented by Chandra et al. [38], employing the FSDT for conducting the dynamic analysis. Furthermore, various FE formulations based on the HSDT [39–46] and zigzag theory [47,48] have been developed to evaluate the thermoelastic stress distribution in the laminated composite and sandwich plates subjected to static loading. In this context, recently Garg and Chalak [49] have provided a state-of-the-art review on the application of various FE formulations for analysis of laminated composite and sandwich plate and shell structures in hygrothermal environment.

Unlike unstiffened laminated composite plates, stiffened laminated composite plates offer reduction in the dynamic deflection, and have thereby become an attractive alternative for response reduction with a minimum weight penalty. Thus, stiffened plate type structures are advantageously used in aircraft fuselages, car bodies, hulls of the ship, and bridge decks for avoiding large deflection and buckling phenomenon. However, it is observed from the literature review that transient response analysis in thermal environments has been primarily restricted to unstiffened plates and shells. Herein, this research gap is addressed by conducting a detailed dynamic analysis of stiffened laminated composite plates in a thermal environment.

With the inception of the idea of applying stiffeners in a structural system, various FE models have been developed to study the bending and dynamic behaviors of isotropic [50–52] and orthotropic [51–54] stiffened plates. Attaf and Hollaway [55] had first presented a vibration study of an eccentrically stiffened glass-reinforced plastic composite plate subjected to in-plane loads using a 4-node plate element. Lee and Lee [56] investigated the influence of the stiffener size and location by conducting a free vibration analysis. They idealized the stiffener as a Timoshenko beam element. Chattopadhyay et al. [57] analyzed a blade-stiffened composite plate using an 8-node isoparametric stiffened plate bending element. Qing et al. [58] studied free vibration behavior of a stiffened laminated composite plate by accounting the compatibility of displacement and stress between the plate and stiffener. In their study, the plate has been modeled by triangular elements whereas the stiffener has been modeled with refined beam and torsional elements. Talebitooti et al. [59] and Golchi et al. [60] used the DQM to study the buckling and dynamic behaviors of FG orthogonally stiffened cylindrical shells and truncated conical shells, respectively. However, due to easier implementation, the FE method was preferred over the DQM for analyzing stiffened structures.

Very limited numbers of study on stiffened laminated composite plates are available in the literature, and the available studies are predominantly related to free vibration analysis using the FE method. Patro et al. [61] presented a brief discussion on free vibration response of stiffened laminated composite plates in thermal environment using the FE model. Sit and Ray [62] evaluated natural frequencies of a bridge deck with closely-spaced box stiffeners made of a glass fiber-reinforced polymer (GFRP) composite plate with increasing temperature. Moreover, Ray and Satsangi [63] presented stress analysis of hat-stiffened laminated composite plates subjected to transverse static

loading. Yu et al. [64] presented a composite plate–plate element model which describes the mechanical behavior of a stiffened plate structure using an absolute nodal coordinate formulation. This model is more appropriate for solving a large deformation problem. The eigenfrequency and random modal damping of a stiffened laminated composite plate for various lamina sequences were studied using the FSDT by Chandra et al. [65]. Assuming the importance of the stability aspect of stiffened composite structures, the maximum buckling load of stiffened laminated shell panels, based on the particle swarm optimization (PSO) and genetic algorithm (GA), was evaluated in [66]. Finally, some experimental modal analyses of stiffened laminated composite plates in thermal environment were reported [67,68] in recent years.

Limited literature is available on the studies related to transient response of stiffened laminated composite plates. Kumar and Mukhopadhyay [69] presented the transient response analysis of an arbitrarily oriented stiffened laminated composite plate using the FSDT and triangular plate bending elements. Free and forced vibration response of stiffened laminated and sandwich folded plates for various crank angles have been studied by Pal and Niyogi [70]. They modeled the plate and stiffener using 9-node plate elements considering an additional drilling DOF per node with proper transformation based on the FSDT which was originally proposed by Niyogi et al. [71] for analysis of laminated composite folded plate structures. Additionally, a few studies [72–74] on transient analysis of stiffened plates and shells subjected to air blast loading are available in the literature. Goel et al. [75] investigated the dynamic response of different stiffener configurations for a rectangular plate subjected to air blast loading. However, these studies did not account for any thermal effect.

A careful synthesis of the literature suggests that a significant research contribution, especially on understanding bending and free vibration [8,9,14,15,32] behaviors of the composite structures in thermal environment, using various plate theories have been reported for laminated composite plates and shells. However, dynamic analysis of stiffened laminated composite plates in thermal environment is almost absent in the literature, and it would be necessary to investigate the dynamic deflection experienced, and stress induced in these plates at different thermal environments. This analysis, further contributes to understand response reduction characteristics of stiffened laminated composite plates in comparison to the corresponding unstiffened plates in varying thermal environments. Moreover, sequential development of a generalized FE formulation based on the energy equation for analysis of unstiffened and stiffened laminated composite plates in thermal environment is not readily available in the literature. In this context, the novel contributions of this study are in two folds: firstly, a systematic development of the generalized FE formulation for dynamic analysis of unstiffened and stiffened laminated composite plates with reference to the Hamilton's variational principle including the effect of temperature variation, and secondly, a detailed dynamic analysis for stiffened laminated composite plates in thermal environment for different orientations of the stiffener and lamina sequences and subsequently understand the response reduction characteristics of the stiffened plates. The systematic development of the generalized FE formulation can further be extended for dynamic analysis of stiffened shells, and unstiffened and stiffened folded plates in thermal environment. Overall, the detailed dynamic analysis gives a deep insight on the dynamic behavior of these plates for their industrial application in thermal environment.

To address the efficient application of stiffened laminated composite plates in a real-life situation, various parametric studies have been conducted in thermal environment that varies between 0 °C and 125 °C temperature. Here, dynamic response of the deflection and normal stress for stiffened laminated composite plates at different temperatures is evaluated for various parameters such as lamina sequences, plates thickness, stiffener orientations and depths. The main objectives of the present study include the following: (a) to conduct a comparative study of eigenfrequency in terms of non-dimensional frequency (NDF) of unstiffened and stiffened IM7-PEEK laminated composite plates for various lamina sequences at different temperatures; (b) to assess the transient response of the deflection and normal stress of unstiffened and stiffened IM7-PEEK laminated composite plates considering various lamina sequences and depths of stiffener at different temperatures; (c) to investigate the effect of the addition of the stiffeners for reducing the amplitude of transient response of the deflection and normal stress with reference to an unstiffened plate in various thermal environments.

The layout of this paper can briefly be summarized as follows. Section 2 describes the FE formulation developed for dynamic analysis of unstiffened and stiffened laminated composite plates in a thermal environment. Next, a detailed validation study is carried out and presented in Section 3. In Section 4, results from various parametric studies are reported to understand the behavior of stiffened laminated composite plates in thermal environment. Finally, conclusions derived from the present study are summarized in Section 5.

2. Mathematical formulation

In this section, an FE formulation is presented for unstiffened and stiffened laminated composite plates to evaluate their transient response of the deflection and normal stress in various thermal environments. The FE formulation is established to analyze a stiffened laminated composite plate (cf. Fig. 1(a)) with length, L; width, W; uniform thickness, h; and stiffener depth, d_s. A laminate consisting of n numbers of unidirectional lamina with equal thickness is considered for the analysis. The FE formulation is developed by employing the FSDT, assuming that the thickness of the laminate is very small in comparison with the in-plane dimensions. It is assumed during analysis of stiffened plates that the plate and stiffener are in perfect contact. An 8-node isoparametric plate element with five DOFs and one drilling DOF per node (cf. Fig. 1(b)) has been implemented here with the proper transformation to establish a generalized formulation for analyzing unstiffened and stiffened laminated composite plates in thermal environments. The constitutive relationship of unstiffened plate and the stiffener are developed based on the five DOFs, and then the drilling DOF of the plate element has been included into the FE formulation to perform the transformation to consider the stiffener orientation. The formulation adopted here for analyzing stiffened plates is known as folded plate formulation [71].

2.1. Constitutive relationship of the composite laminate

In equivalent single layer theory such as the FSDT, the mid-plane is considered as the reference plane to evaluate the displacement field. A generalized displacement vector, $\{\bar{d}\} = \{u \quad v \quad w \quad \theta_x \quad \theta_y\}^T$, based on the FSDT is expressed, assuming that the normal to the mid-plane of the plate remains straight before and after bending. In FSDT, the non-linear distribution of the transverse shear strain is considered by employing a shear correction factor, $\varkappa = (5/6)$ [8]. The generalized displacement field of the composite laminate at a distance z from the mid-plane (Fig. 1(a)) is expressed as

$$\begin{aligned} u &= u_0 + z\theta_y, \\ v &= v_0 - z\theta_x, \\ w &= w_0. \end{aligned} \tag{1}$$

Here, u and v are in-plane translations along the x and y axes, respectively; w is out-of-plane deformation along the z axis; and rotations of the transverse normal about the x and y axes are denoted by θ_x and θ_y, respectively. In Fig. 1(a), rotation about the z axis is denoted by θ_z. Parameters u_0, v_0, and w_0 are mid-plane displacements along the x, y, and z axes, respectively. Shear rotations, φ_x and φ_y, in the $x-z$ and $y-z$ planes of the composite plate are evaluated as

$$\begin{aligned} \varphi_x &= w_{,x} + \theta_y, \\ \varphi_y &= w_{,y} - \theta_x. \end{aligned} \tag{2}$$

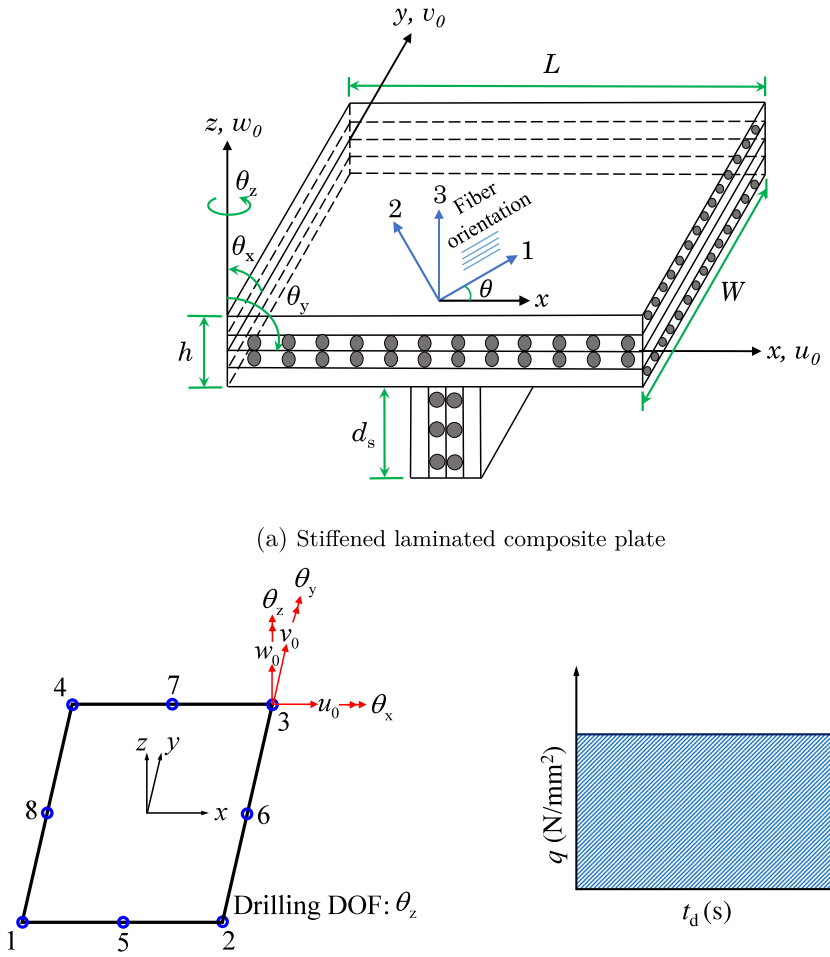

(a) Stiffened laminated composite plate

(b) 8-node isoparametric element

(c) Pulse loading

Fig. 1. (a) Stiffened laminated composite plate, showing the positive direction of the displacement components of a laminate in the laminate coordinate (x, y, z) system, and fiber orientation, θ, for a particular lamina in the lamina coordinate (1, 2, 3) system; (b) 8-node C^0 isoparametric element showing DOFs at each node including θ_z drilling DOF; (c) Time history of pulse loading for a duration of t_d s with a amplitude of q N/mm^2.

The elements of the linear strains vector, $\{\varepsilon\} = \{\varepsilon_x \ \varepsilon_y \ \gamma_{xy} \ \gamma_{xz} \ \gamma_{yz}\}^T$, at a distance z from the mid-plane of the laminate is derived from Eqs. (1) and (2), and written in the form of

$$\begin{aligned}
\varepsilon_x &= u_{0,x} + z\theta_{y,x},\\
\varepsilon_y &= v_{0,y} - z\theta_{x,y},\\
\gamma_{xy} &= u_{0,y} + v_{0,x} + z(\theta_{y,y} - \theta_{x,x}),\\
\gamma_{xz} &= \varphi_x,\\
\gamma_{yz} &= \varphi_y.
\end{aligned} \tag{3}$$

The linear mid-plane strain terms from Eq. (3) are now defined as $\varepsilon_{0x} = u_{0,x}$, $\varepsilon_{0y} = v_{0,y}$, $\gamma_{0xy} = (u_{0,y} + v_{0,x})$, $\kappa_x = \theta_{y,x}$, $\kappa_y = -\theta_{x,y}$, and $\kappa_{xy} = (\theta_{y,y} - \theta_{x,x})$. The stress–strain relationship for the k^{th} lamina is expressed in terms of the laminate coordinate (x, y, z) system for uniform increment in temperature, ΔT, as

$$\{\sigma\}_k = [Q]_k\{\{\varepsilon\}_k - \{\alpha\}_k\Delta T\}. \tag{4}$$

In this equation, the stress vector, $\{\sigma\}_k = \{\sigma_x \ \sigma_y \ \tau_{xy} \ \tau_{xz} \ \tau_{yz}\}_k^T$, for the k^{th} lamina is obtained by relating linear and thermal strains employing the transformed reduced stiffness matrix, $[Q]_k$, for the k^{th} lamina represented in terms of the fiber angle, θ, and elastic constants of the lamina [8]. The coefficients of thermal expansion of a lamina is expressed in the laminate coordinate (x, y, z) system, as $\{\alpha\} = \{\alpha_x \ \alpha_y \ \alpha_{xy} \ 0 \ 0\}^T$. Henceforth, the stress–strain relationship of a lamina in thermal environment is expressed in the laminate coordinate (x, y, z) system.

The stress–strain relationship of the lamina is then integrated over the thickness of the laminate. As a consequence, the stress vector, $\{\sigma\}$, leads to stress-resultant vector, $\{F_r\} = \{N_x \ N_y \ N_{xy} \ M_x \ M_y \ M_{xy} \ Q_x \ Q_y\}^T$, and the corresponding strain vector, $\{\varepsilon\}$, leads to mid-plane strain vector, $\{\varepsilon^*\}$. Thus, stress-resultant vector, $\{F_r\}$, of the laminate is derived by integrating Eq. (4) over the thickness of the laminate comprising of all n numbers of lamina, and can be expressed as

$$\{F_r\} = [D]\{\{\varepsilon^*\} - \{e^*\}\}, \tag{5}$$

where the mid-plane strain vector, $\{\varepsilon^*\}$, of the composite laminate is given by

$$\{\varepsilon^*\} = \{\varepsilon_{0x} \ \varepsilon_{0y} \ \gamma_{0xy} \ \kappa_x \ \kappa_y \ \kappa_{xy} \ \gamma_{xz} \ \gamma_{yz}\}^T, \tag{6}$$

and the corresponding mid-plane thermal strain vector, $\{e^*\}$, is given by

$$\{e^*\} = \{e_x \ \ e_y \ \ e_{xy} \ \ 0 \ \ 0 \ \ 0 \ \ 0 \ \ 0\}^T. \tag{7}$$

Here, thermal stress-resultant vector, $\{F_N\} = [D]\{e^*\}$, is defining as, $\{F_N\} = \{N_{Nx} \ N_{Ny} \ N_{Nxy} \ M_{Nx} \ M_{Ny} \ M_{Nxy} \ 0 \ 0\}^T$. In Eq. (5), the stress-resultant and mid-plane strain relationship matrix, $[D]$, is

given as

$$[D]=\left[\begin{array}{ccc|ccc|cc} A_{11} & A_{12} & A_{16} & B_{11} & B_{12} & B_{16} & 0 & 0 \\ A_{21} & A_{22} & A_{26} & B_{21} & B_{22} & B_{26} & 0 & 0 \\ A_{61} & A_{62} & A_{66} & B_{61} & B_{62} & B_{66} & 0 & 0 \\ \hline B_{11} & B_{12} & B_{16} & D_{11} & D_{12} & D_{16} & 0 & 0 \\ B_{21} & B_{22} & B_{26} & D_{21} & D_{22} & D_{26} & 0 & 0 \\ B_{61} & B_{62} & B_{66} & D_{61} & D_{62} & D_{66} & 0 & 0 \\ \hline 0 & 0 & 0 & 0 & 0 & 0 & \bar{A}_{44} & \bar{A}_{45} \\ 0 & 0 & 0 & 0 & 0 & 0 & \bar{A}_{54} & \bar{A}_{55} \end{array}\right], \tag{8}$$

with $[D]$ being a symmetric-matrix, i.e., $A_{ij} = A_{ji}$, $B_{ij} = B_{ji}$, $D_{ij} = D_{ji}$, and $\bar{A}_{ij} = \bar{A}_{ji}$, where

$$\begin{aligned} A_{ij} &= \sum_{k=1}^{n}\int_{z_{k-1}}^{z_k}[Q_{ij}]_k \mathrm{d}z, \quad i,j=1,2,6 \\ B_{ij} &= \sum_{k=1}^{n}\int_{z_{k-1}}^{z_k}[Q_{ij}]_k (z)\mathrm{d}z, \quad i,j=1,2,6 \\ D_{ij} &= \sum_{k=1}^{n}\int_{z_{k-1}}^{z_k}[Q_{ij}]_k (z^2)\mathrm{d}z, \quad i,j=1,2,6 \end{aligned} \tag{9}$$

and

$$\bar{A}_{ij} = \sum_{k=1}^{n}\int_{z_{k-1}}^{z_k}\varkappa[Q_{ij}]_k \mathrm{d}z, \quad i,j=4,5 \text{ and } \varkappa = 5/6. \tag{10}$$

Here, $[Q_{ij}]_k$ (cf. Eq. (A.1)) is transformed reduced stiffness matrix of the k^{th} lamina in the laminate coordinate (x, y, z) system, and elements of the corresponding matrix are denoted by $(Q_{ij})_k$ for the kth lamina. Thus, $[D]$ matrix is obtained by $(Q_{ij})_k$ are obtained from $(C_{ij})_k$, after proper transformation from the lamina coordinate (1, 2, 3) system based on the fiber orientation to the laminate coordinate (x, y, z) system for the k^{th} lamina. $(C_{ij})_k$ are the elements of the stress–strain matrix $[C]_k$ (cf. Eq. (A.2)) for the k^{th} lamina in the lamina coordinate (1, 2, 3) system. Here, E_{11} and E_{22} are elastic moduli; G_{12}, G_{13}, and G_{23} are shear moduli; and ν_{12} and ν_{21} denote Poisson's ratios of the lamina in the lamina coordinate (1, 2, 3) system. Moreover, while calculating the $[D]$ matrix at a given temperature, the corresponding temperature-dependent elastic moduli, shear moduli, and Poisson's ratio of the composite lamina are considered.

Components of the initial strain vector, $\{\varepsilon_{nt}\} = \{\varepsilon_{x_{nt}} \ \varepsilon_{y_{nt}} \ \gamma_{xy_{nt}} \ \gamma_{xz_{nt}} \ \gamma_{yz_{nt}}\}^T$, due to the thermal load in static condition are described by the non-linear portion of the overall strain, and are given as

$$\begin{aligned} \varepsilon_{x_{nt}} &= \frac{1}{2}(u_{,x}^2 + v_{,x}^2 + w_{,x}^2), \\ \varepsilon_{y_{nt}} &= \frac{1}{2}(u_{,y}^2 + v_{,y}^2 + w_{,y}^2), \\ \gamma_{xy_{nt}} &= (u_{,x}u_{,y} + v_{,x}v_{,y} + w_{,x}w_{,y}), \\ \gamma_{xz_{nt}} &= (u_{,x}u_{,z} + v_{,x}v_{,z}), \\ \gamma_{yz_{nt}} &= (u_{,y}u_{,z} + v_{,y}v_{,z}). \end{aligned} \tag{11}$$

The displacement terms (i.e., u, v, and w) in right side of Eq. (11) are expressed in terms of the mid-plane displacement with reference to Eq. (1). In this way, the initial strain vector, $\{\varepsilon_{nt}\}$, can be written in a compact from, as

$$\{\varepsilon_{nt}\} = \frac{1}{2}[R]\{d^*\}, \tag{12}$$

where $[R]$ is relationship matrix of non-linear strain vector, $\{\varepsilon_{nt}\}$, and vector of partial derivative of displacement, $\{d^*\}$, (cf. Eq. (A.3)). The vector of partial derivative of displacement, $\{d^*\} = [G]\{d\}$, is written as

$$\{d^*\} = \{u_{0,x} \ u_{0,y} \ v_{0,x} \ v_{0,y} \ w_{0,x} \ w_{0,y} \ \theta_{x,x} \ \theta_{x,y} \ \theta_{y,x} \ \theta_{y,y} \ \theta_x \ \theta_y\}^T, \tag{13}$$

where $[G]$ is the shape function matrix (cf. Eq. (A.4)) correspond to $\{d^*\}$, and $\{d\} = \{u_0 \ v_0 \ w_0 \ \theta_x \ \theta_y\}^T$ is the mid-plane displacement of laminate.

2.2. Equations of motion

The equations of motion of the composite laminate in thermal environment are derived based on the Hamilton's variational principle, as

$$\int_{t_1}^{t_2}\delta(\mathbb{E}-\mathbb{K})\mathrm{d}t = 0. \tag{14}$$

Here, $\mathbb{E}$ and $\mathbb{K}$ are total potential and kinetic energies, respectively, within an arbitrary time interval (t_1, t_2). The total potential energy, $\mathbb{E}$, can be written as a summation of strain energy, $\mathbb{U}$, of the laminate, and work done, $\mathbb{W}$, by externally applied uniformly distributed pulse loading, $q(t)$, (cf. Fig. 1(c)) for a duration of t_d s in the direction of the generalized displacement vector, $\{d\}$, i.e., $\mathbb{E} = \mathbb{U} - \mathbb{W}$. The total potential energy, $\mathbb{E}$, can be stated for the composite laminate in the thermal environment, which is expressed as

$$\begin{aligned} \mathbb{E} = &\left(\frac{1}{2}\int_A\{\varepsilon^*\}^T[D]\{\varepsilon^*\}\mathrm{d}A + \frac{1}{2}\int_A\{d^*\}^T[S_r]\{d^*\}\mathrm{d}A\right) \\ &- \left(\int_A\{d\}^T\{q(t)\}\mathrm{d}A\right), \end{aligned} \tag{15}$$

in which $[S_r]$ (cf. Box II) is the initial-stress resultant matrix. The initial stress-resultant vector, $\{F^i\} = \{N_x^i \ N_y^i \ N_{xy}^i \ M_x^i \ M_y^i \ M_{xy}^i \ Q_x^i \ Q_y^i\}^T$, is induced into the composite laminate due to variation in the temperature under static condition. The externally applied load vector is denoted by $\{q(t)\}$.

The kinetic energy, $\mathbb{K}$, of the composite laminate is presented as

$$\mathbb{K} = \frac{1}{2}\int_A\{\dot{d}\}^T[\bar{M}]\{\dot{d}\}\mathrm{d}A, \tag{16}$$

where $\{\dot{d}\}$ is the velocity vector in accordance with $\{d\}$. In Eq. (16), $[\bar{M}]$ is the inertia matrix of the composite laminate, and given as

$$[\bar{M}] = \begin{bmatrix} \bar{p} & 0 & 0 & 0 & 0 \\ 0 & \bar{p} & 0 & 0 & 0 \\ 0 & 0 & \bar{p} & 0 & 0 \\ 0 & 0 & 0 & \bar{q} & 0 \\ 0 & 0 & 0 & 0 & \bar{q} \end{bmatrix}, \tag{17}$$

in which $(\bar{p}, \bar{q}) = \int_{-h/2}^{h/2}\rho(1, z^2)\mathrm{d}z$, and ρ denotes the density of the composite laminate. The expression for equation of motion is formed by combining Eqs. (15) and (16) into the Hamilton's variational statement in Eq. (14), and presented as

$$\begin{aligned} \delta\int_{t_1}^{t_2}\Bigg[&\frac{1}{2}\int_A\{\varepsilon^*\}^T[D]\{\varepsilon^*\}\mathrm{d}A + \frac{1}{2}\int_A\{d^*\}^T[S_r]\{d^*\}\mathrm{d}A - \\ &\int_A\{d\}^T\{q(t)\}\mathrm{d}A - \frac{1}{2}\int_A\{\dot{d}\}^T[\bar{M}]\{\dot{d}\}\mathrm{d}A\Bigg]\mathrm{d}t = 0. \end{aligned} \tag{18}$$

The Hamilton's variational principle as derived in Eq. (18) is further used to develop the FE formulation of the composite laminate under thermal environment in the next section.

2.3. Finite element formulation

The orthotropic laminated composite plate is mathematically modeled by employing the finite element method (FEM) where solution domain is discretized into finite subdomains. The entire structural domain is discretized by an 8-node C^0 isoparametric plate elements with five DOFs, i.e., u_0, v_0, w_0, θ_x, and θ_y, at each node, as shown in Fig. 1(b). The time dependent mid-plane displacement vector, $\{d(t)\}$ of an element, 'e' is expressed in terms of the elemental nodal displacement vector, $\{d_e(t)\}$, using an 8-node serendipity interpolation functions, $[N]$, [8], and is expressed as

$$\{d(t)\} = [N]\{d_e(t)\}. \tag{19}$$

$$\begin{Bmatrix} u_0 \\ v_0 \\ w_0 \\ \theta_x \\ \theta_y \\ \theta_z \end{Bmatrix} = \begin{bmatrix} \cos(x',x) & \cos(y',x) & \cos(z',x) & 0 & 0 & 0 \\ \cos(x',y) & \cos(y',y) & \cos(z',y) & 0 & 0 & 0 \\ \cos(x',z) & \cos(y',z) & \cos(z',z) & 0 & 0 & 0 \\ 0 & 0 & 0 & \cos(x',x) & \cos(y',x) & \cos(z',x) \\ 0 & 0 & 0 & \cos(x',y) & \cos(y',y) & \cos(z',y) \\ 0 & 0 & 0 & \cos(x',z) & \cos(y',z) & \cos(z',z) \end{bmatrix} \begin{Bmatrix} u'_0 \\ v'_0 \\ w'_0 \\ \theta'_x \\ \theta'_y \\ \theta'_z \end{Bmatrix}, \tag{26}$$

Box I.

Accordingly, the mid-plane strain vector, $\{\varepsilon^*(t)\}$, is calculated from the known nodal displacement vector employing the strain–displacement matrix, $[B]$, [71] with reference to Eqs. (6) and (19), as

$$\{\varepsilon^*(t)\} = [B]\{d_e(t)\}. \tag{20}$$

The mathematical statement of the Hamilton's variational principle for the element, '*e*', is derived with reference to Eq. (18), and presented as

$$\int_{t_1}^{t_2} \Bigg[\int_{A_e} \delta\{d_e(t)\}^T [B]^T [D][B]\{d_e(t)\} dA_e + \int_{A_e} \delta\{d_e(t)\}^T [G]^T [S_r][G]\{d_e(t)\} dA_e - \int_{A_e} \delta\{d_e(t)\}^T [N]^T \{q(t)\} dA_e + \int_{A_e} \delta\{d_e(t)\}^T [N]^T [\bar{M}][N]\{\ddot{d}_e(t)\} dA_e \Bigg] dt = 0, \tag{21}$$

where $[G]$ is the matrix of shape functions which is given in Eq. (A.4). Shape function matrix for 8-node isoparametric element is shown by $[N]$. Since, the virtual displacement vector, $\delta\{d_e(t)\}$, is arbitrary in nature, Eq. (21) is valid for any virtual displacement, and the FE model for the element, '*e*', of the laminated composite plate is written in the form of

$$\left[[K_e]+[K_{Ge}]\right]\{d_e(t)\}+\left[M_e\right]\{\ddot{d}_e(t)\}=\{P_e(t)\}. \tag{22}$$

Here, the elemental stiffness matrix, $[K_e]$; the elemental geometric stiffness matrix, $[K_{Ge}]$; and the elemental mass matrix, $[M_e]$, are obtained as

$$\begin{aligned} [K_e] &= \int_{A_e} [B]^T [D][B] dA_e, \\ [K_{Ge}] &= \int_{A_e} [G]^T [S_r][G] dA_e, \\ [M_e] &= \int_{A_e} [N]^T [\bar{M}][N] dA_e. \end{aligned} \tag{23}$$

The elemental geometric stiffness matrix, $[K_{Ge}]$, is developed for initial deformation due to thermal load. The elemental dynamic load vector, $\{P_e(t)\}$, is given by

$$\{P_e(t)\} = \int_{A_e} [N]^T \{q(t)\} dA_e. \tag{24}$$

Elemental thermal force vector, $\{P_{Ne}\}$, due to thermal stress-resultant vector, $\{F_N\}$, is evaluated as

$$\{P_{Ne}\} = \int_{A_e} [B]^T \{F_N\} dA_e. \tag{25}$$

2.4. Transformation matrix for stiffened plate

A transformation matrix, $[\bar{\mathcal{T}}]$, is developed to relate the local displacement vector, $\{d\}$, of a unstiffened plate and stiffener, and the global displacement vector, $\{d'\}$, of a stiffened plate as shown in Fig. 2. The displacement vectors, $\{d\}$ and $\{d'\}$, are expanded by appending θ_z drilling DOF (cf. Fig. 1(b)) prior to the transformation. This relationship is given in Box I, where $\cos(x', x)$ represents the direction cosine of the least angle between positive x and x' axes, and the subsequent direction cosine terms also possess the similar meaning. In the FE formulation, transformation matrix, $[\bar{\mathcal{T}}]$, for each nodal displacement is written in compact form with reference to Box I, as

$$\{d\} = [\bar{\mathcal{T}}]\{d'\}. \tag{27}$$

The transformation matrix, $[\bar{\mathcal{T}}]$, possesses the property of orthogonality. Finally, the transformed elemental stiffness matrix, $[K'_e]$; the transformed elemental geometric stiffness matrix, $[K'_{Ge}]$; the transformed elemental mass matrix, $[M'_e]$; the transformed elemental dynamic load vector, $\{P'_e(t)\}$; and transformed elemental thermal force vector, $\{P'_{Ne}\}$, are expressed in the global coordinate system of the stiffened plate, such as

$$\begin{aligned} [K'_e] &= [\mathcal{T}]^T [K_e][\mathcal{T}], \\ [K'_{Ge}] &= [\mathcal{T}]^T [K_{Ge}][\mathcal{T}], \\ [M'_e] &= [\mathcal{T}]^T [M_e][\mathcal{T}], \\ \{P'_e(t)\} &= [\mathcal{T}]^T \{P_e(t)\}, \\ \{P'_{Ne}\} &= [\mathcal{T}]^T \{P_{Ne}\}, \end{aligned} \tag{28}$$

in which $[\mathcal{T}] = [I] \bigotimes [\bar{\mathcal{T}}]$ with $[I]$ being the identity matrix of size 8×8. The $[\mathcal{T}]$ denotes the corresponding elemental transformation matrix of size 48×48. Prior to applying the transformation in Eq. (28), the 40×40 elemental stiffness, elemental geometric stiffness, and elemental mass matrices are expanded to 48×48 size by inserting θ_z drilling DOF, at each node of the element. The off-diagonal terms in the transformed elemental matrices corresponding to θ_z drilling DOF are considered as zero, whereas a very small positive value is inserted in the corresponding leading diagonal terms of the elemental stiffness matrix to avoid numerical instability [76]. In general, the inserted positive value of the leading diagonal is assumed to be 10^5 times smaller than the smallest leading diagonal term. Similarly, the corresponding force vectors are enlarged to 48×1 by inserting zeroes in the corresponding θ_z positions. This formulation is often referred as the folded plate formulation [77,78], and is used here to model the stiffened plate. The transformed elemental stiffness matrix, $[K'_e]$; the transformed elemental geometric stiffness matrix, $[K'_{Ge}]$; the transformed elemental mass matrix, $[M'_e]$; the transformed elemental dynamic load vector, $\{P'_e(t)\}$; and the transformed elemental thermal force vector, $\{P'_{Ne}\}$, are assembled to obtain the global stiffness matrix, $\left[K'\right]$; the global geometric stiffness matrix, $\left[K'_G\right]$; the global mass matrix, $\left[M'\right]$; the global dynamic force vector, $\left\{P'(t)\right\}$; and the global thermal force vector, $\{P'_N\}$, respectively.

2.5. Solution process

Due to variation of the ambient temperature, the temperature of unstiffened and stiffened laminated composite plates is varied uniformly, and an equilibrium state is achieved. The two-stage solution procedure to analyze composite plates in varying temperature is explained in what follows. In the first stage of solution, the initial global displacement, $\{d'^{i}\}$, due to the uniform variations of temperature in static condition is obtained by solving the equation of static deflection, which is expressed as

$$[K']\{d'^{i}\} = \{P'_N\}. \tag{29}$$

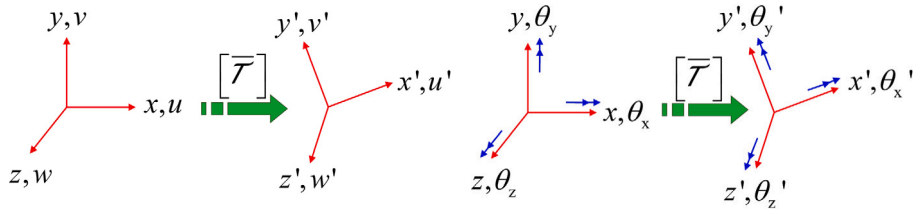

(a) Transformation of translations from local (x, y, z) to global (x', y', z') axes.

(b) Transformation of rotations from local (x, y, z) to global (x', y', z') axes.

Fig. 2. Transformation from local displacement vector, $\{d\}$, to global displacement vector, $\{d'\}$, where the least angle between the positive x and x' axes, y and y' axes, and z and z' axes are represented by (x', x), (y', y), and (z', z), respectively.

Now, initial strain vector, $\{\varepsilon^{*i}\}$, is evaluated from the initial elemental nodal displacement vector, $\{d'^{i}_{e}\}$, by using Eq. (20), and subsequently initial stress-resultant vector, $\{F^{i}\}$, is evaluated with reference to Eq. (5), and given as

$$\{F^{i}\} = [D]\{\varepsilon^{*i}\} - \{F_{N}\}. \tag{30}$$

The elements of the initial stress-resultant vector, $\{F^{i}\}$, are used to develop the initial-stress stiffness matrix, $[S_r]$, cf. Eq. (A.5).

The second stage of solution involves free and forced vibration analysis of unstiffened and stiffened laminated composite plates due to uniform variation of the temperature. The global FE model for the forced vibration in thermal environment is presented in the following form

$$\left[[K'] + [K'_G]\right]\{d'(t)\} + [M']\{\ddot{d}'(t)\} = \{P'(t)\}. \tag{31}$$

The transient response in terms of deflection, w, and normal stress, σ_x, for unstiffened and stiffened laminated composite plates with uniform temperature distribution subjected to a pulse loading (cf. Fig. 1(c)) is sought by solving Eq. (31) using Newmark's average integration technique. Furthermore, the homogeneous solution of Eq. (31) yields the eigenfrequencies, f_m, for unstiffened and stiffened laminated composite plates in thermal environment.

2.6. Computation of stresses

The global displacement of unstiffened and stiffened laminated composite plates is taken to calculate the nodal mid-plane strain vector, $\{\varepsilon^*\}$, using Eq. (20). To evaluate $\{\varepsilon^*\}$, the global displacement vector, $\{d'\}$, of unstiffened and stiffened laminated composite plates is transformed into the laminate coordinate (x, y, z) system of an element in accordance with Eq. (27). The elements of the strain vector, $\{\varepsilon\}$, at any point on the laminate at a distance z from the mid-plane are evaluated in the laminate coordinate (x, y, z) system with reference to Eq. (3), as

$$\varepsilon_x = \varepsilon_{0x} + z\kappa_x, \quad \varepsilon_y = \varepsilon_{0y} + z\kappa_y, \quad \gamma_{xy} = \gamma_{0xy} + z\kappa_{xy}. \tag{32}$$

The stress at the interface of the laminate for the k^{th} lamina are obtained from these strains using the stress–strain relationship matrix, (cf. Eq. (4)) of the laminate, and is presented as

$$\begin{Bmatrix} \sigma_x \\ \sigma_y \\ \tau_{xy} \end{Bmatrix}_k = \begin{bmatrix} Q_{11} & Q_{12} & Q_{16} \\ Q_{21} & Q_{22} & Q_{26} \\ Q_{61} & Q_{62} & Q_{66} \end{bmatrix}_k \begin{Bmatrix} \varepsilon_x \\ \varepsilon_y \\ \gamma_{xy} \end{Bmatrix}_k, \tag{33}$$

in which $Q_{12} = Q_{21}$, $Q_{16} = Q_{61}$, and $Q_{26} = Q_{62}$. These stresses are expressed in the laminate coordinate (x, y, z) system, and are evaluated at each Gauss point. The stresses are evaluated at 2×2 Gauss points of an element. The nodal stress is computed by averaging the stresses as obtained from the surrounding Gauss points. For instance, a nodal stress at node 'U' (cf. Fig. 3) is evaluated by averaging the stresses

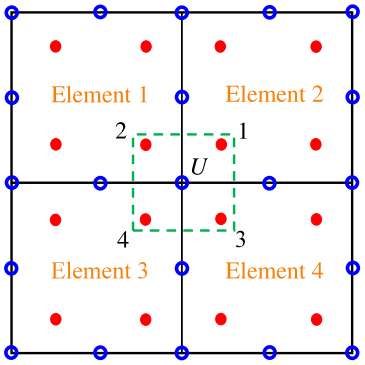

Fig. 3. 2×2 Gauss points (●) in elements for calculation of the nodal stresses at the node (○) 'U'.

computed at the Gauss points 1, 2, 3, and 4. The nodal stresses at each time step are calculated from the corresponding time dependent global displacement vector, $\{d'(t)\}$, and are presented in the time domain.

3. Verification and mesh convergence study

3.1. Verification of FE model

A detailed validation study of the present FE formulation for dynamic analysis of unstiffened and stiffened laminated composite plates in thermal environment has been presented in this section.

3.1.1. Unstiffened plate formulation in thermal environment

A square graphite–epoxy laminated composite plate with a dimension of $(100 \times 100 \times 1)$ mm^3 has been taken for free vibration analysis in thermal environment, and compared with results that reported by Ram and Sinha [8]. The material properties of the graphite–epoxy composite plate at 300 K temperature are presented in Table 1. The coefficients of thermal expansion of the composite lamina in fiber direction and perpendicular to the fiber direction are denoted by α_1 and α_2, respectively. Here, the eigenfrequencies, f_m, are normalized to obtained NDFs, λ_m, which are defined as $\lambda_m = 2\pi f_m L^2(\rho/E_{22}h^2)^{1/2}$.

The NDFs, λ_m, for 0°/90°/90°/0° laminated composite plate with simply-supported boundary conditions at all four edges are computed by discretizing the plate by 4×4 FE mesh, and are presented in Table 2. The NDFs, λ_m, are calculated at 325 K temperature without considering temperature-dependent elastic properties of the graphite–epoxy lamina. It is observed that the calculated NDFs, λ_m, of the graphite–epoxy laminated composite plate at temperature 325 K are in good agreement with the results reported by Ram and Sinha [8]. The good comparison between the calculated and the presented results indicates that the present formulation can be used to conduct a free vibration analysis of laminated composite plates in thermal environment with sufficient accuracy.

Table 1
Properties of the graphite–epoxy composite lamina at 300 K temperature for validation study of FE formulation for analyzing unstiffened laminated composite plate in thermal environment, cf. [8].

E_{11} (GPa)	E_{22} (GPa)	$G_{12} = G_{13}$ (GPa)	G_{23} (GPa)	ν_{12} (–)	ρ (kg/mm^3)	α_1, α_2 (/K)
130	9.5	6.0	3	0.3	1.6×10^{-6}	-0.3×10^{-6}, 28.1×10^{-6}

$\nu_{21} = \nu_{12} \frac{E_{22}}{E_{11}}$.

Table 2
Comparison of the NDFs, λ_m, obtained by using the present FE formulation, and that reported by Ram and Sinha [8] for free vibration analysis of the 0°/90°/90°/0° graphite–epoxy laminated composite plate at 325 K temperature.

Mode, m	NDF, λ_m	
	Present study	Ram and Sinha [8]
1	8.097	8.088
2	19.196	19.297
3	39.324	39.324

$\lambda_m = 2\pi f_m L^2 (\rho / E_{22} h^2)^{1/2}$.

Table 3
Properties of the composite lamina at room temperature (i.e., 25 °C) for validation study of the folded plate formulation for analyzing the stiffened laminated composite plate, cf. [71].

E_{11} (GPa)	E_{22} (GPa)	$G_{12} = G_{13} = G_{23}$ (GPa)	$\nu_{12} = \nu_{21}$ (–)	ρ (kg/mm^3)
60.7	24.8	12	0.23	1.3×10^{-6}

3.1.2. Stiffened plate formulation by using folded plate theory

The folded plate formulation has been used here for modeling a stiffened plate structure with various orientation of the stiffener. The NDFs as presented by Niyogi et al. [71] for the single folded plate are calculated by using the present FE formulation. In this example, NDFs, Λ_m, are defined as $\Lambda_m = 2\pi f_m L\left(\rho(1-\nu_{12}^2)/E_{11}\right)^{1/2}$. The material properties of the composite folded plate are given in Table 3. The length of the folded plate is $L = 1500$ mm, and the length of each fold is taken as $L/2$, as shown in Fig. 4. The crank angle between the two folds is denoted by β. A mesh size of 8 × 4 in each fold is considered for conducting the FE analysis. Two crank angles, such as $\beta = 90°$ and $\beta = 180°$ are taken for calculation of the first three NDFs, Λ_m, for 45°/ − 45°/45° laminated single-folded cantilever plates using the present FE formulation, and commercially available FE software such as ANSYS®. A good agreement between the results is found from Table 4 for the crank angles, $\beta = 90°$ and $\beta = 180°$. It endorses that the present FE formulation can be further considered for analysis of stiffened (i.e., for the crank angle, $\beta = 90°$) laminated composite plates. Similarly, the corresponding results have shown the correctness of the present FE formulation for analysis of unstiffened (i.e., for the crank angle, $\beta = 180°$) laminated composite plates.

3.1.3. Validation of transient response

To verify the transient response of unstiffened and stiffened laminated composite plates in thermal environment, numerical solutions for three examples are compared in this section. In the first example, the transient response in terms of central deflection, w, and normal stress, σ_x, of a laminated composite plate, subjected to a uniformly distributed pulse loading, $q = 10$ N/cm^2 over the entire plate surface for a duration of $t_d = 1.5{\times}10^{-4}$ s, is evaluated, and compared with the results presented by Kant et al. [79]. The size of the plate is (250 × 250 × 50) mm^3. The plate domain is discretized into a 4 × 4 mesh. The material properties of the laminated composite plate considered for this analysis are given in Table 5. The time dependent central deflection, w, and the corresponding normal stress, σ_x, at the bottom of 0°/90°/0° unstiffened laminated composite plate with simply-supported boundary condition at all four edges are calculated, and are illustrated in Fig. 5. Comparison of the transient response in terms of the central deflection, w, and the corresponding normal stress, σ_x, in Fig. 5, confirms a good agreement between the response obtained in the present FE formulation, and those obtained from [79].

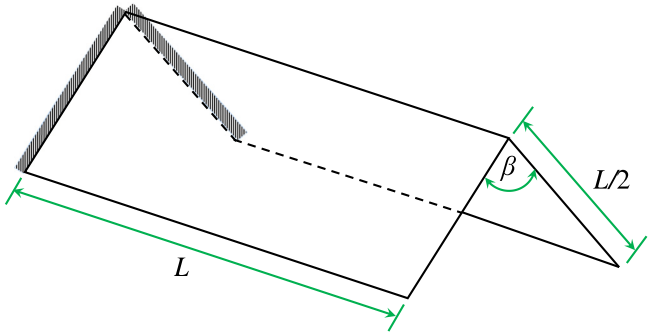

Fig. 4. Geometry of the cantilever single-folded plate with fixed-free boundary conditions.

Table 4
Comparison of the NDFs, Λ_m, obtained by using the present FE formulation, ANSYS® simulations, and that reported by Niyogi et al. [71] for free vibration analysis of 45°/ − 45°/45° laminated single-folded cantilever plates (cf. Fig. 4) with crank angles, $\beta = 90°$ and $\beta = 180°$.

Crank angle, β	Mode, m	NDF, Λ_m		
		Present study	Present ANSYS®	Niyogi et al. [71]
90°	1	0.0383	0.0408	0.0381
	2	0.0763	0.0747	0.0753
	3	0.1422	0.1441	0.1406
180°	1	0.0157	0.0148	0.0158
	2	0.0379	0.0405	0.0378
	3	0.0964	0.0920	0.0948

$\Lambda_m = 2\pi f_m L\left(\rho(1-\nu_{12}^2)/E_{11}\right)^{1/2}$.

Table 5
Properties of the composite lamina at room temperature (i.e., 25 °C) for validation study of the transient response of the unstiffened laminated composite plate, cf. [79].

E_{22} (GPa)	E_{11} (GPa)	$G_{12} = G_{13} = G_{23}$ (GPa)	$\nu_{12} = \nu_{21}$ (–)	ρ (kg/mm^3)
21	$25E_{22}$	$0.5E_{22}$	0.25	0.8×10^{-6}

In order to ensure the accuracy of the present FE code for analysis of stiffened laminated composite plates, the transient response in terms of deflection and normal stress is compared with the results obtained from ANSYS® simulation. In the given verification example a 2-mm thick IM7-PEEK stiffened laminated composite plate with a plan area of (150 × 100) mm^2, and a 12-mm deep centrally placed stiffener parallel to the shorter edge of the plate (cf. Fig. 6) is taken for this validation study. The simply-supported boundary condition at all four edges of the plate including the stiffener is adopted for the analysis of the stiffened plate as shown in Fig. 6. The lamina sequence is taken as 0°/90°/90°/0°. The plan area of the stiffened plate is subdivided into 8 × 6 mesh size, and the corresponding mesh for the stiffener is 6 × 1. A uniformly distributed pulse loading of $q = 0.001$ N/mm^2 for a duration of $t_d = 2 \times 10^{-3}$ s is applied over the entire plate surface, and transient response is evaluated at the mid-span of the half-plate as divided by the stiffener. The elastic properties of the IM7-PEEK composite plate for analysis at room temperature (25 °C) are given in Table 6. The time step for transient analysis is taken as $\Delta t = 10^{-5}$ s. Fig. 7 shows the transient response in terms of deflection, w, and corresponding normal stress, σ_x, at the bottom surface of the plate. The trend of the transient

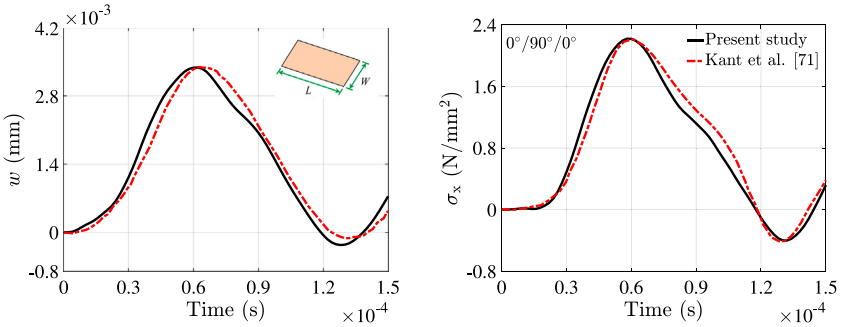

Fig. 5. Comparison of the transient response, w, (left) and the corresponding, σ_x, (right) obtained by using the present FE formulation, and that reported by Kant et al. [79] for 0°/90°/0° laminated composite plate with simply-supported boundary condition at all four edges, subjected to pulse loading, $q = 10$ N/cm^2, over the entire plan area at room temperature (i.e., 25 °C).

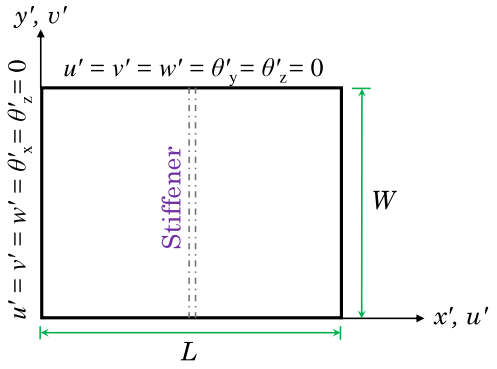

Fig. 6. Top view of a stiffened plate showing the simply-supported boundary condition at $x' = 0$ and L, and $y' = 0$ and W.

Table 6
Properties of the IM7-PEEK composite lamina at 25 °C temperature for validation study of the transient response of the stiffened laminated composite plate, cf. [80].

E_{11} (GPa)	E_{22} (GPa)	$G_{12} = G_{13}$ (GPa)	G_{23} (GPa)	ν_{12} (–)	ρ (kg/mm^3)
160.9	9.7	7.7	3.85	0.289	1.578×10^{-6}

$\nu_{21} = \nu_{12}\frac{E_{22}}{E_{11}}$.

Table 7
Properties of the composite lamina at 300 K and 400 K temperatures for validation study of transient response of unstiffened laminated composite plate in thermal environment, cf. [26].

Temp. (K)	E_{11} (GPa)	E_{22} (GPa)	$G_{12} = G_{13}$ (GPa)	ν_{12} (–)	ρ (kg/mm^3)	α_1, α_2 (/K)
300	172.5	6.9	3.45	0.25	1.6×10^{-6}	-0.3×10^{-6},
400	172.5	5.08	2.73	0.25		28.1×10^{-6}

$G_{23} = 0.4G_{12}$, $\nu_{21} = \nu_{12}\frac{E_{22}}{E_{11}}$.

response in terms of deflection, w, and normal nodal stress, σ_x, is in close agreement with the ANSYS® results.

As the third validation example, transient response of a $(0°/90°)_{10}$ laminated composite plate in thermal environment is compared with that reported by Parhi et al. [26]. The temperature-dependent material properties of the laminated composite plate are presented in Table 7. The transient response in terms of the central deflection, w, of a $(500 \times 500 \times 5)$ mm^3 composite plate subjected to uniformly distributed pulse loading, $q = 100$ N/m^2, for a duration of $t_d = 0.03$ s in thermal environment is evaluated, and is presented in Fig. 8. The analysis of the plate has been carried out with simply-supported boundary condition at all four edges considering the temperature-dependent elastic properties of the lamina. A close match of the transient response in terms of the central deflection, w, at 300 K and 400 K temperatures is observed between that obtained from the present FE formulation and Parhi et al. [26], which confirms that the present FE formulation can adequately predict the trends of transient response, w, of unstiffened laminated composite plates in thermal environment.

Based on the three validation examples presented in this section, the dynamic response of laminated composite plates subjected to the pulse loading in room temperatures and in elevated temperature are calculated by using the present FE formulation. The results are compared with the dynamic response of unstiffened laminated composite plates in thermal environment, and the dynamic response of stiffened laminated composite plates in thermal environment. A detailed dynamic analysis of stiffened laminated composite plates subjected to pulse loading in thermal environment is not available in the literature. Therefore, the present FE formulation is used for studying the NDFs and dynamic response in terms of deflection and normal stress of stiffened laminated composite plates in thermal environment.

3.2. Mesh convergence study

In the present study, the IM7-PEEK composite plate is used for conducting dynamic analysis in various thermal environments. The analysis of IM7-PEEK laminated composite plate is carried out in a temperature range varying from 0 °C to 125 °C, including that at the room temperature, i.e., 25 °C. The temperature-dependent material properties of the IM7-PEEK composite plate are obtained from the experimental data which are presented by Rawal and Misra [80]. The temperature-dependent elastic properties at a specific temperature for the present analysis are computed by linear interpolation and extrapolation based on the available test data at −150 °F, 77 °F (room temperature), and 250 °F [80]. The experimentally identified elastic properties of the unidirectional 0_8 IM7-PEEK laminate at these temperatures are shown in Table 8. The average values of E_{11} and E_{22} are obtained by averaging the corresponding values in tension and compression (cf. Table 8), and used further to compute the temperature-dependent elastic moduli. The experimentally obtained coefficients of the thermal expansion at 77 °F (i.e., 25 °C) are depicted in Table 8. For the purpose of this study, temperature-dependent elastic properties of the IM7-PEEK composite lamina at the specified temperature, namely 0 °C, 25 °C, 50 °C, 75 °C, 100 °C, and 125 °C, are computed using the 'FORECAST' function in the 'MS excel', and presented in Table 9. The elastic properties at 0 °C temperature are evaluated based on the corresponding experimental values at −101 °C and 25 °C. Similarly, the temperature-dependent elastic properties at the remaining temperatures are determined from the experimental elastic properties as known at 25 °C and 121 °C temperatures. The nature of variation of the temperature-dependent elastic properties, as evaluated by the stated procedure based on the available test data, of the IM7-PEEK composite lamina are shown in Fig. 9.

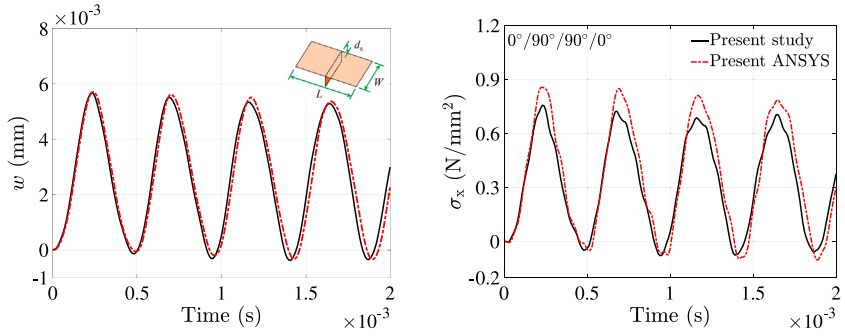

Fig. 7. Comparison of the transient response, w, (left) and the corresponding, σ_x, (right) obtained by using the present FE formulation and ANSYS® simulation for 0°/90°/90°/0° IM7-PEEK stiffened laminated composite plate with stiffener oriented parallel to the shorter edge, for all four edges simply-supported, and subjected to pulse loading, $q = 0.001$ N/mm^2, over the entire plan area at room temperature (i.e., 25 °C).

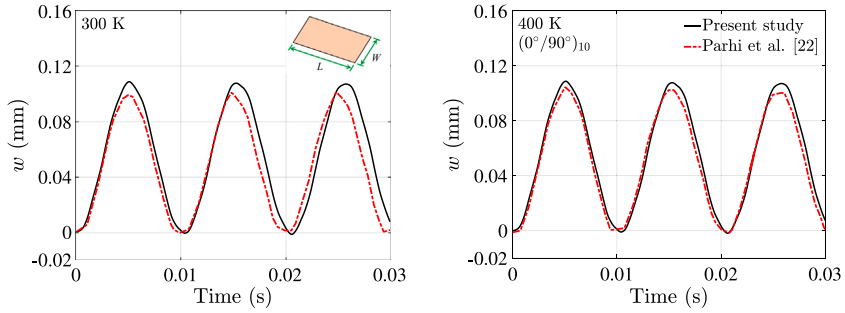

Fig. 8. Comparison of the transient response, w, obtained by using the present FE formulation, and that reported by Parhi et al. [26] for $(0°/90°)_{10}$ laminated composite plate with all four edges simply-supported subjected to pulse loading, $q = 100$ N/m^2, over the entire plan area at 300 K (left) and 400 K (right) temperatures.

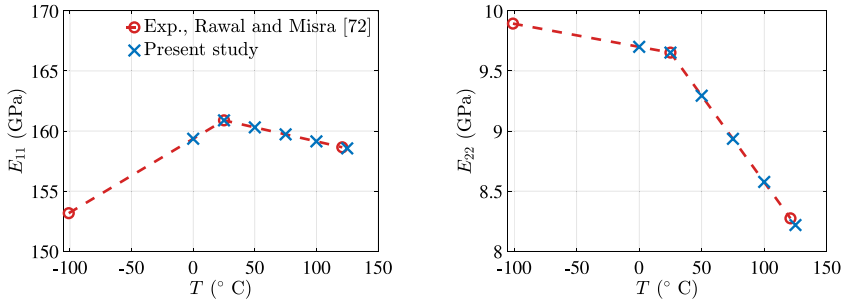

(a) Temperature dependent E_{11}. (b) Temperature dependent E_{22}.

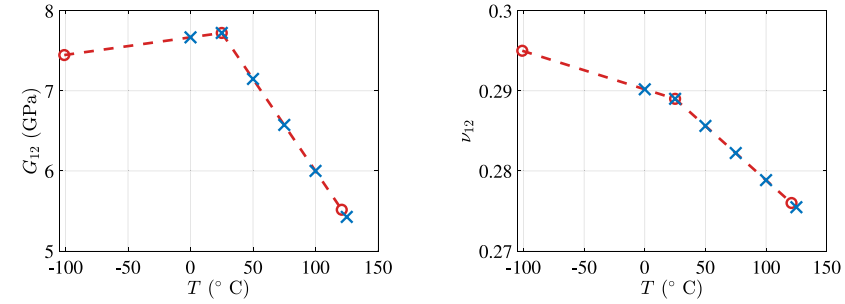

(c) Temperature dependent G_{12}. (d) Temperature dependent ν_{12}.

Fig. 9. Experimentally identified [80] and computed temperature-dependent elastic properties for unidirectional IM7-PEEK composite lamina.

In this study, 25 °C temperature is considered as a reference temperature. The density, ρ, of the IM7-PEEK laminated composite plate is 1.578×10^{-6} kg/mm^3 [80]. The coefficients of thermal expansion of the IM7-PEEK composite lamina are $\alpha_1 = -0.126 \times 10^{-6}$ /°C and $\alpha_2 = 31.3 \times 10^{-6}$ /°C (cf., Table 8), and assumed as the temperature independent. The mesh convergence study is conducted using a $(150 \times 100 \times 2)$ mm^3 rectangular plate with various mesh sizes at three salient temperatures such as 0 °C (below the room temperature), 25 °C (room temperature), and 125 °C (above the room temperature). The mesh convergence study has been carried out for the first three NDFs, λ_1, λ_2,

Table 8
Experimentally identified elastic properties of the unidirectional 0_8 IM7-PEEK laminated composite at −150 °F, 77 °F, and 250 °F temperatures, cf. [80].

Experimental elastic properties	Temperature		
	−150 °F (−101 °C)	77 °F (25 °C)	250 °F (121 °C)
E_{11}, tension (Msi)	21.90	23.87	24.30
E_{11}, compression (Msi)	22.53	22.80	21.72
E_{11}, average (GPa)	153.2	160.9	158.6
E_{22}, tension (Msi)	1.46	1.40	1.18
E_{22}, compression (Msi)	1.41	1.40	1.22
E_{22}, average (GPa)	9.9	9.7	8.3
G_{12} (Msi)	1.08	1.12	0.8
G_{12} (GPa)	7.4	7.7	5.5
ν_{12} (–)	0.295	0.289	0.276
α_1 (μin/in/°F)	–	−0.07	–
α_1 (/°C)	–	-0.126×10^{-6}	–
α_2 (μin/in/°F)	–	17.42	–
α_2 (/°C)	–	31.3×10^{-6}	–

Table 9
The temperature-dependent elastic properties of the IM7-PEEK composite lamina at various temperatures, computed based on the experimental data given in Table 8.

Elastic properties	Temperature					
	0 °C	25 °C	50 °C	75 °C	100 °C	125 °C
E_{11} (GPa)	159.4	160.9	160.3	159.7	159.1	158.6
E_{22} (GPa)	9.7	9.7	9.3	8.9	8.6	8.2
G_{12} (GPa)	7.7	7.7	7.1	6.6	6.0	5.4
ν_{12} (–)	0.290	0.289	0.286	0.282	0.279	0.275

$G_{13} = G_{12}$, $G_{23} = 0.5G_{12}$, $\nu_{21} = \nu_{12}\frac{E_{22}}{E_{11}}$.

Table 10
The first three NDFs, λ_m, and peak dynamic deflection, w, for various mesh sizes using 0°/90°/0°/90° IM7-PEEK laminated composite plate with simply-supported boundary condition at all four edges at 0 °C, 25 °C, and 125 °C temperatures.

Temperature	Dynamic response	Present study, mesh size			
		4 × 2	6 × 4	8 × 6	12 × 8
0 °C	λ_1	24.58	23.98	23.96	23.95
	λ_2	47.15	42.17	42.04	42.01
	λ_3	97.05	74.87	74.01	73.86
	Peak w (mm)	0.0360	0.0368	0.0371	0.0370
25 °C	λ_1	22.72	22.09	22.07	22.06
	λ_2	45.39	40.23	40.10	40.07
	λ_3	95.61	73.23	72.36	72.20
	Peak w (mm)	0.0421	0.0434	0.0432	0.0431
125 °C	λ_1	14.46	13.62	13.59	13.59
	λ_2	38.41	33.16	33.02	32.98
	λ_3	91.21	70.01	69.09	68.93
	Peak w (mm)	0.1229	0.1353	0.1361	0.1359

$\lambda_m = 2\pi f_m L^2(\rho/E_{22}h^2)^{1/2}$.

and λ_3, and the peak dynamic deflection, w, for mesh sizes 4 × 2, 6 × 4, 8 × 6, and 12 × 8 using the present FE formulation. A 0°/90°/0°/90° unstiffened laminated composite plate with simply-supported boundary condition at all four edges is considered for this study, and results are presented in Table 10. Variation in the NDFs for gradually finner mesh sizes such as 6 × 4, 8 × 6, and 12 × 8 are negligible, even with the rise in temperature. Further, the peak dynamic deflection, w, obtained for mesh sizes 6 × 4, 8 × 6, and 12 × 8, has not shown significant variation at different temperatures. However, for accurate computation of average nodal stress, the 8 × 6 mesh size is adopted for further analysis in this paper.

4. Numerical study

4.1. NDFs of the unstiffened and stiffened plates

The effect of rise in temperature for the unstiffened and stiffened laminated composite plates with various lamina sequences on the NDFs, λ_m, is investigated. A 2-mm thick unstiffened plate and stiffened plates with centrally placed stiffeners oriented parallel to the longer and shorter edges are considered for the analysis, cf. Figs. 10(a), 10(b), and 10(c). Plates 1, 2, and 3 are designated for the unstiffened plate, the plate with stiffener oriented parallel to the longer edge, and the plate with stiffener oriented parallel to the shorter edge, respectively. The size of the plan area of the plate is (150×100) mm^2. The depth of the stiffener, d_s, is 12 mm. The simply-supported boundary condition at all edges (cf. Fig. 6) of the laminated composite plates is adopted for the analysis.

The lowest three NDFs of the unstiffened Plate 1 with different lamina sequences for temperature ranging between 0 °C and 125 °C with 25 °C interval are presented in Table 11. Four layered symmetric and antisymmetric cross-ply laminates such as 0°/90°/90°/0° and 0°/90°/0°/90°, respectively, and four layered symmetric and antisymmetric angle-ply laminates such as 45°/ − 45°/ − 45°/45° and 45°/ − 45°/45°/− 45°, respectively (cf. Fig. 10(d)) are taken for the analysis. It is observed from Table 11 that the NDFs, λ_m, of Plate 1 are decreasing with the increment in the temperature due to degradation in the material properties of the IM7-PEEK composite plates above the reference temperature, i.e., 25 °C. The NDFs, λ_m, at 0 °C temperature, i.e., below the reference temperature, are higher than that of the NDFs, λ_m, at the reference temperature, although E_{11} of the IM7-PEEK composite lamina at 0 °C temperature is less than that at 25 °C temperature. The relatively higher NDFs, λ_m, observed at 0 °C temperature are attributed to the stiffening effect caused in the laminated composite plate, as the initial stress induced in the plate below the reference temperature is tensile in nature. Furthermore, the NDFs, λ_m, of the angle-ply laminates are higher than that of the cross-ply laminates for both symmetric and antisymmetric cases. The 45°/ − 45°/45°/ − 45° laminate exhibits the highest NDFs, λ_m, at all temperatures, which is attributed to the non-zero in-plane and bending stiffness coupling, B_{ij}, (cf. Eq. (8)) due to the antisymmetric lamina sequence, and the higher shear stiffness of the angle-ply laminate.

The 0°/90°/90°/0° unstiffened laminated composite plate shows the lowest NDFs at all temperatures, and exhibits instability at 125 °C temperature. The instability arises at 125 °C temperature as the combined stiffness matrix does not remain positive-definite at this temperature. Due to rise in temperature of the laminated composite plate, an initial stress is developed which is compressive in nature, and based on the state of the temperature-dependent initial stress, the geometric stiffness matrix, $[K'_G]$, is developed. Therefore, the combined stiffness matrix, i.e., $\left[[K'] + [K'_G]\right]$, does not remain positive-definite with the rise in temperature above reference temperature, i.e., 25 °C, from 100 °C to 125 °C which leads to instability in the unstiffened Plate 1 with 0°/90°/90°/0° laminate at 125 °C temperature.

The NDFs, λ_m, of the stiffened Plates 2 and 3, made-up with the laminates stated earlier are presented in Tables 12 and 13, respectively. From the tables it is found that the NDFs, λ_m, of the stiffened plates are higher than the corresponding unstiffened plates, as expected. The NDFs, λ_m, of the stiffened plates for a particular laminate are decreasing with the rise in temperature because of the similar reasons as discussed for the unstiffened laminated composite plates. However, no instability is observed at 125 °C temperature for the stiffened plates with 0°/90°/90°/0° laminate.

The first NDF, λ_1, of the stiffened Plate 2 with 0°/90°/90°/0° laminate is higher than the stiffened Plate 3 with same laminate at 0 °C and 25 °C temperatures; whereas, the first NDF, λ_1, of the stiffened Plate 3 with 0°/90°/90°/0° laminate is higher than the stiffened Plate 2 at above 25 °C temperature. It indicates that the stiffness of the stiffened

Table 11
The NDFs, λ_m, of 2-mm thick cross-ply and angle-ply IM7-PEEK unstiffened laminated composite Plate 1 with simply-supported boundary condition at all four edges at various temperatures.

Lamina sequence	Mode, m	NDF, λ_m					
		0 °C	25 °C	50 °C	75 °C	100 °C	125 °C
0°/90°/90°/0°	1	19.84	17.57	15.09	12.22	8.25	–
	2	49.20	47.66	45.97	43.65	40.97	–
	3	50.86	48.30	46.57	45.58	44.29	–
0°/90°/0°/90°	1	23.96	22.07	20.24	18.30	15.99	13.59
	2	42.04	40.10	38.40	36.74	34.76	33.02
	3	74.01	72.36	71.48	70.74	69.64	69.09
45°/ − 45°/ −45°/45°	1	25.90	24.21	22.70	21.15	19.35	17.64
	2	46.22	44.37	42.93	41.53	39.86	38.47
	3	71.76	70.13	69.17	68.36	67.17	66.50
45°/ − 45°/ 45°/ − 45°	1	27.10	25.55	24.26	22.96	21.47	20.15
	2	50.33	48.84	47.95	47.14	46.10	45.46
	3	70.04	68.35	67.31	66.40	65.12	64.35

$\lambda_m = 2\pi f_m L^2(\rho/E_{22}h^2)^{1/2}$.

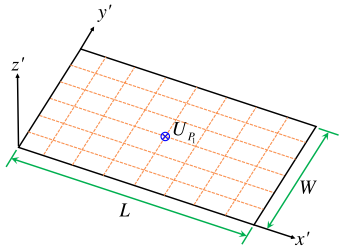

(a) Unstiffened Plate 1 showing nodal point, U_{P_1}.

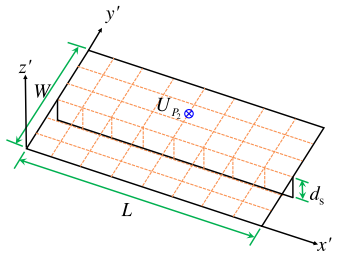

(b) Stiffened Plate 2 with stiffener oriented parallel to the longer edge showing nodal point, U_{P_2}.

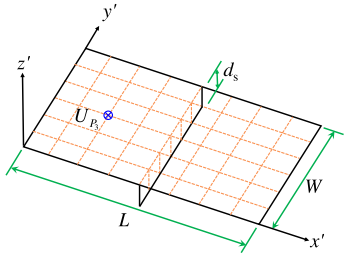

(c) Stiffened Plate 3 with stiffener oriented parallel to the shorter edge showing nodal point, U_{P_3}.

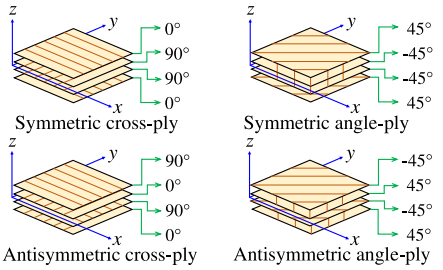

(d) Lamina sequences of symmetric and antisymmetric cross-ply and angle-ply laminates.

Fig. 10. Geometry of the unstiffened Plate 1 and stiffened Plates 2 and 3, and lamina sequences for the laminates.

Table 12
The NDFs, λ_m, of 2-mm thick cross-ply and angle-ply IM7-PEEK stiffened laminated composite Plate 2 with simply-supported boundary condition at all four edges at various temperatures.

Lamina sequence	Mode, m	NDF, λ_m					
		0 °C	25 °C	50 °C	75 °C	100 °C	125 °C
0°/90°/90°/0°	1	51.26	48.27	45.41	42.45	38.97	35.55
	2	53.74	52.70	51.69	50.79	49.42	48.29
	3	73.94	71.52	69.39	67.37	64.80	62.64
0°/90°/0°/90°	1	59.83	59.34	58.82	58.44	57.46	56.70
	2	69.50	71.19	72.71	73.82	74.24	74.95
	3	83.42	83.95	84.47	84.83	84.48	84.54
45°/ − 45°/ −45°/45°	1	56.67	55.91	55.11	54.44	53.22	52.24
	2	71.50	69.50	68.11	66.83	65.12	63.90
	3	97.94	96.22	95.39	94.72	93.52	92.94
45°/ − 45°/ 45°/ − 45°	1	57.00	56.28	55.55	54.97	53.86	53.01
	2	70.53	68.55	67.17	65.91	64.24	63.06
	3	102.51	101.05	100.73	100.58	99.93	100.02

$\lambda_m = 2\pi f_m L^2(\rho/E_{22}h^2)^{1/2}$.

Table 13
The NDFs, λ_m, of 2-mm thick cross-ply and angle-ply IM7-PEEK stiffened laminated composite Plate 3 with simply-supported boundary condition at all four edges at various temperatures.

Lamina sequence	Mode, m	NDF, λ_m					
		0 °C	25 °C	50 °C	75 °C	100 °C	125 °C
0°/90°/90°/0°	1	49.87	48.21	47.00	45.86	44.41	43.32
	2	61.79	60.84	60.29	59.83	58.88	58.26
	3	74.00	71.74	69.89	68.14	65.90	64.10
0°/90°/0°/90°	1	42.73	40.66	38.80	36.95	34.74	32.74
	2	53.05	51.73	50.75	49.88	48.65	47.77
	3	86.65	84.81	83.57	82.51	80.93	79.93
45°/−45°/−45°/45°	1	50.97	49.36	48.29	47.30	46.03	45.14
	2	55.27	53.96	53.11	52.35	51.28	50.58
	3	94.54	92.74	91.70	90.81	89.43	88.64
45°/−45°/45°/−45°	1	51.72	50.18	49.22	48.35	47.21	46.47
	2	56.70	55.53	54.88	54.34	53.48	53.03
	3	101.89	100.54	100.35	100.34	99.84	100.07

$\lambda_m = 2\pi f_m L^2(\rho/E_{22}h^2)^{1/2}$.

laminated composite plates with stiffener oriented parallel to the longer edge has the higher stiffness above the 25 °C temperature for all the considered laminates, except for the 0°/90°/90°/0° laminate. The first NDF, λ_1, of 0°/90°/0°/90°, 45°/−45°/−45°/45° and 45°/−45°/45°/−45° laminates are higher for the plate with the stiffener oriented parallel to the longer edge (Plate 2) than the plate with stiffener oriented parallel to the shorter edge (Plate 3) at all the respective temperatures. This is attributed to the fact that 0°/90°/90°/0° laminate has lower strength due to the null terms, B_{ij} (cf. Eq. (8)) for symmetric lamina sequences, and lower shear strength due to the cross-ply lamina sequence. Further, due to the rectangular plate configuration, 90° lamina in the shorter direction and the stiffener oriented parallel to the longer edge could not increase stiffness of the stiffened Plate 2 than the stiffened Plate 3 in which the stiffener is oriented parallel to the shorter edge. Furthermore, rate of reduction of the first NDF, λ_1, with the increase in temperature is lower for the stiffened Plate 2 with of 0°/90°/0°/90°, 45°/−45°/−45°/45° and 45°/−45°/45°/−45° laminates than that of the stiffened Plate 3. The first NDF, λ_1, for 0°/90°/0°/90° laminate has shown the highest value for the stiffened Plate 2 compared to the Plates 1 and 3 at all respective temperatures, due to fact of antisymmetric lamina sequences and the stiffener orientation parallel to the longer edge. Therefore, it is recommended to use antisymmetric cross-ply laminate and provide a stiffener parallel to the longer direction for the stiffened laminated composite plate with rectangular plan area.

The first NDF, λ_1, of the stiffened Plates 2 and 3 are approximately two times larger in all individual laminates at a specific temperature than the unstiffened Plate 1 with a cost of 12% and 8% mass addition, respectively. The first NDF, λ_1, of the stiffened plate with stiffener oriented parallel to the longer edge (Plate 2) is higher than the stiffened plate with stiffener oriented parallel to the shorter edge (Plate 3) for all the laminates except for the 0°/90°/90°/0° laminate above 25 °C temperature. The stiffened Plate 2 with 0°/90°/0°/90° laminate has appeared as the best configuration due to the fact of providing the highest first NDF, λ_1, in all the considered temperatures, and the lowest rate of reduction of the first NDF, λ_1, with the increase in temperature.

4.2. Transient response of the unstiffened and stiffened plates

The transient response in terms of deflection, w, and the corresponding normal stress, σ_x, are evaluated using the FSDT for the unstiffened and stiffened IM7-PEEK laminated composite plates at different temperatures. The transient response, w and σ_x for the unstiffened Plate 1 are evaluated at mid-span, i.e., at node 'U_{P_1}' (cf. Fig. 10(a)); whereas, for the Plates 2 and 3, the transient response, w and σ_x, are determined at nodes 'U_{P_2}' and 'U_{P_3}' (cf. Figs. 10(b) and 10(c)), respectively. The nodes 'U_{P_2}' and 'U_{P_3}' are the locations of the peak deflection for the Plates 2 and 3, respectively. A uniformly distributed pulse loading, q = 0.001 N/mm^2 is applied over the flat plate surface for a duration of t_d = 0.004 s (cf. Fig. 1(c)), and the corresponding transient response, w and σ_x is evaluated for the same time duration. The boundary conditions, lamina sequences, and dimension of the plates are maintained the same as stated in Section 4.1. A converged time step of $\Delta t = 10^{-5}$ s is adopted for conducting the transient analysis using the Newmark's method. The nodal stress is computed by averaging the stresses obtained from the surrounding Gauss points. The transient response in terms of w and σ_x of the Plates 1, 2, and 3 at the specified location, are shown in Figs. 11, 12, and 13, respectively. Accordingly, the peak dynamic deflection, w, and the corresponding peak normal stress, σ_x, are calculated for the Plates 1, 2, and 3, and are presented in Tables 14–16, respectively in the temperature range varying from 0 °C to 125 °C.

Table 14
Peak dynamic deflection, w, and normal stress, σ_x, at 'U_{P_1}' for the cross-ply and the angle-ply IM7-PEEK laminated composite Plate 1, subjected to pulse loading at various temperatures with simply-supported boundary condition at all four edges.

Temp.	Peak	0°/90°/90°/0°	0°/90°/0°/90°	45°/−45°/−45°/45°	45°/−45°/45°/−45°
0 °C	w (mm)	0.0532	0.0371	0.0314	0.0286
	σ_x (N/mm^2)	1.92	1.18	0.77	0.56
25 °C	w (mm)	0.0686	0.0432	0.0350	0.0323
	σ_x (N/mm^2)	2.53	1.34	0.84	0.65
50 °C	w (mm)	0.0970	0.0540	0.0426	0.0374
	σ_x (N/mm^2)	3.55	1.66	1.06	0.74
75 °C	w (mm)	0.1543	0.0690	0.0519	0.0436
	σ_x (N/mm^2)	5.56	2.14	1.28	0.87
100 °C	w (mm)	0.3503	0.0938	0.0637	0.0519
	σ_x (N/mm^2)	12.52	2.85	1.55	1.03
125 °C	w (mm)	–	0.1361	0.0812	0.0621
	σ_x (N/mm^2)	–	4.14	1.98	1.23

It is observed from the trends in the plots that the amplitude of dynamic deflection of the laminated composite plates is increasing with the rise in temperature from 0 °C to 125 °C due to degradation of the elastic moduli of the IM7-PEEK composite lamina above the reference temperature and initial stress in the composite laminate due to variation in temperatures. The largest peak dynamic deflection is observed for the unstiffened Plate 1 with 0°/90°/90°/0° laminate at 100 °C temperature (cf. Table 14) because of the null terms, B_{ij} (cf. Eq. (8)) owing to the symmetric nature of the laminate, and relatively lesser contribution of shear strength to stiffness in the cross-ply laminate as compared to the other laminates considered in the study. It is also observed from Table 14 that the peak dynamic deflection of the unstiffened Plate 1 with 45°/−45°/45°/−45° laminate has remained the lowest as compared to the other laminates at different temperatures due to imparting highest stiffness as indicated in Section 4.1. It is seen from Figs. 11, 12, and 13 that the amplitude of the transient

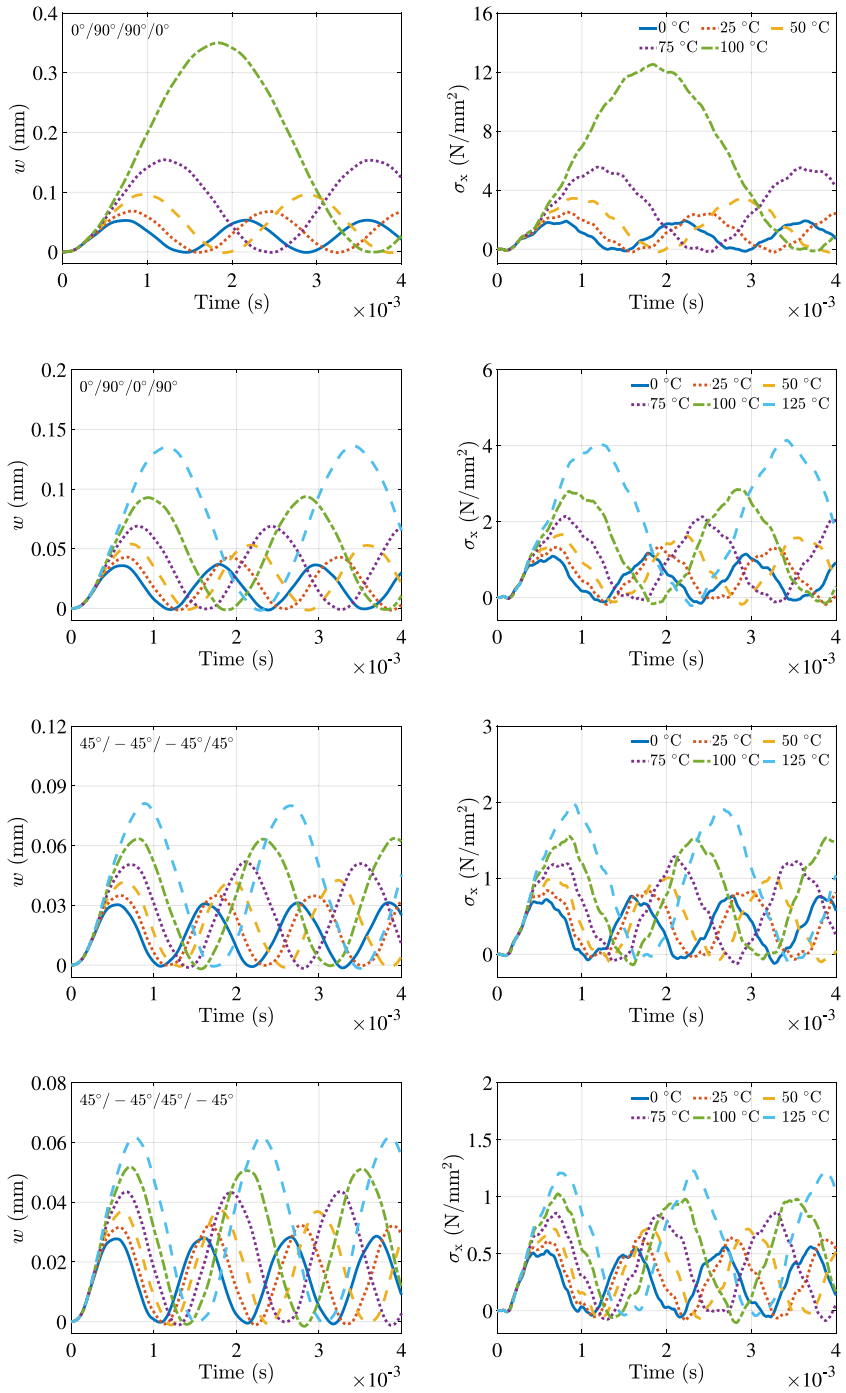

Fig. 11. Dynamic deflection, w, and normal stress, σ_x, at 'U_{P_1}' for the cross-ply and the angle-ply IM7-PEEK laminated composite Plate 1 subjected to pulse loading at various temperatures with simply-supported boundary condition at all four edges.

response in terms of the normal stress is increasing with the increment in temperature for the earlier mentioned laminates of the Plates 1, 2, and 3, as anticipated. It is also observed from Table 14, that the peak normal stress is obtained for the unstiffened Plate 1 with 0°/90°/90°/0° laminate at 100 °C temperature, while the corresponding minimum value is obtained for 45°/ − 45°/45°/ − 45° laminate at all respective temperatures. Moreover, a significant increment in the amplitude of dynamic deflection and the normal stress is observed with the rise in temperature from 75 °C to 100 °C for the unstiffened Plate 1 with 0°/90°/90°/0° laminate. This large magnitude of deflection increment is noticed as the unstiffened Plate 1 with 0°/90°/90°/0° laminate is approaching towards the instability beyond 100 °C temperature.

Addition of stiffeners sufficiently reduces the dynamic deflection and normal stress for the laminates considered. The Tables 15 and 16 reveal that the stiffened Plate 2 with 0°/90°/0°/90° laminate and the stiffened Plate 3 with 0°/90°/90°/0° laminate show the least peak dynamic deflection in thermal environment. The peak dynamic deflection for the unstiffened Plate 1 with 0°/90°/90°/0° laminate is higher than the corresponding response of the unstiffened Plate 1 with 0°/90°/0°/90° laminate at all temperatures, as in-plane and bending stiffness coupling terms, B_{ij}, in $[D]$ matrix become zero for 0°/90°/90°/0° laminate due to the symmetry in the lamina sequence. It is to be noted that the deflection of the stiffened Plate 2 at node U_{P_2} is governed by the cylindrical (i.e., uni-directional) bending, whereas the deflection of

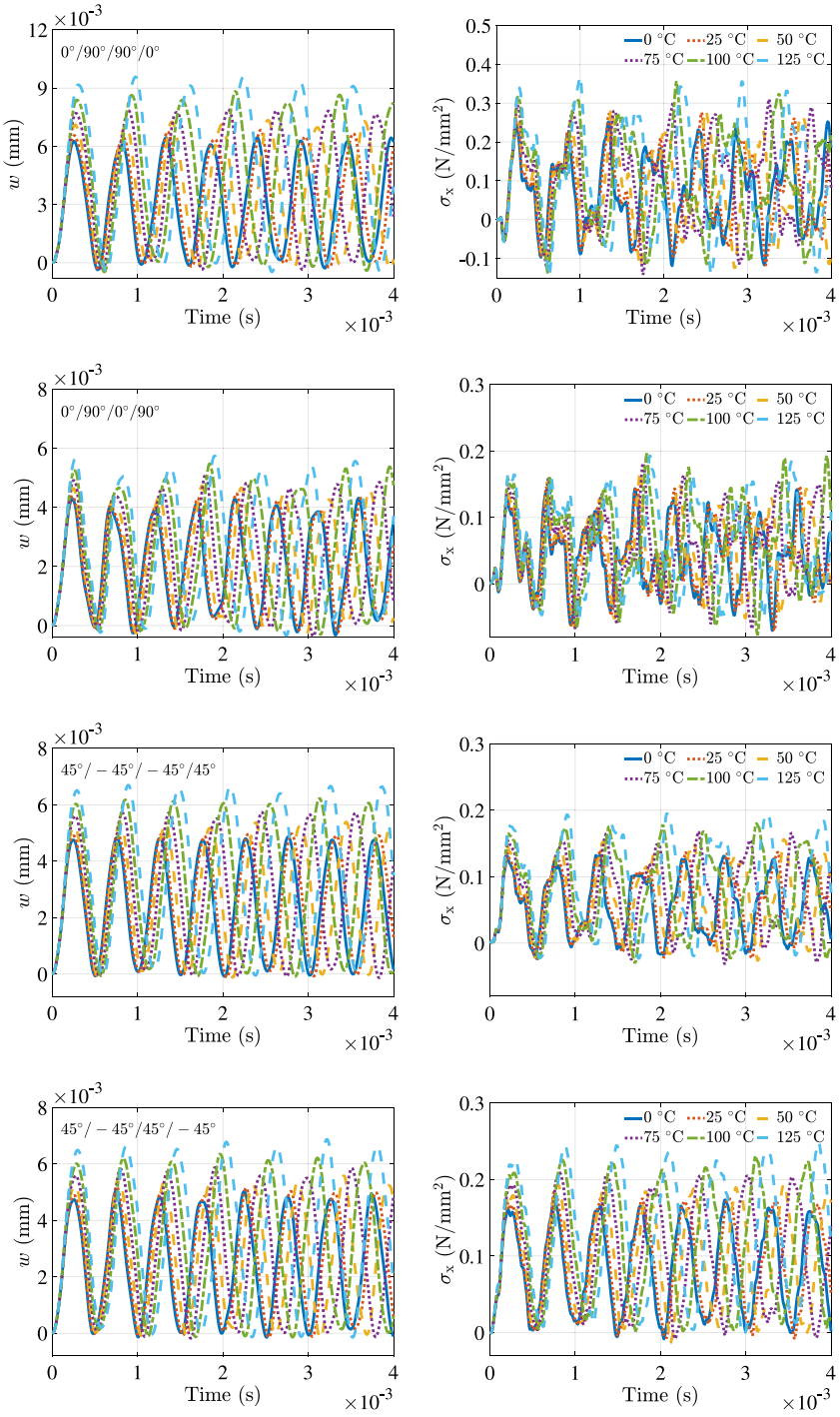

Fig. 12. Dynamic deflection, w, and normal stress, σ_x, at 'U_{P_2}' for the cross-ply and the angle-ply IM7-PEEK laminated composite Plate 2 subjected to pulse loading at various temperatures with simply-supported boundary condition at all four edges.

the stiffened Plate 3 at U_{P_3} is governed by bi-directional bending. In case of the stiffened Plate 2, 0°/90°/90°/0° laminate shows the higher peak dynamic deflection than 0°/90°/0°/90° laminate, similar to the unstiffened Plate 1. In this case, due to the absence of in-plane and bending stiffness coupling terms, B_{ij}, for 0°/90°/90°/0° laminate, the deflection at node, U_{P_2} in cylindrical bending is higher than that of the stiffened Plate 2 with 0°/90°/0°/90° laminate. Whereas, the deflection of the stiffened Plate 3 with 0°/90°/0°/90° laminate is higher than that of the plate with 0°/90°/90°/0° laminate, owing to the null bending-twist coupling terms, D_{16} and D_{26}, which reduces contribution in stiffness when the plate with the antisymmetric laminate undergoes bi-directional bending as compared to that when the symmetric laminate is used in the plate. Hence, the peak dynamic deflection of the stiffened Plate 3 with 0°/90°/90°/0° laminate are less than the corresponding response of the stiffened Plate 3 with 0°/90°/0°/90° laminate at all temperatures. The amplitude of dynamic deflection of the stiffened Plate 2 are the lowest than the stiffened Plate 3 in all respective laminates except 0°/90°/90°/0° laminate at different temperatures. The rate of increment in the peak dynamic response with the rise in temperatures is less for the stiffened plates than the unstiffened plates, as seen from the response reported in Tables 14–16. It is observed from Tables 15 and 16 that the stiffened Plate 2 with 0°/90°/0°/90° laminate shows the lowest peak dynamic deflection and normal stress at all temperature. It is observed that the peak normal stress for the stiffened Plate 2 (Table 15)

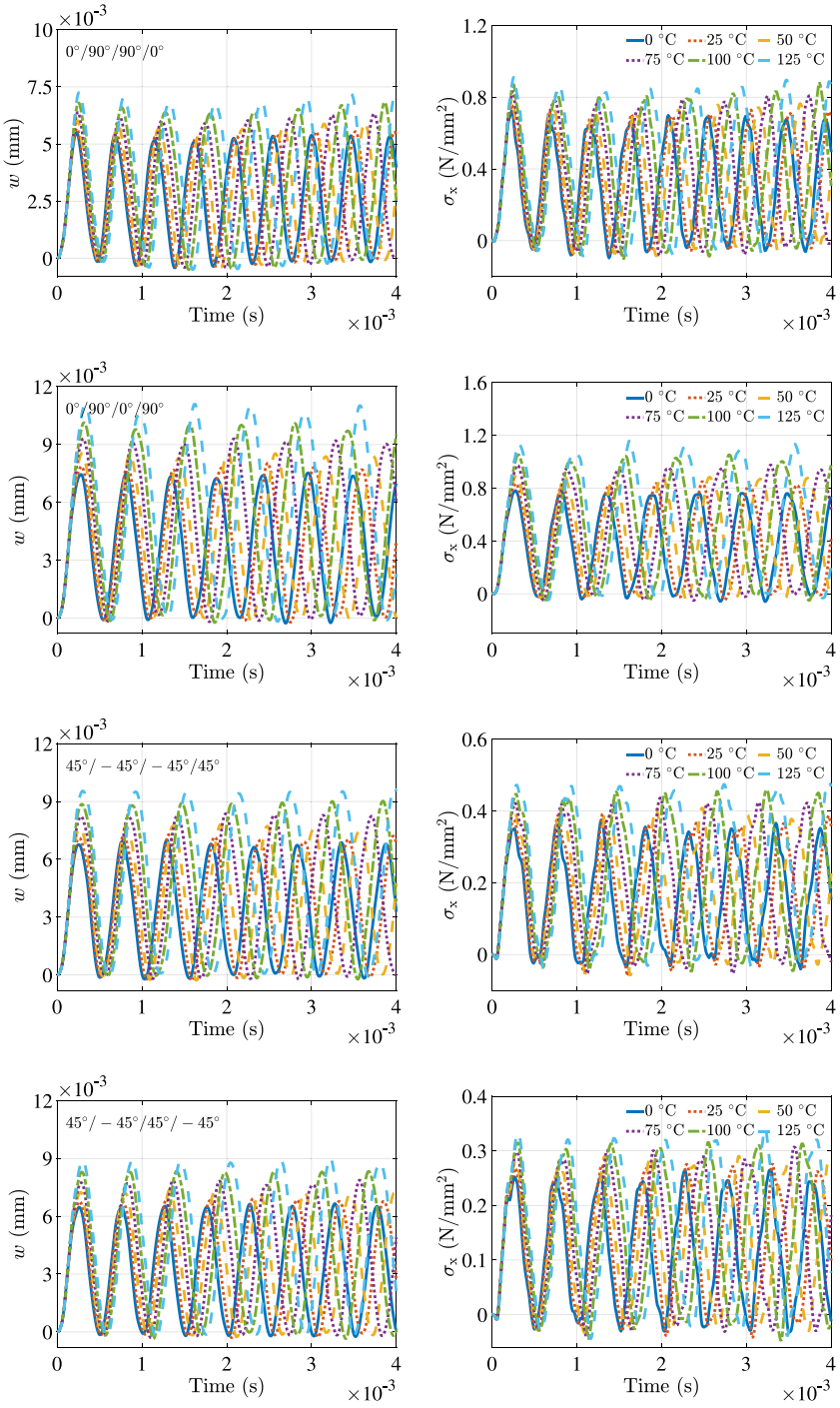

Fig. 13. Dynamic deflection, w, and normal stress, σ_x, at 'U_{P_3}' for the cross-ply and the angle-ply IM7-PEEK laminated composite Plate 3 subjected to pulse loading at various temperatures with simply-supported boundary condition at all four edges.

with 45°/−45°/45°/−45° laminate at all different temperatures show the lowest value however, the peak dynamic deflection of 0°/90°/0°/90° laminate is less than 45°/−45°/45°/−45° laminate at all temperatures.

Thus, stiffened plates are preferred as compared to unstiffened plates for reducing amplitude of the dynamic deflection and the corresponding normal stress. The selection of the stiffener orientation for rectangular plates is governed by the lamina sequence. The 0°/90°/0°/90° stiffened laminated composite plate with the stiffener oriented parallel to the longer edge is recommended to achieve maximum response reduction in terms of deflection at all temperatures.

4.3. Effect of the depth of stiffener

In order to study the effect of the depth of stiffener, d_s, the first NDF, λ_1, is evaluated for the IM7-PEEK stiffened laminated composite Plates 2 and 3 for 0°/90°/90°/0° and 45°/−45°/−45°/45° laminates at 0 °C, 25 °C, and 100 °C temperatures, and are presented in Table 17. The depths of stiffener, d_s, taken for this study are 8 mm, 12 mm, and 16 mm. The stiffened Plate 2 with the stiffener depth 12 mm made-up of 0°/90°/90°/0° laminate shows the highest value of the first NDF, λ_1, than the plate with the stiffeners 8 mm and 16 mm at all respective temperatures.

Table 15
Peak dynamic deflection, w, and normal stress, σ_x, at 'U_{P_2}' for the cross-ply and the angle-ply IM7-PEEK laminated composite Plate 2, subjected to pulse loading at various temperatures with simply-supported boundary condition at all four edges.

Temp.	Peak	0°/90°/ 90°/0°	0°/90°/ 0°/90°	45°/−45°/ −45°/45°	45°/−45°/ 45°/−45°
0 °C	w (mm)	0.0064	0.0043	0.0049	0.0051
	σ_x (N/mm^2)	0.25	0.14	0.13	0.18
25 °C	w (mm)	0.0068	0.0045	0.0050	0.0052
	σ_x (N/mm^2)	0.28	0.15	0.14	0.18
50 °C	w (mm)	0.0073	0.0047	0.0054	0.0056
	σ_x (N/mm^2)	0.29	0.17	0.16	0.19
75 °C	w (mm)	0.0079	0.0051	0.0057	0.0059
	σ_x (N/mm^2)	0.31	0.18	0.17	0.21
100 °C	w (mm)	0.0088	0.0055	0.0062	0.0063
	σ_x (N/mm^2)	0.36	0.20	0.18	0.23
125 °C	w (mm)	0.0096	0.0057	0.0067	0.0069
	σ_x (N/mm^2)	0.37	0.19	0.20	0.25

Table 16
Peak dynamic deflection, w, and normal stress, σ_x, at 'U_{P_3}' for the cross-ply and the angle-ply IM7-PEEK laminated composite Plate 3, subjected to pulse loading at various temperatures with simply-supported boundary condition at all four edges.

Temp.	Peak	0°/90°/ 90°/0°	0°/90°/ 0°/90°	45°/−45°/ −45°/45°	45°/−45°/ 45°/−45°
0 °C	w (mm)	0.0055	0.0075	0.0070	0.0066
	σ_x (N/mm^2)	0.72	0.78	0.38	0.27
25 °C	w (mm)	0.0057	0.0080	0.0073	0.0069
	σ_x (N/mm^2)	0.76	0.85	0.39	0.28
50 °C	w (mm)	0.0060	0.0086	0.0078	0.0074
	σ_x (N/mm^2)	0.80	0.90	0.41	0.29
75 °C	w (mm)	0.0064	0.0093	0.0084	0.0079
	σ_x (N/mm^2)	0.83	0.98	0.44	0.31
100 °C	w (mm)	0.0068	0.0101	0.0090	0.0083
	σ_x (N/mm^2)	0.88	1.05	0.46	0.32
125 °C	w (mm)	0.0073	0.0111	0.0097	0.0090
	σ_x (N/mm^2)	0.91	1.16	0.48	0.34

The first NDF, λ_1, increases in the higher rate with the increment in the depths of stiffener of the stiffened Plate 2 with 45°/−45°/−45°/45° laminate at all respective temperatures. Whereas, with the increment in the depths of stiffener in the stiffened Plate 3 with the corresponding laminate, the first NDF, λ_1, is increased marginally. Symmetric angle-ply laminate, i.e., 45°/−45°/−45°/45° offers comparatively higher shear stiffness than the corresponding symmetric cross-ply laminate, and increment in the depths of stiffener oriented parallel to the longer edge increases bending stiffness of the stiffened plates in higher rate than that of the stiffener oriented parallel to the shorter edge; which advocates the highest rate of increment of the first NDF, λ_1, with the increment of the depths of stiffener for the stiffened Plate 2 with 45°/−45°/−45°/45° laminate at all respective temperatures. As expected, the first NDF, λ_1, of all the stiffened plates decreases with the increment in temperature.

In addition, the corresponding transient response in terms of deflection, w, at nodes 'U_{P_2}' and 'U_{P_3}' of the Plates 2 and 3 are presented in Figs. 14 and 15, respectively. It is observed from the transient response, w, for the stiffened Plate 2 in Fig. 14 that the amplitude of dynamic deflection is decreasing with the increment in the stiffener depth for both the laminates as bending stiffness of the stiffened laminated composite plates increases with increment of the depths of stiffener. The similar trend is also observed for the stiffened Plate 3 with the stiffener oriented parallel to the shorter edge in Fig. 15. The mass of the structure is increased at the rate of 4% and 2.67% with every addition of 4 mm depth to the stiffener in the orientation of the longer and shorter directions, respectively in comparison with the unstiffened plate. It has indicated that the 12-mm deep stiffener oriented parallel to the longer edge becomes more effective as the consecutive rate of reduction in the amplitude of the dynamic deflection is higher than the 16-mm deep stiffener with a marginal increment in the mass. A marginal reduction in the amplitude of the dynamic deflection is observed for the stiffened Plate 3 with the increment of the stiffener depths in the considered temperatures. This dynamic behavior of the stiffened Plate 3 is supported by the earlier observation of marginal increment of the first NDF, λ_1, with the increment of the depths of stiffener. This implies that the stiffness of the Plate 3 has not increased sufficiently with an increment in the stiffener depths. Rate of variation in the amplitude of the dynamic deflection is reducing with the increment in depths of stiffener for a laminate. With the increment of the stiffener depth, the rate of reduction of the amplitude of dynamic deflection is highest for the stiffened Plate 2 (Fig. 14) at 100 °C temperature, which attributed to the fact of higher rate increment of the bending stiffness with the increment of the stiffener depths for the stiffener oriented parallel to the longer edge, and this effect became significant for stiffened Plate 2 at 100 °C temperature.

4.4. Adding stiffener vis-á -vis thickening unstiffened plate

In order to limit the peak dynamic deflection in thermal environment, the stiffness of plates is needed to be increased. The increment in the structural stiffness can be achieved by two ways: (1) by increasing the thickness of the plate, and (2) by addition of stiffener(s) to the plate. The transient response in terms of deflection, w, and normal stress, σ_x, at the node 'U_{P_1}' of the unstiffened Plate 1 for various thicknesses such as 2 mm, 4 mm, and 6 mm are compared with transient response at 'U_{P_2}' and 'U_{P_3}' of 2-mm thick stiffened Plates 2 and 3 with an 8-mm deep stiffener attached parallel to the longer and shorter edges of the plate to investigate effectiveness of adding the stiffener in thermal environment. The corresponding transient response, w and σ_x, are illustrated in Fig. 16, for 0°/90°/0°/90° laminate at 0 °C, 25 °C, and 100 °C temperatures. It is observed that addition of the stiffener oriented parallel to the longer edge can reduce the amplitude of dynamic deflection and normal stress more effectively in comparison to the increment in the thickness of the unstiffened plate at higher temperature. The corresponding peak dynamic deflection, w, and normal stress, σ_x, are computed from the transient response, and are given in Tables 18 and 19, respectively.

The percentage reduction in the peak dynamic deflection and normal stress is computed with respect to the 2-mm thick unstiffened plate (cf. Tables 18 and 19). The percentage reduction in the peak dynamic deflection for 4-mm and 6-mm thick unstiffened plates are 85.7% and 95.7% at 0 °C temperature. However, addition of an 8-mm deep stiffener oriented parallel to the longer and shorter edges with 2-mm thick plate reduces the peak dynamic deflection by 80.3% and 77.1% with the expense of only 8% and 5.3% mass increment, respectively. Further, the stiffened Plate 2 could reduce the peak dynamic deflection by 82.4% and 90.4% at 25 °C and 100 °C temperatures, respectively, and the reduction in the peak dynamic deflection of the stiffened Plate 3 at the corresponding temperatures are 79.2% and 87.1%. The 6-mm thick plate reduces the dynamic deflection marginally with the rise in temperature, in comparison with the 4-mm thick unstiffened plate. Therefore, it can be inferred that the rate of reduction in the dynamic deflection for the unstiffened plates reduces with the increment in the plate thickness. Furthermore, the rate of percentage reduction in the dynamic deflection is increased for the stiffened plate with the increment in temperature as compared to the unstiffened plate. However, percentage of reduction of transient response, w, for the stiffened Plate 3 is less as compared to the stiffened Plate 2. Thus, the stiffened plate with a stiffener oriented parallel to the longer edge could reduce the dynamic deflection sufficiently with very less penalty of adding mass as compared to the increment in plate thickness. Advantage of addition of the stiffener in the longer direction for reducing dynamic deflection also predominant at the higher temperatures. From Table 19, it is also observed that the corresponding peak normal

Table 17
First NDF, λ_1, for 0°/90°/90°/0° and 45°/−45°/−45°/45° IM7-PEEK stiffened laminated composite Plates 2 and 3 with the depths of stiffener, d_s, as 8 mm, 12 mm, and 16 mm at 0 °C, 25 °C, and 100 °C temperatures for simply-supported boundary condition at all four edges.

Types of stiffened plate	d_s	NDF, λ_1					
		0°/90°/90°/0°			45°/−45°/−45°/45°		
		0 °C	25 °C	100 °C	0 °C	25 °C	100 °C
Plate 2	8 mm	42.65	41.63	38.57	41.14	40.08	36.63
	12 mm	51.26	48.27	38.97	56.67	55.91	53.22
	16 mm	50.60	47.50	37.53	70.22	68.10	63.17
Plate 3	8 mm	49.61	47.98	44.28	50.50	48.96	45.64
	12 mm	49.87	48.21	44.41	50.97	49.36	46.03
	16 mm	50.09	48.45	44.61	51.17	49.56	46.23

$\lambda_1 = 2\pi f_1 L^2(\rho/E_{22}h^2)^{1/2}$.

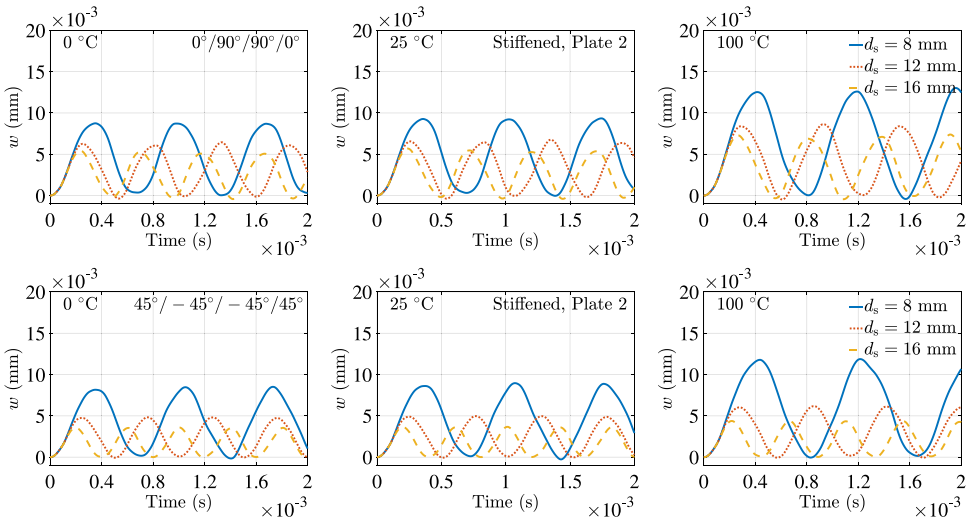

Fig. 14. Dynamic deflection, w, at node 'U_{P_2}' for the Plate 2 with 0°/90°/90°/0° and 45°/−45°/−45°/45° IM7-PEEK laminated composite plates for different depths of stiffener, d_s, subjected to pulse loading at 0 °C, 25 °C, and 100 °C temperatures for simply-supported boundary condition at all four edges.

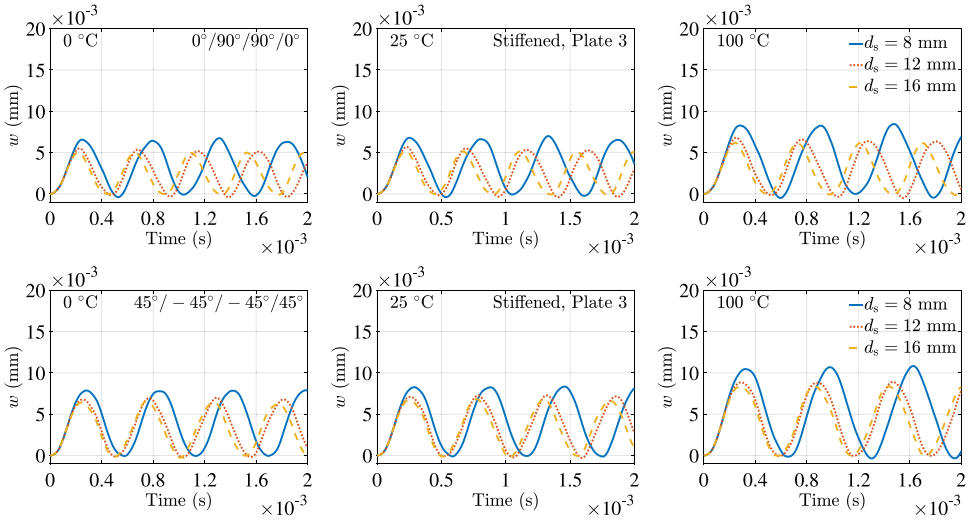

Fig. 15. Dynamic deflection, w, at node 'U_{P_3}' for the Plate 3 with 0°/90°/90°/0° and 45°/−45°/−45°/45° IM7-PEEK laminated composite plates for different depths of stiffener, d_s, subjected to pulse loading at 0 °C, 25 °C, and 100 °C temperatures for simply-supported boundary condition at all four edges.

stress is decreased with the attachment of stiffener oriented parallel to the longer and shorter edges (i.e., Plates 2 and 3, respectively) in comparison to the Plate 1 with 2 mm thickness, specifically at the higher temperature. However, the performance of the reduction of the peak normal stress of the stiffened Plate 3 is less than the Plate 1 with varying thickness and the stiffened Plate 2. The advantages of addition of the stiffener oriented parallel to the longer edge for reducing the dynamic response in thermal environment with some mass increment are also revealed from the tables. Therefore, the stiffened plate with the stiffener oriented parallel to the longer edge is the preferable choice than the stiffened plate with the stiffener oriented parallel to the shorter edge

Table 18
Comparison of the peak dynamic deflection, w, of IM7-PEEK laminated composite Plate 1 with various thicknesses and the Plates 2 and 3 with 8-mm deep stiffener oriented parallel to the longer and shorter edges, respectively at 0 °C, 25 °C, and 100 °C temperatures for 0°/90°/0°/90° laminate with simply-supported boundary condition at all four edges.

Geometry of plate	0 °C		25 °C		100 °C		% of mass diff.
	w (mm)	% of diff.	w (mm)	% of diff.	w (mm)	% of diff.	
Plate 1, $h = 2$ mm	0.0371	–	0.0432	–	0.0929	–	–
Plate 1, $h = 4$ mm	0.0053	−85.7	0.0055	−87.3	0.0067	−92.8	100
Plate 1, $h = 6$ mm	0.0016	−95.7	0.0017	−96.1	0.0019	−97.9	200
Plate 2, $h = 2$ mm, $d_s = 8$ mm	0.0073	−80.3	0.0076	−82.4	0.0089	−90.4	8.0
Plate 3, $h = 2$ mm, $d_s = 8$ mm	0.0085	−77.1	0.0090	−79.2	0.012	−87.1	5.3

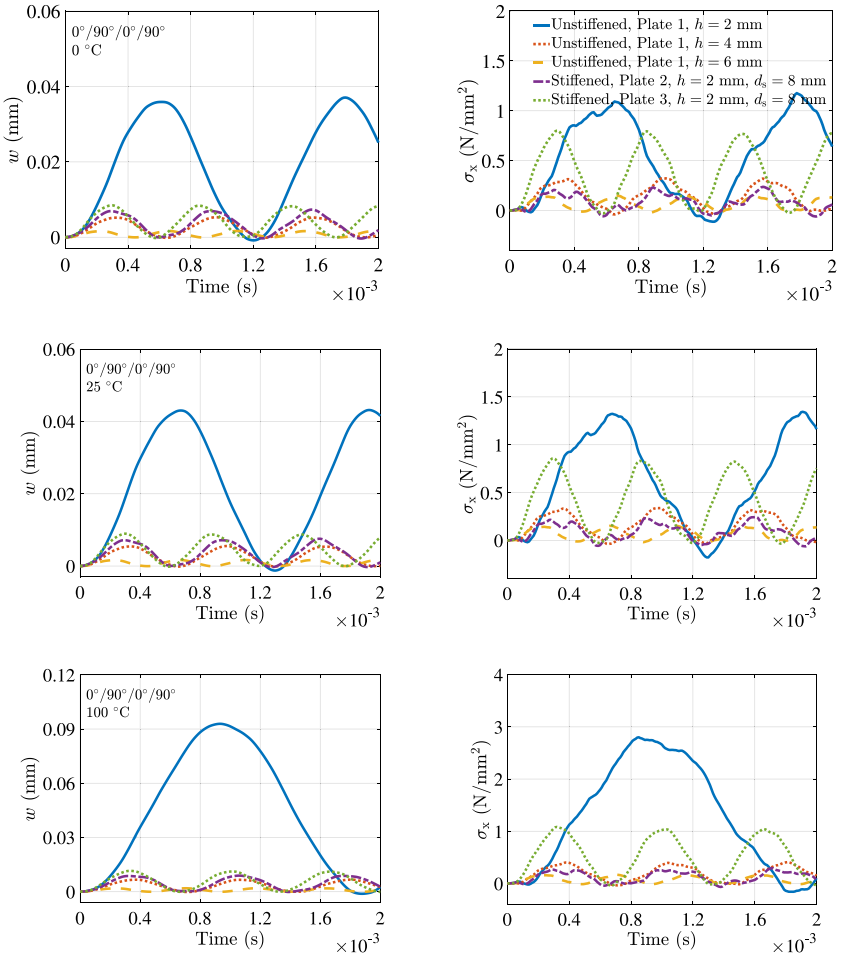

Fig. 16. Dynamic deflection, w, and normal stress, σ_x, at node 'U_{P_1}' for the Plate 1 with various thicknesses, and at node 'U_{P_2}' and 'U_{P_3}' for the Plates 2 and 3, respectively with 8-mm deep stiffener oriented parallel to the longer and shorter edges for 0°/90°/0°/90° IM7-PEEK laminated composite plates with simply-supported boundary condition in all four edges, subjected to the pulse loading at temperatures 0 °C, 25 °C, and 100 °C, respectively.

Table 19
Comparison of the peak normal stress, σ_x, of IM7-PEEK laminated composite Plate 1 with various thicknesses and the Plates 2 and 3 with 8-mm deep stiffener oriented parallel to the longer and shorter edges, respectively at 0 °C, 25 °C, and 100 °C temperatures for 0°/90°/0°/90° laminate with simply-supported boundary condition at all four edges.

Geometry of plate	0 °C		25 °C		100 °C		% of mass diff.
	σ_x (N/mm²)	% of diff.	σ_x (N/mm²)	% of diff.	σ_x (N/mm²)	% of diff.	
Plate 1, $h = 2$ mm	1.18	–	1.34	–	2.8	–	–
Plate 1, $h = 4$ mm	0.32	−72.9	0.34	−74.6	0.4	−85.4	100
Plate 1, $h = 6$ mm	0.15	−87.3	0.16	−88.1	0.17	−93.9	200
Plate 2, $h = 2$ mm, $d_s = 8$ mm	0.24	−79.7	0.250	−81.3	0.29	−89.6	8.0
Plate 3, $h = 2$ mm, $d_s = 8$ mm	0.80	−32.2	0.86	−35.8	1.08	−61.4	5.3

for the response reduction of w and σ_x in thermal environment using 0°/90°/0°/90° laminate.

5. Conclusion

The dynamic analysis of unstiffened and stiffened IM7-PEEK laminated composite plates in thermal environment has been presented by considering the temperature-dependent elastic properties. For this, a generalized finite element formulation, that can analyze unstiffened and stiffened laminated composite plates is developed with reference to the Hamilton's variational principle. In the presented finite element formulation, the first-order shear deformation theory has been implemented by including an additional drilling degree of freedom to account for three translations and three rotations per node, and the thermal effects. The accuracy of the present finite element formulation has been verified with the results reported in the literature and that with ANSYS® simulations, and a good agreement has been obtained. The non-dimensional frequencies and the transient response in terms of deflection and normal stress are studied for different stiffener orientations in various thermal environment including below reference temperature, i.e., at 0 °C. To address the research gap, the performance of the considered stiffened plates with various depth of stiffeners, which are oriented parallel to the longer and shorter edges, are studied in varying thermal environments. The plates are analyzed considering symmetric and antisymmetric cross-ply and angle-ply lamina sequences. It is found that the non-dimensional frequencies decrease with the increment in temperature above the reference temperature for both unstiffened and stiffened plates. Further, the non-dimensional frequencies of unstiffened and stiffened plates below the reference temperature are higher than that at the reference temperature. The stiffened plate with the stiffener oriented parallel to the longer edge with 0°/90°/0°/90° IM7-PEEK laminate exhibits the highest first non-dimensional frequency at all respective temperatures. The stiffener can advantageously be used to avoid dynamic instability, as observed for 0°/90°/90°/0° unstiffened IM7-PEEK laminated composite plate at 125 °C, of unstiffened laminated composite plates at higher temperature.

Lamina sequences play a crucial role in transient response of unstiffened laminated composite plates in thermal environment. The plate with the antisymmetric angle-ply laminate exhibits lower transient response in terms of the deflection and normal stress at all temperatures as compared to the plates with symmetric angle-ply as well as symmetric and antisymmetric cross-ply laminates. Provision of the stiffener reduces the transient response in terms of deflection and normal stress significantly. The stiffened plate with stiffener oriented parallel to the longer edge and made-up of antisymmetric cross-ply laminate offers the lowest transient response in terms of the deflection at all temperatures; whereas, the lowest normal stress is observed in case of the stiffened plate made-up of antisymmetric angle-ply laminate with the stiffener oriented parallel to the longer edge. Moreover, it is observed that the peak dynamic deflection of stiffened plates reduces further by increasing the stiffener depth, although, the rate of reduction decreases with the increment in the stiffener depth. The stiffened plate with stiffener oriented parallel to the longer edge offers higher rate of reduction in the peak dynamic deflection with the increasing stiffener depth, and is notable at the higher temperature. Study shows that the 12-mm deep stiffener can be considered as the most effective depth for achieving significant dynamic response reduction in thermal environment. Further, the rate of reduction in the magnitudes of the peak dynamic deflection and normal stress for stiffened plates with stiffener oriented parallel to the longer edge is higher in comparison with the associated unstiffened plates with incremental thickness, at the higher temperature than at the lower temperature. These outcomes will guide designers and engineers for efficient selection of the stiffener orientation and stiffener depth based on the considered laminae sequences and the operating temperature.

CRediT authorship contribution statement

S. Chandra: Conceptualization, Methodology, Programing, Validation, Investigation, Result analysis, Data curation, Writing – original draft, Writing – review & editing. **K. Sepahvand:** Methodology, Writing – review & editing. **V.A. Matsagar:** Conceptualization, Result analysis, Writing – review & editing, Supervision. **S. Marburg:** Resource, Writing – review & editing, Supervision.

Declaration of competing interest

The authors declare that they have no known competing financial interests or personal relationships that could have appeared to influence the work reported in this paper.

Data availability

Data will be made available on request.

Acknowledgments

The first and third authors gratefully acknowledge the financial support extended by the Deutscher Akademischer Austauschdienst (DAAD), Germany under Research Grants - Doctoral Program in Germany, and that by the Alexander von Humboldt Foundation, Germany under Fellowship for Experienced Researcher.

Appendix

Transformed reduced stiffness matrix of the kth lamina in the laminate coordinate (x, y, z) system:

$$[Q]_k = \begin{bmatrix} Q_{11} & Q_{12} & Q_{16} & 0 & 0 \\ Q_{21} = Q_{12} & Q_{22} & Q_{26} & 0 & 0 \\ Q_{61} = Q_{16} & Q_{62} = Q_{26} & Q_{66} & 0 & 0 \\ 0 & 0 & 0 & Q_{44} & Q_{45} \\ 0 & 0 & 0 & Q_{54} = Q_{45} & Q_{55} \end{bmatrix}. \quad (A.1)$$

Stress–strain relationship matrix of the kth lamina in the lamina coordinate (1, 2, 3) system:

$$[C]_k = \begin{bmatrix} C_{11} = \frac{E_{11}}{1-\nu_{12}\nu_{21}} & C_{12} = \frac{\nu_{12}E_{11}}{1-\nu_{12}\nu_{21}} & 0 & 0 & 0 \\ C_{21} = \frac{\nu_{12}E_{11}}{1-\nu_{12}\nu_{21}} & C_{22} = \frac{E_{22}}{1-\nu_{12}\nu_{21}} & 0 & 0 & 0 \\ 0 & 0 & C_{66} = G_{12} & 0 & 0 \\ 0 & 0 & 0 & C_{44} = G_{13} & 0 \\ 0 & 0 & 0 & 0 & C_{55} = G_{23} \end{bmatrix}. \quad (A.2)$$

Non-linear strain vector, $\{\epsilon_{nt}\}$, and vector of partial derivative of displacement, $\{d^*\}$, relationship matrix:

$$[R]^T = \begin{bmatrix} u_{0,x} + 2z\theta_{y,x} & 0 & u_{0,y} + 2z\theta_{y,y} & 0 & 0 \\ 0 & u_{0,y} + 2z\theta_{y,y} & z\theta_{y,x} & 0 & 0 \\ v_{0,x} - 2z\theta_{x,x} & 0 & \theta_{0,y} - z\theta_{x,y} & 0 & 0 \\ 0 & v_{0,y} - 2z\theta_{x,y} & -z\theta_{x,x} & 0 & 0 \\ w_{0,x} & 0 & 0 & 0 & 0 \\ 0 & w_{0,y} & w_{0,x} & 0 & 0 \\ z^2\theta_{x,x} & 0 & z^2\theta_{x,y} & z\theta_x & 0 \\ 0 & z^2\theta_{x,y} & 0 & 0 & z\theta_x \\ z^2\theta_{y,x} & 0 & z^2\theta_{y,y} & z\theta_y & 0 \\ 0 & z^2\theta_{y,y} & 0 & 0 & z\theta_y \\ 0 & 0 & 0 & -v_{0,x} & -v_{0,y} \\ 0 & 0 & 0 & u_{0,x} & u_{0,y} \end{bmatrix}. \quad (A.3)$$

$$[S_r] = \begin{bmatrix}
N_x^i & N_{xy}^i & 0 & 0 & 0 & 0 & 0 & 0 & M_x^i & M_{xy}^i & 0 & Q_x^i \\
N_{xy}^i & N_y^i & 0 & 0 & 0 & 0 & 0 & 0 & M_{xy}^i & M_y^i & 0 & Q_y^i \\
0 & 0 & N_x^i & N_{xy}^i & 0 & 0 & -M_x^i & -M_{xy}^i & 0 & 0 & -Q_x^i & 0 \\
0 & 0 & N_{xy}^i & N_y^i & 0 & 0 & -M_{xy}^i & -M_y^i & 0 & 0 & -Q_y^i & 0 \\
0 & 0 & 0 & 0 & N_x^i & N_{xy}^i & 0 & 0 & 0 & 0 & 0 & 0 \\
0 & 0 & 0 & 0 & N_{xy}^i & N_y^i & 0 & 0 & 0 & 0 & 0 & 0 \\
0 & 0 & -M_x^i & -M_{xy}^i & 0 & 0 & \frac{N_x^i h^2}{12} & \frac{N_{xy}^i h^2}{12} & 0 & 0 & 0 & 0 \\
0 & 0 & -M_{xy}^i & -M_y^i & 0 & 0 & \frac{N_{xy}^i h^2}{12} & \frac{N_y^i h^2}{12} & 0 & 0 & 0 & 0 \\
M_x^i & M_{xy}^i & 0 & 0 & 0 & 0 & 0 & 0 & \frac{N_x^i h^2}{12} & \frac{N_{xy}^i h^2}{12} & 0 & 0 \\
M_{xy}^i & M_y^i & 0 & 0 & 0 & 0 & 0 & 0 & \frac{N_{xy}^i h^2}{12} & \frac{N_y^i h^2}{12} & 0 & 0 \\
0 & 0 & -Q_x^i & -Q_y^i & 0 & 0 & 0 & 0 & 0 & 0 & 0 & 0 \\
Q_x^i & Q_y^i & 0 & 0 & 0 & 0 & 0 & 0 & 0 & 0 & 0 & 0
\end{bmatrix}. \tag{A.5}$$

Box II.

Shape function matrix corresponding to $\{d^*\}$:

$$[G] = \sum_{i=1}^{8} \begin{bmatrix}
N_{i,x} & 0 & 0 & 0 & 0 \\
N_{i,y} & 0 & 0 & 0 & 0 \\
0 & N_{i,x} & 0 & 0 & 0 \\
0 & N_{i,y} & 0 & 0 & 0 \\
0 & 0 & N_{i,x} & 0 & 0 \\
0 & 0 & N_{i,y} & 0 & 0 \\
0 & 0 & 0 & N_{i,x} & 0 \\
0 & 0 & 0 & N_{i,y} & 0 \\
0 & 0 & 0 & 0 & N_{i,x} \\
0 & 0 & 0 & 0 & N_{i,y} \\
0 & 0 & 0 & N_i & 0 \\
0 & 0 & 0 & 0 & N_i
\end{bmatrix}. \tag{A.4}$$

Here, shape function for the 8-node isoparametric element is denoted by N_i with $i = 1$ to 8.

Initial stress-stiffness matrix: $[S_r]$, see Box II.

References

[1] Halpin J. Effect of environmental factors on composite materials. Techinal report AFML-TR-67-423, 1969, p. 1–61.

[2] Halpin J, Pagano N. Consequences of environmentally induced dilation in solids. Techinal report AFML-TR-68-395, 1969, p. 1–32.

[3] Whitney J, Ashton J. Effect of environment on the elastic response of layered composite plates. AIAA J 1971;9:1708–13.

[4] Gander MJ, Wanner G. From Euler, Ritz, and Galerkin to modern computing. SIAM Rev 2012;54(4):627–66.

[5] Qatu M, Algothani A. Bending analysis of laminated plates and shells by different methods. Comput Struct 1994;52(3):529–39.

[6] Mahi A, Adda Bedia EA, Tounsi A. A new hyperbolic shear deformation theory for bending and free vibration analysis of isotropic, functionally graded, sandwich and laminated composite plates. Appl Math Model 2015;39(9):2489–508.

[7] Kapania RK, Singhvi S. Free vibration analyses of generally laminated tapered skew plates. Compos Eng 1992;2(3):197–212.

[8] Sai Ram K, Sinha P. Hygrothermal effects on the free vibration of laminated composite plates. J Sound Vib 1992;158(1):133–48.

[9] Patel B, Ganapathi M, Makhecha D. Hygrothermal effects on the structural behaviour of thick composite laminates using higher-order theory. Compos Struct 2002;56(1):25–34.

[10] Sepahvand K. Spectral stochastic finite element vibration analysis of fiber-reinforced composites with random fiber orientation. Compos Struct 2016;145:119–28.

[11] Sepahvand K. Stochastic finite element method for random harmonic analysis of composite plates with uncertain modal damping parameters. J Sound Vib 2017;400:1–12.

[12] Sepahvand K, Khosroshahi FS, Geweth CA, Marburg S. Stochastic structural dynamic analysis with random damping parameters. In: Proceedings of the 46th international congress and exposition on noise control engineering. 2017.

[13] Mangala A, Jayasuriya M, Dwivedi SN, Sivaneri NT, Lyons DW. Doubly curved laminated composite shells with hygrothermal conditioning and dynamic loads, part 1: A theoretical development and semielastic solution using a higher-order displacement field. Mech Adv Mater Struct 2002;9(1):53–68.

[14] Mangala A, Jayasuriya M, Dwivedi SN, Louisiana L, Sivaneri NT, Lyons DW. Doubly curved laminated composite shells with hygrothermal conditioning and dynamic loads, part 2: FEA and numerical results of shells of revolution. Mech Adv Mater Struct 2002;9(1):69–97.

[15] Naidu N, Sinha P. Nonlinear finite element analysis of laminated composite shells in hygrothermal environments. Compos Struct 2005;69(4):387–95.

[16] Naidu NS, Sinha P. Nonlinear free vibration analysis of laminated composite shells in hygrothermal environments. Compos Struct 2007;77(4):475–83.

[17] Shen H-S, Yang D-Q. Nonlinear vibration of functionally graded fiber-reinforced composite laminated cylindrical shells in hygrothermal environments. Appl Math Model 2015;39(5–6):1480–99.

[18] Shen H-S, Xiang Y, Fan Y. Nonlinear vibration of functionally graded graphene-reinforced composite laminated cylindrical shells in thermal environments. Compos Struct 2017;182:447–56.

[19] Sai Ram K, Sinha P. Hygrothermal effects on the buckling of laminated composite plates. Compos Struct 1992;21(4):233–47.

[20] Sreehari V, Maiti D. Buckling and post buckling analysis of laminated composite plates in hygrothermal environment using an inverse hyperbolic shear deformation theory. Compos Struct 2015;129:250–5.

[21] Zhai Y, Su J, Liang S. Free vibration and buckling analysis of composite sandwich plates in thermal environment. J Sandwich Struct Mater 2020;22(8):2604–28.

[22] Malekzadeh P. Differential quadrature large amplitude free vibration analysis of laminated skew plates based on FSDT. Compos Struct 2008;83(2):189–200.

[23] Malekzadeh P, Vosoughi A. Large amplitude free vibration analysis of composite plates with rotationally restrained edges using DQM. J Reinf Plast Compos 2008;27(4):409–30.

[24] Tornabene F, Fantuzzi N, Ubertini F, Viola E. Strong formulation finite element method based on differential quadrature: A survey. Appl Mech Rev 2015;67(2).

[25] Mohammadimehr M, Salemi M, Rousta Navi B. Bending, buckling, and free vibration analysis of MSGT microcomposite reddy plate reinforced by FG-SWCNTs with temperature-dependent material properties under hydro-thermo-mechanical loadings using DQM. Compos Struct 2016;138:361–80.

[26] Parhi P, Bhattacharyya S, Sinha P. Hygrothermal effects on the dynamic behavior of multiple delaminated composite plates and shells. J Sound Vib 2001;248(2):195–214.

[27] Huang X-L, Shen H-S, Zheng J-J. Nonlinear vibration and dynamic response of shear deformable laminated plates in hygrothermal environments. Compos Sci Technol 2004;64(10–11):1419–35.

[28] Shen H-S, Zheng J-J, Huang X-L. Dynamic response of shear deformable laminated plates under thermomechanical loading and resting on elastic foundations. Compos Struct 2003;60(1):57–66.
[29] Shen H-S, Zheng J-J, Huang X-L. The effects of hygrothermal conditions on the dynamic response of shear deformable laminated plates resting on elastic foundations. J Reinf Plast Compos 2004;23(10):1095–113.
[30] Reddy J. Mechanics of laminated composite plates and shells: Theory and analysis. second ed. London, UK: CRC Press; 2001, p. 109–12.
[31] Makhecha D, Ganapathi M, Patel B. Dynamic analysis of laminated composite plates subjected to thermal/mechanical loads using an accurate theory. Compos Struct 2001;51(3):221–36.
[32] Swamy Naidu N, Sinha P. Nonlinear transient analysis of laminated composite shells in hygrothermal environments. Compos Struct 2006;72(3):280–8.
[33] Nanda N, Pradyumna S. Nonlinear dynamic response of laminated shells with imperfections in hygrothermal environments. J Compos Mater 2011;45(20):2103–12.
[34] Bandyopadhyay T, Karmakar A, Kishimoto K. Transient response of delaminated composite conical shells due to multiple low velocity impacts in hygrothermal environment. Compos Struct 2016;143:202–19.
[35] Malekzadeh P, Monajjemzadeh S. Dynamic response of functionally graded plates in thermal environment under moving load. Composites B 2013;45(1):1521–33.
[36] Niu Y, Wang Z, Zhang W. Nonlinear thermal flutter analysis of supersonic composite laminated panels using differential quadrature method. Int J Struct Stab Dyn 2014;14(07):1450030.
[37] Liu L, Li J-M, Kardomateas GA. Nonlinear vibration of a composite plate to harmonic excitation with initial geometric imperfection in thermal environments. Compos Struct 2019;209:401–23.
[38] Chandra S, Sepahvand K, Matsagar VA, Marburg S. Stochastic dynamic analysis of composite plate with random temperature increment. Compos Struct 2019;226:111159.
[39] Kant T, Arora C, Varaiya J. Finite element transient analysis of composite and sandwich plates based on a refined theory and a mode superposition method. Compos Struct 1992;22(2):109–20.
[40] Kommineni J, Kant T. Large deflection elastic and inelastic transient analyses of composite and sandwich plates with a refined theory. J Reinf Plast Compos 1993;12(11):1150–70.
[41] Jonnalagadda K, Tauchert T, Blandford G. High-order thermoelastic composite plate theories: An analytic comparison. J Therm Stresses 1993;16(3):265–84.
[42] Khare R, Kant T, Garg A. Closed-form thermo-mechanical solutions of higher-order theories of cross-ply laminated shallow shells. Compos Struct 2003;59(3):313–40.
[43] Kant T, Khare R. Finite element thermal stress analysis of composite laminates using a higher-order theory. J Therm Stresses 1994;17(2):229–55.
[44] Sit M, Ray C, Biswas D. Thermal stress analysis of laminated composite plates using third order shear deformation theory. In: Advances in structural engineering: Mechanics. Vol. 1, 2015, p. 149–56.
[45] Punera D, Kant T, Desai Y. Thermoelastic analysis of laminated and functionally graded sandwich cylindrical shells with two refined higher order models. J Therm Stresses 2018;41(1):54–79.
[46] Naik N, Sayyad A. An accurate computational model for thermal analysis of laminated composite and sandwich plates. J Therm Stresses 2019;42(5):559–79.
[47] Kapuria S, Achary G. An efficient higher order zigzag theory for laminated plates subjected to thermal loading. Int J Solids Struct 2004;41(16):4661–84.
[48] Dumir P, Nath J, Kumari P, Kapuria S. Improved efficient zigzag and third order theories for circular cylindrical shells under thermal loading. J Therm Stresses 2008;31(4):343–67.
[49] Garg A, Chalak HD. A review on analysis of laminated composite and sandwich structures under hygrothermal conditions. Thin-Wall Struct 2019;142:205–26.
[50] Olson M, Hazell C. Vibration studies on some integral rib-stiffened plates. J Sound Vib 1977;50(1):43–61.
[51] Deb A, Booton M. Finite element models for stiffened plates under transverse loading. Comput Struct 1988;28:361–72.
[52] Mukherjee A, Mukhopadhyay M. Review of dynamic behaviour of stiffened plates. Shock Vib Dig 1986;338(18):3–8.
[53] Mukhopadhyay M, Mukherjee A. Recent advances on the dynamic behaviour of stiffened plates. Shock Vib Dig 1989;69(21):6–9.
[54] Thompson PA, Bettess P, Caldwell JB. An isoparametric eccentrically stiffened plate bending element. Eng Comput 1989;5:110–6.
[55] Attaf B, Hollaway L. Vibrational analyses of stiffened and unstiffened composite plates subjected to in-plane loads. Composites 1990;21(2):117–26.
[56] Lee D-M, Lee I. Vibration analysis of anisotropic plates with eccentric stiffeners. Comput Struct 1995;57(1):99–105.
[57] Chattopadhyay B, Sinha P, Mukhopadhyay M. Finite element analysis of blade-stiffened composite plates under transverse loads. J Reinf Plast Compos 1993;12(1):76–100.
[58] Qing G, Qiu J, Liu Y. Free vibration analysis of stiffened laminted plates. Int J Solids Struct 2006;43:1357–71.
[59] Talebitooti M, Daneshjou K, Talebitooti R. Vibration and critical speed of orthogonally stiffened rotating FG cylindrical shell under thermo-mechanical loads using differential quadrature method. J Therm Stresses 2013;36(2):160–88.
[60] Golchi M, Talebitooti M, Talebitooti R. Thermal buckling and free vibration of FG truncated conical shells with stringer and ring stiffeners using differential quadrature method. Mech Based Des Struct Mach 2019;47(3):255–82.
[61] Patro SS, Sutradhar D, Behera RK, Sharma N. Free vibration analysis of stiffened laminated composite plate in a thermal environment. IOP Conf Ser: Mater Sci Eng 2018;390:012040.
[62] Sit M, Ray C. Temperature induced nonlinear effect on free vibration characteristics of fibre reinforced polymer bridge deck. J Inst Eng (India) A 2019;100(1):147–55.
[63] Ray C, Satsangi SK. Finite element analysis of laminated hat-stiffened plates. J Reinf Plast Compos 1996;15(12):1174–93.
[64] Yu H, Zhao Z, Yang D, Gao C. A new composite plate/plate element for stiffened plate structures via absolute nodal coordinate formulation. Compos Struct 2020;247:112431.
[65] Chandra S, Sepahvand K, Matsagar V, Marburg S. Stochastic modal damping analysis of stiffened laminated composite plate. In: Saha SK, Mukherjee M, editors. Recent advances in computational mechanics and simulations. Singapore: Springer Singapore; 2021, p. 635–50.
[66] Moradi S, Vosoughi A, Anjabin N. Maximum buckling load of stiffened laminated composite panel by an improved hybrid PSO-GA optimization technique. Thin-Walled Struct 2021;160:107382.
[67] Sit M, Ray C. A third order nonlinear model to study the dynamic behaviour of composite laminated structures under thermal effect with experimental verification. Compos Struct 2019;212:106–17.
[68] Sinha L, Mishra S, Nayak A, Sahu S. Free vibration characteristics of laminated composite stiffened plates: Experimental and numerical investigation. Compos Struct 2020;233:111557.
[69] Kumar YVS, Mukhopadhyay M. Transient response analysis of laminated stiffened plates. Compos Struct 2002;58(1):97–107.
[70] Pal S, Guha Niyogi A. Application of folded plate formulation in analyzing stiffened laminated composite and sandwich folded plate vibration. J Reinf Plast Compos 2008;27(7):693–710.
[71] Guha Niyogi A, Laha M, Sinha P. Finite element vibration analysis of laminated composite folded plate structures. Shock Vib 1999;6(5–6):273–83.
[72] Balkan D, Demir O, Arikoğlu A. Dynamic analysis of a stiffened composite plate under blast load: A new model and experimental validation. Int J Impact Eng 2020;143:103591.
[73] Matsagar VA. Comparative performance of composite sandwich panels and non-composite panels under blast loading. Mater Struct 2016;49(1):611–29.
[74] Prusty BG, Satsangi S. Finite element transient dynamic analysis of laminated stiffened shells. J Sound Vib 2001;248(2):215–33.
[75] Goel M, Matsagar V, Gupta A. Dynamic response of stiffened plates under air blast. Int J Prot Struct 2011;2:139–56.
[76] Bathe K. Finite element procedures in engineering analysis. updated ed. Upper Saddle River, New Jersy 07458: Prentice Hall; 1982.
[77] Crisfield M. Shear-constraints and folded-plated structures. Eng Comput 1985;2:238–46.
[78] Thakur BR, Verma S, Singh B, Maiti D. Dynamic analysis of folded laminated composite plate using nonpolynomial shear deformation theory. Aerosp Sci Technol 2020;106:106083.
[79] Kant T, Varaiya J, Arora C. Finite element transient analysis of composite and sandwiched plates based on a refined theory and implicit time integration schemes. Comput Struct 1990;36(3):401–20.
[80] Rawal S, Misra M. Measurement of mechanical and thermophysical properties of dimensionally stable materials for space applications. NASA Contractor Report 18552, 1992, p. 1–159.

Publication 2

Reference: S. Chandra, M. Maeder, K. Sepahvand, V.A. Matsagar, S. Marburg, Damping analysis of stiffened laminated composite plates in thermal environment. *Composite Structures*, 300, 116163, 2022.

Composite Structures 300 (2022) 116163

Contents lists available at ScienceDirect

Composite Structures

journal homepage: www.elsevier.com/locate/compstruct

Damping analysis of stiffened laminated composite plates in thermal environment

S. Chandra [a,*], M. Maeder [a], K. Sepahvand [a], V.A. Matsagar [b], S. Marburg [a]

[a] Chair of Vibroacoustics of Vehicles and Machines, TUM School of Engineering and Design, Technical University of Munich (TUM), 85748 Garching b. Munich, Germany

[b] Department of Civil Engineering, Indian Institute of Technology (IIT) Delhi, Hauz Khas, New Delhi 110 016, India

ARTICLE INFO

Keywords:
Loss factor
Rayleigh damping
Modal expansion damping
Logarithmic decrement
Energy-based damping analysis
Stiffened laminated composite plate
Thermal environment

ABSTRACT

High-strength and lightweight composites used in high-speed vehicles and aircraft experience increased temperature owing to aerodynamic friction. Because of the rise in temperature, the elastic moduli of the composites are degraded and inherent viscous damping is increased to the glass transition temperature. In this work, the damping performance of unstiffened and stiffened polyetheretherketone (PEEK) based intermediate modulus (IM7) carbon fiber laminated composite plates is evaluated at various temperatures using displacement- and energy-based approaches. In the displacement-based approach, the logarithmic decrement of the damped vibration is determined to investigate the effect of lamina sequences, stiffener orientation, and stiffener depth at different temperatures. A first-order shear deformation theory considering the viscoelastic property of the composite lamina is implemented to simulate the damped dynamic response of the laminated composite plates in a thermal environment. The best suitable damping model, among Rayleigh damping and modal expansion damping, has been identified to evaluate the damping matrix. Furthermore, the energy-based damping analysis appeared to be a robust approach to evaluate the damping performance as compared to the displacement-based analysis. It is concluded that stiffened plates effectively suppress the dynamic response at elevated temperature, whereas the unstiffened plates show relatively better damping performance at lower temperature.

1. Introduction

Excessive vibration in lightweight composite structures subjected to various kinds of dynamic loading needs to be controlled or prevented. Nowadays, lightweight composite plates are used to manufacture different important components of aircraft, sportscars, high-speed trains, etc. During high-speed maneuvering, the temperature of structural components increases owing to the aerodynamic friction and the rise in the surrounding temperature due to the heat exchange from drive units. This affects the material properties of the composite materials as well as damping characteristics. To withstand harsh and hazardous environmental conditions, high-strength composite materials such as graphite-epoxy, carbon-epoxy, and intermediate modulus (IM7) carbon-polyetheretherketone (PEEK) are used as a principal material. In addition, these composite materials possess sufficient structural stability in thermal environment. However, the elastic properties degrade with the increment in temperature whereas damping increases with the rise in temperature to the glass transition temperature [1]. Beyond this temperature, damping is reduced with further increase in temperature. The thin high-strength laminated composite plates subjected to dynamic loading in a thermal environment show large magnitudes of vibration. This may reduce the fatigue life of plates and often cause fracture. These issues lead to a significant loss of the structural integrity of the high-strength composite plates during operating condition. Therefore, controlling the dynamic response is essential in a thermal environment and can be achieved by considering the damping under the thermal influence.

Damping can be added through various strategies, such as active, passive, and active–passive hybrid vibration controls that are implemented to suppress the vibration amplitude of laminated composite plates. A substantial advancement in the research on the active vibration control using piezoelectric materials [2,3] and shape memory alloys [4,5] has been observed in the past few decades. The active vibration control using such materials has been widely studied and is implemented to suppress the dynamic response of laminated composite plates [6,7]. In contrast, passive vibration control using inherent damping capacity and interleaved viscoelastic damping layers is relatively simple to implement and perhaps inexpensive relatively. Generally,

* Corresponding author.
E-mail address: sourav.chandra@tum.de (S. Chandra).

https://doi.org/10.1016/j.compstruct.2022.116163
Received 16 December 2021; Received in revised form 6 June 2022; Accepted 14 August 2022
Available online 22 August 2022
0263-8223/© 2022 Elsevier Ltd. All rights reserved.

active vibration control offers better vibration abatement than passive control by requiring additional power supply to the dynamic system along with the proper implementation of the control algorithm. However, in the case of a simple and cost-effective implementation of vibration control, passive vibration control can be used conveniently to achieve a sufficient suppression of the vibration amplitude. Therefore, this study intends to investigate the damping performance of laminated composite plates due to the inherent damping capacity in various thermal environments.

The need to investigate on temperature-dependent damping in laminated composite plates emerges evidently upon reviewing the state-of-the-art in detail. A free vibration analysis of the laminated composite plates in thermal environment using the first-order shear deformation theory (FSDT) has been studied by Whitney and Ashton [8] and Sai Ram and Sinha [9]. Similarly, the free vibration analysis based on higher-order shear deformation theory (HSDT) in a hygrothermal environment was presented by Patel et al. [10]. Furthermore, free and forced vibration analyses of composite shells using the HSDT has been studied by various researchers including Mangala et al. [11,12], Huang et al. [13], Naidu and Sinha [14,15], and Nanda and Pradyumna [16]. Parhi et al. [17] has studied the transient response of the delaminated composite plates and shells in hygrothermal environment using the FSDT. Chandra et al. [18] has presented a stochastic dynamic analysis of graphite-epoxy laminated composite plate in thermal environment using the FSDT in an uncertain thermal environment, however did not account for the variation in temperature-dependent damping.

To reduce the amplitude of the dynamic response without much addition of structural mass, stiffener(s) can be added to the laminated composite plates. Nowadays, stiffened laminated composite plates are efficiently used in various structural components such as wings of aircraft to increase structural stiffness and thereby contribute to stability of the structural systems [19,20]. For numerical simulation, various finite element (FE) formulations using beam and plate elements have been developed. Chattopadhyay et al. [21], Kumar and Mukhopadhyay [22], Pal and Niyogi [23], and Yu et al. [24] have investigated the dynamic response of the stiffened laminated composite plates by utilizing plate elements in modeling the stiffener. In contrast, Lee and Lee [25] and Qing et al. [26] have analyzed stiffened plates by using beam elements. Ray and Satsangi [27] have modeled the stiffener independently, wherein the corresponding stiffness matrix was included with the unstiffened plate element during the analysis.

The energy dissipation in the laminated composite plates is determined to calculate the inherent damping capacity which is due to the viscoelastic behavior of the matrix part of the composite material. The damping capacity of the laminated composite plates is evaluated by a complex modulus approach [28–30]. Bouadi and Sun [31] have adopted the complex modulus approach to investigate the effect of temperature and moisture on the storage moduli and the damping loss factors of composite plates, numerically and experimentally. Some experimental studies [32–34] have been reported with an aim to maximize the damping loss factors in various thermal environments. The dissipation of energy from composite plates is represented by specific damping capacities (SDCs). It is expressed as a ratio between the dissipated energy and the total strain energy per stress cycle [35–39]. Further, Saravanos and Chemis [40] have studied the effect of temperature and moisture on the damping capacity of a graphite-epoxy laminated composite plate using the micromechanical damping theory. Some researchers [41–44] have shown interest in examining the variation in the SDCs due to the influence of temperature and frequency for different types of composite plates, both numerically and experimentally. Uncertainty in frequency response functions (FRFs) due to random modal damping has been studied by Sepahvand [45,46]. Stochastic modal damping analysis for stiffened laminated composite plates has been presented by Chandra et al. [47] using the complex modulus approach. Some research contributions on damping in composite plates have been summarized in [48,49].

To study the efficacy in suppressing the dynamic response due to inherent damping, the corresponding damped dynamic response in the time domain and/or frequency domain was evaluated. Zabaras and Pervez [50,51] have evaluated the modal SDCs of the laminated composite plates due to inherent damping, where the damping matrix was incorporated into the FE modeling with the definition of Rayleigh damping to calculate the damped dynamic response in the time domain. The implementation of Rayleigh damping to calculate the damping matrix assuming well-separated eigenfrequencies has been reported in [52]. Zabaras and Pervez [50,51] have illustrated the damped dynamic response of laminated composite plates due to inherent damping based on the viscoelastic theory. Further, Yi et al. [53] have studied the influence of temperature on the damped dynamic response of cross-ply and angle-ply cylindrical shells without considering temperature-dependent elastic and damping properties. Kiral [54] has investigated the damped dynamic response of composite beam due to harmonic excitation using Rayleigh damping formulation. Şahan [55] determined the damped dynamic response of a shallow spherical shell using Laplace transformation subjected to a impulsive loading where the damping matrix has been estimated in accordance with the Kelvin viscoelastic model. In addition to the time domain analysis, Jeyaraj et al. [56] have presented frequency domain analysis of the laminated composite plates in different thermal environments using the complex modulus method. Many researchers [50,51,53] have determined the damping matrix based on the concept of Rayleigh (mass and/or stiffness proportional) damping considering the modal damping values of the first two modes without considering the thermal effect. However, the application of the Rayleigh damping model considering the first two modes may not be suitable for engineering structures with complex geometry as they are subjected to non-proportional damping [57]. Moreover, energy analysis is primarily conducted to assess the seismic performance of ductile structures [58] which includes energy dissipation due to hysteretic behavior [59] and damping [60,61]. Moreover, various response control strategies have been developed based on energy assessment criteria [62–64].

However, the authors have yet not found any study evaluating the damping performance of unstiffened and stiffened laminated composite plates considering temperature-dependent elastic and damping properties at different temperatures. In this context, research to date is limited and does not account for the effect of temperature-dependent damping in FE formulation. Even though Zabaras and Pervez [50,51] have studied the damped response of laminated composite plates, it was without considering any thermal effects. Therefore, it is essential to study the effect of the temperature-dependent damping of unstiffened and stiffened laminated composite plates and their performance at different temperatures when subjected to thermo-mechanical loading. This paper intends to investigate the inherent damping performance of such composite plates using displacement-based and energy-based approaches. The decay in the damped dynamic deflection is determined, denoted as displacement-based approach, to evaluate the damping performance of the unstiffened and stiffened laminated composite plates. Furthermore, energy-based assessment of the damping performance for these plates in thermal environment is presented. Particularly, this study investigates the inherent damping performance of high-strength IM7-PEEK unstiffened and stiffened laminated composite plates based on the displacement-based and energy-based approaches in thermal environment considering temperature-dependent elastic and damping properties. The FE formulation for the unstiffened and stiffened laminated composite plates is developed by employing the FSDT using an 8-node isoparametric plate element with six degrees of freedom (DOFs) per node, which includes conventional five DOFs (three translational DOFs and two rotational DOFs) and one additional drilling DOF. The modal damping values for unstiffened and stiffened laminated composite plates are evaluated based on the complex modulus approach by implementing the viscoelastic damping principle. The damping performance of the unstiffened and stiffened laminated composite plates

in various thermal environments is evaluated based on the decay in the damped dynamic response and assessment of the inherent damping energy.

The main objectives of the current study are: (a) to evaluate the modal damping values of the unstiffened and stiffened laminated composite plates in thermal environment; (b) to identify the best suitable approach to calculate the damping matrix for the purpose of evaluating the damped dynamic response in thermal environment; (c) to investigate the influence of various parameters of the unstiffened and stiffened laminated composite plates such as lamina sequences, stiffener orientations, depths of the stiffener, and operating harmonic frequency for efficient vibration control in thermal environment using the logarithmic decrement; and (d) to assess damping energy while evaluating the damping performance of such plates in thermal environment. Thus, the novelty of this work is in developing the FE formulation taking modal damping into account to evaluate the damped dynamic response of the unstiffened and stiffened laminated composite plates at various thermal environment realistically. Furthermore, this paper has furnished a detailed comparative study to identify the best possible methodology for evaluating the damping performance.

In what follows, a mathematical framework is introduced in Section 2, which includes a generalized FE formulation to analyze the unstiffened and stiffened laminated composite plates, while determining the damping matrix based on Rayleigh damping and modal expansion damping, respectively. The algorithm of the FE formulation to determine the damped dynamic response is illustrated in Section 3. Next in Section 4, the best suitable damping approach between Rayleigh damping and modal expansion damping is identified, and results from various parametric studies are reported using the selected damping model to understand damping performance of the unstiffened and stiffened laminated composite plates at different temperatures using displacement-based and energy-based approaches. Finally, conclusions as derived from the present study are written in Section 5.

2. Mathematical formulations

An FE formulation has been developed to calculate the damped dynamic response of the unstiffened and stiffened laminated composite plates subjected to dynamic loading in thermal environment. It is assumed that the stiffeners are in perfect connection with the plate. The geometry of the laminated composite plate consisting of length, L; width, W; and uniform thickness, h, is shown in Fig. 1. Primarily, the FE formulation of a thin unstiffened laminate has been developed using an 8-node isoparametric plate element with five DOFs per node, based on the FSDT for n number of unidirectional lamina of equal thickness. Furthermore, the FE formulation for stiffened laminated composite plates is developed by using folded plate theory [23] by considering five conventional DOFs and a drilling DOF per node of a plate element.

2.1. Constitutive relationship

A generalized displacement field, $\bar{\boldsymbol{d}} = \{u \quad v \quad w \quad \theta_x \quad \theta_y\}^T$, (cf. Fig. 1) of the composite laminate is considered for developing a constitutive relationship based on the FSDT. According to the FSDT, the displacement field, $\bar{\boldsymbol{d}}$, is calculated with the assumption that the normal of the mid-plane of the composite laminate remains orthogonal during deformation. Here, the mid-plane is assumed as a reference plane for evaluating the components of $\bar{\boldsymbol{d}}$ of the laminate at a distance z from the mid-plane, and the components of $\bar{\boldsymbol{d}}$ are expressed as

$$\begin{aligned} u &= u_0 + z\theta_y, \\ v &= v_0 - z\theta_x, \\ w &= w_0, \end{aligned} \tag{1}$$

where u and v are in-plane translations along the x and y axes, respectively, w is out-of-plane deformation along the z axis, and rotations of the transverse normal about the x and y axes are defined by θ_x and θ_y, respectively. The mid-plane displacements along the x, y, and z directions are represented by u_0, v_0, and w_0. The shear rotations, φ_x and φ_y, in the $x-z$ and $y-z$ planes are presented as

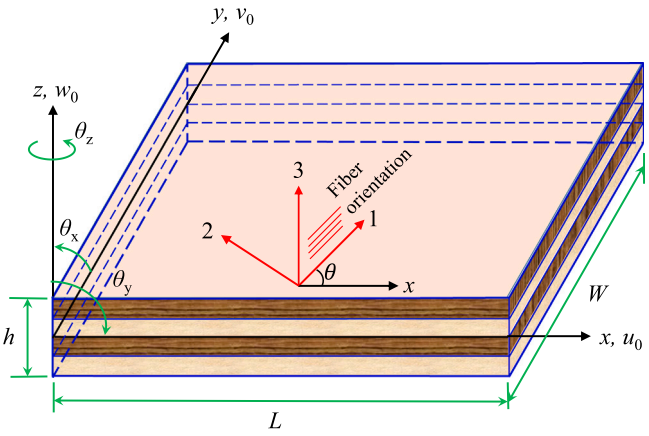

Fig. 1. Laminated composite plate, showing the positive direction of laminate axes in the laminate coordinate (x, y, z) system, the corresponding displacement components, and fiber orientation, θ, for a particular lamina in the lamina coordinate (1, 2, 3) system.

$$\begin{aligned} \varphi_x &= w_{,x} + \theta_y, \\ \varphi_y &= w_{,y} - \theta_x. \end{aligned} \tag{2}$$

In Eq. (2), first derivatives of w with respect to the x and y axes are denoted by $w_{,x}$ and $w_{,y}$. The mid-plane displacement vector is shown by $\boldsymbol{d} = \{u_0 \quad v_0 \quad w_0 \quad \theta_x \quad \theta_y\}^T$. The linear strain vector, $\boldsymbol{\varepsilon} = \{\varepsilon_x \quad \varepsilon_y \quad \gamma_{xy} \quad \gamma_{xz} \quad \gamma_{yz}\}^T$, at a distance z from the mid-plane contains

$$\begin{aligned} \varepsilon_x &= u_{0,x} + z\theta_{y,x}, \\ \varepsilon_y &= v_{0,y} - z\theta_{x,y}, \\ \gamma_{xy} &= u_{0,y} + v_{0,x} + z(\theta_{y,y} - \theta_{x,x}), \\ \gamma_{xz} &= \varphi_x, \\ \gamma_{yz} &= \varphi_y, \end{aligned} \tag{3}$$

as its individual components. The mid-plane strain terms in Eq. (1) are compactly presented as $\varepsilon_{0x} = u_{0,x}$, $\varepsilon_{0y} = v_{0,y}$, $\gamma_{0xy} = (u_{0,y} + v_{0,x})$, $\kappa_x = \theta_{y,x}$, $\kappa_y = -\theta_{x,y}$, and $\kappa_{xy} = (\theta_{y,y} - \theta_{x,x})$. For the uniform increment in the temperature, ΔT, the stress–strain relationship for the k^{th} lamina is presented with reference to the laminate axes (x, y, z) system, which is expressed as

$$\boldsymbol{\sigma}_k = \boldsymbol{Q}_k\{\varepsilon_k - \boldsymbol{\alpha}_k \Delta T\}, \tag{4}$$

where the stress vector, $\boldsymbol{\sigma}_k = \{\sigma_x \quad \sigma_y \quad \tau_{xy} \quad \tau_{xz} \quad \tau_{yz}\}_k^T$, of the k^{th} lamina is derived from the linear strain vector, $\boldsymbol{\varepsilon}_k$, and the thermal strain vector, $\boldsymbol{\alpha}_k \Delta T$. The coefficient of thermal expansion (CTE) of the k^{th} lamina is expressed in the laminate coordinate system (x, y, z) as

$$\boldsymbol{\alpha}_k = \{\alpha_x \quad \alpha_y \quad \alpha_{xy} \quad 0 \quad 0\}_k^T. \tag{5}$$

The transformed reduced stiffness matrix, $\boldsymbol{Q}_k$, [65] for the k^{th} lamina in Eq. (4) is derived from the stress–strain relationship matrix, $\boldsymbol{C}_k$, of the k^{th} lamina in the laminate coordinate system (x, y, z) after proper transformation due to fiber angle orientation, θ. For the plane stress problem, the elements of the $\boldsymbol{C}_k$ matrix, i.e., $(C_{ij})_k$ are evaluated from the elastic moduli of the lamina [9]. In the lamina coordinate (1, 2, 3) system, the elastic moduli of a lamina are denoted by E_{11} and E_{22}; the shear moduli are shown by G_{12}, G_{13}, and G_{23}; and the Poisson's ratios are denoted by ν_{12} and ν_{21}.

The stress–strain relationship of the lamina (cf. Eq. (4)) is integrated over the thickness of the laminate to establish the stress–strain relationship of the laminate. Due to integration, the stress vector for a

particular lamina ($\boldsymbol{\sigma}_k$) is transformed into the stress-resultant vector, $\boldsymbol{F}_r = \{N_x \;\; N_y \;\; N_{xy} \;\; M_x \;\; M_y \;\; M_{xy} \;\; Q_x \;\; Q_y\}^T$, of the laminate and the corresponding strain vector ($\boldsymbol{\varepsilon}_k$) leads to the mid-plane strain vector, $\boldsymbol{\varepsilon}^*$. The stress-resultant and mid-plane strain vector relationship of the composite laminate consisting of n number of the composite lamina is presented as

$$\boldsymbol{F}_r = \boldsymbol{D}\boldsymbol{\varepsilon}^* - \boldsymbol{F}_N. \tag{6}$$

Here, the mid-plane strain vector, $\boldsymbol{\varepsilon}^*$, is presented as

$$\boldsymbol{\varepsilon}^* = \{\varepsilon_{0x} \;\; \varepsilon_{0y} \;\; \gamma_{0xy} \;\; \kappa_x \;\; \kappa_y \;\; \kappa_{xy} \;\; \gamma_{xz} \;\; \gamma_{yz}\}^T, \tag{7}$$

and the thermal stress-resultant vector, $\boldsymbol{F}_N = \boldsymbol{D}\boldsymbol{e}^*$, is given by

$$\boldsymbol{F}_N = \{N_{Nx} \;\; N_{Ny} \;\; N_{Nxy} \;\; M_{Nx} \;\; M_{Ny} \;\; M_{Nxy} \;\; 0 \;\; 0\}^T, \tag{8}$$

in which the thermal strain vector, $\boldsymbol{e}^*$, is written as

$$\boldsymbol{e}^* = \{e_x \;\; e_y \;\; e_{xy} \;\; 0 \;\; 0 \;\; 0 \;\; 0 \;\; 0\}^T. \tag{9}$$

The stress-resultant and mid-plane strain vectors relationship matrix, $\boldsymbol{D}$, in Eq. (6) is written as

$$\boldsymbol{D} = \left[\begin{array}{cccccc|cc} A_{11} & A_{12} & A_{16} & B_{11} & B_{12} & B_{16} & 0 & 0 \\ A_{21} & A_{22} & A_{26} & B_{21} & B_{22} & B_{26} & 0 & 0 \\ A_{61} & A_{62} & A_{66} & B_{61} & B_{62} & B_{66} & 0 & 0 \\ \hline B_{11} & B_{12} & B_{16} & D_{11} & D_{12} & D_{16} & 0 & 0 \\ B_{21} & B_{22} & B_{26} & D_{21} & D_{22} & D_{26} & 0 & 0 \\ B_{61} & B_{62} & B_{66} & D_{61} & D_{62} & D_{66} & 0 & 0 \\ \hline 0 & 0 & 0 & 0 & 0 & 0 & \bar{A}_{44} & \bar{A}_{45} \\ 0 & 0 & 0 & 0 & 0 & 0 & \bar{A}_{54} & \bar{A}_{55} \end{array}\right], \tag{10}$$

where $\boldsymbol{D}$ is a symmetric matrix with $A_{ij} = A_{ji}$, $B_{ij} = B_{ji}$, $D_{ij} = D_{ji}$, and $\bar{A}_{ij} = \bar{A}_{ji}$. The elements of $\boldsymbol{D}$ matrix are stated in compact form, as

$$A_{ij}, B_{ij}, D_{ij} = \sum_{k=1}^{n} \int_{z_{k-1}}^{z_k} \boldsymbol{Q}_k(1, z, z^2)\mathrm{d}z, \quad i, j = 1, 2, 6, \tag{11}$$

and

$$\bar{A}_{ij} = \sum_{k=1}^{n} \int_{z_{k-1}}^{z_k} \varkappa \boldsymbol{Q}_k \mathrm{d}z, \quad i, j = 4, 5 \text{ and } \varkappa = 5/6. \tag{12}$$

In Eq. (12), $\varkappa = 5/6$ is the shear correction factor [9] to consider nonlinear distribution of the transverse shear strain along the thickness of the laminate.

The initial strain vector, $\boldsymbol{\varepsilon}_{nt} = \{\varepsilon_{x_{nt}} \;\; \varepsilon_{y_{nt}} \;\; \gamma_{xy_{nt}} \;\; \gamma_{xz_{nt}} \;\; \gamma_{yz_{nt}}\}^T$, due to the uniform variation of temperature in the entire laminate is presented by the nonlinear portion of the overall strain. The components of the nonlinear thermal strain vector, $\boldsymbol{\varepsilon}_{nt}$, are expressed as

$$\begin{aligned} \varepsilon_{x_{nt}} &= \frac{1}{2}(u_{,x}^2 + v_{,x}^2 + w_{,x}^2), \\ \varepsilon_{y_{nt}} &= \frac{1}{2}(u_{,y}^2 + v_{,y}^2 + w_{,y}^2), \\ \gamma_{xy_{nt}} &= (u_{,x}u_{,y} + v_{,x}v_{,y} + w_{,x}w_{,y}), \\ \gamma_{xz_{nt}} &= (u_{,x}u_{,z} + v_{,x}v_{,z}), \\ \gamma_{yz_{nt}} &= (u_{,y}u_{,z} + v_{,y}v_{,z}). \end{aligned} \tag{13}$$

The displacement terms i.e, u, v, and (w), in Eq. (13) are further expressed in terms of mid-plane displacement (cf. Eq. (1)). Henceforth, the nonlinear thermal strain vector, $\boldsymbol{\varepsilon}_{nt}$, is written in terms of the vector of partial derivative of displacement, $\boldsymbol{d}^*$, as

$$\{\varepsilon_{nt}\} = \frac{1}{2}\boldsymbol{R}\boldsymbol{d}^*. \tag{14}$$

Here, $\boldsymbol{R}$ is a relationship matrix between $\boldsymbol{\varepsilon}_{nt}$ and $\boldsymbol{d}^*$ [65], and the corresponding displacement vector, $\boldsymbol{d}^*$, is described by

$$\boldsymbol{d}^* = \{u_{0,x} \;\; u_{0,y} \;\; v_{0,x} \;\; v_{0,y} \;\; w_{,x} \;\; w_{,y} \;\; \theta_{x,x} \;\; \theta_{x,y} \;\; \theta_{y,x} \;\; \theta_{y,y} \;\; \theta_x \;\; \theta_y\}^T. \tag{15}$$

2.2. Equations of motion

The Hamilton variational principle is used to develop the equation of motion of the laminated composite plates subjected to the dynamic loading in thermal environment. The equation of motion can be expressed within an arbitrary time interval (t_1, t_2) as [52,66,67]

$$\int_{t_1}^{t_2} \delta(\mathbb{E} - \mathbb{K} + \mathbb{Q})\mathrm{d}t = 0, \tag{16}$$

where total potential and kinetic energies are denoted by $\mathbb{E}$ and $\mathbb{K}$, respectively. The damping energy due to the dissipative force vector, $\boldsymbol{f}_{diss}$, is expressed by $\mathbb{Q}$. The total potential energy, $\mathbb{E}$, is the summation of strain energy, $\mathbb{U}$, and work done, $\mathbb{W}$, by conservative forces. Thus, the total potential energy, $\mathbb{E} = \mathbb{U} - \mathbb{W}$, is expressed as

$$\begin{aligned} \mathbb{E} = &\left(\frac{1}{2}\int_A \boldsymbol{\varepsilon}^{*T}\boldsymbol{D}\boldsymbol{\varepsilon}^* \mathrm{d}A + \frac{1}{2}\int_A \boldsymbol{d}^{*T}\boldsymbol{S}_r\boldsymbol{d}^* \mathrm{d}A\right) \\ &- \left(\int_A \boldsymbol{d}^T\boldsymbol{q}(t)\mathrm{d}A\right), \end{aligned} \tag{17}$$

where $\boldsymbol{S}_r$ is the initial stress-stiffness matrix, cf. Eq. (A.2), and $\boldsymbol{q}(t)$ is the externally applied dynamic (transverse) load vector. The initial stress-stiffness matrix, $\boldsymbol{S}_r$, is considered in Eq. (17) to incorporate the effect of initial-stress resultant vector, $\boldsymbol{F}^i = \{N_x^i \;\; N_y^i \;\; N_{xy}^i \;\; M_x^i \;\; M_y^i \;\; M_{xy}^i \;\; Q_x^i \;\; Q_y^i\}^T$, which is induced into the composite laminate due to the uniform variation in temperature.

The kinetic energy, $\mathbb{K}$, of the composite laminate is given by

$$\mathbb{K} = \frac{1}{2}\int_A \dot{\boldsymbol{d}}^T\bar{\boldsymbol{M}}\dot{\boldsymbol{d}}\mathrm{d}A, \tag{18}$$

where $\bar{\boldsymbol{M}}$ is the inertia matrix of the laminate and is written as

$$\bar{\boldsymbol{M}} = \begin{bmatrix} \bar{p} & 0 & 0 & 0 & 0 \\ 0 & \bar{p} & 0 & 0 & 0 \\ 0 & 0 & \bar{p} & 0 & 0 \\ 0 & 0 & 0 & \bar{q} & 0 \\ 0 & 0 & 0 & 0 & \bar{q} \end{bmatrix}. \tag{19}$$

In Eq. (19), the elements $\bar{p}$ and $\bar{q}$ are compactly written as $(\bar{p}, \bar{q}) = \int_{-h/2}^{h/2} \rho(1, z^2)\mathrm{d}z$, and ρ is the density of the composite material. Furthermore, the damping energy, $\mathbb{Q}$, is presented by

$$\mathbb{Q} = \int_A \boldsymbol{d}^T\boldsymbol{f}_{diss}\mathrm{d}A. \tag{20}$$

In the case of viscoelastic damping dissipative force, $\boldsymbol{f}_{diss}$, is proportional to the structural velocity, $\dot{\boldsymbol{d}}$, and can be represented as

$$\boldsymbol{f}_{diss} = \bar{\boldsymbol{C}}\dot{\boldsymbol{d}}, \tag{21}$$

in which $\bar{\boldsymbol{C}}$ is a proportional matrix which represents the energy dissipation mechanism due to the viscoelastic behavior of the composite material.

Finally, the expression of the Hamiltonian variational principle of the composite laminate in thermal environment subjected to the dynamic loading is developed by considering the expression of the total potential, kinetic, and damping energies, and is presented as

$$\begin{aligned} \delta\int_{t_1}^{t_2} \Bigg[&\frac{1}{2}\int_A \boldsymbol{\varepsilon}^{*T}\boldsymbol{D}\boldsymbol{\varepsilon}^*\mathrm{d}A + \frac{1}{2}\int_A \boldsymbol{d}^{*T}\boldsymbol{S}_r\boldsymbol{d}^*\mathrm{d}A \\ &- \int_A \boldsymbol{d}^T\boldsymbol{q}(t)\mathrm{d}A + \int_A \boldsymbol{d}^T\bar{\boldsymbol{C}}\dot{\boldsymbol{d}}\mathrm{d}A - \frac{1}{2}\int_A \dot{\boldsymbol{d}}^T\bar{\boldsymbol{M}}\dot{\boldsymbol{d}}\mathrm{d}A \Bigg] \mathrm{d}t = 0. \end{aligned} \tag{22}$$

The expression of the Hamilton variational statement as derived in Eq. (22) is further used to develop the governing equations of damped dynamic motion for the stiffened laminated composite plates in thermal environment using FE modeling in the next section.

2.3. Finite element formulation

An 8-node C^0 isoparametric plate element with five DOFs (i.e., u, v, (w), θ_x, and θ_y) at each node is implemented for FE analysis of the laminate. The mid-plane displacement vector, $\boldsymbol{d}$, at any location within the element 'e' can be described in terms of the nodal mid-plane displacement vector, $\boldsymbol{d}_e$, of the element by

$$\boldsymbol{d} = \boldsymbol{N}\boldsymbol{d}_e, \tag{23}$$

where $\boldsymbol{N}$ is the matrix of shape functions for the 8-node isoparametric element. Accordingly, the mid-plane strain vector, $\boldsymbol{\epsilon}^*$, is expressed in terms of the nodal mid-plane displacement vector, $\boldsymbol{d}_e$, in relation to the strain–displacement matrix, $\boldsymbol{B}$, [68] as

$$\boldsymbol{\epsilon}^* = \boldsymbol{B}\boldsymbol{d}_e. \tag{24}$$

Similarly, the vector of partial derivatives of displacement, $\boldsymbol{d}^*$, in Eq. (14) is expressed in terms of the nodal displacement vector, $\boldsymbol{d}_e$, as

$$\boldsymbol{d}^* = \boldsymbol{G}\boldsymbol{d}_e, \tag{25}$$

where $\boldsymbol{G}$ (cf. Eq. (A.1)) is the corresponding shape function matrix.

Now, using the Hamilton variational principle for the composite laminate in thermal environment, the inherent viscoelastic damping property is expressed for an element 'e' in the form of

$$\begin{aligned}\int_{t_1}^{t_2}\Bigg[&\int_{A_e}\delta\boldsymbol{d}_e(t)^T\boldsymbol{B}^T\boldsymbol{D}\boldsymbol{B}\boldsymbol{d}_e(t)\mathrm{d}A_e\\ &+\int_{A_e}\delta\boldsymbol{d}_e(t)^T\boldsymbol{G}^T\boldsymbol{S}_r\boldsymbol{G}\boldsymbol{d}_e(t)\mathrm{d}A_e-\int_{A_e}\delta\boldsymbol{d}_e(t)^T\boldsymbol{N}^T\boldsymbol{q}(t)\mathrm{d}A_e\\ &+\int_{A_e}\delta\boldsymbol{d}_e(t)^T\boldsymbol{N}^T\bar{\boldsymbol{C}}\boldsymbol{N}\dot{\boldsymbol{d}}(t)\mathrm{d}A_e-\int_{A_e}\delta\boldsymbol{d}_e(t)^T\boldsymbol{N}^T\bar{\boldsymbol{M}}\boldsymbol{N}\ddot{\boldsymbol{d}}_e(t)\mathrm{d}A_e\Bigg]\mathrm{d}t=0.\end{aligned} \tag{26}$$

Since, the virtual displacement $\delta\boldsymbol{d}_e(t)$ in Eq. (26) is arbitrary in nature, the governing equation of the element 'e' for the composite laminate is

$$\left[\boldsymbol{K}_e+\boldsymbol{K}_{Ge}\right]\boldsymbol{d}(t)+\boldsymbol{C}_e\dot{\boldsymbol{d}}(t)+\boldsymbol{M}_e\ddot{\boldsymbol{d}}(t)=\boldsymbol{P}_e(t). \tag{27}$$

Here, the elemental stiffness matrix, $\boldsymbol{K}_e$, of the composite laminate takes the form of

$$\boldsymbol{K}_e=\int_{A_e}\boldsymbol{B}^T\boldsymbol{D}\boldsymbol{B}\mathrm{d}A_e, \tag{28}$$

the elemental geometric stiffness matrix, $\boldsymbol{K}_{Ge}$, due to the initial thermal stress is expressed as

$$\boldsymbol{K}_{Ge}=\int_{A_e}\boldsymbol{G}^T\boldsymbol{S}_r\boldsymbol{G}\mathrm{d}A_e, \tag{29}$$

the elemental mass matrix, $\boldsymbol{M}_e$, is expressed as

$$\boldsymbol{M}_e=\int_{A_e}\boldsymbol{N}^T\bar{\boldsymbol{M}}\boldsymbol{N}\mathrm{d}A_e, \tag{30}$$

the elemental damping matrix, $\boldsymbol{C}_e$, is given by

$$\boldsymbol{C}_e=\int_{A_e}\boldsymbol{N}^T\bar{\boldsymbol{C}}\boldsymbol{N}\mathrm{d}A_e, \tag{31}$$

and the elemental external load vector, $\boldsymbol{P}_e(t)$, is expressed as

$$\boldsymbol{P}_e(t)=\int_{A_e}\boldsymbol{N}^T\boldsymbol{q}(t)\mathrm{d}A_e. \tag{32}$$

Furthermore, the elemental thermal force vector, $\boldsymbol{P}_{Ne}$, is evaluated as

$$\boldsymbol{P}_{Ne}=\int_{A_e}\boldsymbol{B}^T\boldsymbol{F}_N\mathrm{d}A_e. \tag{33}$$

A 3-point Gauss quadrature rule is adopted for calculating the elemental bending stiffness matrix; whereas a 2-point Gauss quadrature rule is implemented to derive the shear stiffness, the mass matrices, and the elemental force vector.

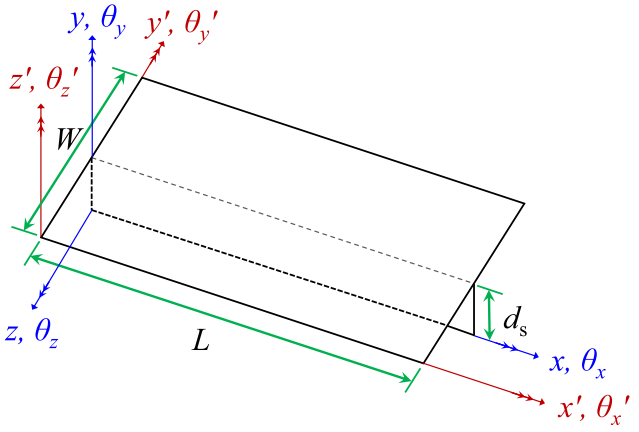

Fig. 2. Local coordinate (x, y, z) system for a laminate and global coordinate (x', y', z') system for a typical stiffened plate, where the least angle between the positive x and x' axes is represented by (x', x), typically.

2.3.1. Transformation matrix due to stiffener

The stiffener(s) is (are) modeled as a plate element along with proper transformation due to their orientation. The transformation matrix is developed to relate the local displacements vector, $\boldsymbol{d}$, of the unstiffened plate and stiffener, and the global displacement vector, $\boldsymbol{d}'$, for the stiffened plate with reference to Fig. 2. The displacement vectors, $\boldsymbol{d}$, and $\boldsymbol{d}'$, are expanded by including θ_z drilling DOF. The local and global mid-plane displacement vectors with six DOFs are presented as

$$\boldsymbol{d}=\{u_0\quad v_0\quad w_0\quad \theta_x\quad \theta_y\quad \theta_z\}^T, \tag{34}$$

$$\boldsymbol{d}'=\{u_0'\quad v_0'\quad w_0'\quad \theta_x'\quad \theta_y'\quad \theta_z'\}^T. \tag{35}$$

In Fig. 2, the depth of the stiffener is denoted by d_s. An orthogonal transformation matrix, $\mathcal{T}$, (see, [65]) for an element with six DOFs per node is developed with reference to Fig. 2, and is given by

$$\boldsymbol{d}_e=\mathcal{T}\boldsymbol{d}_e'. \tag{36}$$

The elemental matrices and vectors in Eqs. (28)–(33) are taken to develop the transformed elemental stiffness, geometric stiffness, mass and damping matrices; and the transformed elemental external load, and thermal force vectors, as

$$\begin{aligned}\boldsymbol{K}_e'&=\mathcal{T}^T\boldsymbol{K}_e\mathcal{T},\\ \boldsymbol{K}_{Ge}'&=\mathcal{T}^T\boldsymbol{K}_{Ge}\mathcal{T},\\ \boldsymbol{M}_e'&=\mathcal{T}^T\boldsymbol{M}_e\mathcal{T},\\ \boldsymbol{C}_e'&=\mathcal{T}^T\boldsymbol{C}_e\mathcal{T},\\ \boldsymbol{P}_e'(t)&=\mathcal{T}^T\boldsymbol{P}_e(t),\\ \boldsymbol{P}_{Ne}'&=\mathcal{T}^T\boldsymbol{P}_{Ne}.\end{aligned} \tag{37}$$

Prior to the transformation in Eq. (37), θ_z drilling DOF is inserted into each node of the element by expanding 40 × 40 elemental matrices to 48 × 48. The off-diagonal terms of the expanded elemental matrices corresponding to θ_z drilling DOF are considered as zero, however a very small positive value is inserted into the corresponding leading diagonal terms of the elemental stiffness and mass matrices to avoid numerical instability [69]. The inserted positive value of the leading diagonal is assumed as 10^5 times smaller than the smallest leading diagonal terms. Furthermore, the 40 × 1 elemental load vector is also enlarged to 48 × 1 by inserting zeros in the corresponding θ_z positions.

Elemental matrices of the plate and stiffeners are assembled after implementing proper transformation to develop the global stiffness matrix, $\boldsymbol{K}'$; the global geometric stiffness matrix, $\boldsymbol{G}_{e'}$; the global damping matrix, $\boldsymbol{C}'$; the global mass matrix, $\boldsymbol{M}'$; the global external load

vector, $\boldsymbol{P}'(t)$; and the global thermal force vector, $\boldsymbol{P}'_{\mathrm{N}}$, for the stiffened laminated composite plates. Therefore, the governing equation of the unstiffened and stiffened laminated composite plates in a thermal environment is expressed by

$$\left[\boldsymbol{K}'+\boldsymbol{K}'_{\mathrm{G}}\right]\boldsymbol{d}'(t)+\boldsymbol{C}'\dot{\boldsymbol{d}}'(t)+\boldsymbol{M}'\ddot{\boldsymbol{d}}'(t)=\boldsymbol{P}'(t). \tag{38}$$

The development of the global damping matrix ($\boldsymbol{C}'$) is illustrated in the subsequent sections.

2.4. Viscoelastic damping formulation of composite materials

The viscoelastic damping (VED) model is adopted to formulate the mechanism for energy dissipation from the laminate during vibration. The basic idea of the VED model is to approximate the energy dissipation from the composite laminate by knowing the elastic and damping properties of the unidirectional lamina. The temperature-dependent elastic moduli and damping parameters of the unidirectional lamina are evaluated experimentally. According to the VED model, stress, σ, and strain, ε, are harmonically time dependent at a frequency, ω (rad/s), as

$$\begin{aligned}\sigma(t) &= \sigma_0 \mathrm{e}^{\mathrm{i}\omega t},\\ \varepsilon(t) &= \varepsilon_0 \mathrm{e}^{\mathrm{i}\omega t}.\end{aligned} \tag{39}$$

A linear viscoelastic constitutive relationship is developed with consideration that the stress state at a time, t, is a superposition of stress steps from all the strain changes at all times, τ, before t, and is mathematically presented as [70,71]

$$\sigma(t) = \int_{-\infty}^{t} h(t-\tau)\mathrm{d}\varepsilon(\tau), \tag{40}$$

where $h(t)$ is the relaxation modulus. The constitutive relationship of the isotropic linear viscoelastic material is written as

$$\sigma(\omega) = E^*(\omega)\varepsilon(\omega). \tag{41}$$

Here, $E^*(\omega)$ is the complex elastic modulus which accounted for the energy dissipation under hermonic vibration and is written as

$$E^*(\omega) = E(\omega) + \mathrm{i}E'(\omega), \tag{42}$$

in which the real part, $E(\omega)$, is termed as the storage modulus, and the imaginary part, $E'(\omega)$, is termed as the loss modulus. The ratio between the loss and storage moduli is defined as the loss factor, η. Accordingly, the complex elastic modulus, $E^*(\omega)$, is shown as

$$E^*(\omega) = E(\omega)\big(1+\mathrm{i}\eta(\omega)\big). \tag{43}$$

Now, the frequency-independent complex elastic moduli of the composite lamina are represented in lamina coordinate (1, 2, 3) system as

$$E^*_{11} = E_{11}(1+\mathrm{i}\eta_{11}), \quad E^*_{22} = E_{22}(1+\mathrm{i}\eta_{22}), \quad G^*_{12} = G_{12}(1+\mathrm{i}\eta_{12}), \tag{44}$$

where η_{11}, η_{22}, and η_{12} are the damping loss factors along the longitudinal, transverse, and shear directions of the composite lamina, respectively. These loss factors of the composite lamina can be determined experimentally using the dynamic mechanical analysis (DMA) [43] and inverse methods [44,72,73].

2.5. Modal damping in composite plates

In this section, the modal damping values of the laminated composite plates are evaluated from the free vibration analysis without considering the damping matrix, $\boldsymbol{C}'$. As, the laminated composite plates are lightly damped structures, ignoring the damping matrix ($\boldsymbol{C}'$) does not have significant influence on the calculated modal damping values. The global complex stiffness matrix, $\boldsymbol{K}'^*$, and the global complex geometric stiffness matrix, $\boldsymbol{K}'^*_{\mathrm{G}}$, of the laminated composite plates are determined by considering complex elastic moduli (cf. Eq. (44)) of the composite lamina. Hence, the equation of the free vibration of the laminated composite plates, by considering viscoelastic properties of the composite lamina, in thermal environment is written as

$$\left[\boldsymbol{K}'^*+\boldsymbol{K}'^*_{\mathrm{G}}\right]\boldsymbol{d}'(t)+\boldsymbol{M}'\ddot{\boldsymbol{d}}'(t)=0. \tag{45}$$

The general solution of Eq. (45) is assumed as $\boldsymbol{d}'(t) = \boldsymbol{\phi}^*_{\mathrm{m}}\mathrm{e}^{\mathrm{i}\omega^*_{\mathrm{dm}}\mathrm{t}}$, in which $\boldsymbol{\phi}^*_{\mathrm{m}}$ and ω^*_{dm} (i.e., $2\pi f^*_{\mathrm{dm}}$) are the m^{th} complex eigenmode and complex damped eigenfrequency in rad/s, respectively, and are obtained by the complex eigenvalue solution. The complex damped eigenfrequencies, f^*_{dm}, is expressed as [30,74]

$$f^*_{\mathrm{dm}} = f_{\mathrm{dm}}\sqrt{(1+\mathrm{i}\eta_{\mathrm{m}})}, \tag{46}$$

where f_{dm} is the damped eigenfrequencies in Hz, and η_{m} is the modal loss factors of laminated composite plates. The modal loss factors (η_{m}) are represented as

$$\eta_{\mathrm{m}} = \frac{\mathrm{Im}(f^{*2}_{\mathrm{dm}})}{\mathrm{Re}(f^{*2}_{\mathrm{dm}})}. \tag{47}$$

The modal SDCs, Ψ_{m}, for the unstiffened and stiffened laminated composite plates are calculated from the modal loss factors, η_{m}, using the relation $\Psi_{\mathrm{m}} = 2\pi\eta_{\mathrm{m}}$. Further, the modal damping ratios, ξ_{m}, relate with the modal loss factors (η_{m}) as $\xi_{\mathrm{m}} = \frac{\eta_{\mathrm{m}}}{2}$.

2.6. Damping matrix for composite plates

For the lightly damped structure with well-spaced eigenfrequencies, the damping matrix ($\boldsymbol{C}'$) can be developed using the definition of Rayleigh damping, i.e., stiffness and mass proportional damping. The Rayleigh damping matrix ($\boldsymbol{C}'_{\mathrm{Rayleigh}}$) is expressed as a linear combination of the stiffness and mass matrices with coefficients a and b, as

$$\boldsymbol{C}'_{\mathrm{Rayleigh}} = a\left[\boldsymbol{K}'+\boldsymbol{K}'_{\mathrm{G}}\right] + b\boldsymbol{M}'. \tag{48}$$

The coefficients, a and b, are evaluated by fitting two sets of modal data, as

$$\begin{aligned}a + b\omega^2_{\mathrm{d1}} &= 2\xi_1\omega_{\mathrm{d1}},\\ a + b\omega^2_{\mathrm{d2}} &= 2\xi_2\omega_{\mathrm{d2}}.\end{aligned} \tag{49}$$

A set of modal data includes modal damped eigenfrequencies and modal damping ratios. Generally, the data from the first two modes is considered to calculate the coefficients, a and b, and subsequently the Rayleigh damping matrix, $\boldsymbol{C}'_{\mathrm{Rayleigh}}$ is developed using Eq. (48). However, for structures with complex geometry, the first two modes are not enough to correctly estimate the damping matrix [57]. In these cases, the damping matrix can be determined by considering data from sufficient numbers of modes. A modal expansion approach, as suggested in [52], is implemented to develop the damping matrix ($\boldsymbol{C}'_{\mathrm{ModalExp}}$) by considering the initial N_{c} numbers of modes in the form of

$$\boldsymbol{C}'_{\mathrm{ModalExp}} = \sum_{m=1}^{N_{\mathrm{c}}} \boldsymbol{M}'\boldsymbol{\phi}_{\mathrm{m}}\frac{2\xi_{\mathrm{m}}\omega_{\mathrm{dm}}}{\mu_{\mathrm{m}}}\boldsymbol{\phi}^{\mathrm{T}}_{\mathrm{m}}\boldsymbol{M}', \tag{50}$$

where μ_{m} is m^{th} modal mass of the vibrating plate. Hence, the global damping matrix ($\boldsymbol{C}'$) of the unstiffened and stiffened laminated composite plates is estimated either using the Rayleigh damping matrix ($\boldsymbol{C}'_{\mathrm{Rayleigh}}$) or the modal expansion damping matrix, $\boldsymbol{C}'_{\mathrm{ModalExp}}$.

2.7. Governing equation of motion

The governing equations of motion of the unstiffened and stiffened laminated composite plates subjected to the dynamic loading in thermal environment with inherent viscoelastic damping properties are expressed as

$$\left[\boldsymbol{K}'+\boldsymbol{K}'_{\mathrm{G}}\right]\boldsymbol{d}'(t)+\boldsymbol{C}'\dot{\boldsymbol{d}}'(t)+\boldsymbol{M}'\ddot{\boldsymbol{d}}'(t)=\boldsymbol{P}'(t). \tag{51}$$

The equations of motion in Eq. (51) are solved numerically in the time domain using the Newmark's integration method using average acceleration approach.

3. Solution algorithm

A two-stage solution algorithm is used to analyze the damped dynamic response of the unstiffened and stiffened laminated composite plates in a thermal environment considering the temperature-dependent elastic and damping properties. In the first stage, the initial stress-resultant vector, $\boldsymbol{F}^{\mathrm{i}}$, is evaluated due to the uniform variation in temperature in the entire laminate. The initial static displacement vector, $\boldsymbol{d}'^{\mathrm{i}}$, is derived by solving the equation of static deflection, as

$$\boldsymbol{K}'\boldsymbol{d}'^{\mathrm{i}} = \boldsymbol{P}'_{\mathrm{N}}. \tag{52}$$

By using Eq. (24), the initial strain vector ($\boldsymbol{\varepsilon}^{*\mathrm{i}}$) is calculated from the nodal initial elemental displacement vector, $\boldsymbol{d}'^{\mathrm{i}}_{\mathrm{e}}$. The initial stress-resultant vector ($\boldsymbol{F}^{\mathrm{i}}$) is calculated from

$$\boldsymbol{F}^{\mathrm{i}} = \boldsymbol{D}\boldsymbol{\varepsilon}^{*\mathrm{i}} - \boldsymbol{F}_{\mathrm{N}}, \tag{53}$$

and is used to develop the initial-stress stiffness matrix, $\boldsymbol{S}_{\mathrm{r}}$, which is subsequently used to develop the global geometric stiffness matrix, $\boldsymbol{K}'_{\mathrm{G}}$.

The damped dynamic response for the unstiffened and stiffened laminated composite plates in terms of deflection is evaluated in second stage of the solution procedure. The global complex stiffness matrix ($\boldsymbol{K}'^{*}$) and the global complex geometric stiffness matrix ($\boldsymbol{K}'^{*}_{\mathrm{G}}$) are calculated by considering elastic moduli and loss factors of the composite lamina. The modal loss factors (η_{m}) are determined from complex eigenvalue solution, and these modal loss factors (η_{m}) are used to determine the global damping matrix, $\boldsymbol{C}'$. A comparative study of the dynamic deflection using the two kinds of damping matrices, i.e., $\boldsymbol{C}'_{\mathrm{Rayleigh}}$ and $\boldsymbol{C}'_{\mathrm{ModalExp}}$, was conducted further to identify the best suitable damping matrix. The underlying step-by-step procedure in obtaining the solution is described here.

Algorithm 1: The damped dynamic response for the unstiffened and stiffened laminated composite plates in thermal environment.

1. Develop the global complex stiffness matrix, $\boldsymbol{K}'^{*}$; the global complex geometric stiffness matrix, $\boldsymbol{K}'^{*}_{\mathrm{G}}$; the global mass matrix, $\boldsymbol{M}'$; and the global load vector, $\boldsymbol{P}'(t)$, of the unstiffened and stiffened laminated composite plate at a predefined temperature, cf. Eq. (37);
2. Determine the complex eigenfrequencies, f^{*}_{m}, and the complex mode shapes, ϕ^{*}_{m}, of the unstiffened and stiffened laminated composite plates in thermal environment via complex eigenvalue solution of Eq. (45);
3. Determine the modal loss factors, η_{m}, cf. Eq. (47);
4. Develop the global damping matrix ($\boldsymbol{C}'$) based on either by the Rayleigh damping ($\boldsymbol{C}'_{\mathrm{Rayleigh}}$) (cf. Eq. (48)); or by the modal expansion damping matrix ($\boldsymbol{C}'_{\mathrm{ModalExp}}$) (cf. Eq. (50));
5. Evaluate the damped dynamic response of the unstiffened and stiffened laminated composite plates due to the dynamic loading with inherent damping in thermal environment, via Newmark's integration technique of average acceleration cf. Eq. (51).

Additionally, a detailed flowchart of the algorithm is presented in Fig. 3.

4. Numerical studies

The damped dynamic response for the unstiffened and stiffened laminated composite plates subjected to the pulse loading is evaluated using the temperature-dependent elastic and damping properties of IM7-PEEK composite, and presented in this section. A 2-mm thick unstiffened Plate 1 and stiffened Plates 2 and 3 with a centrally placed stiffener in the longer and shorter directions, respectively are taken for the analysis with the simply-supported boundary condition at all four edges. The geometry of the unstiffened Plate 1 and the stiffened Plates 2 and 3 is shown in Fig. 4, and the points for maximum deflection of the plates are U_{P_1}, U_{P_2}, and U_{P_3}, respectively as shown in the figures. The transient response of Plates 1, 2, and 3 is calculated at these nodes.

Table 1
Elastic moduli and damping properties of IM7-PEEK lamina at various temperatures, cf. [43,75].

Elastic moduli	Temperature					
	0 °C	25 °C	50 °C	75 °C	100 °C	125 °C
E_{11} (GPa)	159.4	160.9	160.3	159.7	159.1	158.6
E_{22} (GPa)	9.7	9.7	9.3	8.9	8.6	8.2
G_{12} (GPa)	7.7	7.7	7.1	6.6	6.0	5.4
ν_{12} (-)	0.290	0.289	0.286	0.282	0.279	0.275
η_{11} (%)	0.45	0.51	0.55	0.65	0.72	0.70
η_{22} (%)	0.75	0.73	0.81	0.91	1.01	1.26
η_{22} (%)	1.05	1.01	1.09	1.43	1.48	1.49

$G_{13} = G_{12}$, $G_{23} = 0.5G_{12}$, $\nu_{21} = \nu_{12}\frac{E_{22}}{E_{11}}$.

Table 2
dNDFs, λ_{dm}, and modal SDCs, Ψ_{m}, of 2-mm thick unstiffened IM7-PEEK composite Plate 1 with the simply-supported boundary condition at all four edges in thermal environment.

Lamina sequence	Mode,	0 °C		25 °C		75 °C		125 °C	
	m	λ_{dm}	Ψ_{m}	λ_{dm}	Ψ_{m}	λ_{dm}	Ψ_{m}	λ_{dm}	Ψ_{m}
0°/90°/ 90°/0°	1	19.84	3.91	17.57	3.97	12.22	4.75	–	–
	2	49.20	3.39	47.66	3.60	43.65	4.81	–	–
	3	50.86	3.77	48.30	3.88	45.58	4.52	–	–
	4	72.26	3.85	70.02	4.00	66.34	5.13	–	–
45°/−45°/ −45°/45°	1	25.90	3.33	22.07	3.67	18.30	4.61	13.59	2.11
	2	46.22	3.38	40.10	3.81	36.74	4.84	33.02	4.21
	3	71.76	3.42	72.36	3.54	70.74	4.51	69.09	4.66
	4	74.54	3.50	77.09	3.66	75.33	4.64	73.47	4.67

$\lambda_{\mathrm{dm}} = 2\pi f_{\mathrm{dm}} L^2(\rho/E_{22}h^2)^{1/2}$.

The dimension of the plan area for all plates is $(150 \times 100 \times 2)\mathrm{mm}^3$, and a uniformly distributed pulse loading, $q(t) = 0.001\ \mathrm{N/mm}^2$ is applied over the plate surface for a duration of t_{d}, along the normal to the plate surface. The depth of the stiffener is represented by d_{s}. The temperature-dependent elastic properties of IM7-PEEK composite plate were experimentally evaluated and reported by Rawal and Misra [75], and are taken to determine the elastic properties at 25 °C interval by linear interpolation, and are presented in Table 1. The temperature-dependent damping properties of the IM7-PEEK lamina are also illustrated in Table 1, and adopted from [43] by linear interpolation at 25 °C interval. The density of the IM7-PEEK composite is 1.578×10^{-6} kg/mm^3. The CTE of the IM7-PEEK lamina are $\alpha_1 = -0.126 \times 10^{-6}$ /°C and $\alpha_2 = 31.3 \times 10^{-6}$ /°C [75].

4.1. Modal damping values for the unstiffened and stiffened plates

The modal damping values of the IM7-PEEK laminated composite Plates 1, 2, and 3 in the thermal environment are calculated in this section in terms of modal SDCs, Ψ_{m}. The depth of the stiffener (d_{s}) for the stiffened plate is taken as 12 mm. The temperature-dependent elastic and damping properties of the IM7-PEEK composite laminate, as shown in Table 1, are considered for the analysis. In this analysis, the simply-supported boundary condition (cf. Fig. 5) at all four edges is implemented. The first four modal data sets in terms of damped NDFs (dNDFs), λ_{dm}, and modal SDCs, Ψ_{m}, are calculated for the unstiffened Plate 1 and stiffened Plates 2 and 3 with the lamina sequences of 0°/90°/90°/0° and 45°/ − 45°/ − 45°/45°. The modal data sets are calculated at different temperatures such as 0 °C, 25 °C, 75 °C, and 125 °C, and presented in Tables 2, 3, and 4 for the Plates 1, 2, and 3, respectively. It is observed from Tables 2, 3, and 4 that the dNDFs (λ_{m}) decrease as expected with the increment in the temperature due to degradation in the elastic properties with the rise in the temperature. The modal SDCs (Ψ_{m}) for the unstiffened and stiffened laminated composite plates for a particular mode are varied nonlinearly with the increment in temperature. It is difficult to distinguish the

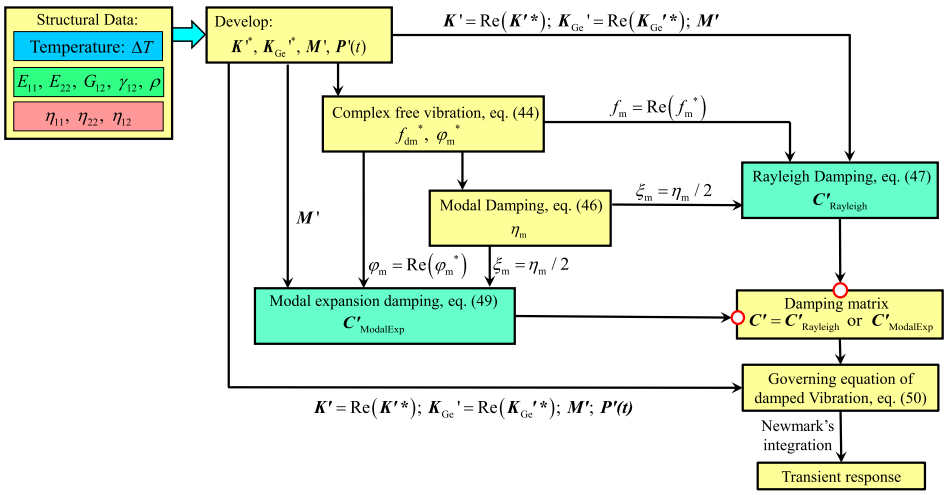

Fig. 3. Flowchart of the Algorithm 1 to evaluate the damped dynamic response of the unstiffened and stiffened laminated composite plates in thermal environment.

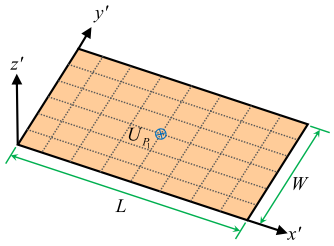

(a) Plate 1: Unstiffened plate.

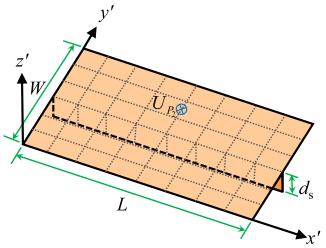

(b) Plate 2: Stiffened plate with centrally placed stiffener oriented parallel to the longer edge.

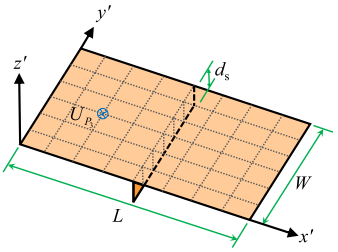

(c) Plate 3: Stiffened plate with centrally placed stiffener oriented parallel to the shorter edge.

Fig. 4. Geometry of the unstiffened Plate 1 and stiffened Plates 2 and 3, by showing the nodes, U_{P_1}, U_{P_2}, and U_{P_3}, respectively where dynamic response is evaluated.

damping efficiency for the unstiffened Plate 1, and stiffened Plates 2 and 3 by observing the modal SDCs (Ψ_m) at different temperatures. Further, the modal SDCs (Ψ_m) are varied nonlinearly with the increment in the mode number. To evaluate the damping performance, one needs to study the damped dynamic response for the unstiffened and stiffened laminated composite plates at different temperatures. The corresponding damped dynamic analysis is presented in the next sections.

4.2. Selection of damping model

The damped dynamic deflection (w) of the Plates 1, 2, and 3 made-up of IM7-PEEK 45°/−45°/−45°/45° laminate is shown in Figs. 6, 7, and 8, respectively at 25 °C and 75 °C temperatures. The damped dynamic deflection (w) of the plates subjected to the uniformly distributed pulse loading, $q(t) = 0.001$ N/mm^2, for a duration of $t_d = 0.003$ s is evaluated. The damping matrix is calculated using the Rayleigh damping approach considering the first two modal data sets and the modal expansion damping considering the initial 20 and 200 modal data sets. The modal data set includes damped eigenfrequencies and modal damping values.

The damped dynamic deflection (w) for the unstiffened Plate 1 at 25 °C and 75 °C temperatures, as calculated by the Rayleigh damping matrix, and the modal expansion damping using the modal data sets of initial $N_c = 20$ and $N_c = 200$ modes, is shown in Fig. 6. These damped response for the unstiffened Plate 1 at the specified temperatures are in good agreement, which indicates that the global damping matrices calculated using $\boldsymbol{C}'_{\text{Rayleigh}}$ and $\boldsymbol{C}'_{\text{ModalExp}}$ can predict the damped dynamic response for the unstiffened plate in thermal environment with sufficient accuracy. A similar response is evaluated and shown in Fig. 7 for the stiffened Plate 2 with stiffener oriented parallel to the longer edge, and held at 25 °C and 75 °C temperatures. It is observed from Fig. 7 that the damped dynamic deflections (w) are quite well in agreement at room temperature, i.e., 25 °C; however, the damped dynamic deflection (w) calculated by using the Rayleigh damping at 75 °C temperature become unbounded in the delayed time domain. The damped dynamic response for the stiffened Plate 2, as calculated by the

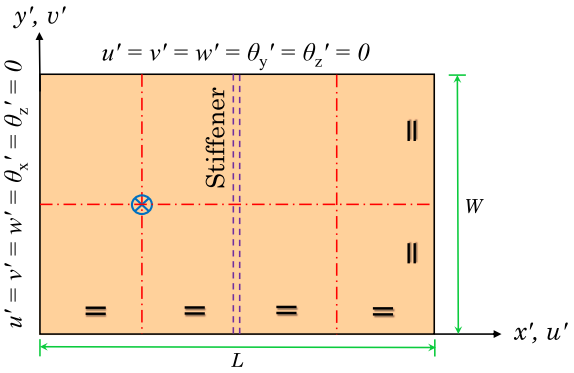

Fig. 5. Top view of a typical stiffened plate showing the simply-supported boundary condition at $x' = 0$ and L, and $y' = 0$ and W.

Table 3
dNDFs, λ_{dm}, and modal SDCs, Ψ_m, of 2-mm thick stiffened IM7-PEEK composite Plate 2 with the simply-supported boundary condition at all four edges in thermal environment.

Lamina sequence	Mode,	0 °C		25 °C		75 °C		125 °C	
	m	λ_{dm}	Ψ_m	λ_{dm}	Ψ_m	λ_{dm}	Ψ_m	λ_{dm}	Ψ_m
	1	51.26	3.83	48.27	3.93	42.45	4.90	35.55	4.02
0°/90°/	2	53.74	4.35	52.70	4.42	50.79	5.94	48.29	6.27
90°/0°	3	73.94	3.92	71.52	4.07	67.37	5.26	62.64	5.07
	4	85.53	3.94	83.89	4.07	81.57	5.27	78.85	5.48
	1	56.67	4.51	55.91	4.60	54.44	6.30	52.24	6.60
45°/−45°/	2	71.50	3.48	69.50	3.68	66.83	4.66	63.90	4.51
−45°/45°	3	97.94	3.46	96.22	3.68	94.72	4.71	92.94	4.92
	4	104.14	3.86	103.03	4.03	102.15	5.30	100.66	5.62

$\lambda_{dm} = 2\pi f_{dm} L^2 (\rho / E_{22} h^2)^{1/2}$.

modal expansion damping considering modal contribution of $N_c = 20$ and $N_c = 200$ numbers of modes, do remain stable and match with sufficient accuracy. The unbounded damped dynamic response which is calculated by the Rayleigh damping matrix ($\boldsymbol{C}'_{\text{Rayleigh}}$) considering the first two modal data sets arises due to the existence of the negative term in the leading diagonal of the Rayleigh damping matrix, $\boldsymbol{C}'_{\text{Rayleigh}}$. The selection of the modes is important while calculating the coefficients a and b for the Rayleigh damping matrix ($\boldsymbol{C}'_{\text{Rayleigh}}$) so that coefficients a and b remain positive and the corresponding Rayleigh damping matrix become positive semi-definite. The modal data sets of the first fundamental mode and a dominant mode can be used for evaluating coefficients a and b which would fulfill the criteria of the non-negativity of the coefficients a and b, and development of positive semi-definite Rayleigh damping matrix, $\boldsymbol{C}'_{\text{Rayleigh}}$. For structures with complex geometry such as stiffened plates, in thermal environment, first and second modes are always not suitable to evaluate the positive semi-definite Rayleigh damping matrix, $\boldsymbol{C}'_{\text{Rayleigh}}$. In Fig. 9, the damped dynamic deflection (w) for the stiffened Plate 2 at 75 °C temperature is evaluated by using the Rayleigh damping matrix ($\boldsymbol{C}'_{\text{Rayleigh}}$) by considering the first and third modal data sets, and found in a good agreement with that of the damped response obtained by the modal expansion damping matrix, $\boldsymbol{C}'_{\text{ModalExp}}$. In this case, the third mode is the second dominant mode. Therefore, it is important to identify the dominant modes of the dynamic system for proper implementation of the Rayleigh damping for the structures with complex geometry in thermal environment.

Further, the damped dynamic deflection (w) for the stiffened Plate 3 with a stiffener oriented parallel to the shorter edge is presented in Fig. 8. In this figure, the three responses are seen to be matching well at room temperature (i.e., 25 °C) and higher temperature (i.e., 75 °C) regimes. Therefore, it can be summarized that the damped dynamic deflection (w) for the stiffened laminated composite plates in thermal environment can be evaluated with sufficient accuracy by using the Rayleigh damping matrix ($\boldsymbol{C}'_{\text{Rayleigh}}$) considering judicial selection

Table 4
dNDFs, λ_{dm}, and modal SDCs, Ψ_m, of 2-mm thick stiffened IM7-PEEK composite Plate 3 with the simply-supported boundary condition at all four edges in thermal environment.

Lamina sequence	Mode,	0 °C		25 °C		75 °C		125 °C	
	m	λ_{dm}	Ψ_m	λ_{dm}	Ψ_m	λ_{dm}	Ψ_m	λ_{dm}	Ψ_m
	1	49.87	3.43	48.21	3.64	45.86	4.59	43.32	4.13
0°/90°/	2	61.79	3.90	60.84	4.07	59.83	5.46	58.26	5.70
90°/0°	3	74.00	3.87	71.74	4.02	68.14	5.18	64.10	5.07
	4	87.01	3.78	85.23	3.96	82.94	5.14	80.22	5.23
	1	50.97	3.27	49.36	3.49	47.30	4.34	45.14	4.16
45°/−45°/	2	55.27	3.53	53.96	3.72	52.35	4.74	50.58	4.76
−45°/45°	3	94.54	3.57	92.74	3.76	90.81	4.79	88.64	5.02
	4	94.79	3.60	93.19	3.80	91.68	4.92	89.81	5.21

$\lambda_{dm} = 2\pi f_{dm} L^2 (\rho / E_{22} h^2)^{1/2}$.

of the modal data sets and the modal expansion damping matrix ($\boldsymbol{C}'_{\text{ModalExp}}$) considering sufficient numbers of modal data sets.

It is also observed that the prediction of the damped dynamic deflections (w) for the unstiffened and stiffened IM7-PEEK laminated composite plates in thermal environment using the modal expansion damping matrix ($\boldsymbol{C}'_{\text{ModalExp}}$) considering the first 20 modal data sets and the first 200 modal data sets show a good correlation. Therefore, by considering the accuracy and numerical efficiency, the modal expansion damping matrix ($\boldsymbol{C}'_{\text{ModalExp}}$) with modal contribution $N_c = 20$ is adopted to develop the global damping matrix ($\boldsymbol{C}'$) and implemented in the later part of this paper to evaluate the damped dynamic response for the unstiffened and stiffened laminated composite plates in thermal environment.

4.3. Calculation of the logarithmic decrement

The damped dynamic response for the unstiffened Plate 1 and stiffened Plates 2 and 3 is evaluated at nodes U_{P_1}, U_{P_2}, and U_{P_3}, respectively to evaluate the inherent damping performance of the IM7-PEEK laminated composite plates at various thermal environments. The displacement-based approach based on calculation of the logarithmic decrement, δ, is implemented to evaluate the damping performance. The rate of oscillation decay of the damped dynamic deflection under the free vibration condition is measured using logarithmic decrement, δ, as

$$\delta = \frac{1}{j} \ln \left(\frac{w_{\text{ini}}}{w_{\text{ini+j}}} \right). \tag{54}$$

Here, decay in the amplitude for j oscillations apart from w_{ini} to $w_{\text{ini+j}}$ is represented by the logarithmic decrement, δ. The logarithmic decrement for the pulse loading is expressed as

$$\delta_p = \frac{1}{j} \ln \left(\frac{w_{\text{ini}} - w_s}{w_{\text{ini+j}} - w_s} \right), \tag{55}$$

where w_s denotes the static deflection subjected to the pulse loading. The upper and lower envelope curves, w_{up} and w_{lp}, represent the dynamic decay of the maximum and minimum amplitudes of the damped dynamic deflection (w) subjected to the pulse loading, and the equations of the corresponding curves are obtained by fitting the maximum and minimum amplitudes of the damped dynamic deflection (w) by linear regression. For the damped dynamic deflection of the laminated composite plate at a specific temperature, $w_{up} = w_s + w_{0u} \exp(-\xi_{up} \omega_1 t)$ where parameters w_{0u} and the damping ratio (ξ_{up}) of the maximum amplitude of the damped dynamic deflection are evaluated by the linear regression. The logarithmic decrement (δ_{up}) of the maximum amplitude of the damped dynamic deflection is evaluated from the identified damping ratio (ξ_{up}) using the relationship

$$\delta_{up} = \frac{2\pi \xi_{up}}{\sqrt{(1 - \xi_{up}^2)}}. \tag{56}$$

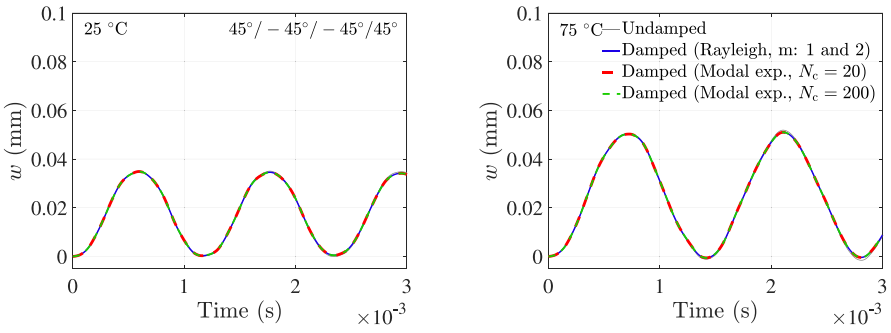

Fig. 6. Damped dynamic response (w) of 45°/ − 45°/ − 45°/45° IM7-PEEK unstiffened laminated composite Plate 1 at 25 °C and 75 °C temperatures.

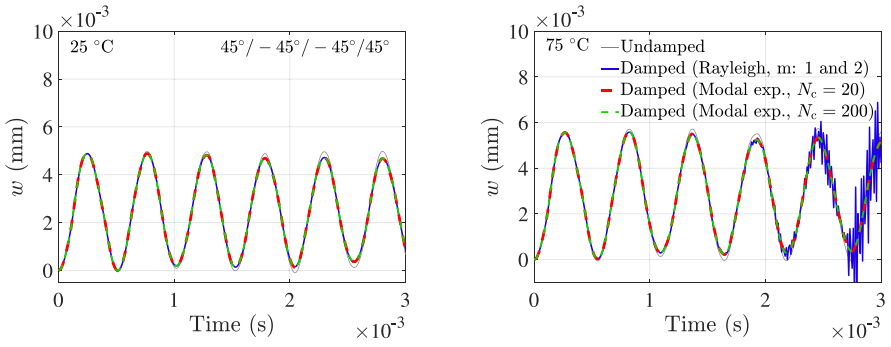

Fig. 7. Damped dynamic response (w) of 45°/ − 45°/ − 45°/45° IM7-PEEK stiffened laminated composite Plate 2 at 25 °C and 75 °C temperatures.

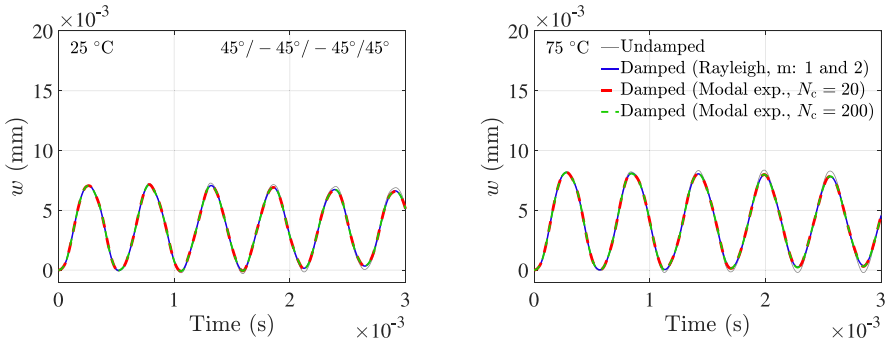

Fig. 8. Damped dynamic response (w) of 45°/ − 45°/ − 45°/45° IM7-PEEK stiffened laminated composite Plate 3 at 25 °C and 75 °C temperatures.

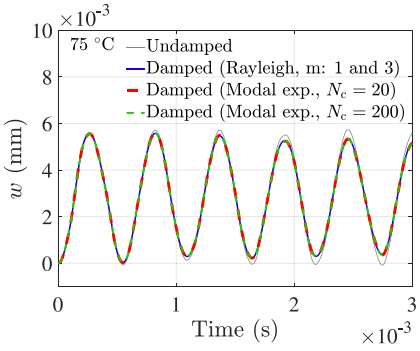

Fig. 9. Damped dynamic response (w) of 45°/ − 45°/ − 45°/45° IM7-PEEK stiffened laminated composite Plate 2 at 75 °C temperature, where Rayleigh damping is calculated based on 1st and 3rd modal data.

Similarly, the equation of the lower envelope curve, $w_{\text{lp}} = w_{\text{s}} + w_{0\text{l}} \exp(-\xi_{\text{lp}}\omega_1 t)$, representing the dynamic decay of the minimum amplitude of the damped dynamic deflection (w) and the corresponding logarithmic decrement, δ_{lp}, is determined. The logarithmic decrements, δ_{up} and δ_{lp}, are considered to measure the equivalent decay of the maximum and minimum amplitudes of the damped dynamic deflection (w), respectively of the laminated composite plate subjected to the pulse loading due to the inherent damping.

The best fitted upper and lower envelope curves of the dynamic decay of the maximum and minimum amplitudes of the damped dynamic deflection (w) for the unstiffened Plate 1 and stiffened Plates 2 and 3 are evaluated at the specified nodes (cf. Fig. 4) at 75 °C temperature and shown in Fig. 10. The IM7-PEEK laminated composite plate with 45°/ − 45°/ − 45°/45° lamina sequence is used for the analysis. The damped dynamic deflection (w) for the unstiffened and stiffened laminated composite plates subjected to the uniformly distributed pulse loading, $q(t) = 0.001$ N/mm^2, is determined for a duration of $t_{\text{d}} = 0.05$ s. It is observed from Fig. 10 that the upper and lower envelop curves, w_{up} and w_{lp}, are fitted with sufficient accuracy to represent the equivalent decay in the maximum and minimum amplitudes of the damped dynamic deflection (w) and the equations of the developed envelop curves are also shown therein. Due to the activation of the higher order modes, a nominal variation in the maximum and minimum amplitudes of the damped dynamic deflection (w) and the fitted upper and lower

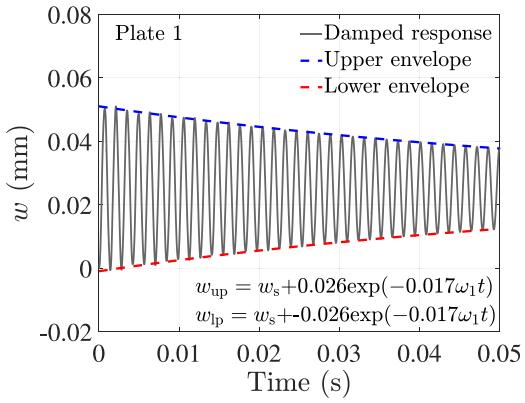

(a) Logarithmic decrement for the unstiffened Plate 1.

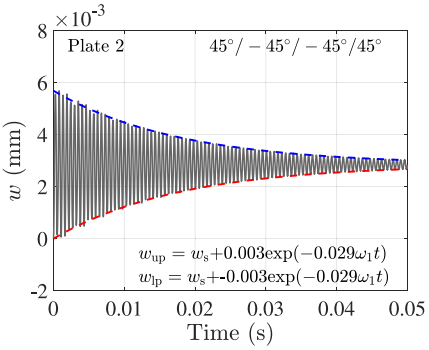

(b) Logarithmic decrement for the stiffened Plate 2.

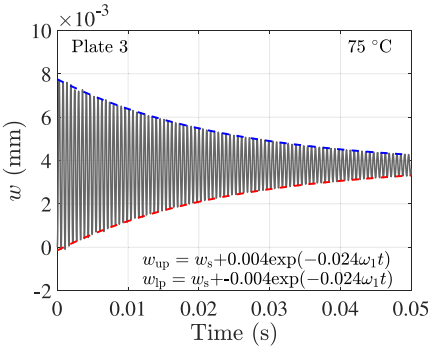

(c) Logarithmic decrement for the stiffened Plate 3.

Fig. 10. Upper and lower envelops of the logarithmic decrements, δ_{up} and δ_{lp}, of 45°/ − 45°/ − 45°/45° IM7-PEEK unstiffened Plate 1 and stiffened Plates 2 and 3 with the simply-supported boundary condition at all four edges at 75 °C temperature subjected to the pulse loading.

envelope curves of the dynamic decay is observed initially in time domain.

The logarithmic decrements, δ_{up} and δ_{lp}, of the maximum and minimum amplitudes of the damped dynamic deflection (w) are also calculated from the evaluated damping ratios, ξ_{up} and ξ_{lp}, respectively. The corresponding logarithmic decrements, δ_{up} and δ_{lp}, for the unstiffened Plate 1 are 0.107 and 0.108. Furthermore, δ_{up} for the stiffened Plates 2 and 3 are 0.198 and 0.152, respectively, and δ_{lp} for these plates are 0.199 and 0.152, respectively. Because of presenting the higher values of δ_{up} and δ_{lp}, the stiffened Plates 2 exhibits better damping performance than the unstiffened Plate 1 and stiffened Plate 3 at 75 °C temperature using 45°/ − 45°/ − 45°/45° laminate as is evident from the figure. Therefore, the calculated logarithmic decrements, δ_{up} and δ_{lp}, can be used to determine the damping performance of the unstiffened and stiffened laminated composite plates in various thermal environments.

4.4. Damped dynamic response of the unstiffened and stiffened composite plates in thermal environment

The damped dynamic response of the unstiffened and stiffened IM7-PEEK laminated composite plates is evaluated at different temperatures. The modal expansion damping matrix ($\boldsymbol{C}'_{\text{ModalExp}}$) considering $N_c = 20$ modal contribution is used to calculate the global damping matrix, $\boldsymbol{C}'$. The damped dynamic deflection (w) for the unstiffened and stiffened laminated composite plates is calculated in the time domain between 0 s to 0.05 s, and the corresponding dynamic response is evaluated for the time step $\Delta t = 0.00001$ s. The entire plan (surface) area of the plate is subjected to the uniformly distributed pulse loading, $q(t) = 0.001$ N/mm^2, for a duration of $t_d = 0.05$ s. The damped dynamic deflection (w) for the unstiffened Plate 1 using 0°/90°/90°/0°, 0°/90°/0°/90°, 45°/ − 45°/ − 45°/45°, and 45°/ − 45°/45°/ − 45° IM7-PEEK laminates at 0 °C, 25 °C, 75 °C, 100 °C, and 125 °C temperatures is shown in Fig. 11. Similarly, the damped dynamic deflection (w) for the stiffened Plates 2 and 3 at the specified temperatures is illustrated in Figs. 12 and 13, respectively. In this study, the logarithmic decrements, δ_{up} and δ_{lp}, as determined in Section 4.3 are used to evaluate the damping performance of the IM7-PEEK laminated composite plates to mitigate the dynamic deflection in thermal environment. The logarithmic decrements, δ_{up} and δ_{lp}, quantify the decay of the maximum and minimum amplitudes of the damped dynamic deflections (w) for the IM7-PEEK unstiffened and stiffened laminated composite plates subjected to the pulse loading. However, for the better visibility, upper and lower envelop curves of the dynamic decay are not shown in Figs. 11, 12, and 13. It is to be noted that for better suppression of the dynamic response, the logarithmic decrements, δ_{up} and δ_{lp}, should be higher.

The logarithmic decrements, δ_{up} and δ_{lp}, for the Plates 1, 2, and 3 with symmetric and antisymmetric cross-ply and angle-ply laminates are calculated for a temperature range varies from 0 °C to 125 °C with a interval of 25 °C. The logarithmic decrements, δ_{up} and δ_{lp}, for the Plates 1, 2, and 3 are shown in Tables 5, 6, and 7, respectively. In these tables, the higher values of δ_{up} and δ_{lp} for a specific laminate are denoted in bold. Further, the highest values of δ_{up} and δ_{lp} among all the considered laminates for a particular plate type are identified by the underline '__'.

It is observed from the figures that the amplitude of the dynamic deflection (w) of the unstiffened and stiffened laminated composite plates increases with the increment in temperature; however, the amplitude of the dynamic deflection (w) decays in the time domain due

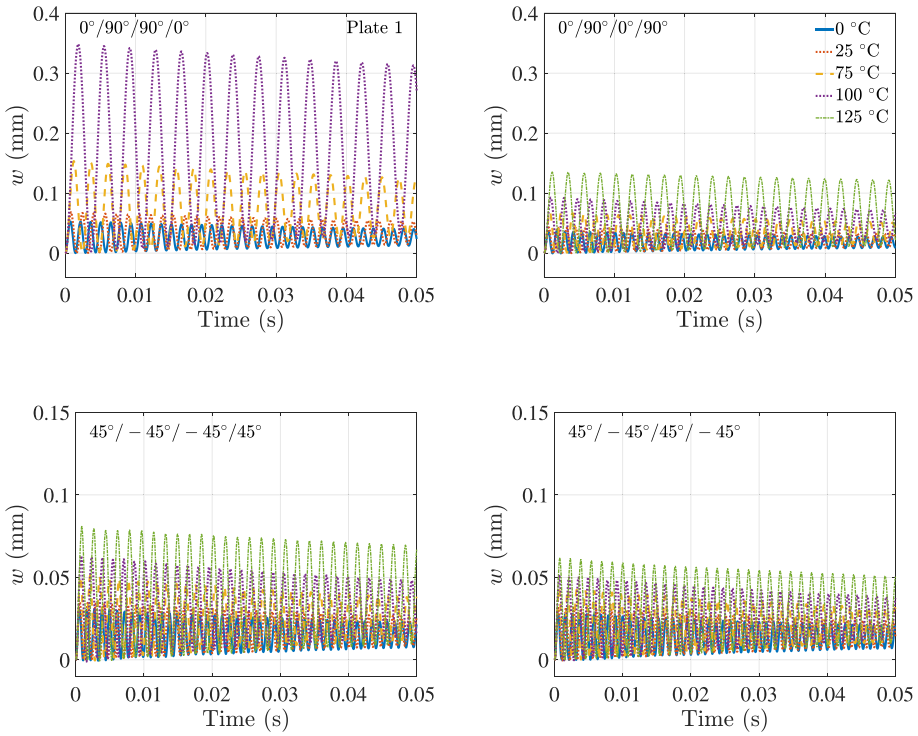

Fig. 11. Damped dynamic response for the unstiffened IM7-PEEK laminated composite Plate 1 at node 'U_{P_1}' with the simply-supported boundary condition at all four edges in thermal environment.

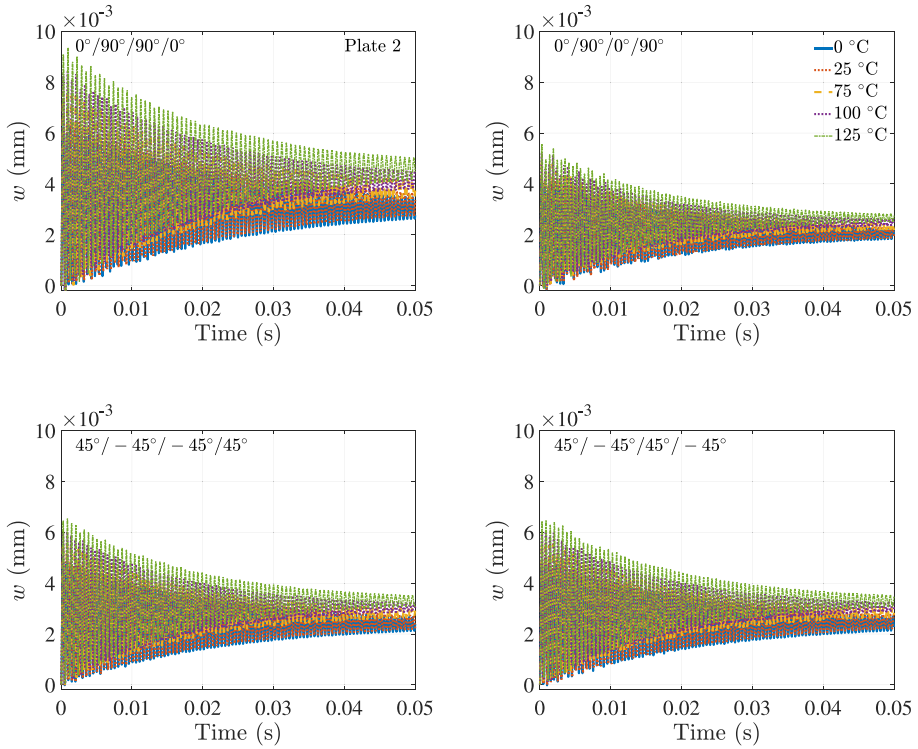

Fig. 12. Damped dynamic response for the IM7-PEEK stiffened laminated composite Plate 2 at node 'U_{P_2}' with the simply-supported boundary condition at all four edges in thermal environment.

to the inherent damping capacity of the IM7-PEEK lamina. It is also evident that the addition of the stiffener reduces the amplitude of the dynamic deflection (w) and the corresponding damping performance is also increased by showing higher rate of decay of the damped dynamic deflection (w) in the time domain. The damping performance of the unstiffened and stiffened laminated composite plates at different temperatures is studied in detailed with reference to the logarithmic decrements, δ_{up} and δ_{lp}.

It is observed from Fig. 11 that the amplitude of the dynamic deflection (w) for the unstiffened Plate 1 with 45°/ – 45°/45°/ – 45°

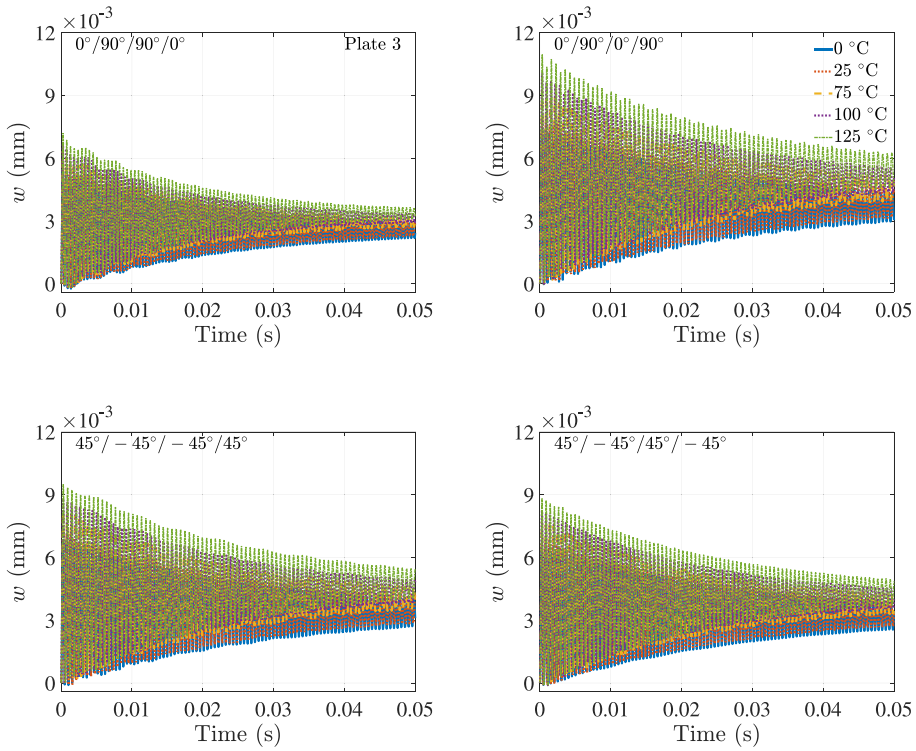

Fig. 13. Damped dynamic response for the IM7-PEEK stiffened laminated composite Plate 3 at node 'U_{P_3}' with the simply-supported boundary condition at all four edges in thermal environment.

Table 5
Logarithmic decrements, δ_{up} and δ_{lp}, for the unstiffened Plate 1 using IM7-PEEK cross-ply and angle-ply laminates with the simply-supported boundary conditions at all four edges at various temperatures.

	Lamina sequences	Temperature	δ_{up}	δ_{lp}
Plate 1	0°/90°/90°/0°	0 °C	**0.139**	**0.140**
		25 °C	0.125	0.125
		50 °C	0.101	0.102
		75 °C	0.102	0.102
		100 °C	0.050	0.050
		125 °C	–	–
	0°/90°/0°/90°	0 °C	**0.120**	**0.120**
		25 °C	0.116	0.116
		50 °C	0.105	0.106
		75 °C	0.117	0.117
		100 °C	0.105	0.104
		125 °C	0.039	0.039
	45°/−45°/−45°/45°	0 °C	**0.112**	**0.113**
		25 °C	0.103	0.103
		50 °C	0.103	0.103
		75 °C	0.107	0.108
		100 °C	0.098	0.098
		125 °C	0.048	0.048
	45°/−45°/45°/−45°	0 °C	0.108	0.108
		25 °C	0.107	0.107
		50 °C	0.102	0.102
		75 °C	**0.109**	**0.109**
		100 °C	0.103	0.103
		125 °C	0.061	0.060

laminate shows the least amplitude of the damped dynamic deflection (w) at all respective temperatures in comparison to the other laminates. The stiffness of 45°/−45°/45°/−45° laminate is higher than that of the remaining laminates due to the antisymmetric lamina sequence and higher shear strength for the angle-ply lamina orientation. The variation of the logarithmic decrements, δ_{up} and δ_{lp}, for the unstiffened Plate 1 with various laminates at different temperatures is presented in Table 5. It is seen from Table 5 that for the unstiffened laminated composite Plate 1 with 0°/90°/90°/0° lamina sequence, the highest values of logarithmic decrements, δ_{up} and δ_{lp}, are observed at 0 °C temperature among all the considered laminates. However, the unstiffened Plate 1 with 45°/−45°/45°/−45° laminate presents the higher values of the logarithmic decrements, δ_{up} and δ_{lp}, at a temperature of 75 °C. It is revealed from the table that best damping performance of the unstiffened plate is obtained at the lower temperature, i.e., 0 °C. However, unstiffened Plate 1 with 45°/−45°/45°/−45° laminate, having the highest stiffness, has shown better damping performance at 75 °C temperature. Further, the variation in the dynamic decays of the upper and lower envelopes is negligible by exhibiting negligible variation between δ_{up} and δ_{lp}. From these observations, it can be stated that, to obtain the better damping performance for the unstiffened laminated composite plates at higher temperature, the stiffness of the plate has to be increased by adopting a suitable lamina sequence which minimize the effect of the stiffness loss at the higher temperature due to the degradation of the material properties of the IM7-PEEK composite.

The addition of the stiffener reduces the magnitude of the dynamic response for the stiffened Plates 2 and 3, as shown in Figs. 12 and 13, respectively in comparison to the unstiffened Plate 1 at different temperatures. The results presented in Fig. 12 depict that the stiffened Plate 2 with 0°/90°/0°/90° laminate showed the least amplitude of the damped dynamic deflection (w) in thermal environment in comparison to the other laminates. This implies that 0°/90°/0°/90° stiffened laminated composite Plate 2 with stiffener oriented parallel to the longer edge imparts the highest structural stiffness due to antisymmetric lamina sequence. By reviewing Table 6, it is observed that the stiffened Plate 2 with 45°/−45°/−45°/45° laminate shown the highest value of the logarithmic decrements, δ_{up} and δ_{lp}, at 100 °C temperatures, thus exhibiting the best damping performance among all the laminates studied herein, adopting displacement-based approach. Furthermore, the higher values of the logarithmic decrement, δ_{up} and δ_{lp}, for the stiffened Plate 2 is observed at 100 °C for each laminate, and the variation of the corresponding values is very nominal.

Table 6
Logarithmic decrements, δ_{up} and δ_{lp}, for the stiffened Plate 2 using IM7-PEEK cross-ply and angle-ply laminates with the simply-supported boundary conditions at all four edges at various temperatures.

	Lamina sequences	Temperature	δ_{up}	δ_{lp}
Plate 2	0°/90°/90°/0°	0 °C	0.152	0.152
		25 °C	0.151	0.151
		50 °C	0.146	0.146
		75 °C	0.189	0.188
		100 °C	**0.196**	**0.196**
		125 °C	0.186	0.187
	0°/90°/0°/90°	0 °C	0.142	0.142
		25 °C	0.142	0.142
		50 °C	0.137	0.137
		75 °C	0.188	0.188
		100 °C	**0.197**	**0.198**
		125 °C	0.193	0.193
	45°/−45°/−45°/45°	0 °C	0.143	0.142
		25 °C	0.143	0.143
		50 °C	0.137	0.137
		75 °C	0.189	0.189
		100 °C	**0.198**	**0.199**
		125 °C	0.192	0.192
	45°/−45°/45°/−45°	0 °C	0.140	0.140
		25 °C	0.141	0.141
		50 °C	0.134	0.134
		75 °C	0.185	0.185
		100 °C	**0.194**	**0.194**
		125 °C	0.189	0.186

Table 7
Logarithmic decrements, δ_{up} and δ_{lp}, for the stiffened Plate 3 using the IM7-PEEK cross-ply and angle-ply laminates with the simply-supported boundary conditions at all four edges at various temperatures.

	Lamina sequences	Temperature	δ_{up}	δ_{lp}
Plate 3	0°/90°/90°/0°	0 °C	0.156	0.156
		25 °C	0.160	0.160
		50 °C	0.157	0.156
		75 °C	0.207	0.204
		100 °C	**0.215**	**0.215**
		125 °C	0.200	0.200
	0°/90°/0°/90°	0 °C	0.152	0.152
		25 °C	0.155	0.154
		50 °C	0.152	0.152
		75 °C	**0.190**	**0.189**
		100 °C	0.197	0.197
		125 °C	0.179	0.178
	45°/−45°/−45°/45°	0 °C	0.124	0.124
		25 °C	0.127	0.127
		50 °C	0.126	0.127
		75 °C	0.152	0.152
		100 °C	**0.158**	**0.158**
		125 °C	0.143	0.143
	45°/−45°/45°/−45°	0 °C	0.123	0.123
		25 °C	0.127	0.127
		50 °C	0.127	0.127
		75 °C	0.153	0.152
		100 °C	**0.160**	**0.160**
		125 °C	0.146	0.146

A comparison of the damped dynamic deflection (w) for the stiffened Plate 3, as shown in Fig. 13, reveals that the stiffened Plate 3 with 0°/90°/90°/0° laminate presents the lowest amplitude of the dynamic deflection (w) at all temperatures, which indicates that the stiffened Plate 3 with 0°/90°/90°/0° laminate presents the highest stiffness. Furthermore, the stiffened Plate 3 with 0°/90°/90°/0° laminate represents the best damping performance at 100 °C temperature by showing the highest values of the logarithmic decrements, δ_{up} and δ_{lp}, among all the considered laminates.

Evaluating the damping performance based on the displacement-based approach shows that the stiffened Plate 3 with 0°/90°/90°/0° laminate has the highest value of δ_{up} and δ_{lp} at 100 °C temperature which indicates that this plate offers the best damping performance by suppressing the maximum and minimum damped dynamic deflections (w) at 100 °C. However, the stiffened Plate 2 with stiffener oriented parallel to the longer edge offers overall better damping performance for all the considered laminates at the higher temperature varies between 75 °C and 125 °C.

It is observed that stiffened plates showed better response reduction near 100 °C temperature, and the corresponding damping performance of a laminate depends on the orientation of the stiffener for the stiffened plate. As the addition of the stiffener increases the stiffness of the composite plates, the stiffened plates offer better damping performance at 100 °C by utilizing the higher damping capacity of the IM7-PEEK lamina at the higher temperature, whereas the unstiffened plate offers better damping performance at lower temperature. The logarithmic decrements, δ_{up} and δ_{lp}, for the stiffened Plates 2 and 3 for a particular laminate are higher than the corresponding unstiffened Plate 1 at a specific temperature, which indicates the better damping performance for the stiffened plates than the corresponding unstiffened plate.

Therefore, it can be stated that a combination of the lamina sequences and stiffener orientation which offers the higher stiffness for the unstiffened and stiffened laminated composite plates at a specific thermal environment would present the better damping performance at that temperature. The stiffened plates offer better damping performance at the higher temperature than does the unstiffened plates. The study also indicates that the stiffened plates maximize the damping performance compared to the unstiffened plates by addition of the small amount of structural mass at higher temperature.

4.5. Effect of the depth of the stiffener on the dynamic response for stiffened plates in thermal environment

To investigate the influence of the depth of stiffeners, the damped dynamic deflection (w) for the stiffened laminated composite Plates 2 and 3 with stiffener depths 8 mm, 12 mm, and 16 mm is evaluated for the symmetric and antisymmetric cross-ply and angle-ply laminates at 25 °C and 100 °C temperatures. The damped dynamic deflection (w) for the stiffened Plates 2 and 3 is illustrated in Figs. 14 and 15, respectively at 25 °C and 100 °C temperatures. The rate of decay of the damped dynamic response for the stiffened laminated composite plates with the given depths of stiffener is evaluated in terms of the logarithmic decrements, δ_{up} and δ_{lp}, and presented in Tables 8 and 9. The higher values of δ_{up} and δ_{lp} for a lamina sequence are shown in bold, and the corresponding highest values of δ_{up} and δ_{lp} at a specific temperature is identified by the underline '__'.

Figs. 14 and 15 show that with the increment of the stiffener depth from 8 mm to 16 mm, the amplitude of the damped dynamic deflection (w) of the corresponding stiffened plate decreases at a specific temperature; however, for a given stiffener depth, the corresponding amplitude increases while temperature is raised from 25 °C to 100 °C. The higher values of the logarithmic decrements, δ_{up} and δ_{lp}, are observed for the stiffened Plate 2 with symmetric and antisymmetric angle-ply laminates with the 12-mm deep stiffener oriented parallel to the longer edge at both temperatures. The stiffened Plate 2 with symmetric and antisymmetric cross-ply laminates showed higher values of the logarithmic decrements, δ_{up} and δ_{lp}, for the 16-mm deep stiffener at 100 °C temperature. Further, it is observed that stiffened Plate 2 with 0°/90°/90°/0° laminate showed the highest values of logarithmic decrements, δ_{up} and δ_{lp}, at 25 °C and 100 °C temperatures separately for the 16-mm deep stiffener, and thus offers the best damping performance at the stated temperatures.

It is observed from Table 9 that for the stiffened Plate 3 with antisymmetric cross-ply and angle-ply laminates, the stiffener depth which shows the higher logarithmic decrements, δ_{up} and δ_{lp}, is varied at 25 °C and 100 °C temperatures. The stiffened Plate 3 with 45°/−45°/−45°/45° laminate showed better dynamic decrement for

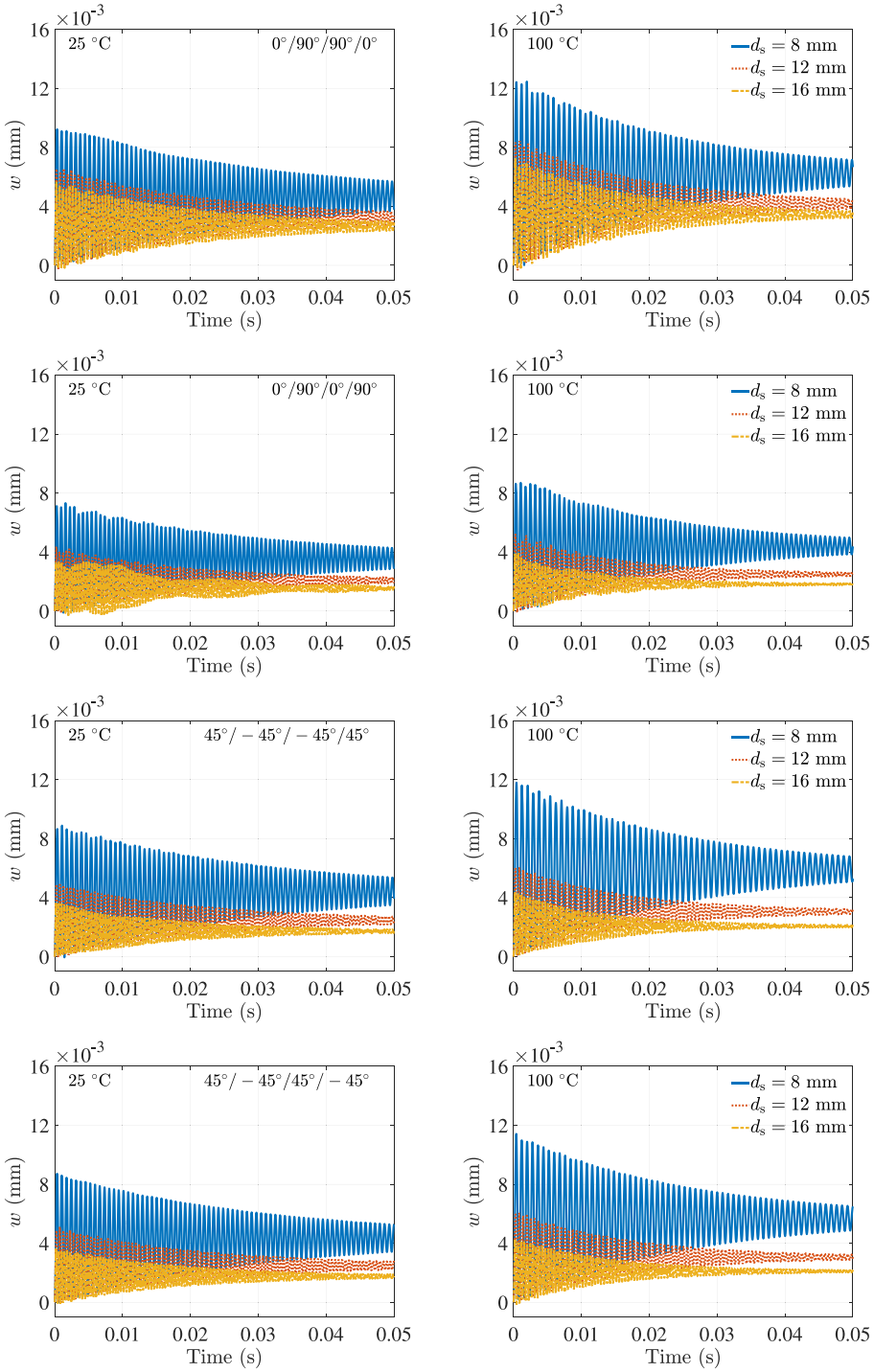

Fig. 14. Damped dynamic deflection (w) of the IM7-PEEK stiffened laminated composite Plate 2 with the simply-supported boundary condition at all four edges for various depths of stiffener at 25 °C and 100 °C temperatures.

8-mm deep stiffener at 25 °C and 100 °C temperatures by showing higher values of the logarithmic decrements, δ_{up} and δ_{lp}. The stiffened Plate 3 with the 16-mm deep stiffener showed the highest values of the logarithmic decrements, δ_{up} and δ_{lp}, for 0°/90°/90°/0° laminate at both temperatures. The variation of the magnitude of the δ_{up} and δ_{lp} is inconsequential with the variation of the stiffener depth from 12 mm to 16 mm for the stiffened Plate 3 in thermal environment. It is concluded that increment in the stiffener depths shows a nonlinear variation of the logarithmic decrement for various lamina sequences in thermal environment.

Therefore, the displacement-based study indicates that the symmetric cross-ply, i.e., 0°/90°/90°/0° laminate showed the best damping performance to mitigate the dynamic deflection for stiffened plates with the 16-mm deep stiffener oriented parallel to the longer and shorter edges at 100 °C. The 12-mm deep stiffener with stiffened Plate 2 for symmetric and antisymmetric angle-ply laminates and the 12-mm deep stiffener with stiffened Plate 3 for antisymmetric angle-ply laminate showed better dynamic decays in damped dynamic deflection at 100 °C temperature. Thus, selection of optimum depth of the stiffener to maximize the dynamic decay at a particular temperature is made based on the lamina sequence and the stiffener orientation.

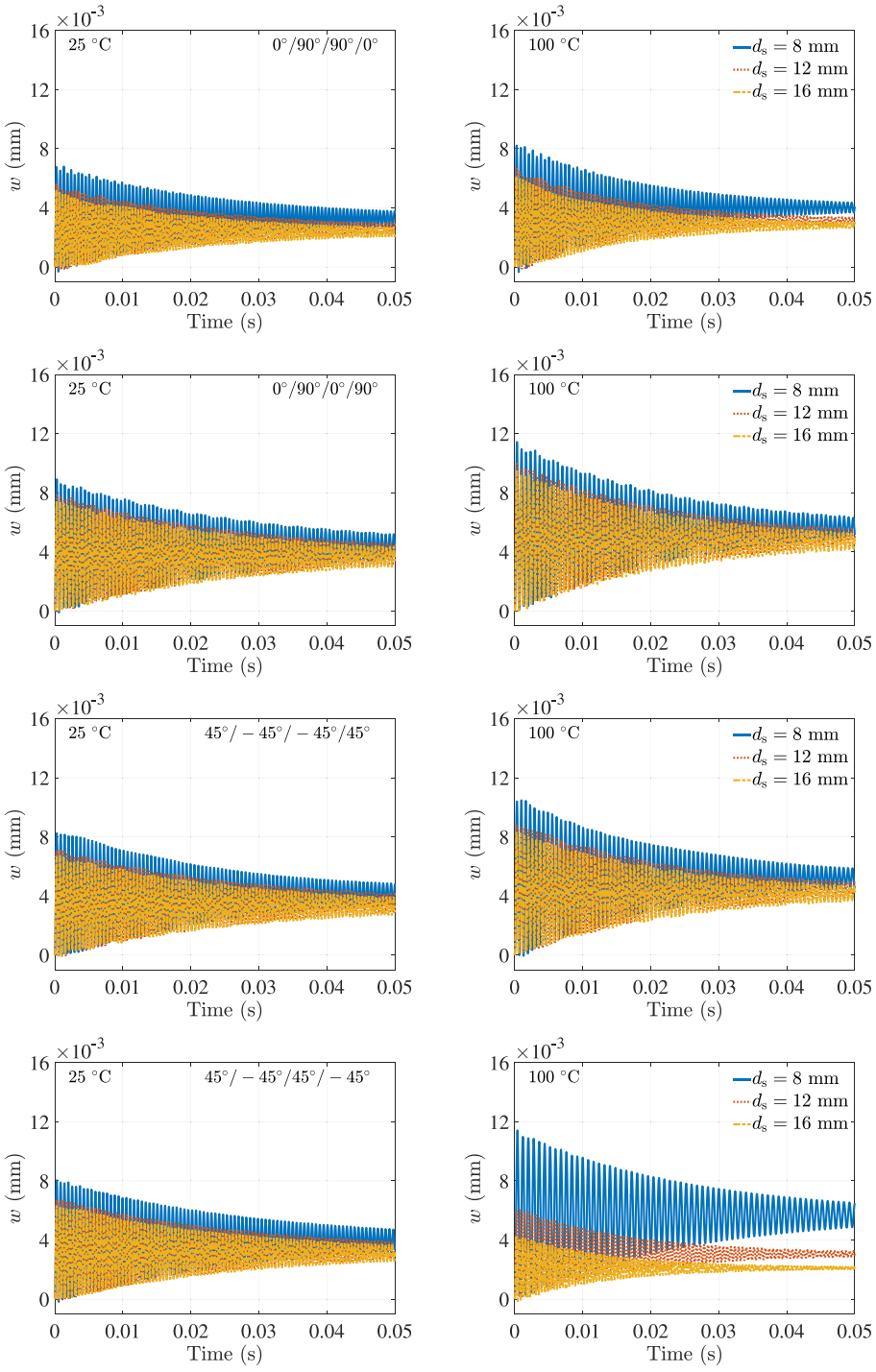

Fig. 15. Damped dynamic deflection (w) of IM7-PEEK stiffened laminated composite Plate 3 with the simply-supported boundary condition at all four edges for various depths of stiffener at 25 °C and 100 °C temperatures.

4.6. Energy-based damping assessment in thermal environment

An energy-based assessment of the damping performance for the unstiffened and stiffened laminated composite plates at different temperatures is presented in this section. The damping performance of the laminated composite plates is evaluated using the energy criteria considering the global behavior of the laminated composite plates by accounting the exact amplitude of the dynamic response for each nodes and contribution of the higher frequency content.

During the damped vibration of the laminated composite plates, damping energy, E_d, is dissipated at every time instant due to the viscoelastic behavior of the composite materials, and remaining mechanical energy is stored in the structure in the form of interchangeable strain energy, E_s, and kinetic energy, E_k. The strain energy, E_s, kinetic energy, E_k, and damping energy, E_d, are expressed in terms of structural properties and the time-dependent nodal response of the

Table 8
Logarithmic decrements, δ_{up} and δ_{lp}, for IM7-PEEK stiffened laminated composite Plate 2 with the simply-supported boundary condition at all four edges for various depths of stiffener at 25 °C and 100 °C temperatures.

	Lamina sequence	Depth of stiffener d_s	δ_{up}	δ_{lp}
Plate 2, 25 °C	0°/90°/90°/0°	8 mm	0.135	0.134
		12 mm	0.151	0.151
		16 mm	**0.167**	**0.168**
	0°/90°/0°/90°	8 mm	0.133	0.133
		12 mm	**0.142**	**0.142**
		16 mm	0.142	0.141
	45°/−45°/−45°/45°	8 mm	0.140	0.141
		12 mm	**0.143**	**0.143**
		16 mm	0.142	0.140
	45°/−45°/45°/−45°	8 mm	0.137	0.137
		12 mm	**0.141**	**0.141**
		16 mm	0.140	0.141
Plate 2, 100 °C	0°/90°/90°/0°	8 mm	0.179	0.179
		12 mm	0.196	0.196
		16 mm	**0.218**	**0.215**
	0°/90°/0°/90°	8 mm	0.178	0.178
		12 mm	0.197	0.198
		16 mm	**0.200**	**0.199**
	45°/−45°/−45°/45°	8 mm	0.185	0.185
		12 mm	**0.198**	**0.198**
		16 mm	0.189	0.187
	45°/−45°/45°/−45°	8 mm	0.179	0.179
		12 mm	**0.194**	**0.194**
		16 mm	0.186	0.186

Table 9
Logarithmic decrements, δ_{up} and δ_{lp}, for IM7-PEEK stiffened laminated composite Plate 3 with the simply-supported boundary condition at all four edges for various depths of stiffener at 25 °C and 100 °C temperatures.

	Lamina sequence	Depth of stiffener d_s	δ_{up}	δ_{lp}
Plate 3, 25 °C	0°/90°/90°/0°	8 mm	0.147	0.147
		12 mm	0.160	0.160
		16 mm	**0.162**	**0.162**
	0°/90°/0°/90°	8 mm	0.149	0.150
		12 mm	0.155	0.154
		16 mm	**0.155**	**0.154**
	45°/−45°/−45°/45°	8 mm	**0.135**	**0.135**
		12 mm	0.127	0.127
		16 mm	0.128	0.128
	45°/−45°/45°/−45°	8 mm	0.123	0.123
		12 mm	0.127	0.127
		16 mm	**0.127**	**0.127**
Plate 3, 100 °C	0°/90°/90°/0°	8 mm	0.197	0.198
		12 mm	0.215	0.215
		16 mm	**0.216**	**0.216**
	0°/90°/0°/90°	8 mm	0.192	0.192
		12 mm	**0.197**	**0.197**
		16 mm	0.197	0.196
	45°/−45°/−45°/45°	8 mm	**0.159**	**0.159**
		12 mm	0.158	0.158
		16 mm	0.157	0.157
	45°/−45°/45°/−45°	8 mm	0.157	0.158
		12 mm	**0.160**	**0.160**
		16 mm	0.160	0.160

laminated composite plates as

$$E_s(t) = \boldsymbol{d}'(t)^T\left[\boldsymbol{K}' + \boldsymbol{K}'_G\right]\boldsymbol{d}'(t),$$
$$E_k(t) = \dot{\boldsymbol{d}}'(t)^T\boldsymbol{M}'\dot{\boldsymbol{d}}'(t),$$
$$E_d(t) = \sum_{i=1}^{nt_{step}} \mathrm{d}\boldsymbol{d}'(t)^T\boldsymbol{C}'\dot{\boldsymbol{d}}'(t), \quad (57)$$

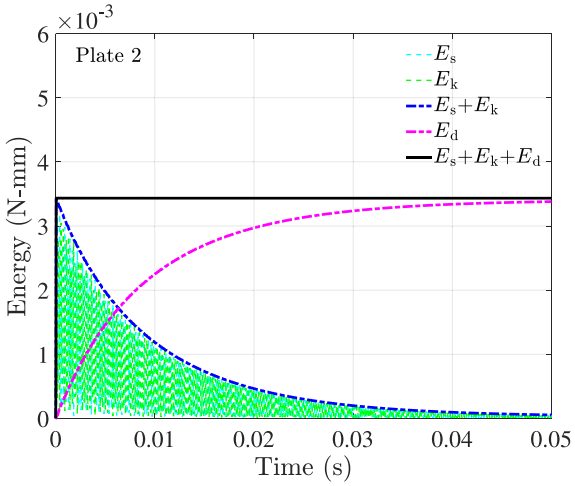

Fig. 16. Time histories of the energy components for the stiffened laminated composite Plate 2 with stiffener oriented parallel to the longer edge with 45°/−45°/−45°/45° laminate, subjected to the impulse loading for a duration of 0.00004 s at 25 °C temperature.

where nt_{step} is the total number of time steps in the dynamic response, and $\mathrm{d}\boldsymbol{d}'(t)$ denotes vector of the change of nodal displacement of various DOFs at each time step. The total energy, E_T, at each time instant is presented as the summation of the all energy components

$$E_T(t) = E_s(t) + E_k(t) + E_d(t). \quad (58)$$

The time history of the energy components for the stiffened laminated composite Plate 2 with 45°/−45°/−45°/45° laminate is shown in Fig. 16, at 25 °C temperature. A simply-supported boundary condition at all four edges is considered for the analysis. An impulse loading, $q(t) = 0.001$ N/mm^2, for a duration of $t_d = 0.00004$ s is applied, and the time history of the energy components is shown for 0.05 s in Fig. 16. The figure shows that the total energy, E_T, remains constant after removal of the impulse loading, and the damping energy, E_d, increases with the increment of time. Further, the total mechanical energy, $(E_s + E_k)$, diminishes in the delayed time domain. This figure validates the energy balance equation.

The time history of the damping energy (E_d) for the unstiffened Plate 1 and the stiffened Plates 2 and 3 subjected to the pulse loading is shown for 0°/90°/90°/0°, 0°/90°/0°/90°, 45°/−45°/−45°/45°, and 45°/−45°/45°/−45° laminates at various temperatures in Figs. 17, 18, and 19, respectively. It is observed from Fig. 17 that the damping energy (E_d) for the unstiffened Plate 1 for all considered laminates is higher at 100 °C temperature in the time domain. The time history of the damping energy (E_d) at 125 °C temperature for 0°/90°/0°/90° and 45°/−45°/−45°/45° laminates is lower than the time history of E_d at 75 °C temperature. The time history of the damping energy (E_d) for the unstiffened Plate 1 with 45°/−45°/45°/−45° laminate at 125 °C is lower in the initial time domain than that of the time history of the damping energy (E_d) at 75 °C temperature, and subsequently increases in the later time domain. The unstiffened Plate 1 with 0°/90°/90°/0° laminate shows the higher dissipation of damping energy (E_d) at all respective temperatures.

The time history of the damping energy (E_d) for the stiffened Plates 2 and 3 at 125 °C temperature is the higher for all respective laminates. Further, 0°/90°/90°/0° and 0°/90°/0°/90° laminates showed a higher amplitude of damping energy (E_d) for the stiffened Plates 2 and 3, respectively. This indicates that energy dissipation characteristic for the unstiffened and stiffened laminated composite plates depends on the stiffness of the structural system. However, higher energy dissipation alone does not indicate better damping performance.

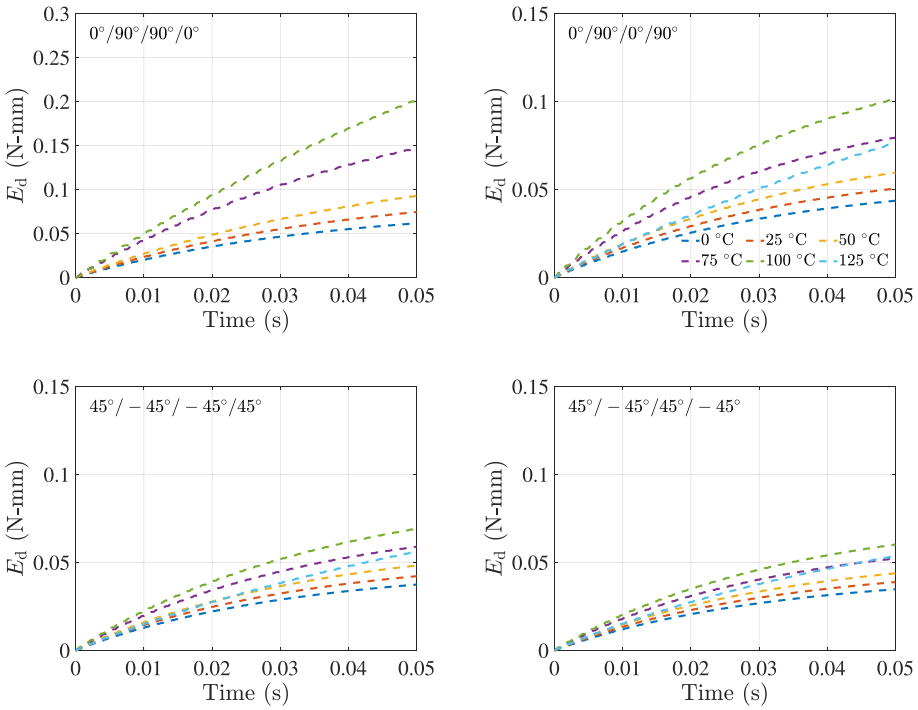

Fig. 17. Time history of the damping energy, E_d, of IM7-PEEK unstiffened laminated composite Plate 1 subjected to the pulse loading with the simply-supported boundary condition at all four edges in thermal environment.

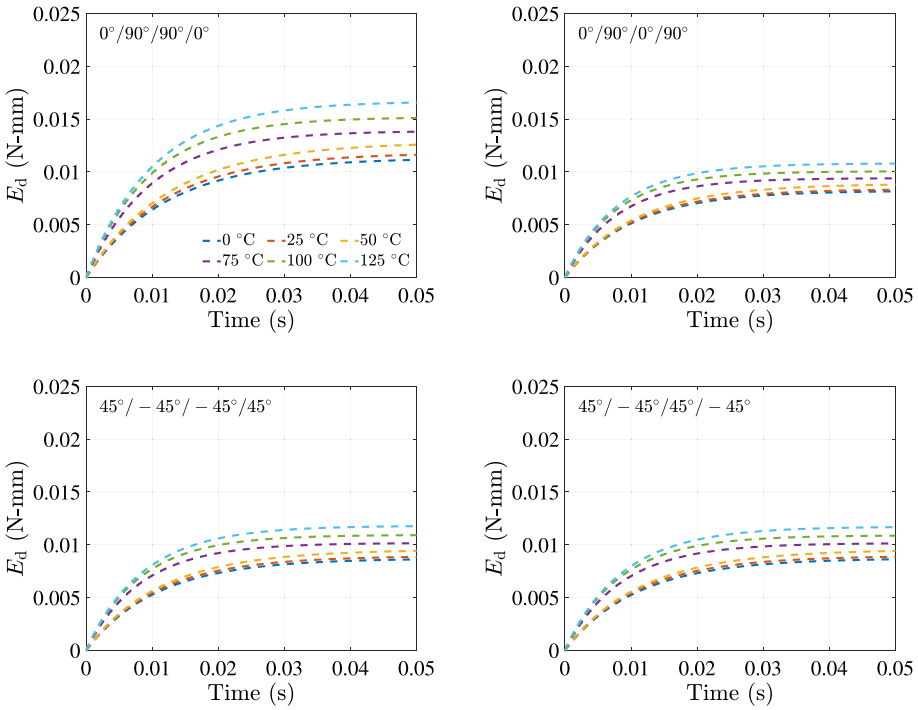

Fig. 18. Time history of the damping energy, E_d, of IM7-PEEK stiffened laminated composite Plate 2 subjected to the pulse loading with the simply-supported boundary condition at all four edges in thermal environment.

The damping performance for the unstiffened and stiffened laminated composite plates at different temperatures is evaluated by determining damping efficiency, J, as

$$J = \frac{E_{td}}{E_{ts} + E_{tk} + E_{td}}, \tag{59}$$

where E_{ts}, E_{tk}, and E_{td} are the total strain energy, total kinetic energy, and total damping energy, respectively, which are obtained by integrating the corresponding time-dependent energy within the limits of the considered time domain. The damping efficiency (J) for the unstiffened Plate 1 and the stiffened Plates 2 and 3 at various temperatures is presented in Table 10.

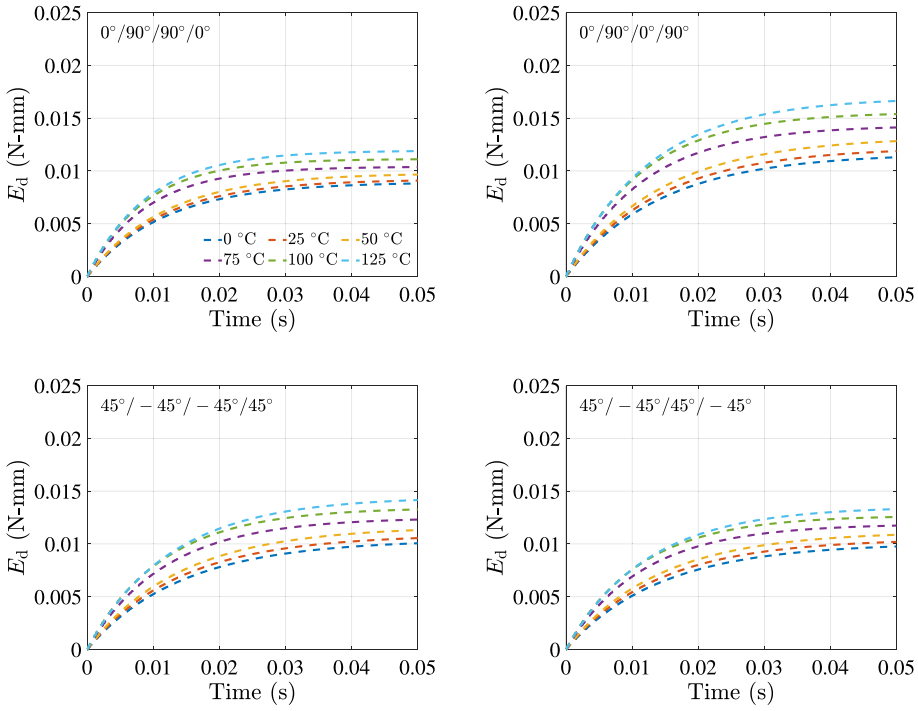

Fig. 19. Time history of the damping energy, E_d, of IM7-PEEK stiffened laminated composite Plate 3 subjected to the pulse loading with the simply-supported boundary condition at all four edges in thermal environment.

Table 10
Damping efficiency, J, for the IM7-PEEK unstiffened laminated composite Plate 1 and stiffened laminated composite Plates 2 and 3 with the simply-supported boundary condition at all four edges at different temperatures.

	J (%)						
	Temperature →	0 °C	25 °C	50 °C	75 °C	100 °C	125 °C
	Lamina sequence ↓						
Plate 1	0°/90°/0°/90°	**22.8**	21.2	18.2	18.1	10.1	–
	0°/90°/90°/0°	**16.0**	15.6	14.6	15.6	14.5	6.7
	45°/−45°/−45°/45°	**24.6**	24.2	23.1	23.7	22.3	13.2
	45°/−45°/45°/−45°	**24.7**	24.5	23.8	24.6	23.8	16.5
Plate 2	0°/90°/90°/0°	38.1	38.1	37.5	40.2	**40.4**	39.8
	0°/90°/0°/90°	39.7	39.8	39.2	42.0	**42.2**	41.8
	45°/−45°/−45°/45°	39.2	39.3	38.7	41.5	**41.7**	41.3
	45°/−45°/45°/−45°	39.1	39.2	38.5	41.4	**41.6**	41.1
Plate 3	0°/90°/90°/0°	38.4	38.7	38.4	41.0	**41.3**	40.7
	0°/90°/0°/90°	36.0	36.3	36.0	38.4	**38.7**	37.5
	45°/−45°/−45°/45°	36.0	36.4	36.3	38.3	**38.7**	37.5
	45°/−45°/45°/−45°	36.1	36.5	36.5	38.5	**39.0**	37.9

It is observed from Table 10 that for the unstiffened Plate 1, the higher value of the damping efficiency (J) is obtained at 0 °C temperature for all considered laminates. The highest value of the damping efficiency (J) is observed for the unstiffened Plate 1 with 45°/−45°/45°/−45° laminate at 0 °C temperature which indicates that the unstiffened Plate 1 with 45°/−45°/45°/−45° offers best damping performance at 0 °C. However, the best damping performance for the unstiffened Plate 1 is identified for 0°/90°/90°/0° laminate at 0 °C temperature during evaluation of the damping performance using the displacement-based approach (cf. Table 5) in Section 4.4.

The higher damping efficiency (J) for the stiffened Plates 2 and 3 is observed at 100 °C temperature which implies the better damping performance for the stiffened plates at 100 °C temperature for all considered laminates. This observation is also supported by the displacement-based damping analysis (cf. Tables 6 and 7) in Section 4.4. Notably, energy dissipation in unstiffened plates is higher than that in case of the stiffened plates (cf. Figs. 17, 18, and 19), because the dissipated energy (cf. Eq. (57)) depends on the displacement. However, damping performance (J), which is a non-dimensional quantity, is better for the stiffened plates as compared to the unstiffened plates. The damping matrix is stiffness proportional (cf. Eq. (48) and (50)), and thus explains the underlying cause of better damping performance in the stiffened plates. According to the energy-based damping analysis 0°/90°/0°/90° laminate exhibits the best damping performance for the stiffened Plate 2 at 100 °C temperature which is in contrast to the best damping performance of 45°/−45°/−45°/45° laminate, as identified based on studying the values of the logarithmic decrements, δ_{up} and δ_{lp}. Furthermore, symmetric cross-ply laminate, i.e., 0°/90°/90°/0° showed the best damping performance at 100 °C for the stiffened Plate 3 according to both the energy-based and displacement-based damping analysis approaches. Moreover, the stiffened laminated composite Plate 2 with 0°/90°/0°/90° laminate presents the best damping performance among all considered unstiffened and stiffened plates at 100 °C temperature.

The lamina sequence identified for the considered unstiffened and stiffened plates in terms of the best damping performance in the displacement-based approach is different from the one identified in the energy-based approach. It is to be noted that the determination of the logarithmic decrements is based on the optimally fitted upper and lower envelope curves of the dynamic decays of the maximum and minimum amplitudes of the damped dynamic deflection, which accounted for a nominal approximation error. On the other hand, the calculation of the damping efficiency is based on the exact displacement components of all nodes of the laminated composite plates, and no error due to the approximation existed. Therefore, the energy-based damping assessment technique emerge as a more robust approach to quantify the inherent damping performance of the laminated composite plates, considering the global behavior, in a thermal environment over the displacement-based approach using logarithmic decrement. Moreover, the lamina sequence which offers the highest stiffness for the unstiffened and stiffened laminated composite plates is identified as offering the best damping performance at a specific temperature using the energy-based damping assessment criteria appeared as a most convincing outcome.

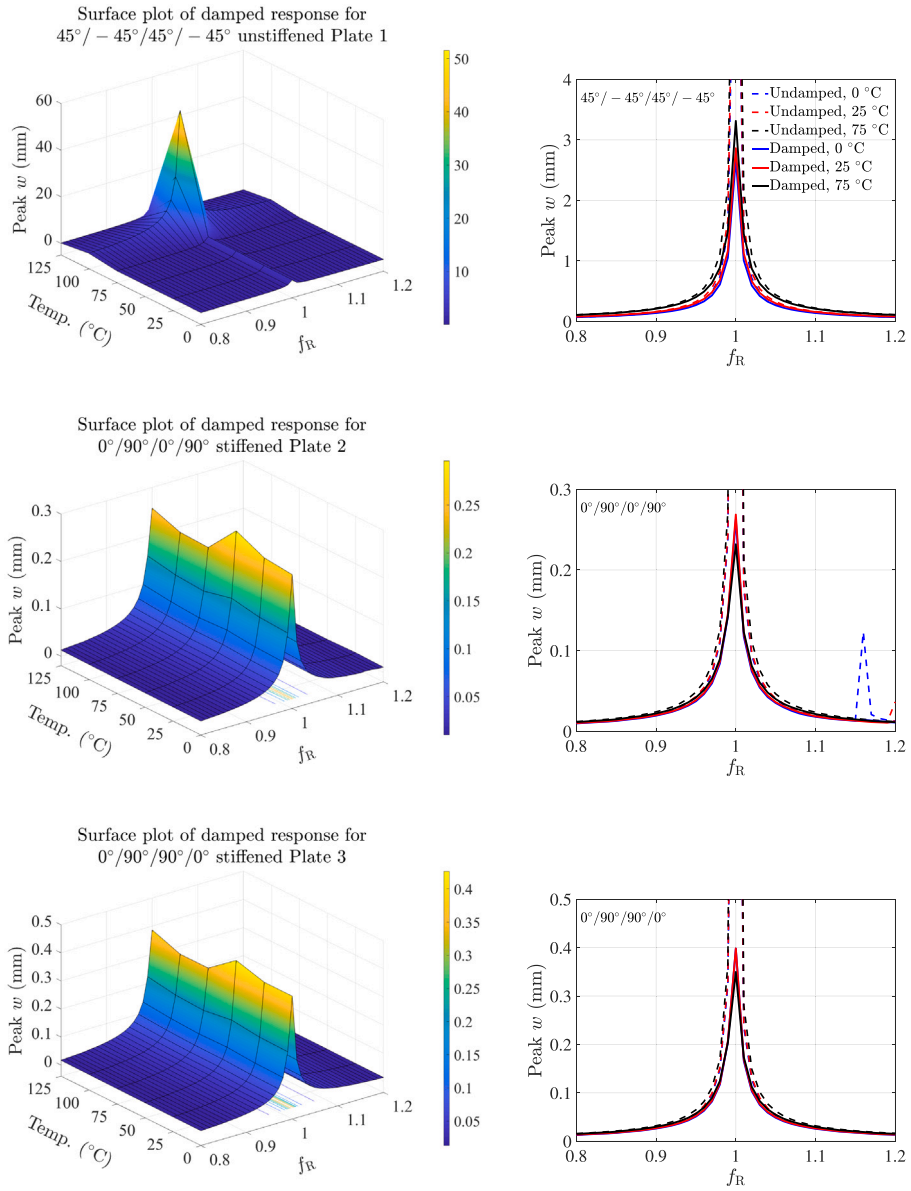

Fig. 20. Influence of the excitation frequency ratio, f_R, on the undamped and damped response for the unstiffened Plate 1 and stiffened Plates 2 and 3 at different temperatures.

4.7. Effect of the excitation frequency ratio

The damping performance of the laminated composite plates is influenced by the temperature and excitation frequency ratio, f_R. For the unstiffened Plate 1 and the stiffened Plate 2, the first mode shapes are in phase and the frequency ratio is considered as $f_R = f_{ext}/f_{d1}$. However, for the case of the stiffened Plate 3 the first mode shape is out phase and the second mode shape is in phase, hence the frequency ratio for such case is considered as $f_R = f_{ext}/f_{d2}$. In this investigation, a sinusoidal loading of various excitation frequencies, f_{ext}, having an amplitude of 0.001 N/mm^2 is applied. The sinusoidal loading at time instant t is stated as $q(t) = 0.001 \sin\left((2\pi f_{ext})t\right)$, where f_{ext} is given in Hz and t is given in s. The range of the excitation frequency ratio (f_R) used in this study varies between 0.8–1.2. The laminates which have identified as exhibiting the best damping performance for the unstiffened and stiffened plates using the energy-based damping analysis in Section 4.6 are considered in this study.

The effect of the excitation frequency ratio (f_R) on the peak dynamic deflection (w) for the unstiffened Plate 1 with 45°/ − 45°/45°/ − 45° laminate, the stiffened Plate 2 with 0°/90°/0°/90° laminate, and the stiffened Plate 3 with 0°/90°/90°/0° laminate is shown in Fig. 20. The depth of the stiffener for the stiffened plate is considered as 12 mm. It is observed from Fig. 20 that the peak dynamic deflection obtained for the unstiffened Plate 1 is more than that of the stiffened Plates 2 and 3 in thermal environment. For the unstiffened Plate 1, the peak dynamic deflection (w) at 100 °C temperature is sufficiently large near $f_R = 1$. On the other hand, a temperature range from 75 °C to 100 °C gives better reduction in the peak dynamic deflection near $f_R = 1$ for the stiffened Plates 2 and 3. Further, the damped dynamic response minimizes the peak developed in case of the undamped dynamic response at 0 °C and 25 °C temperatures near the second eigenfrequency for the stiffened Plate 2.

5. Conclusions

The damped dynamic response for the unstiffened and stiffened laminated composite plates has been studied in various thermal environments using finite element technique. The first-order shear deformation theory has been implemented in the finite element formulation to model such plates by incorporating the drilling degree of freedom

to account six degrees of freedom per node of the plate element. The uniform variation of temperature in the entire composite plate has been incorporated into the finite element formulation by developing the geometric stiffness matrix. The complex modulus approach has been implemented to calculate the modal damping values based on the viscoelastic damping principle at various temperatures. The numerical efficiency of the two damping models, i.e., the Rayleigh damping model and the modal expansion damping model, has been studied to identify the best damping formulation for analysis of the stiffened laminated composite plates in thermal environment. Comparison of the dynamic decay for the unstiffened and stiffened laminated composite plates at different temperatures has been carried out for symmetric and antisymmetric cross-ply and angle-ply laminates by calculating the logarithmic decrement. Further, the damping performance of the unstiffened and stiffened laminated composite plates has been evaluated based on the damping efficiency using energy assessment of the laminated composite plates. Based on the present study, the following conclusions are drawn:

1. Damped non-dimensional frequencies for the unstiffened and stiffened IM7-PEEK laminated composite plates decrease with the increment in temperature. However, the addition of stiffener increases the damped non-dimensional frequencies of stiffened plates in comparison to unstiffened plates.
2. The modal damping values of the IM7-PEEK unstiffened and stiffened laminated composite plates vary nonlinearly with the increment in temperature and mode.
3. The comparative study of the damped dynamic response, calculated by considering the damping matrix as developed by using either the Rayleigh damping model or the modal expansion damping, for the stiffened laminated composite plates in thermal environment shows that the modal expansion damping can be efficiently used to develop the damping matrix. The implementation of the modal expansion damping avoids numerical instability in the damped dynamic response over the implementation of the Rayleigh damping model using the first two modes.
4. The successful implementation of the Rayleigh damping model to calculate the damping matrix relies on the identification of the suitable modes for calculating the Rayleigh damping coefficients a and b, so that the damping matrix remains positive semi-definite.
5. Predicting the damped dynamic response for the unstiffened and stiffened laminated composite plates in thermal environment by implementing modal expansion damping considering the first twenty modes imparts sufficient accuracy in comparison with the consideration of the first two hundred modes.
6. The unstiffened laminated composite plate exhibits better damping performance at the lower temperature, i.e., 0 °C, because with increasing temperature degradation of the plate stiffness diminishes the damping performance at the higher temperature. The unstiffened plate with antisymmetric angle-ply laminate exhibits best damping performance.
7. The damping performance of the laminated composite plates improves with the addition of the stiffener. The damping performance of the stiffened plates is better at a higher temperature, i.e., 100 °C, owing to the lower rate of degradation of the plate stiffness than that of the unstiffened plates with increasing temperature, therefore the stiffened plates utilize the higher damping properties of composites at the elevated temperature for vibration control.
8. Based on the energy assessment criteria, the stiffened plates with stiffener oriented parallel to the longer and shorter edges exhibit the best damping performance by adopting antisymmetric and symmetric cross-ply laminates, respectively at 100 °C temperature.
9. The energy-based assessment of the damping performance appears as most robust technique, and better than the displacement-based damping assessment technique.
10. There is a specific temperature range where the performance of the temperature-dependent inherent damping is better near $f_R = 1$ for unstiffened and stiffened plates. For the unstiffened plate studied in this paper, this temperature range is 0–75 °C, whereas for the stiffened plates with stiffener oriented parallel to the longer and shorter edges, 75–100 °C temperature range is suitable for reduced dynamic deflection near the resonance frequency.
11. For obtaining increased response reduction for the unstiffened and stiffened laminated composite plates at a specific temperature, due to the inherent damping capacity of the composite lamina, stiffener orientation, depth of the stiffener, and lamina sequence must to be optimized.

This study has primarily implemented numerical procedures for damping analysis of unstiffened and stiffened laminated plates in thermal environment. However, experimental verification remains an open task and will be considered in future work by the authors.

CRediT authorship contribution statement

S. Chandra: Conceptualization, Methodology, Programming, Validation, Investigation, Result analysis, Data curation, Writing – original draft, Writing – review & editing. **M. Maeder:** Conceptualization, Writing – review & editing. **K. Sepahvand:** Methodology, Writing – review & editing. **V.A. Matsagar:** Conceptualization, Result analysis, Writing – review & editing, Supervision. **S. Marburg:** Resource, Writing – review & editing, Supervision.

Declaration of competing interest

The authors declare that they have no known competing financial interests or personal relationships that could have appeared to influence the work reported in this paper.

Data availability

Data will be made available on request.

Acknowledgments

The first and fourth authors gratefully acknowledge the financial support extended by the Deutscher Akademischer Austauschdienst (DAAD) under Research Grants- Doctoral Program in Germany, and that by the Alexander von Humboldt Foundation under Fellowship for Experienced Researcher, respectively.

Appendix

Shape function matrix corresponding to $\{d^*\}$:

$$[G] = \sum_{i=1}^{8} \begin{bmatrix} N_{i,x} & 0 & 0 & 0 & 0 \\ N_{i,y} & 0 & 0 & 0 & 0 \\ 0 & N_{i,x} & 0 & 0 & 0 \\ 0 & N_{i,y} & 0 & 0 & 0 \\ 0 & 0 & N_{i,x} & 0 & 0 \\ 0 & 0 & N_{i,y} & 0 & 0 \\ 0 & 0 & 0 & N_{i,x} & 0 \\ 0 & 0 & 0 & N_{i,y} & 0 \\ 0 & 0 & 0 & 0 & N_{i,x} \\ 0 & 0 & 0 & 0 & N_{i,y} \\ 0 & 0 & 0 & N_i & 0 \\ 0 & 0 & 0 & 0 & N_i \end{bmatrix}. \tag{A.1}$$

Here, shape function for the 8-node isoparametric element is denoted by N_i with $i = 1$ to 8.

Initial stress-stiffness matrix:

$$[S_r] = \begin{bmatrix}
N_x^i & N_{xy}^i & 0 & 0 & 0 & 0 & 0 & 0 & M_x^i & M_{xy}^i & 0 & Q_x^i \\
N_{xy}^i & N_y^i & 0 & 0 & 0 & 0 & 0 & 0 & M_{xy}^i & M_y^i & 0 & Q_y^i \\
0 & 0 & N_x^i & N_{xy}^i & 0 & 0 & -M_x^i & -M_{xy}^i & 0 & 0 & -Q_x^i & 0 \\
0 & 0 & N_{xy}^i & N_y^i & 0 & 0 & -M_{xy}^i & -M_y^i & 0 & 0 & -Q_y^i & 0 \\
0 & 0 & 0 & 0 & N_x^i & N_{xy}^i & 0 & 0 & 0 & 0 & 0 & 0 \\
0 & 0 & 0 & 0 & N_{xy}^i & N_y^i & 0 & 0 & 0 & 0 & 0 & 0 \\
0 & 0 & -M_x^i & -M_{xy}^i & 0 & 0 & \frac{N_x^i h^2}{12} & \frac{N_{xy}^i h^2}{12} & 0 & 0 & 0 & 0 \\
0 & 0 & -M_{xy}^i & -M_y^i & 0 & 0 & \frac{N_{xy}^i h^2}{12} & \frac{N_y^i h^2}{12} & 0 & 0 & 0 & 0 \\
M_x^i & M_{xy}^i & 0 & 0 & 0 & 0 & 0 & 0 & \frac{N_x^i h^2}{12} & \frac{N_{xy}^i h^2}{12} & 0 & 0 \\
M_{xy}^i & M_y^i & 0 & 0 & 0 & 0 & 0 & 0 & \frac{N_{xy}^i h^2}{12} & \frac{N_y^i h^2}{12} & 0 & 0 \\
0 & 0 & -Q_x^i & -Q_y^i & 0 & 0 & 0 & 0 & 0 & 0 & 0 & 0 \\
Q_x^i & Q_y^i & 0 & 0 & 0 & 0 & 0 & 0 & 0 & 0 & 0 & 0
\end{bmatrix}. \tag{A.2}$$

References

[1] Nguyen T, Jerry Qi H, Castro F, Long K. A thermoviscoelastic model for amorphous shape memory polymers: Incorporating structural and stress relaxation. J Mech Phys Solids 2008;56(9):2792–814.

[2] Qatu M. Recent research advances in the dynamic behavior of shells: 1989 - 2000, Part 1: Laminated composite shells. Appl Mech Rev 2002;55(4):325–49.

[3] Qatu M. Recent research advances in the dynamic behavior of shells: 1989–2000, Part 2: Homogeneous shells. Appl Mech Rev 2002;55(5):415–34.

[4] Yang J. A review of a few topics in piezoelectricity. Appl Mech Rev 2006;59(1–6):335–45.

[5] Altay G, Dökmeci M. Variational principles for piezoelectric, thermopiezoelectric, and hygrothermopiezoelectric continua revisited. Mech Adv Mater Struct 2007;14(7):549–62.

[6] Bhattacharya P, Suhail H, Sinha PK. Finite element analysis and distributed control of laminated composite shells using LQR/IMSC approach. Aerosp Sci Technol 2002;6(4):273–81.

[7] Ghosh S, Sahu A, Bhattacharya P. Observer-based H2-robust controller for active vibration control of laminated composite plates with an optimally placed IDE-PFC actuator. J Aerosp Eng 2016;29(3).

[8] Whitney J, Ashton J. Effect of environment on the elastic response of layered composite plates. AIAA J 1971;9:1708–13.

[9] Sai Ram K, Sinha P. Hygrothermal effects on the free vibration of laminated composite plates. J Sound Vib 1992;158(1):133–48.

[10] Patel B, Ganapathi M, Makhecha D. Hygrothermal effects on the structural behaviour of thick composite laminates using higher-order theory. Compos Struct 2002;56(1):25–34.

[11] Mangala A, Jayasuriya M, Dwivedi SN, Sivaneri NT, Lyons DW. Doubly curved laminated composite shells with hygrothermal conditioning and dynamic loads, Part 1: A theoretical development and semielastic solution using a higher-order displacement field. Mech Adv Mater Struct 2002;9(1):53–68.

[12] Mangala A, Jayasuriya M, Dwivedi SN, Louisiana L, Sivaneri NT, Lyons DW. Doubly curved laminated composite shells with hygrothermal conditioning and dynamic loads, Part 2: FEA and numerical results of shells of revolution. Mech Adv Mater Struct 2002;9(1):69–97.

[13] Huang X-L, Shen H-S, Zheng J-J. Nonlinear vibration and dynamic response of shear deformable laminated plates in hygrothermal environments. Compos Sci Technol 2004;64(10–11):1419–35.

[14] Naidu N, Sinha P. Nonlinear finite element analysis of laminated composite shells in hygrothermal environments. Compos Struct 2005;69(4):387–95.

[15] Swamy Naidu N, Sinha P. Nonlinear transient analysis of laminated composite shells in hygrothermal environments. Compos Struct 2006;72(3):280–8.

[16] Nanda N, Pradyumna S. Nonlinear dynamic response of laminated shells with imperfections in hygrothermal environments. J Compos Mater 2011;45(20):2103–12.

[17] Parhi P, Bhattacharyya S, Sinha P. Hygrothermal effects on the dynamic behavior of multiple delaminated composite plates and shells. J Sound Vib 2001;248(2):195–214.

[18] Chandra S, Sepahvand K, Matsagar VA, Marburg S. Stochastic dynamic analysis of composite plate with random temperature increment. Compos Struct 2019;226:111159.

[19] Card M, Starnes J. Current research in composite structures at NASA's langley research center. Sadhana 1987;11(3–4):277–98.

[20] Carrera E, Pagani A, Jamshed R. Refined beam finite elements for static and dynamic analysis of hull structures. Comput Struct 2016;167:37–49.

[21] Chattopadhyay B, Sinha P, Mukhopadhyay M. Finite element analysis of blade-stiffened composite plates under transverse loads. J Reinf Plast Compos 1993;12(1):76–100.

[22] Kumar YS, Mukhopadhyay M. Transient response analysis of laminated stiffened plates. Compos Struct 2002;58(1):97–107.

[23] Pal S, Niyogi AG. Application of folded plate formulation in analyzing stiffened laminated composite and sandwich folded plate vibration. J Reinf Plast Compos 2008;27(7):693–710.

[24] Yu H, Zhao Z, Yang D, Gao C. A new composite plate/plate element for stiffened plate structures via absolute nodal coordinate formulation. Compos Struct 2020;247:112431.

[25] Lee D-M, Lee I. Vibration analysis of anisotropic plates with eccentric stiffeners. Comput Struct 1995;57(1):99–105.

[26] Qing G, Qiu J, Liu Y. Free vibration analysis of stiffened laminted plates. Int J Solids Struct 2006;43:1357–71.

[27] Ray C, Satsangi SK. Laminated stiffened plate - A first ply failure analysis. J Reinf Plast Compos 1999;18(12):1061–76.

[28] Neumark S. Concept of complex stiffness applied to problems of oscillations with viscous and hysteretic damping. Tech. rep., Aeronautical Research Council, London, U.K.; 1962.

[29] Hashin Z. Viscoelastic fiber reinforced materials. AIAA J 1966;4(8):1411–7.

[30] Hu B-G, Dokainish M. Damped vibration of laminated composite plates-Modeling and finite element analysis. Finite Elem Anal Des 1993;15(2):103–24.

[31] Bouadi H, Sun CT. Hygrothermal effects on structural stiffness and structural damping of laminated composites. J Mater Sci 1990;25(1):499–505.

[32] Dobson B, Drew R. Experimental investigation of the effects of temperature on the dynamic properties of a carbon fibre-reinforced plate. Composites 1991;22(3):199–203.

[33] Hanselka H, Hoffmann U. Damping characteristics of fiber reinforced polymers. Tech. Mech. 1999;10(2):91–101.

[34] Zhang P, Ruan J, Li W. Influence of some factors on the damping property of fiber-reinforced epoxy composites at low temperature. Cryogenics 2001;41(4):245–51.

[35] Ungar EE, Kerwin EM. Loss factors of viscoelastic systems in terms of energy concepts. J Acoust Soc Am 1962;34:954–7.

[36] Adams R, Bacon D. Effect of fibre orientation and laminate geometry on the dynamic properties of CFRP. J Compos Mater 1973;7(4):402–28.

[37] Saravanos DA, Chamis CC. Unified micromechanics of damping for unidirectional fiber reinforced composites. NASA; 1989, p. 1–27.

[38] Klaerner M, Wuehrl M, Kroll L, Marburg S. Modelling and FEA-simulation of the anisotropic damping of thermoplastic composites. Adv. Aircr. Spacecr. Sci. 2016;3(3):331–49.

[39] Klaerner M, Wuehrl M, Kroll L, Marburg S. Amplitude-dependent damping: Experimental determination and functional interpretation for metal-plastic composites. Int J Struct Stab Dyn 2019;19(5):1941001.

[40] Saravanos DA, Chamis CC. Mechanics of damping for fiber composite laminates including hygro-thermal effects. AIAA J 1990;28(10):1813–9.

[41] Mustafa RJ. Temperature dependence of dynamic modulus and damping in continuous fiber-reinforced Al-(alloy) matrix composites at elevated temperatures. Jordan J. Mech. Ind. Eng. 2008;2(1):15–21.

[42] Maheri M, Adams R, Gaitonde J. The effect of temperature on the dynamic characteristics of heat-resistant thermoplastic composites. Compos Sci Technol 1996;56(12):1425–34.

[43] Melo JDD, Radford DW. Time and temperature dependence of the viscoelastic properties of CFRP by dynamic mechanical analysis. Compos Struct 2005;70(2):240–53.

[44] Sefrani Y, Berthelot J-M. Temperature effect on the damping properties of unidirectional glass fibre composites. Composites B 2006;37(4):346–55.

[45] Sepahvand K. Stochastic finite element method for random harmonic analysis of composite plates with uncertain modal damping parameters. J Sound Vib 2017;400:1–12.

[46] Sepahvand K, Khosroshahi FS, Geweth CA, Marburg S. Stochastic structural dynamic analysis with random damping parameters. In: Proceedings of the 46th International Congress and Exposition on Noise Control Engineering. 2017.

[47] Chandra S, Sepahvand K, Matsagar VA, Marburg S. Stochastic modal damping analysis of stiffened laminated composite plate. In: Saha SK, Mukherjee M, editors. Recent Advances in Computational Mechanics and Simulations. Singapore: Springer Singapore; 2021, p. 635–50.

[48] Chandra R, Singh S, Gupta K. Damping studies in fiber-reinforced composites - a review. Compos Struct 1999;46(1):41–51.

[49] Treviso A, Genechten BV, Mundo D, Tournour M. Damping in composite materials: Properties and models. Composites B 2015;78:144–52.

[50] Zabaras N, Pervez T. Viscous damping approximation of laminated anisotropic composite plates using the finite element method. Comput Methods Appl Mech Engrg 1990;81(3):291–316.
[51] Pervez T, Zabaras N. Transient dynamic and damping analysis of laminated anisotropic plates using a refined plate theory. Internat J Numer Methods Engrg 1992;33(5):1059–80.
[52] Geradin M, Rixen D. Mechanical Vibrations: Theory and Application to Structural Dynamics. West Sussex, U.K.: Wiley; 2015.
[53] Yi S, Pollock G, Ahmad M, Hilton H. Time-dependent analysis of anisotropic viscoelastic composite shell structures. Comput. Syst. Eng. 1992;3(1–4):457–67.
[54] Kiral Z. Numerical investigation of the dynamic response of symmetric laminated composite beams to harmonic excitations. Adv Compos Lett 2009;18(5):163–72.
[55] Şahan M. Viscoelastic damped response of cross-ply laminated shallow spherical shells subjected to various impulsive loads. Mech. Time-Depend. Mater. 2017;21(4):499–518.
[56] Jeyaraj P, Ganesan N, Padmanabhan C. Vibration and acoustic response of a composite plate with inherent material damping in a thermal environment. J Sound Vib 2009;320(1):322–38.
[57] Adhikari S. Damping modelling using generalized proportional damping. J Sound Vib 2006;293(1):156–70.
[58] Priestley MJN. Displacement-based seismic assessment of reinforced concrete buildings. J. Earthq. Eng. 1997;1(1):157–92.
[59] Mezgebo MG, Lui EM. A new methodology for energy-based seismic design of steel moment frames. Earthq. Eng. Eng. Vib. 2017;16(9):131–52.
[60] Zahrah TF, Hall WJ. Earthquake energy absorption in SDOF structures. J Struct Eng 1984;110(8):1757–72.
[61] Elias S. Seismic energy assessment of buildings with tuned vibration absorbers. Shock Vib 2018;2018(2051687).
[62] Austin MA, Lin W-J. Energy balance assessment of base-isolated structures. J Eng Mech 2004;130(3):347–58.
[63] Bhardwaj A, Matsagar V, Nagpal AK. Energy balance assessment of tall buildings equipped with friction dampers for earthquake response control. J Struct Eng 2016;43(1):91–101.
[64] Zelleke DH, Matsagar VA. Semi-active algorithm for energy-based predictive structural control using tuned mass dampers. Comput-Aided Civ Infrastruct Eng 2019;34(11):1010–25.
[65] Chandra S, Sepahvand K, Matsagar VA, Marburg S. Dynamic response of stiffened laminated composite plate in thermal environment. Compos. Struct. 2022;116049.
[66] Wang QA, Wang R. Is it possible to formulate least action principle for dissipative systems?. 2015, arXiv:1201.6309.
[67] Salamon R, Kamiński H, Fritzkowski P. Estimation of parameters of various damping models in planar motion of a pendulum. Meccanica 2020;55(9):1655–77.
[68] Reddy JN. Mechanics of Laminated Composite Plates and Shells: Theory and Analysis. second ed. London, U.K.: CRC Press; 2001.
[69] Bathe KJ. Finite Element Procedures in Engineering Analysis. updated ed. New Jersy, U.S.A.: Prentice Hall; 1982.
[70] Christensen RM. Theory of Viscoelasticity: An Introduction. second ed. London, U.K.: Academic Press; 1982.
[71] Baz AM. Active and Passive Vibration Damping. U.K.: Wiley; 2019.
[72] Li H, Wu T, Gao Z, Wang X, Ma H, Han Q, Qin Z. An iterative method for identification of temperature and amplitude dependent material parameters of fiber-reinforced polymer composites. Int J Mech Sci 2020;184:105818.
[73] Zu X, Wu H, Lv H, Zheng Y, Li H. An amplitude- and temperature-dependent vibration model of fiber-reinforced composite thin plates in a thermal environment. Materials (Basel) 2020;13(7):1590.
[74] Rikards R. Finite element analysis of vibration and damping of laminated composites. Compos Struct 1993;24(3):193–204, Special Issue Advances in Polymer Composites.
[75] Rawal S, Misra M. Measurement of mechanical and thermophysical properties of dimensionally stable materials for space applications. NASA Contractor Report 18552 1992;1–159.

Publication 3

Reference: S. Chandra, M. Maeder, J. Bienert, H. Beinersdorf, W. Jiang, V.A. Matsagar, S. Marburg, Identification of temperature-dependent elastic and damping Parameters of carbon-epoxy composite plates based on experimental modal data. *Mechanical Systems and Signal Processing*, 187, 109945, 2022.

Mechanical Systems and Signal Processing 187 (2023) 109945

Contents lists available at ScienceDirect

Mechanical Systems and Signal Processing

journal homepage: www.elsevier.com/locate/ymssp

Identification of temperature-dependent elastic and damping parameters of carbon–epoxy composite plates based on experimental modal data

S. Chandra [a,*], M. Maeder [a], J. Bienert [b], H. Beinersdorf [c], W. Jiang [d], V.A. Matsagar [e], S. Marburg [a]

[a] Chair of Vibroacoustics of Vehicles and Machines, TUM School of Engineering and Design, Technical University of Munich (TUM), 85748 Garching b. Munich, Germany
[b] Faculty of Mechanical Engineering, Technische Hochschule Ingolstadt, Esplanade 10, 85049 Ingolstadt, Germany
[c] Material Research and Testing Institute, Bauhaus University Weimar, Coudraystraße 9, 99423 Weimar, Germany
[d] State Key Laboratory of Mechanical System and Vibration, Shanghai Jiao Tong University, Shanghai 200240, China
[e] Multi-Hazard Protective Structures (MHPS) Laboratory, Department of Civil Engineering, Indian Institute of Technology (IIT) Delhi, Hauz Khas, New Delhi 110 016, India

ARTICLE INFO

Communicated by J.E. Mottershead

Keywords:
Operational modal analysis
T700 carbon–epoxy
Thermal environment
Experimental test
Inverse method
Temperature-dependent elastic and damping parameters

ABSTRACT

High-strength composite materials are receiving increased attention within the aerospace and transportation industries. These materials, although light in weight, still impart high stiffness when compared to conventional structural materials, e.g., aluminum and steel. Fibers and matrix are the basic constituents of composite materials. During high-speed maneuvering of aircraft and high-speed trains, the composite materials are subjected to dynamic loads in changing temperatures. The dynamic behavior of composites strongly depends on the ambient thermal environment. Furthermore, during the in-situ operation, the quantification of real-time dynamic loads is a challenging task. Therefore, the experimental investigation of the dynamic behavior of several carbon-fiber epoxy laminated composite plates at different temperatures, namely 0 °C, 25 °C, 50 °C, 75 °C, 100 °C, and 125 °C, is carried out using operational modal analysis, to identify the modal characteristics of the structure, and the temperature-dependent modal data of the tested composite plates is given in the supplementary data. The temperature-dependent elastic and damping parameters of the carbon–epoxy laminate are estimated using a genetic algorithm-based parameter identification scheme for different sets of modal contribution. A combined experimental and numerical simulation procedure is implemented to estimate deterministic material parameters at different temperatures. To obtain the in-situ material parameters for a given operating frequency range, the modal contribution is selected such that the operating frequency of interest lies within the considered resonance modes. As an example of matrix-dominated elastic parameter, the shear modulus, has been found to degrade significantly with increasing temperature, and shown a strong correlation with temperature.

1. Introduction

Over recent decades, the application of fiber reinforced composite materials as an alternative to conventional structural materials has attracted a lot of interest in a number of manufacturing sectors. These composite materials possess various excellent properties,

* Corresponding author.
E-mail address: sourav.chandra@tum.de (S. Chandra).

https://doi.org/10.1016/j.ymssp.2022.109945
Received 9 June 2022; Received in revised form 10 September 2022; Accepted 8 November 2022
Available online 30 November 2022
0888-3270/© 2022 Elsevier Ltd. All rights reserved.

such as high structural stiffness, high strength-to-weight ratio, and high structural stability in a high temperature environment. With the rapid development of the aerospace and high-speed transportation sectors, a requirement for high-strength and light-weight structural materials has evolved. In high-speed vehicles, composite structures can effectively withstand prolonged structural vibration together with harsh aerodynamic heating. Overall, high-strength composite materials such as graphite–epoxy, carbon–epoxy, intermediate modulus (IM7) carbon fiber–polyetheretherketone (PEEK), and carbon–carbon are extensively used in different components of aircraft, satellite launch vehicles, and high-speed trains. For example, carbon–epoxy and carbon–PEEK composite shell panels are used in the front and rear fuselages, and stiffened carbon–epoxy composite panels are implemented in the wing box of commercial aircraft [1]. However, temperature variations modify the elastic and damping properties of these composite panels, which also modify the natural frequencies, mode shapes, and the transient response of the structure. Ultimately, the variation in the response influences the flutter characteristics, controllability, and failure characteristics of these structures. Based on the loading characteristics and structural requirements, different composite plates such as laminated composite plates, sandwich plates, and functionally graded plates are used in different components of aircraft and high-speed vehicles. Therefore, for reliable design of these composite structures, sufficient knowledge of the temperature-dependent elastic and damping properties is required within the operating frequency range.

To identify the appropriate material parameters of composites, various identification strategies have been investigated based on different static and dynamic experimental procedures. Material parameters of a laminated composite lamina can be identified from the standardized direct static tests which include the tension test [2], the three/ four points bending test [3], the compression test [4], and the shear tests [5,6]. Recently, Kodur et al. [7] presented a detailed review on direct static test protocols of polymer reinforced composites for evaluating their properties at elevated temperatures. Noted that a composite laminate consists of a finite number of laminae staked together in different directions, which are attached together by resin-type materials such as epoxy, PEEK, etc. Furthermore, various experimental procedures [8–10] have been developed to evaluate the elastic and damping properties of unidirectional composite laminates based on combined bending and torsion tests of beam-type samples. The accuracy of these types of measurement relies on the boundary conditions and geometry of these laminates. In addition, micromechanical theories [11] of a composite lamina have been implemented to predict the corresponding elastic and damping properties. Typically, the finite element (FE) method is used in such cases, where properties of the constituent materials, i.e., fiber and matrix, must be known a priori. Researchers, such as Saravanos et al. [12] and Hwang et al. [13], used a strain energy-based micromechanical formulation to determine the modal damping values of composite plates. Furthermore, Saravanos and Chemis [14] proposed a micromechanical formulation of composite lamina by considering the hygrothermal effect. This formulation along with macromechanical formulation can be used to calculate the elastic and damping properties of the laminate by knowing the properties of the fibers, matrix, and fiber volume fraction in a lamina. However, accuracy of the micromechanical formulation depends on the prior knowledge of the properties and percentage of the constituent materials as well as the application of a suitable numerical model. The incorporation of the effect of temperature and moisture in micromechanics-based modeling [14] is a challenging task when implemented by considering proper assumptions. Hence, the direct approaches [3–6] have some limitations in their methodology, when aiming at extracting the in-situ material properties of laminated composite plates while subjected to dynamic loads with specific attention towards the environmental conditions and operating frequencies. Additionally, static methods are time consuming procedures because evaluating all relevant material properties in a single test is hardly possible so far. Moreover, the micromechanical theory ignores the interaction between fibers and matrix [15,16], which plays a crucial role when predicting the mechanical behavior of the composite plate when subjected to a complex stress envelope.

The realistic identification of the elastic and damping properties can be achieved by implementing inverse methods [17,18] using data from static and dynamic tests in which the actual stresses domain and environmental conditions have been considered. The inverse methods, which adopt a mixed experimental and numerical strategy, have received significant attention from researchers in recent years. Employing inverse analogy, Lecompte et al. [19], Wang et al. [20], and Mi et al. [21] identified the elastic properties of composite laminates based on different static test procedures. However, these static test procedures are often time consuming and fail to impose realistic conditions during material properties identification specially when the composite structures are subjected to dynamic loads.

The material properties of a laminated composite plate can be identified by implementing a suitable inverse technique [22–24], which involves combined application of the in-situ dynamic measurement and the FE modeling of the laminated composite plate. The dynamic behavior of a structure is described by its modal characteristics, therefore the experimental and numerical modal data in terms of eigenfrequencies and modal damping values are used to identify the elastic and damping properties of composite lamina. Soares et al. [25], Bledzki et al. [26], and Rikards et al. [27] proposed an inverse method to evaluate the elastic parameters by using the FE method and a response surface-based meta-model. Frederiksen [28–30] presented a detailed investigation on the application of a first-order shear deformation theory (FSDT) and various higher-order shear deformation theories to estimate the elastic properties of thick laminated composite plates by use of inverse schemes. In inverse methods, the parameters were estimated by minimizing an error function, which includes measured and simulated modal values. It is also noted that various higher-order shear deformation theories [31–35] were developed for the accurate prediction of modal responses for thick laminated composite plates. Chandra et al. [36,37] have presented a generalized FE formulation to analyze undamped and damped dynamic response of laminated composite plates in thermal environment using the FSDT. In addition, the modal damping values of laminated composite plates were evaluated numerically using the strain energy principle [38–41] and the viscoelastic damping model [38,42]. Furthermore, Täger et al. [43] analytically studied the damping-dominated sound radiation pattern of laminated composites.

To identify the damping properties, Sol et al. [44,45] and Visscher et al. [46,47] conducted an experimental modal analysis with free–free boundary conditions. The plates are excited by an impact hammer or acoustic excitation. Klaerner et al. [48,49]

evaluated the amplitude-dependent non-linear damping of metal–plastic composites experimentally and this non-linearity is retraced by the developed FE-based numerical procedure. The determination of the damping loss factors for the carbon–epoxy composite lamina is presented by Li et al. [50] by minimizing the error function, which is developed using the experimental and simulated modal damping values of certain numbers of modes. They used the strain energy principle for the numerical analysis. Due to manufacturing-related uncertainty in composite plates, extracted modal responses [51] and subsequently identified elastic and damping parameters [52–54] exhibit substantial uncertainty. Furthermore, a randomness in temperature also leads to uncertainty in eigenfrequency values and the transient response [55]. It is observed from the literature that experimental and numerical modal data are efficiently exploited instead of other dynamic response, e.g., time history of displacement, to estimate the elastic and damping properties of composite lamina using an inverse approach.

Inverse methods for evaluating the elastic and damping parameters of laminated composite plates appear to possess great potential. Since a thermal environment has a great influence on the elastic and damping properties, identification of the temperature-dependent properties is essential. Often, a dynamic mechanical analysis (DMA) is used to measure the elastic and damping properties of composite lamina within a limited frequency range, i.e., $0-100$ Hz. Furthermore, this quasi-static experimental procedure allows direct evaluation of the five elastic parameters and the three damping parameters of the underlying material model, see Melo et al. [56]. In a subsequent study, Melo et al. [57] have evaluated the temperature and frequency dependent elastic and damping properties of IM7–PEEK lamina using the DMA. Generally, a DMA is conducted using a small composite beam sample. It therefore remains questionable whether the determined properties reflect realistic values for real structures under operating conditions.

While concerned with the applicability of the DMA, the experiment can be conducted within a thermal chamber, and the temperature-dependent material properties are identified by implementing a suitable inverse method. Inspired by this idea, Frederiksen [58] and Pedersen and Frederiksen [59] identified the temperature-dependent elastic properties of glass-epoxy and carbon–epoxy plates. Sefrani and Berthelot [40] determined the temperature-dependent damping parameters of a unidirectional glass-fiber composite plate by conducting a flexural vibration test within a thermal chamber (0 °C–90 °C). Here, an impulse hammer technique, where a suitable modification to the technique had been implemented, was used to excite the clamped composite plate. Li et al. [60] proposed an experimental methodology to identify the temperature-dependent elastic and damping properties taking into consideration the effect of material non-linearity, where the fixed laminated composite plate has been excited by aerodynamic loading. Adopting a similar experimental strategy, Li et al. [61] identified the temperature and amplitude dependent elastic and damping properties of composite lamina at varying temperatures. These studies [60,61] used the classical laminated plate theory, which ignores the effect of shear deformation, for the numerical analysis. An computationally extensive exhaustive search optimization technique is used by Maeder et al. [62] to estimate temperature-dependent elastic properties of composite lamina.

Conducting an experimental modal analysis on laminated composite plates inside a thermal chamber subjected to multiple challenges, e.g., influence of boundary conditions, excitation methodology, and input and output data acquisition during measurement. The composite plates are lightly damped structures. Therefore, fixing the composite plate [40,60,61] at one-edge (i.e., fixed-free boundary conditions) or all-edges (i.e., fixed–fixed boundary conditions) can modify the energy dissipation characteristics of the plate. In contrast, with free–free boundary conditions [46,47] chance of energy dissipation through the boundary is mostly avoided. Geweth et al. [63] discussed the influence of the boundary conditions on experimentally obtained damping values for solid plates. The excitation of laminated composite plates using the impulse hammer technique [40,58] is challenging if the impulse hammer is not temperature-resistant. Moreover, sensor-based excitation requires judicial positioning of the sensor together with consideration of the extra mass within the corresponding FE analysis and is preferably to be avoided in such situations. Note that, Li et al. [60,61] excited the plate, which was clamped inside the thermal enclosure, by use of a steel ball actuated using the aerodynamic pressure. The experimental data acquisition was performed by a laser Doppler vibrometer (LDV) instead of attaching sensors to the plate [58,60,61].

In-depth study of the literature suggests that the temperature-dependent elastic and damping parameters can be evaluated by employing a suitable inverse method using experimental modal data extracted at different temperatures. However, the stated experimental challenges need to be addressed. The present study endeavors to develop a simple experimental procedure for modal analysis of laminated composite plates inside a thermal chamber. Herein, free–free boundary conditions are adopted to limit experimental and numerical complexity, thus ensuring a maximum comparability between experimental tests and simulations. Furthermore, free–free boundary conditions avoid the introduction of any thermal-stress induced stiffness matrix, e.g., the geometric stiffness matrix. Note that the geometric stiffness matrix has no influence on the identified material properties. In order to simulate free–free boundary conditions, the suspension system is selected in such a way that it has only a minor influence on the rigid-body modes of each sample. Difficulties associated with impulse hammer excitation are avoided by utilizing a white noise sound source. In this way, the output-only operational modal analysis (OMA) is applied. Furthermore, the OMA not only yields the model of the structure but also includes the effects of the operational environment and boundary conditions [64] which are consequently part of the identified system. To the best of the authors' knowledge, the application of the OMA to identify the modal parameters for laminated composite plates has yet to be reported in literature. Therefore, this study presents a simple experimental strategy for conducting an OMA applied to laminated composite plates in identifying the material properties are studied. A genetic algorithm-based optimization technique is implemented to estimate the temperature-dependent material parameters. The FE formulation as suggested in [37] is implemented within the optimization framework as the forward model. Therefore, the novel objectives of the present study are: (1) provide a simple and output-only experimental procedure to extract the modal responses of a laminated composite plate inside a thermal chamber; (2) study the behavior of the experimentally obtained temperature-dependent modal responses; (3) present a deterministic identification of the temperature-dependent elastic and damping properties of the laminate composite plate by considering the FSDT in the FE formulation.

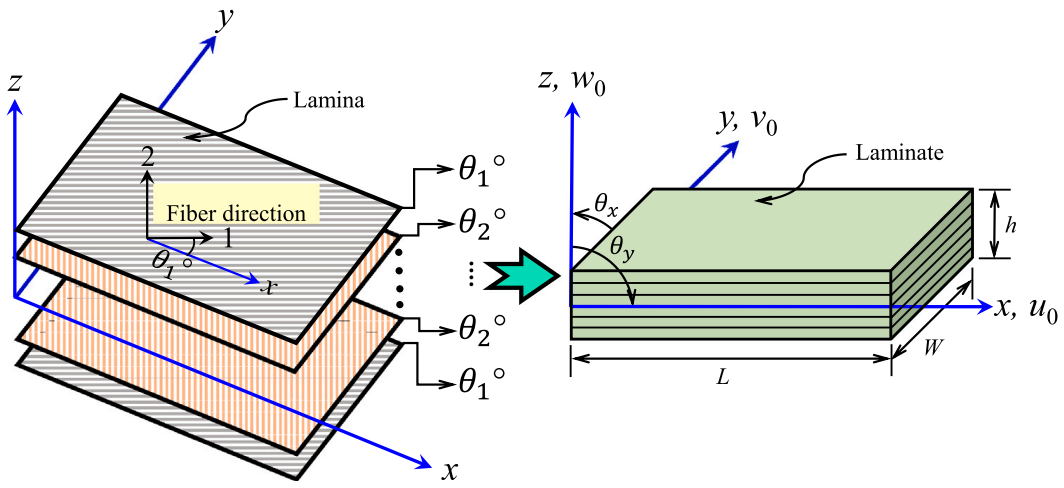

Fig. 1. Sequence of lamina, showing fiber orientation for a lamina in the lamina coordinate (1, 2, 3) system, to develop a (symmetric) laminate, and showing the positive direction of the mid-plane displacement components, u_0, v_0, w_0, θ_x, and θ_y, of the laminate in the global coordinate (x, y, z) system.

This paper is organized as follows: Section 2 describes the FE-based numerical procedure for computing the dynamic responses of laminated composite plates, the theoretical background of OMA, and the optimization procedure for evaluating the temperature-dependent elastic and damping parameters. The proposed experimental protocol is illustrated in Section 3, while in Section 4, the experimentally obtained modal responses and the evaluated temperature-dependent elastic and damping parameters are reported. Finally, the outcomes are summarized in Section 5.

2. Theory

Temperature-dependent elastic and damping properties of a composite lamina are identified by developing an inverse method; this is a combined experimental–numerical modeling technique. First, a FE model for conducting a numerical modal analysis of a laminated composite plate in a thermal environment is developed. Second, the identification of the elastic and damping properties at different temperatures is carried out by minimizing the error between numerically and experimentally estimated eigenfrequencies and modal damping values.

2.1. FE model in thermal environment

A laminated composite plate consists of a number of n thin unidirectional laminae of equal thickness (Fig. 1). Here, the FSDT is used to model the plate of length, L, width, W, and uniform thickness, h. A Cartesian coordinate (x, y, z) system at the mid-plane of the laminated composite plate is assumed (Fig. 1).

According to the FSDT, the generalized displacement field is described by a vector with five components, $\bar{\boldsymbol{d}} = \{u \quad v \quad w \quad \theta_x \quad \theta_y\}^T$. The displacement components at a distance z from the mid-plane are expressed within the laminate coordinate (x, y, z) system as

$$\begin{aligned} &u = u_0 + z\theta_y, \qquad v = v_0 - z\theta_x, \qquad w = w_0, \\ &\theta_x = w_{,y} - \varphi_y, \qquad \theta_y = -w_{,x} + \varphi_x, \end{aligned} \tag{1}$$

where u_0, v_0, and w_0 are the mid-plane displacements along x, y, and z axes, respectively, θ_x and θ_y are rotations about x and y axes, respectively, and φ_x and φ_y are the shear rotations in $x-z$ and $y-z$ planes. The mid-plane displacement vector is given by $\boldsymbol{d} = \{u_0 \quad v_0 \quad w_0 \quad \theta_x \quad \theta_y\}^T$. To account for the non-linear distribution of the shear strain, a shear correction factor, i.e., $\varkappa = 5/6$, is considered. Furthermore, the total strain is considered as a combination of linear strain, $\boldsymbol{\varepsilon}$, and non-linear thermal strain, $\boldsymbol{\varepsilon}_{\mathbf{nt}}$, where the linear part, $\boldsymbol{\varepsilon} = \{\varepsilon_x \ \varepsilon_y \ \gamma_{xy} \ \gamma_{xz} \ \gamma_{yz}\}^T$, reads as

$$\begin{aligned} &\varepsilon_x = u_{0,x} + z\theta_{y,x}, \qquad \varepsilon_y = v_{0,y} - z\theta_{x,y}, \\ &\gamma_{xy} = u_{0,y} + v_{0,x} + z(\theta_{y,y} - \theta_{x,x}), \\ &\gamma_{xz} = \varphi_x, \qquad \gamma_{yz} = \varphi_y. \end{aligned} \tag{2}$$

The elements of the mid-plain strain vector, $\boldsymbol{\varepsilon}^*$, are defined as: $\varepsilon_{0x} = u_{0,x}$, $\varepsilon_{0y} = v_{0,y}$, $\gamma_{0xy} = (u_{0,y} + v_{0,x})$, $\kappa_x = \theta_{y,x}$, $\kappa_y = -\theta_{x,y}$, and $\kappa_{xy} = (\theta_{y,y} - \theta_{x,x})$, and presented in the vector form, as

$$\boldsymbol{\varepsilon}^* = \{\varepsilon_{0x} \quad \varepsilon_{0y} \quad \gamma_{0xy} \quad \kappa_x \quad \kappa_y \quad \kappa_{xy} \quad \gamma_{xz} \quad \gamma_{yz}\}^T. \tag{3}$$

For a uniform increment in the temperature, ΔT, the thermal-strain vector, $\boldsymbol{\varepsilon}_{T_k}$, is shown as

$$\boldsymbol{\varepsilon}_{T_k} = \boldsymbol{\alpha}_k \Delta T, \tag{4}$$

in which, the vector of coefficients of thermal expansion for the k^{th} lamina is expressed in the laminate coordinate (x, y, z) system as $\boldsymbol{\alpha}_k = \{\alpha_x \;\; \alpha_y \;\; \alpha_{xy} \;\; 0 \;\; 0\}_k^T$. Due to the uniform increment of the temperature (ΔT), the stress vector, $\boldsymbol{\sigma}_k$, for the k^{th} lamina of the laminated composite plate is evaluated as

$$\boldsymbol{\sigma}_k = \boldsymbol{Q}_k \{\boldsymbol{\varepsilon}_k - \boldsymbol{\varepsilon}_{T_k}\}. \tag{5}$$

Here, $\boldsymbol{Q}_k$ (cf., Eq. (A.1)) is the transformed reduced stiffness matrix for the k^{th} lamina in the laminate coordinate (x, y, z) system and is obtained from the stress–strain relationship matrix, $\boldsymbol{C}_k$, following the proper transformation from the k^{th} lamina coordinate (1, 2, 3) system. Consequently, the elements of the stress–strain relationship matrix ($\boldsymbol{C}_k$) for the k^{th} lamina are evaluated by knowing the elastic moduli, E_{11}, E_{22}, G_{12}, G_{13}, and G_{23}, and Poisson's ratios, ν_{12} and ν_{21} (cf. Eq. (A.2)).

To evaluate the stress-resultant, the stress–strain relationship (cf., Eq. (5)) of n laminae is integrated over the thickness (h). Following the integration, the stress vector ($\boldsymbol{\sigma}_k$) of a lamina leads to develop the stress-resultant vector, $\boldsymbol{F}_r = \{N_x \;\; N_y \;\; N_{xy} \;\; M_x \;\; M_y \;\; M_{xy} \;\; Q_x \;\; Q_y\}^T$, of the laminate and the corresponding strain vector ($\boldsymbol{\varepsilon}_k$) is transformed into the mid-plane strain vector, $\boldsymbol{\varepsilon}^* = \{\varepsilon_{0x} \;\; \varepsilon_{0y} \;\; \gamma_{0xy} \;\; \kappa_x \;\; \kappa_y \;\; \kappa_{xy} \;\; \gamma_{xz} \;\; \gamma_{yz}\}^T$. Similarly, $\boldsymbol{\varepsilon}_T$ leads to the mid-plane thermal strain vector, $\boldsymbol{e}^*$, and is presented as

$$\boldsymbol{e}^* = \{e_x \;\; e_y \;\; e_{xy} \;\; 0 \;\; 0 \;\; 0 \;\; 0 \;\; 0\}^T. \tag{6}$$

Now, the stress-resultant and mid-plane strain relationship of the laminate is given by

$$\boldsymbol{F}_r = \boldsymbol{D}\boldsymbol{\varepsilon}^* - \boldsymbol{F}_N, \tag{7}$$

where, $\boldsymbol{F}_N = \{N_{Nx} \;\; N_{Ny} \;\; N_{Nxy} \;\; M_{Nx} \;\; M_{Ny} \;\; M_{Nxy}\}^T$ is the thermal stress-resultant vector which is evaluated as

$$\boldsymbol{F}_N = \boldsymbol{D}\boldsymbol{e}^*. \tag{8}$$

Here, $\boldsymbol{D}$ denotes the stress-resultant and mid-plane strain relationship matrix [36,65].

The developed initial strain, due to the uniform temperature variation, is described by the non-linear portion of the overall strain, $\boldsymbol{\varepsilon}_{nt} = \{\varepsilon_{x_{nt}} \;\; \varepsilon_{y_{nt}} \;\; \gamma_{xy_{nt}} \;\; \gamma_{xz_{nt}} \;\; \gamma_{yz_{nt}}\}^T$, and defined by

$$\begin{aligned}
&\varepsilon_{x_{nt}} = \frac{1}{2}(u_{,x}^2 + v_{,x}^2 + w_{,x}^2), \qquad \varepsilon_{y_{nt}} = \frac{1}{2}(u_{,y}^2 + v_{,y}^2 + w_{,y}^2),\\
&\gamma_{xy_{nt}} = (u_{,x}u_{,y} + v_{,x}v_{,y} + w_{,x}w_{,y}),\\
&\gamma_{xz_{nt}} = (u_{,x}u_{,z} + v_{,x}v_{,z}), \qquad \gamma_{yz_{nt}} = (u_{,y}u_{,z} + v_{,y}v_{,z}).
\end{aligned} \tag{9}$$

This equation is expressed in terms of the partial derivative of the mid-plane displacement vector, $\boldsymbol{d}^*$, and is illustrated in the compact form as [66]

$$\boldsymbol{\varepsilon}_{nt} = \frac{1}{2}\boldsymbol{R}\boldsymbol{d}^*, \tag{10}$$

where $\boldsymbol{R}$ is the non-linear strain–displacement relationship matrix, and the corresponding partial derivative of the mid-plane displacement vector reads as $\boldsymbol{d}^* = \{u_{0,x} \;\; u_{0,y} \;\; v_{0,x} \;\; v_{0,y} \;\; w_{,x} \;\; w_{,y} \;\; \theta_{x,x} \;\; \theta_{x,y} \;\; \theta_{y,x} \;\; \theta_{y,y} \;\; \theta_x \;\; \theta_y\}^T$.

2.1.1. Governing equation

The equations of motion of laminated composite plates are developed by minimization of the total energy. The FE method is implemented to develop the governing equation of the undamped free vibration in the thermal environment. The 2-dimensional plate domain is discretized using 8-node isoparametric elements and the governing equation [36,65] is presented as

$$\left[\boldsymbol{K} + \boldsymbol{K}_G\right]\boldsymbol{d}(t) + \boldsymbol{M}\ddot{\boldsymbol{d}}(t) = 0. \tag{11}$$

Here, $\boldsymbol{K}$ and $\boldsymbol{K}_G$ are the global stiffness and geometric stiffness matrices, respectively, and $\boldsymbol{M}$ is the global mass matrix. The global stiffness matrix, the geometric stiffness matrix, and the global mass matrix, ($\boldsymbol{K}$, $\boldsymbol{K}_G$, and $\boldsymbol{M}$) are obtained by assembling the corresponding elemental matrices, i.e., $\boldsymbol{K}_e$, $\boldsymbol{K}_{Ge}$, and $\boldsymbol{M}_e$, respectively. The elemental stiffness matrix ($\boldsymbol{K}_e$), the elemental geometric stiffness matrix ($\boldsymbol{K}_{Ge}$), and the elemental mass matrix ($\boldsymbol{M}_e$) are illustrated in Eqs. (A.3), (A.4), and (A.6), respectively.

2.1.2. Modeling of damping

A viscoelastic damping model is implemented to develop the governing equation for damped free vibration of the laminated composite plate in a thermal environment. The viscoelastic principle assumed stress, σ, and strain, ϵ, are harmonically time dependent at a frequency, ω, and reads as

$$\sigma(t) = \sigma_0 e^{i\omega t}, \quad \varepsilon(t) = \varepsilon_0 e^{i\omega t}. \tag{12}$$

The energy dissipation from the vibrating plate can be represented by the complex modulus approach. According to the viscoelastic damping model, the complex value expressions of the elastic moduli are given by

$$E_{11}^* = E_{11}(1 + i\eta_{11}), \quad E_{22}^* = E_{22}(1 + i\eta_{22}), \quad G_{12}^* = G_{12}(1 + i\eta_{12}), \tag{13}$$

where η_{11}, η_{22}, and η_{12} are the damping loss factors of the lamina in the lamina coordinate (1, 2, 3) system. The complex elastic moduli of the composite lamina are inserted into Eq. (5) and subsequently the global complex stiffness matrix, $\boldsymbol{K}^*$, and the global complex geometric stiffness matrix, $\boldsymbol{K}_{\mathbf{G}}^*$, are obtained. For free vibration, the equation for the complex eigenvalue problem of the laminated composite plate in a thermal environment is stated as [37,55]

$$\left(\left[\boldsymbol{K}^* + \boldsymbol{K}_{\mathbf{G}}^*\right] - \omega_{\mathrm{dm}}^{*2}\boldsymbol{M}\right)\left\{\phi^*\right\} = 0. \tag{14}$$

The complex eigenvalue solution of Eq. (14) results in complex angular eigenfrequencies, ω_{dm}^*, and complex eigenmodes, ϕ^*. The real part of the complex frequency in Hz related to the angular frequency as: $\omega_{\mathrm{dm}} = 2\pi f_{\mathrm{dm}}$. The m^{th} damped complex eigenfrequency is expressed as

$$f_{\mathrm{dm}}^* = f_{\mathrm{dm}}\sqrt{(1 + \mathrm{i}\eta_{\mathrm{m}})}, \tag{15}$$

where f_{dm} is the damped eigenfrequency, and η_{m} is the modal loss factor of the associated mode. Here, the modal loss factor is calculated as

$$\eta_{\mathrm{m}} = \frac{\mathrm{Im}(f_{\mathrm{dm}}^{*2})}{\mathrm{Re}(f_{\mathrm{dm}}^{*2})}. \tag{16}$$

The modal damping can be defined in terms of modal specific damping capacity, Ψ_{m}, and modal damping ratio, ξ_{m}. They can be determined in terms of modal loss factors, η_{m}, as

$$\Psi_{\mathrm{m}} = 2\pi\eta_{\mathrm{m}}, \qquad \xi_{\mathrm{m}} = \frac{\eta_{\mathrm{m}}}{2}. \tag{17}$$

Thus, the real part of the complex eigenfrequency (f_{dm}^*) is described as the damped eigenfrequency, $f_{\mathrm{dm}} = \mathrm{Re}(f_{\mathrm{dm}}^*)$, of the plate, and the corresponding modal loss factor (η_{m}) is evaluated from Eq. (16). In the remaining part of the paper, these numerically calculated damped eigenfrequency and modal loss factor are designated as $f_{\mathrm{dm}}^{\mathrm{num}}$ and $\eta_{\mathrm{m}}^{\mathrm{num}}$, respectively.

2.2. Operational modal analysis

Modal analysis is a well established method for the parameter identification of linear systems. As the test object in this paper is described as a linear mechanical system, the aim is to identify modal parameters and then relate them to the material properties. The assumption is a linear time-invariant system with symmetric matrices for mass, damping, and stiffness. In this case, the modal parameters are the

- natural frequency,
- modal damping,
- mode shapes with scaling.

They represent each mode, and the number of modes is equal to the number of degrees of freedom (DOFs).

The symmetry of the matrices leads to right-hand side eigenvectors only. They are equal to the solution of the classical eigenvalue problem. The extension to non-symmetric problems, e.g., caused by gyroscopic effects, and time-variant modal analysis is not necessary in this case. Another question relates to the complex representation of the mode shapes. Complex mode shapes allow the description of natural vibrations including a phase difference between the degrees of freedom. It can be shown that for systems that have equally distributed damping, the mode shapes do not show relative phases. This is expected in this study as the damping distribution will be proportional to the mass and/or stiffness matrix. Nevertheless, the used algorithm includes complex mode shapes, but the phase between the DOFs will be expected as negligible.

The modal analysis community distinguishes between the classical modal analysis (i.e., experimental modal analysis) and the OMA [67]. The classical experimental modal analysis is based on frequency response functions in the frequency domain. The full system information is included in the relationship between output and input. All modal parameters in the measured frequency range can be extracted. The input must be known in the experimental modal analysis test which means that the excitation force must be measured. For lightweight structures a sensitive measurement setup is required because the attachment of an exciter or the use of an impact hammer has an influence on the structure. Non-contact based excitation by sound pressure excitation of a loudspeaker improves the situation, but the approximation of the input force by a microphone is not satisfactory. Therefore, the OMA without system input measurements is preferred in this study. Using a laser vibrometer, the system response can also be measured in a non-contact manner. In general the OMA has some significant advantages:

- the excitation is applied in a distribution similar to that of the real operation,
- the level of the excitation is somehow as in reality; this helps if the structure has slight non-linearities, as we work at the linearization point,
- conditions that cannot be controlled are in the right setup, e.g., boundary conditions under operation or temperature-dependent variations.

These advantages are most relevant for powered machines or civil engineering structures under environmental changes.

On the other side, the lack of information with respect to the excitation has an influence to the result. As the input force is not known, the scaling of the mode shapes, as it is necessary to synthesize the frequency response functions, is not possible. This

disadvantage is not relevant in this study because the results for the material properties are derived from the experimentally obtained eigenfrequencies, $f_{\mathrm{m}}^{\mathrm{exp}}$, and the modal damping, $\eta_{\mathrm{m}}^{\mathrm{exp}}$. Each measurement from the scanning laser vibrometer delivers the vibration response of each DOF sequentially. A second single point laser was used as a reference channel to construct the mode shape vector. This allows to develop the correct amplitude and phase relation between each DOF.

Different options for the analysis algorithms are available for the OMA analysis based on the acquired data. Comparable with the classical experimental modal analysis the OMA can be distinguished between

- time domain methods,
- frequency domain methods.

In the class of time domain methods, the Stochastic Subspace Iteration (SSI) is one of the most elaborate procedures, which has been utilized in this study together with an Enhanced Frequency Domain Decomposition (EFDD) to ensure the reliability of the estimated modal parameters. For deeper insight, the reader can refer to the literature on the SSI method [68–70] and the EFDD method [71–74].

2.3. Identification of temperature-dependent elastic and damping parameters

The identification of the elastic moduli and damping loss factors of the composite lamina is posed as an optimization problem, where the discrepancy between the eigenfrequencies of the OMA and the numerically obtained eigenfrequencies is minimized. The FE formulation for numerical determination of the damped eigenfrequencies ($f_{\mathrm{dm}}^{\mathrm{num}}$) and modal loss factors ($\eta_{\mathrm{m}}^{\mathrm{num}}$) of the laminated composite plate at different temperatures has been discussed in Section 2.1. For a given dimension and density, the eigenfrequencies and modal loss factors of the plate are predicted as a function of identifiable variables. A two-stage identification strategy is implemented to identify the elastic moduli and the damping loss factors at different temperatures. Initially, the elastic moduli are identified by minimizing the discrepancy between the experimentally and numerically predicted damped eigenfrequencies, i.e., $f_{\mathrm{m}}^{\mathrm{exp}}$ and $f_{\mathrm{dm}}^{\mathrm{num}}$, respectively. In a second stage, the damping loss factors are identified by minimizing the experimental and numerically predicted modal loss factors, i.e., $\eta_{\mathrm{m}}^{\mathrm{exp}}$, and $\eta_{\mathrm{m}}^{\mathrm{num}}$, respectively.

In the first stage of the optimization, $\bar{\boldsymbol{r}}_{\mathbf{1}} = \{E_{11} \;\; E_{11}/E_{22} \;\; E_{11}/G_{12}\}^{\mathrm{T}}$ is considered as evaluated vector. Since the sensitivity of the Poisson's ratio, ν_{12}, is very small, this parameter is not identified in the present study. The remaining elastic moduli are related as $G_{13} = G_{12}$ and $G_{23} = 0.5G_{12}$ [28,75–77], and can be determined once $\bar{\boldsymbol{r}}_{\mathbf{1}}$ is identified. The average density of the composite plate is determined by knowing the geometry and mass of the individual plate among all the plates considered for the measurement. The optimization problem for the inverse method is stated as

$$\begin{aligned} \bar{r}_1^* &= \underset{\bar{r}_1}{\operatorname{argmin}} \;\; C(\bar{\boldsymbol{r}}_{\mathbf{1}}), \\ \text{subject to} \;\; & \bar{\boldsymbol{r}}_{\mathbf{1_{min}}} < \bar{\boldsymbol{r}}_{\mathbf{1}} < \bar{\boldsymbol{r}}_{\mathbf{1_{max}}}, \end{aligned} \tag{18}$$

where

$$C(\bar{\boldsymbol{r}}_{\mathbf{1}}) = \sum_{m=N_{\mathrm{ini}}}^{N_{\mathrm{fin}}} \left(\frac{f_{\mathrm{m}}^{\mathrm{exp}} - f_{\mathrm{m}}^{\mathrm{num}}}{f_{\mathrm{m}}^{\mathrm{exp}}} \right)^2, \tag{19}$$

in which N_{ini} and N_{fin} are initial and final mode numbers that are considered to develop the objective function ($C(\bar{\boldsymbol{r}}_{\mathbf{1}})$) for minimization. The gradient-less genetic algorithm available in MATLAB is used in this context.

In the second stage of optimization, the damping loss factors are evaluated by incorporating the identified elastic parameters, i.e., E_{11}, E_{22}, and G_{12}. The design variables in this stage of optimization are stated as $\bar{\boldsymbol{r}}_{\mathbf{2}} = \{\eta_{11} \;\; \eta_{22} \;\; \eta_{12}\}^{\mathrm{T}}$, and the associated optimization problem is defined as

$$\begin{aligned} \bar{\boldsymbol{r}}_{\mathbf{2}}^* &= \underset{\bar{r}_2}{\operatorname{argmin}} \;\; C(\bar{\boldsymbol{r}}_{\mathbf{2}}), \\ \text{subject to} \;\; & \bar{\boldsymbol{r}}_{\mathbf{2_{min}}} < \bar{\boldsymbol{r}}_{\mathbf{2}} < \bar{\boldsymbol{r}}_{\mathbf{2_{max}}}, \end{aligned} \tag{20}$$

where

$$C(\bar{\boldsymbol{r}}_{\mathbf{2}}) = \sum_{m=N_{\mathrm{ini}}}^{N_{\mathrm{fin}}} \left(\frac{\eta_{\mathrm{m}}^{\mathrm{exp}} - \eta_{\mathrm{m}}^{\mathrm{num}}}{\eta_{\mathrm{m}}^{\mathrm{exp}}} \right)^2. \tag{21}$$

This two-stage optimization procedure was conducted at each temperature state to evaluate temperature-dependent material properties using an in-housely developed MATLAB code. For better understanding of the analysis framework, a flowchart is provided (cf., Fig. 2).

In these two deterministic inverse problems, a genetic algorithm is applied to achieve the global minimum of the given objective functions. For successful implementation of the genetic algorithm various strategies are applied. These strategies are: (1) starting values of the identified parameters are given based on the known data by supplier and the experiences gathered during trial runs; (2) the interdependency ratios between the elastic constants are considered as the identified parameters instead of identifying the parameters directly [27]; (3) provide realistic limits of the identified parameters; and (4) various parameters of the genetic algorithm, e.g., 'ConstraintTolerance', 'MaxGenerations', 'PopulationSize' [78] are given by keeping a balance between accuracy and computational time.

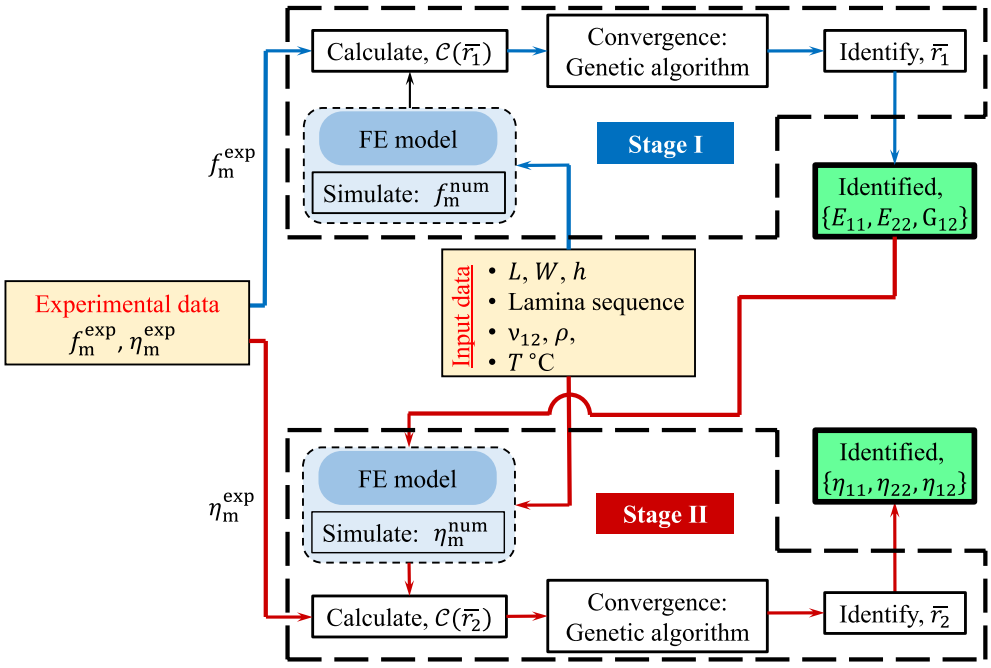

Fig. 2. Framework of the inverse method to evaluate the temperature-dependent elastic parameters (E_{11}, E_{22}, and G_{12}) and damping parameters (η_{11}, η_{22}, and η_{12}) of the T700 carbon–epoxy composite lamina.

3. Experimental setup

In the present experimental study, the eigenfrequencies of the damped system and the modal loss factors of a 14-layered T700 carbon–epoxy laminated composite plate, manufactured by Connova[1], were determined experimentally at varying temperatures. To ensure the reliability of the measurement and resulting lamina properties, two symmetric cross-ply and two symmetric angle-ply laminated composite plates have been tested and further analyzed using modal analysis. Inside the environmental chamber, the plate excitation and corresponding measurements were carried out by a non-contact based method using a loudspeaker and two LDVs.

3.1. Experimental procedure

The experimental setup consists of a thermal chamber in which the carbon–epoxy laminated plate is suspended using elastic strings. An environmental chamber, which accurately controls temperature and moisture, is used for this investigation. The chamber has an inner volume of $1.09 \times 1.01 \times 1.10$ m^3. The chamber has two circular openings in two opposite faces which are covered by glass windows. The plate inside the chamber is excited by a white noise signal generated using a loudspeaker and the sound pressure level is measured using a microphone (cf., Fig. 3). The non-contact based measurement on the vibrating plate is done through two openings using LDVs. Prior to initiate each measurement, the humidity and temperature inside the environmental chamber were controlled through an automatic controller and a 10 min. delay was set to achieve equilibrium condition.

To achieve free–free boundary conditions for the plate during measurement, the plate is suspended vertically using Kevlar wires (cf., Fig. 3). The influence of the suspension is minimized by mounting the plate in the nodal lines [63] of the first elastic deformation mode (cf., Figs. 3 and 4). This method of suspension ensured that the frequencies of the rigid body motions remained at a very low value compared to the fundamental eigenfrequency of the plate.

A graphical representation of the experimental setup is provided in Fig. 4. As shown, the loudspeaker is placed in the corner of the thermal chamber (cf., Figs. 3 and 4). The full experimental setup is designed in such way that the acoustic excitation produces a diffuse acoustic field which is a necessary condition for subsequently applying the OMA. The main advantages of the presented approach rely on the thermal resilience of the loudspeaker as well as the continuous excitation signal for sequential measurements. Despite the lower energy input compared to standard impulse excitation, the sensitivity of LDV is sufficient to still achieve accurate measurement. Furthermore, use of electrodynamic contact excitation was not possible because of the need to avoid additional mass coupling. Similarly, magnetic excitation involves additional mass coupling because the composite is not magnetic and the exact excitation force is unknown. All limitations are avoided by presenting a non-contact based excitation strategy. Moreover, the microphone placed inside the chamber tracks the sound pressure level inside the thermal chamber, thus, tracking the coherence.

[1] Connova Deutschland GmbH, Schücostrasse 8, 01900 Grossröhrsdorf, Germany.

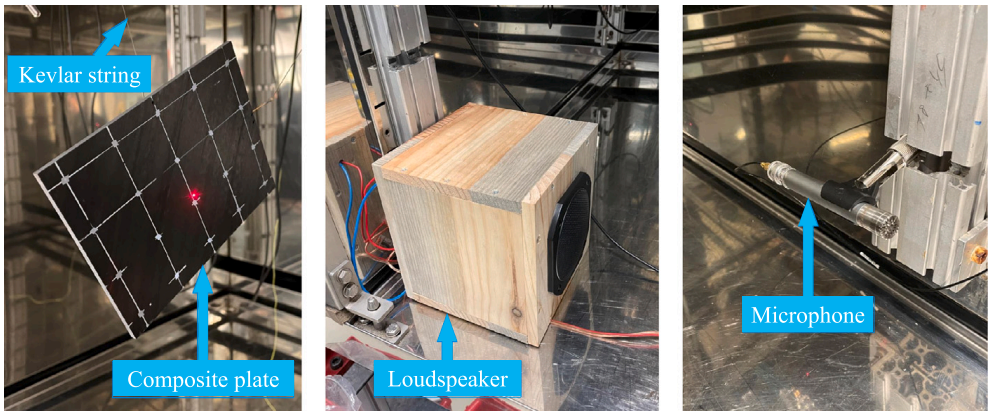

Fig. 3. Suspension system with free–free boundary conditions to the composite plate (left), loudspeaker (middle), and microphone (right) inside the thermal chamber.

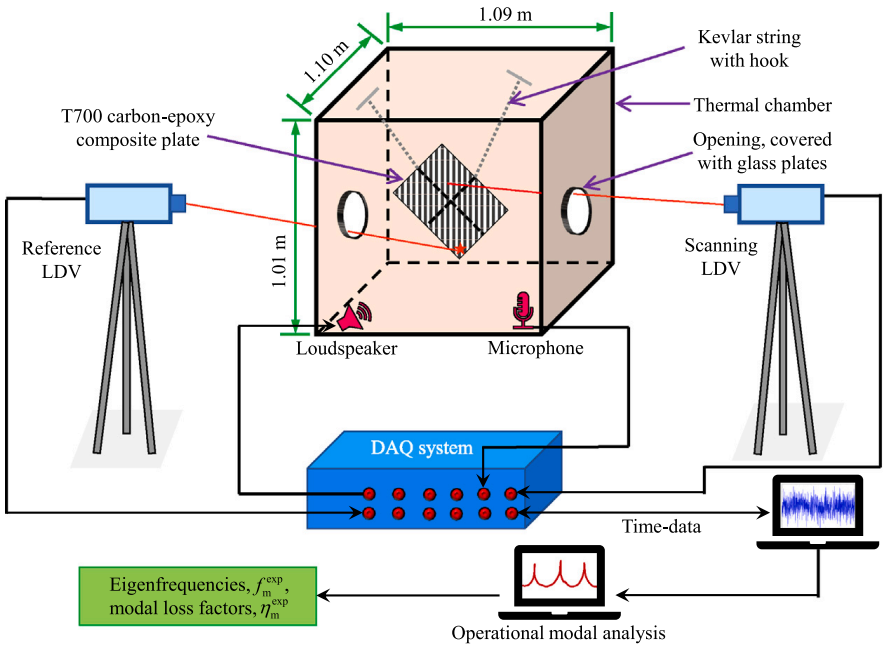

Fig. 4. Flowchart of the experimental setup for evaluating experimental eigenfrequencies, (f_m^{exp}) and modal loss factors, (η_m^{exp}) of the T700 carbon–epoxy laminated composite plate inside the environmental chamber.

Table 1
Apparatus used in the experiments conducted to identify modal parameters of composite plates at different temperatures.

Apparatus	Manufacturer	Product model
Thermal Chamber	Clima temperature system (CTS)	–
Reference LDV	Polytec GmbH, Waldbronn, Germany	PDV100
Scanning LDV	Polytec GmbH, Waldbronn, Germany	PSV500
Loudspeaker	Visaton GmbH & Co., Haan, Germany	FRS 10 WP
Microphone	Brüel & Kjær, Virum, Denmark	1/2’ Diffuse-field Microphone, 6.3 Hz to 16 kHz
Mobile DAQ	Polytec GmbH, Waldbronn, Germany	–

The photograph (cf., Fig. 5) of the experimental setup in the laboratory illustrates how the measurement is performed. Two LDVs are used to collect response data: one LDV measures the plate vibration through scanning sequentially all DOFs (scanning LDV), and the other LDV remains at a fixed position and serves as a reference channel (reference LDV). The measurement is conducted at each DOF of the plate for a duration of 50 s. This time block corresponds to approximately 30,000 times the period of the fundamental mode, and is sufficiently long to enable the extraction of low damping modes [64,79]. During the experiment, controlling the input, i.e., white noise, and collecting measured data are performed by the data acquisition (DAQ) system. Details of the apparatus used during measurements are presented in Table 1.

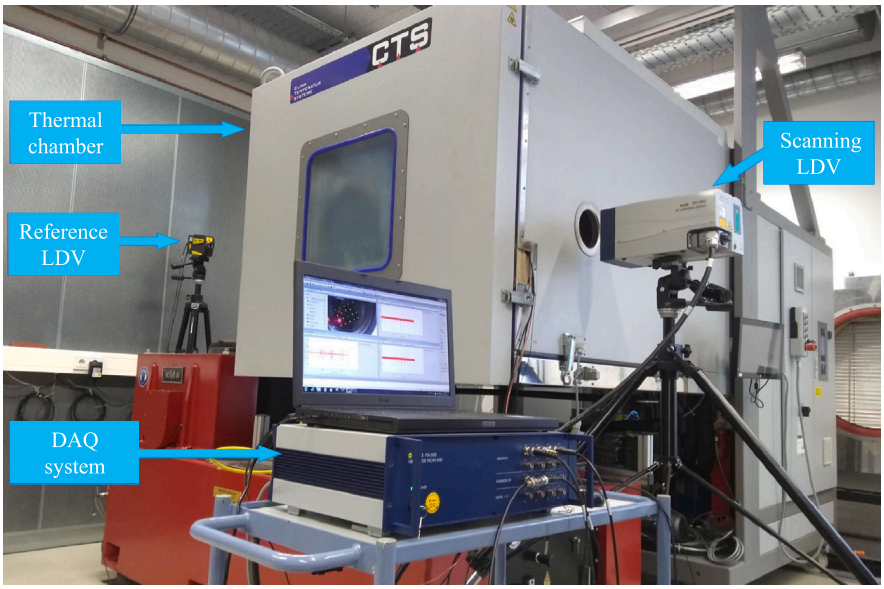

Fig. 5. Pictorial illustration of the experimental setup available at the Material Research and Testing Institute, Bauhaus University, Weimar, Germany.

3.2. Test samples

Two 14-layered symmetric angle-ply, $(45°/-45°)_{7s}$, laminates, namely SA2 and SA10; and two 14-layered symmetric cross-ply, $(0°/90°)_{7s}$, laminates, namely SC5 and SC6, of carbon–epoxy are used as samples for the experiment. The unidirectional lamina is fabricated from T700 carbon fibers which were cured at 135 °C within the epoxy resin. Note that the glass transition temperature of the applied epoxy resin is approximately 170 °C. The thickness of each lamina is 0.287 mm. These laminates are cut from a large-size plate. The volume of the carbon–epoxy laminated composite plates is $150\times110\times4.018$ mm^3. Moreover, the dimensions of the plate are selected such that the first fundamental frequency remains in high-frequency regime as compared to the resonance frequency of the acoustic cavity. The experiment was conducted at varying temperatures, namely 0 °C, 25 °C, 50 °C, 75 °C, 100 °C, and 125 °C. A 0% humidity level is maintained inside the thermal chamber. The average density, ρ, of the laminate is 1603.7 kg/m^3. The temperature independent Poisson's ratio, ν_{12}, is assumed as 0.32.

3.3. Post-processing of experimental data

The measured time data was analyzed using the Brüel & Kjær OMA software[2], where the data was transferred by using an uff-file format to ensure compatibility between the DAQ and the OMA software. Before analyzing the measured data to obtain the corresponding modal parameters, the time signals were filtered using an 8th order Butterworth low-pass filter with a cut-off frequency of 5000 Hz after removing outliers and any mean values. In this way, no drift of the time data could violate the subsequent modal parameter estimation. The quality of the time data was checked by evaluating the coherence between each DOF and the reference LDV channel signal which was above 0.8 within the frequency range around the corresponding resonances of interest.

After applying the SSI as well as the EFDD method, the results were compared to ensure a reliable result quality. Furthermore, the quality of the corresponding mode shapes were checked by evaluating the MAC-matrix. It is noted that the off-diagonal values of the MAC-matrix remained below a value of 0.05.

4. Results

4.1. Experimental modal responses

The modal parameters, i.e., the eigenfrequencies and loss factors of the tested carbon–epoxy laminated composite plates are evaluated from the experimentally obtained time domain data at different temperatures for the plates SA2, SA10, SC5, and SC6. The extracted six eigenfrequencies and the associated mode shapes for these plates are illustrated with reference to the variation in temperature in Fig. 6. For plates SA2 and SA10, the first six experimental eigenfrequencies (cf., Figs. 6(a), 6(b), and 6(c)) are presented. Prior to the experiment, mode shapes and associated eigenfrequencies were calculated using initial guess values for the elastic parameters. However, for plates SC5 and SC6, 2nd to 7th experimental eigenfrequencies (cf., Figs. 6(d), 6(e), and 6(f)) are extracted. The first eigenfrequency of the symmetric cross-ply laminates could not be identified experimentally. The first

[2] PULSE Operational Modal Analysis, 5.2.0.2 - x64, Built Date: 11.06.2018.

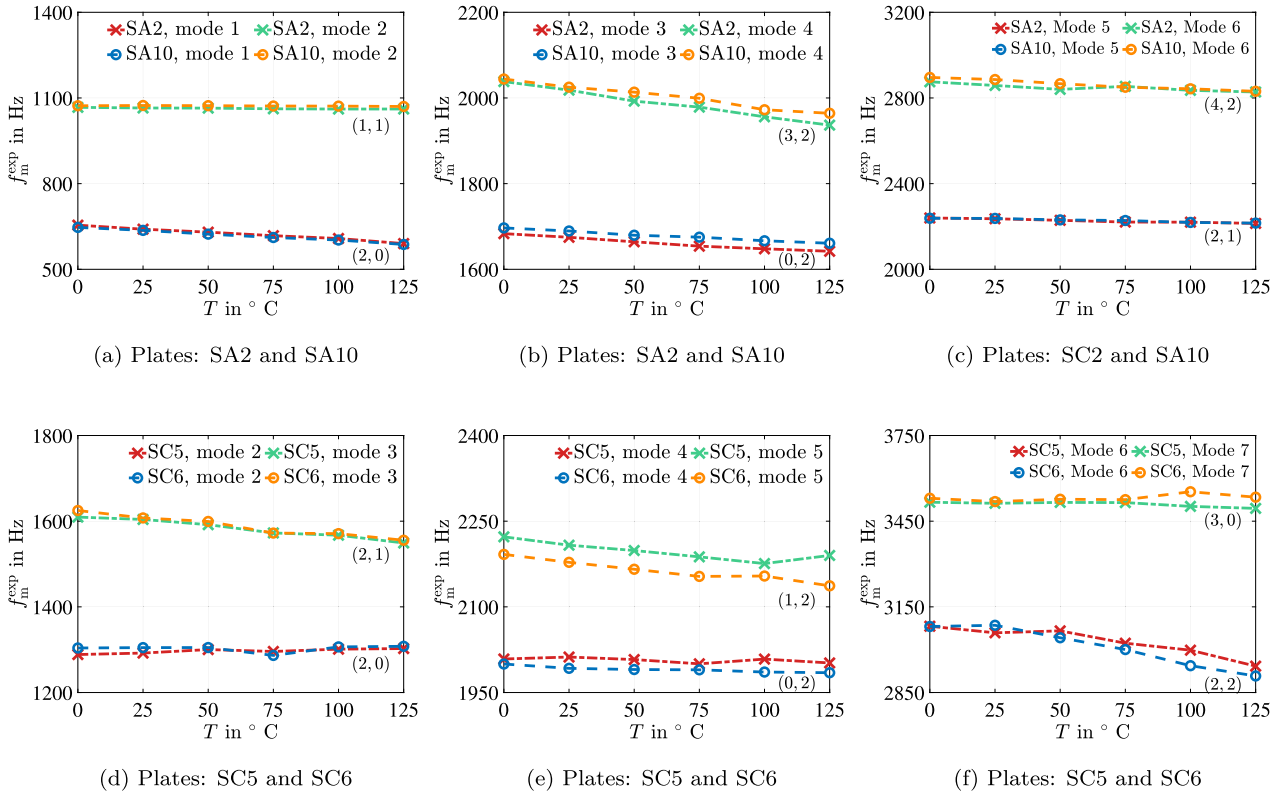

(a) Plates: SA2 and SA10 (b) Plates: SA2 and SA10 (c) Plates: SC2 and SA10

(d) Plates: SC5 and SC6 (e) Plates: SC5 and SC6 (f) Plates: SC5 and SC6

Fig. 6. Variation in the experimentally obtained eigenfrequencies (f_m^{exp}) plotted with temperatures for associated mode shapes, plotted for plates SA2, SA10, SC5, and SC6.

eigenfrequency of this laminate is lowest in magnitude, and radiation efficiency of the corresponding mode is also lowest. To excite this low frequency mode a larger sound source is necessary, however within the present experimental setup, size of the loudspeaker is too small in diameter. Therefore, possible explanations regarding unidentification of the first mode for the symmetric cross-ply laminates could be: firstly, low radiation efficiency of the first mode and secondly, too small diameter of power output of the loudspeaker.

For the symmetric angle-ply laminates (cf., SA2 and SA10) it is observed that the 1st, 3rd, 4th, and 6th experimentally determined eigenfrequencies decrease as the temperature increases, whereas, the 2nd and 5th experimental eigenfrequencies are not very sensitive to the temperature variation. On the other hand, the 3rd, 5th, and 6th experimental eigenfrequencies decrease with increasing temperature for the symmetric cross-ply laminates (cf., SC5 and SC6). The variation in the experimentally determined eigenfrequencies with respect to temperature can be explained by observing mode shapes of a plate and the associated fiber orientations (cf., Fig. 6). The mode shapes of the plates SA2 and SC5 at 25 °C are given in Appendix C (cf., Figs. 13 and 14) to understand the nodal line representation of the mode shapes for two types of plate configurations. It is observed that for the case of the symmetric angle-ply laminates, which have diagonal fibers orientation, the modes in which the eigenfrequencies remained unaffected by an increase in temperature are not bending modes. In these modes, major extension occurs along the directions of the fibers. Since the fibers are unaffected by the temperature variation, the associated eigenfrequencies did not decrease with increasing temperature. Moreover, for the cross-ply laminates, modes corresponding to the unaffected eigenfrequencies are the bending modes. In these bending modes, the longitudinally and transversely oriented fibers are not influenced by the increasing temperature, thus, the corresponding eigenfrequencies remained constant across the temperature range. It is apparent from Fig. 6 that the experimental eigenfrequencies for the symmetric angle-ply laminates, and symmetric cross-ply laminates are in good agreement with each other which proves the reliability of the extracted eigenfrequencies.

The associated experimental modal loss factors of these plates are plotted against temperature in Fig. 7. It is observed that the first six experimental modal loss factors (cf., Figs. 7(a), 7(b), and 7(c)) for the plates SA2 and SA10 vary non-linearly with increasing temperature. Furthermore, the experimental modal loss factors for the plates SA2 and SA10 do not agree well at a specific temperature. The non-agreement and non-linear behavior of experimentally evaluated modal damping values are primarily due to the manufacturing-related uncertainty, and the measurement precision. Furthermore, the curve-fitting algorithm within the SSI may influence the accuracy of the estimated modal loss factors. The uncertainty involved in identifying modal damping values for lightly damped structures is extensively discussed in the literature [74,80].

The 1st experimental modal loss factors for the plates SA2 and SA10 show an increasing trend and this trend is depicted by the best fitted line in Fig. 7(a). The variation in the 3rd and 4th experimental modal loss factors remain within a shallow envelope. Relatively good agreement is observed for mode 5, where the experimental modal loss factors for both plates remain constant with increasing

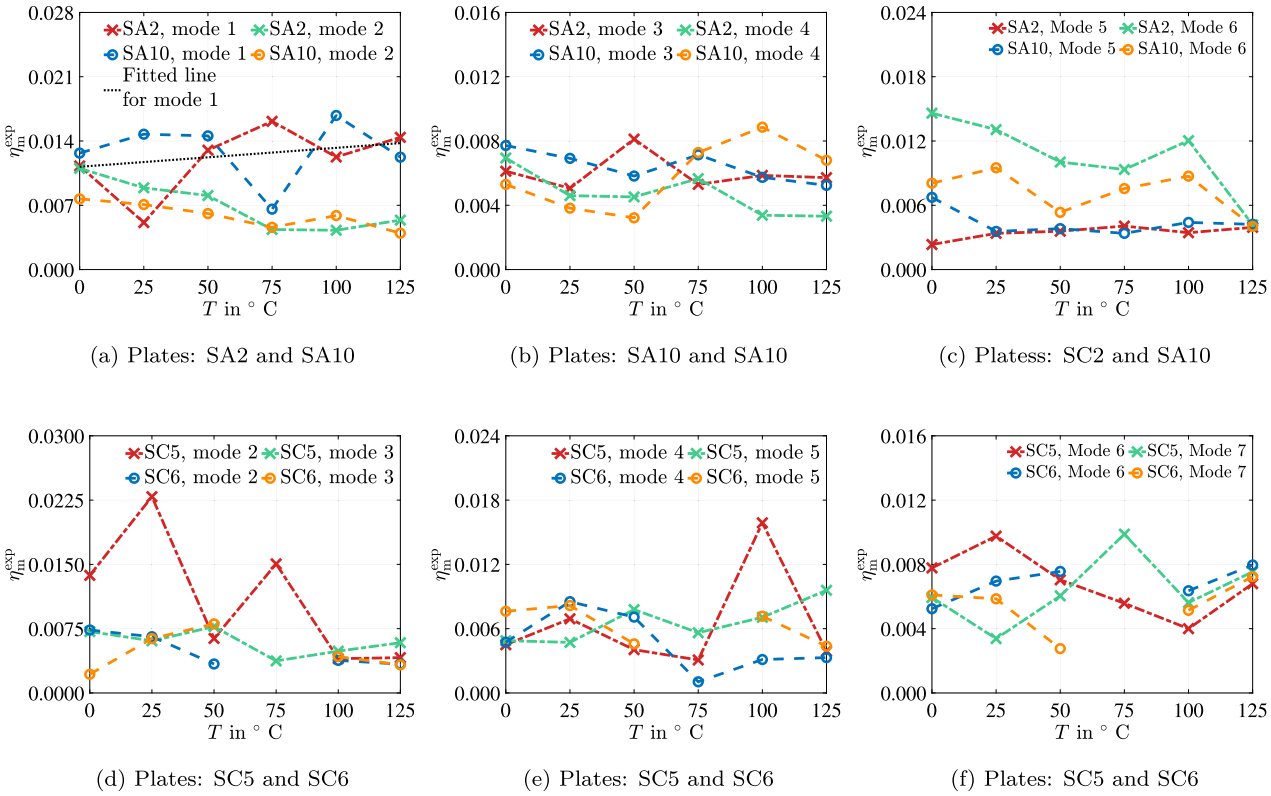

(a) Plates: SA2 and SA10 (b) Plates: SA10 and SA10 (c) Platess: SC2 and SA10

(d) Plates: SC5 and SC6 (e) Plates: SC5 and SC6 (f) Plates: SC5 and SC6

Fig. 7. Variation in the experimentally obtained modal loss factors (η_m^{exp}) plotted with temperatures for the plates SA2, SA10, SC5, and SC6.

temperature. Further, this behavior matches intuitively with the temperature-independent behavior of the 5th experimental modal frequency in Fig. 6(c). For the plates SC5 and SC6 (cf., Figs. 7(d), 7(e), and 7(f)), it is very difficult to identify any pattern in the variation of the experimental modal loss factors with respect to increasing temperature. Moreover, some experimental data, e.g., for modes 2, 3, 5, 6, and 7 for plate SC6, at 75 °C are omitted in the figures due to unrealistically high values being obtained. The experimentally obtained eigenfrequencies and modal loss factors of these plates are given in the supplementary document.

To assess the overall damping behavior of these composite plates at varying temperatures, a concept of pressure-normalized velocity is introduced. In this way, the output amplitude of the vibration velocity is scaled to the input amplitude of the sound pressure, which represents the overall reciprocal damping. It was stated earlier that each plate was excited by a white noise signal and the associated experimental time data in terms of velocity has been collected for 50 s (t_{tot}). During digitization of the velocity response data, a window of 0.5 s (t_w) is considered. The characteristic of the experimental velocity at every nodal point is evaluated using the root mean square value, V_{rms}, of the velocity data for each window. In a similar way, the root mean square values of sound pressure, p_{rms}, obtained from the microphone, for each time window are also calculated. Only 97 percentile (V_{rms}) data, and the corresponding p_{rms} are selected to evaluate the pressure-normalized velocity, V_{norm}, at each node. The pressure-normalized velocity $V_{norm,i,j}$ for the i^{th} window of the j^{th} nodal data is given as

$$V_{norm,i,j} = \frac{V_{rms,i,j}}{p_{rms,i}}, \quad i = 1, 2, \ldots, n_{w,sel}, \quad j = 1, 2, \ldots, n_{node}, \tag{22}$$

where $n_{w,sel}$ $\left(< \frac{t_{tot}}{t_w}\right)$ is the number of windows selected considering the 97 percentile criterion and n_{node} denotes the total number of nodes on the composite plate for which measurements were performed. Based on this, an average pressure-normalized velocity, $V_{norm,avg}$, is calculated, as

$$V_{norm,avg} = \frac{1}{n_{node}} \left\{ \sum_{j=1}^{n_{node}} \left(\frac{1}{n_{w,sel}} \sum_{i=1}^{n_{w,sel}} V_{norm,i,j} \right) \right\}. \tag{23}$$

The calculated average pressure-normalized velocity of the plate is shown plotted against temperature in Fig. 8. For the plates SA2 and SA10, the minimum value of the average pressure-normalized velocity ($V_{norm,avg}$) is obtained at 100 °C (cf., Fig. 8(a)), which signifies that the maximum response control occurs at 100 °C. Furthermore, in the case of the considered cross-ply laminates, i.e., SC5 and SC6 (cf., Fig. 8(b)), overall damping is varies non-linearly with varying temperature.

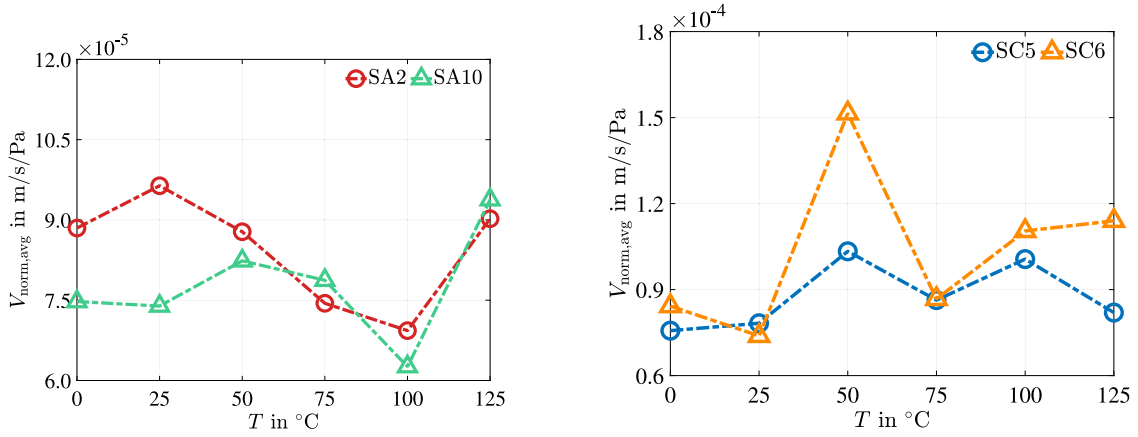

(a) Plates: SA2 and SA10 (b) Plates: SC5 and SC6

Fig. 8. Experimentally obtained average normalized-velocity ($V_{\text{norm,avg}}$) plotted against temperatures for the plates SA2, SA10, SC5, and SC6.

4.2. Identified temperature-dependent elastic properties

The temperature-dependent elastic parameters of the carbon–epoxy lamina are evaluated from the eigenfrequencies of the symmetric angle-ply (i.e., SA2 and SA10) and symmetric cross-ply (i.e., SC5 and SC6) laminates. The identification procedure was explained in Section 2.3. The identified temperature-dependent elastic properties, i.e., E_{11}, E_{22}, and G_{12}, of the carbon–epoxy lamina are illustrated in Fig. 9. Furthermore, values of these identified parameters are given in Appendix B (cf., Table 2). During the identification, three different sets of modes are considered to study the influence of modal contribution on the identified properties. For the symmetric angle-ply laminates modes considered are: 1–3, 4–6, and 1–6, and for the symmetric cross-ply laminates modes considered are: 2–4, 5–7, and 2–7. A minimum of three modes is considered to avoid a non-unique solution of the optimization algorithm. Additionally, three sets of modal contributions are provided, intended to explain the frequency dependency of the elastic parameters. A 2^{nd} order fitted curve for each elastic parameter is plotted separately for each laminate, and the corresponding equation is presented below each sub-figure. The 2^{nd} order fitted curve can represent a non-linear variation in the elastic properties with respect to temperature, although avoiding the over-fitting phenomenon.

The temperature dependency of the identified E_{11} for the symmetric angle-ply and symmetric cross-ply laminates is depicted in Figs. 9(a), 9(d), and 9(g), and fitted curves are plotted for each type of laminate. Although, two fitted curves for the identified E_{11} show a modest increasing trend with increasing temperature, individual values of the identified E_{11} are vary non-linearly with temperature. Moreover, these fitted curves have very low gradient. Hence, it can be stated that the fiber-dominated E_{11} is a temperature independent parameter. For the identified E_{22}, a downward slope is apparent for the associated fitted curves (cf., Figs. 9(b), 9(e), and 9(h)). The negative slope of these fitted curves indicates that the identified E_{22} are temperature-dependent and the magnitudes of these identified E_{22} decrease with increasing temperature. E_{22} is not a fiber-dominated parameter, thus is influenced by the temperature-dependent behavior of the matrix. A steep negative slope of the fitted curves for the identified G_{12} of the symmetric angle-ply and symmetric cross-ply laminates is observed in Figs. 9(c), 9(f), and 9(i), which indicates significant degradation of the shear modulus with an increase in temperature. The coefficient of determination, R^2, for the identified G_{12} fitted curves is calculated. It is observed that R^2 is greater than 0.95 in the cases where an initial three (cf., Figs. 9(c)) and an initial six (cf., Fig. 9(i)) experimental modes are considered during the identification procedure, which indicates a strong correlation between the identified G_{12} and temperature. Whereas, in the remaining case, R^2 is greater than 0.85 (cf., Fig. 9(f)) that also denotes a sufficiently good correlation between the identified G_{12} and temperature. It is noted that G_{12} is a matrix-dominated property, and stiffness of the matrix degrades with increasing temperature, which proves the underlying cause of strong correlation between G_{12} and temperature. Due to the dissimilarity in inter-laminar stress for angle-ply and cross-ply laminates, the pattern of the temperature dependency for the identified elastic parameters is not exactly the same, although, the extent of this variability remains within the acceptable limit. The variability of the identified parameters indicates that adaptation of a stochastic identification technique could explore these variabilities in a more rational way.

Until now, the temperature dependency of elastic moduli for carbon–epoxy lamina have been discussed in the lamina coordinate system (1, 2, 3). In addition to this, temperature-dependency pattern of homogenized elastic properties, i.e., E_{xx}, E_{yy}, and G_{xy}, for symmetric angle-ply and symmetric cross-ply laminates is worthy of study. The homogenized elastic properties are expressed in the laminate coordinate (x, y, z) system of the plate, see Fig. 1 for an explanation of the coordinate systems. To understand the temperature dependency of the homogenized elastic parameters of two types of laminates, the corresponding E_{xx}, E_{yy}, and G_{xy} at each temperature state are evaluated based on the modal contribution of 1–3, and shown in Fig. 10. The fitted curves for the identified parameters are plotted separately for the symmetric angle-ply and symmetric cross-ply laminates. Based on the fitted curves for the identified E_{xx} (cf., Fig. 10(a)), it is found that the identified E_{xx} is a temperature independent parameter for the symmetric cross-ply laminates, whereas the identified value of E_{xx} decreases with the increasing temperature for symmetric angle-ply

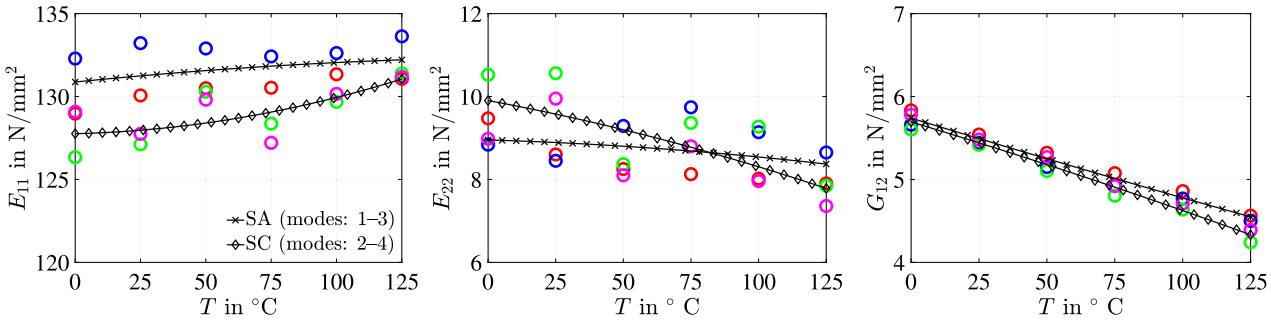

(a) Considered modes: 1–3 and 2–4
$E_{11,\mathrm{SA}} = 130.88 + 1.58\times10^{-2}T - 4.10\times10^{-5}T^2$
$E_{11,\mathrm{SC}} = 127.76 + 3.89\times10^{-3}T + 1.80\times10^{-4}T^2$

(b) Considered modes: 1–3 and 2–4
$E_{22,\mathrm{SA}} = 8.95 - 1.96\times10^{-3}T - 2.16\times10^{-5}T^2$
$E_{22,\mathrm{SC}} = 9.90 - 1.21\times10^{-2}T - 3.87\times10^{-5}T^2$

(c) Considered modes: 1–3 and 2–4
$G_{12,\mathrm{SA}} = 5.74 - 9.99\times10^{-3}T + 3.70\times10^{-6}T^2$ $(R^2 = 0.9729)$
$G_{12,\mathrm{SC}} = 5.69 - 9.90\times10^{-3}T - 7.90\times10^{-6}T^2$ $(R^2 = 0.9769)$

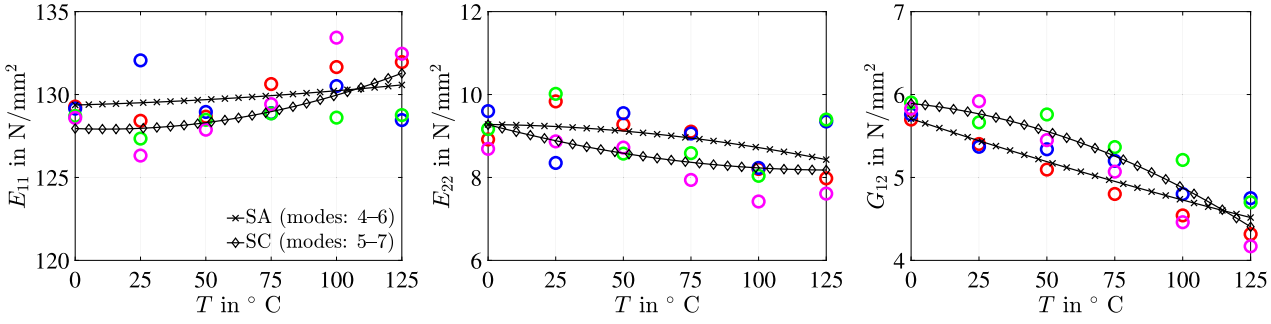

(d) Considered modes: 4–6 and 5–7
$E_{11,\mathrm{SA}} = 129.37 + 4.24\times10^{-3}T - 4.35\times10^{-5}T^2$
$E_{11,\mathrm{SC}} = 127.95 - 6.03\times10^{-3}T + 2.62\times10^{-4}T^2$

(e) Considered modes: $4-6$ and 5–7
$E_{22,\mathrm{SA}} = 9.28 - 7.57\times10^{-4}T - 4.81\times10^{-5}T^2$
$E_{22,\mathrm{SC}} = 9.27 - 1.71\times10^{-2}T + 6.70\times10^{-5}T^2$

(f) Considered modes: $4-6$ and 5–7
$G_{12,\mathrm{SA}} = 5.71 - 1.09\times10^{-2}T + 1.10\times10^{-5}T^2$ $(R^2 = 0.8848)$
$G_{12,\mathrm{SC}} = 5.89 - 3.29\times10^{-3}T - 6.89\times10^{-5}T^2$ $(R^2 = 0.8513)$

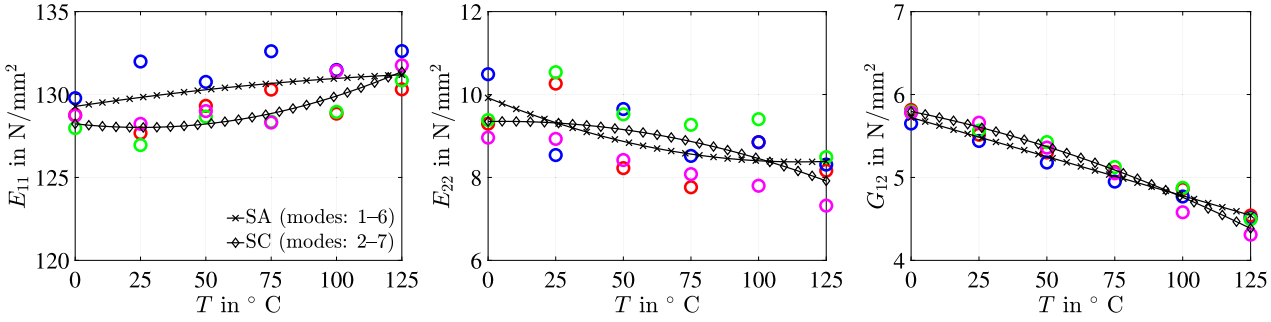

(g) Considered modes: 1–6 and 2–7
$E_{11,\mathrm{SA}} = 129.28 + 2.33\times10^{-2}T - 6.43\times10^{-5}T^2$
$E_{11,\mathrm{SC}} = 128.23 - 1.70\times10^{-2}T + 3.38\times10^{-4}T^2$

(h) Considered modes: 1–6 and 2–7
$E_{22,\mathrm{SA}} = 9.92 - 2.68\times10^{-2}T - 1.17\times10^{-4}T^2$
$E_{22,\mathrm{SC}} = 9.35 + 1.17\times10^{-3}T - 1.01\times10^{-4}T^2$

(i) Considered modes: 1–6 and 2–7
$G_{12,\mathrm{SA}} = 5.72 - 9.43\times10^{-3}T - 1.95\times10^{-9}T^2$ $(R^2 = 0.9806)$
$G_{12,\mathrm{SC}} = 5.80 - 6.60\times10^{-3}T - 3.75\times10^{-5}T^2$ $(R^2 = 0.9744)$

Fig. 9. Variation in the identified elastic parameters (E_{11}, E_{22}, and G_{12}) for the plates SA2 ( ), SA10 ( ), SC5 ( ), and SC6 ( ) at different temperatures.

laminates. In the case of the symmetric cross-ply laminate, fibers are oriented along the x- and y-axes depending upon the lamina sequences, moreover, elastic properties of fibers are not influenced by the temperature. Hence, the identified E_{xx} for symmetric cross-ply laminates does not vary with the change in temperature. On the other hand, for the symmetric angle-ply laminate, fibers are not oriented along the x- or y-axis. Thus, the identified E_{xx} degrades with increasing temperature and is influenced by the temperature-dependent matrix behavior. The flat fitted curves for the identified E_{yy}, as shown in Fig. 10(b), indicate the temperature independency of the identified E_{yy} for both laminates. Fig. 10(c) shows that the identified G_{xy} decreases with increasing temperature for both types of laminates. Moreover, the identified G_{xy} exhibits a strong correlation with temperature because R^2 values for the fitted curves are greater than 0.98. It is worthy to mention here that a strong temperature dependency is also observed for the shear

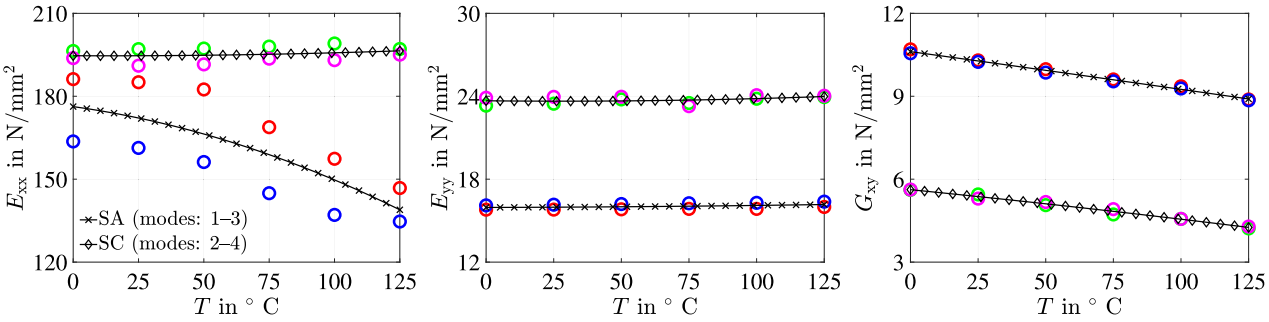

(a) Considered modes: 1–3 and 2–4
$E_{xx,SA} = 176.26 - 1.31 \times 10^{-1} T - 1.34 \times 10^{-3} T^2$
$E_{xx,SC} = 194.66 - 3.76 \times 10^{-3} T + 1.44 \times 10^{-4} T^2$

(b) Considered modes: 1–3 and 2–4
$E_{yy,SA} = 15.95 + 4.80 \times 10^{-4} T + 9.78 \times 10^{-6} T^2$
$E_{yy,SC} = 23.67 - 2.02 \times 10^{-2} T + 3.59 \times 10^{-5} T^2$

(c) Considered modes: 1–3 and 2–4
$G_{xy,SA} = 10.61 - 1.34 \times 10^{-2} T - 2.29 \times 10^{-6} T^2$ $(R^2 = 0.9906)$
$G_{xy,SC} = 5.62 - 9.74 \times 10^{-3} T - 9.44 \times 10^{-6} T^2$ $(R^2 = 0.9851)$

Fig. 10. Variation in the identified homogenized elastic parameters (E_{xx}, E_{yy}, and G_{xy}) for the plates SA2 ( ), SA10 ( ), SC5 ( ), and SC6 ( ) at different temperatures.

modulus (G_{12}) of the carbon–epoxy lamina. Similarly to G_{12}, G_{xy} is a matrix-dominated property of a laminate, thus it degrades with increasing temperature.

In this study, three sets of modal contribution have been considered for the identification of the elastic parameters. The damped eigenfrequencies of these plates are calculated using the identified elastic parameters at each temperature. The corresponding numerical error, $\epsilon_{m,nT}$, for the m^{th} frequency at the temperature T is determined as

$$\epsilon_{m,nT} = \left| \frac{f^{exp}_{m,nT} - f^{num}_{dm,nT}}{f^{exp}_{m,nT}} \right|, \tag{24}$$

where $nT = 1$ for a specific temperature T. Average numerical error, $\epsilon_{m,avg}$, for the m^{th} frequency for the six temperature states is calculated as

$$\epsilon_{m,avg} = \sum_{nT=1}^{6} \epsilon_{m,nT}, \quad nT = 1, 2, \ldots, 6 \tag{25}$$

and shown in Fig. 11 for the plates SA2, SA10, SC5, and SC6. A general observation is derived from Figs. 11(a) and 11(b). It is that $\epsilon_{m,avg}$ is less for the modes 1, 2, and 3 than for the modes 4, 5, and 6, when modes 1–3 are adopted during identification for the plates SA2 and SA10. Similarly, the $\epsilon_{m,avg}$ for the modes 4, 5, and 6 is lower than for the modes 1, 2, and 3, when the modes considered for the identification are 4–6. It is correspondingly observed for the plate SC5 that the modes which are considered for the identification impart the low magnitude of $\epsilon_{m,avg}$. However, this behavior has not been followed for the plate SC6 (cf., Fig. 11(d)), which appears to have arisen due to existing manufacturing-related uncertainty in the plate. Moreover, when all the six modes are used for material properties identification, the corresponding $\epsilon_{m,avg}$ are distributed over all these modes in an average sense.

This outcome is important for a number of reasons, which are highlighted here in a more detailed fashion. When conducting numerical simulations, knowledge of the correct material properties is crucial. In most cases, these parameters are measured quasi-statically by a suitable DMA for different temperatures. However, it could be argued that such a parameter set is only valid for low frequency analysis because the corresponding material property measurements have been conducted in a low frequency regime. This behavior would be in accordance with the widely known phenomena that when conducting a numerical modal analysis and a corresponding experimental modal analysis, the errors between the modal frequencies are for instance small for low mode numbers and increase for higher modes. From the presented results it can be concluded that when using a mode set of higher mode numbers for the material parameter estimation, the errors between experiment and simulation for the used set of higher modes is smaller and for other modes, i.e., lower modes and even higher modes, the errors increase again. Ultimately, the simulation engineers must be provided with a set of material parameters that are determined from measurements that are similar to the final operating conditions in which the final product will operate. A direct consequence is that in order to improve the simulation quality within the framework of numerical modal analysis, we need measurements of similar prototypes acquired under similar operating conditions in order to determine material properties that capture the dynamic behavior correctly. Here, the choice of a suitable material model is crucial.

4.3. Identified temperature-dependent damping properties

Based on the experimental modal loss factors of all the considered plates the damping loss factors (η_{11}, η_{22}, and η_{12}) of the carbon–epoxy lamina are determined, and plotted in Fig. 12. Three different sets of modal contribution, stated in Section 4.2, are used during identification. For further reference, the numerical values of the identified damping parameters are furnished in Appendix B (cf., Table 3). As the experimentally extracted modal loss factors of the composite plates vary non-linearly, the identified damping

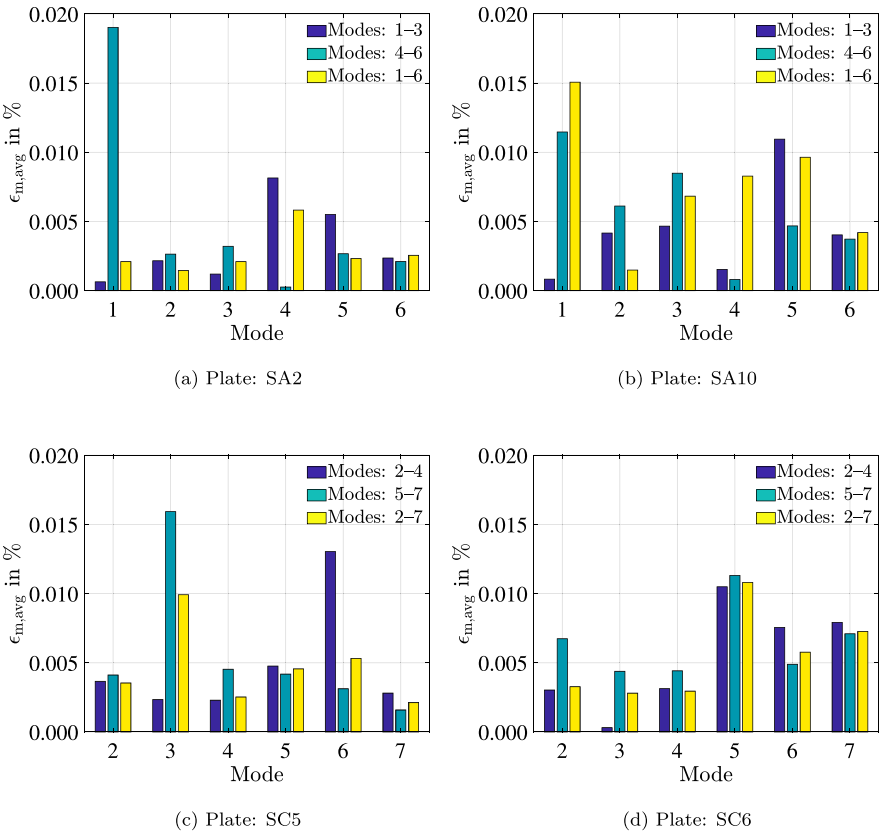

Fig. 11. Average numerical error ($\epsilon_{m,avg}$) between experimental and simulated eigenfrequencies for the plates SA2, SA10, SC5, and SC6 considering different modal contributions.

parameters also vary non-linearly in temperature scale. The counter-intuitive variation in the identified loss factors with temperature is most likely due to the existence of an inherent uncertainty in the extracted modal damping values. To restrict error related to uncertainty within the identified damping parameters, a two-stage identification algorithm is introduced in this deterministic inverse method. Several trials with different optimization techniques were carried out before selecting the two-stage optimization strategy. Instead of considering a deterministic identification methodology, adaptation of stochastic identification procedure for evaluating underlying uncertainty in the damping parameters is suggested. The stochastic identification of the temperature-dependent elastic and damping parameters is subject of future scope of research.

5. Conclusion

The present investigation addresses the experimental estimation of the temperature-dependent modal response and material properties of laminated composite plates and comprehends two main contributions: firstly, implementing a test program by proposing an experimental protocol and then extracting the modal responses, and secondly, deterministic identification of the temperature-dependent material properties of the composite lamina based on the experimental modal data.

The dynamic behavior of the carbon–epoxy symmetric cross-ply and angle-ply laminates has been investigated, experimentally and numerically in varying thermal environments. An efficient experimental strategy was proposed to conduct the modal analysis of composite plates inside the thermal chamber. The experiments had adopted the non-contact based excitation and measurement strategies, which are most worthwhile to implement inside the enclosed environmental chamber. The temperature-dependent eigenfrequencies and modal loss factors of these laminates are estimated by conducting the operational modal analysis (OMA), which is an output-only modal identification technique. The eigenfrequencies estimated from the OMA at different temperatures correlate well, thus, indicating the adopted time-domain modal identification technique is both user-friendly and robust for eigenfrequency identification. The reduction of the identified eigenfrequencies for some specific modes reveals degradation in the matrix-based stiffness properties with increasing temperature. However, due to the existence of an inherent uncertainty in the test samples, it is difficult to propose a distinctive temperature-dependent damping behavior from the experimental modal loss factors. Furthermore, the low-valued modal loss factors are more sensitive than the eigenfrequencies, and require higher precision within the identification algorithm.

The temperature-dependent elastic and damping properties of the composite lamina are identified by implementing an inverse method. The experimental program has been carried out on symmetric cross-ply and symmetric angle-ply laminates to ensure

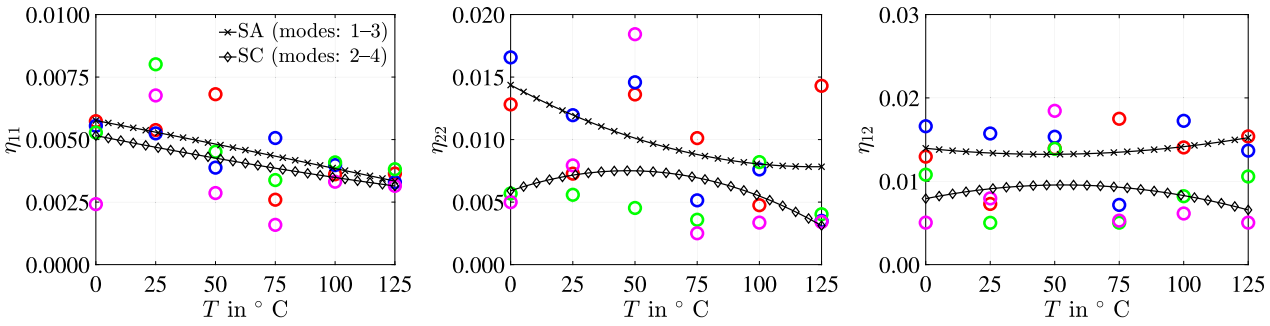

(a) Considered modes: 1–3 and 2–4
$\eta_{11,\mathrm{SA}} = 5.76\times10^{-3} - 1.84\times10^{-5}T - 7.48\times10^{-9}T^2$
$\eta_{11,\mathrm{SC}} = 5.16\times10^{-3} - 1.93\times10^{-5}T - 2.51\times10^{-8}T^2$

(b) Considered modes: 1–3 and 2–4
$\eta_{22,\mathrm{SA}} = 1.44\times10^{-2} - 1.07\times10^{-4}T + 4.36\times10^{-7}T^2$
$\eta_{22,\mathrm{SC}} = 5.91\times10^{-3} + 6.82\times10^{-5}T - 7.24\times10^{-7}T^2$

(c) Considered modes: 1–3 and 2–4
$\eta_{12,\mathrm{SA}} = 1.40\times10^{-2} - 3.08\times10^{-5}T - 3.28\times10^{-7}T^2$
$\eta_{12,\mathrm{SC}} = 7.91\times10^{-3} + 6.19\times10^{-5}T - 5.28\times10^{-7}T^2$

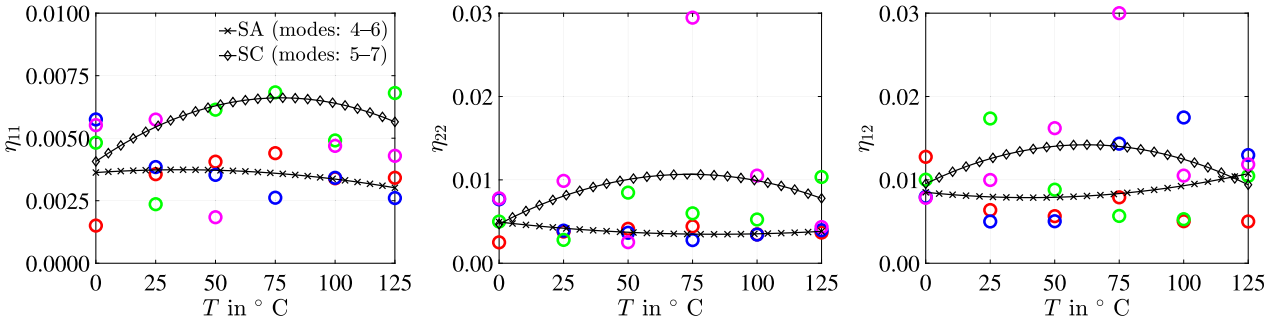

(d) Considered modes: $4-6$ and 5–7
$\eta_{11,\mathrm{SA}} = 3.63\times10^{-3} + 6.36\times10^{-6}T - 8.98\times10^{-8}T^2$
$\eta_{11,\mathrm{SC}} = 4.07\times10^{-3} + 6.58\times10^{-5}T - 4.25\times10^{-7}T^2$

(e) Considered modes: $4-6$ and 5–7
$\eta_{22,\mathrm{SA}} = 4.94\times10^{-3} - 3.49\times10^{-5}T + 2.08\times10^{-7}T^2$
$\eta_{22,\mathrm{SC}} = 4.70\times10^{-3} + 1.62\times10^{-4}T - 1.10\times10^{-6}T^2$

(f) Considered modes: $4-6$ and 5–7
$\eta_{12,\mathrm{SA}} = 8.51\times10^{-3} - 3.19\times10^{-5}T + 3.98\times10^{-7}T^2$
$\eta_{12,\mathrm{SC}} = 9.54\times10^{-3} + 1.51\times10^{-4}T - 1.21\times10^{-6}T^2$

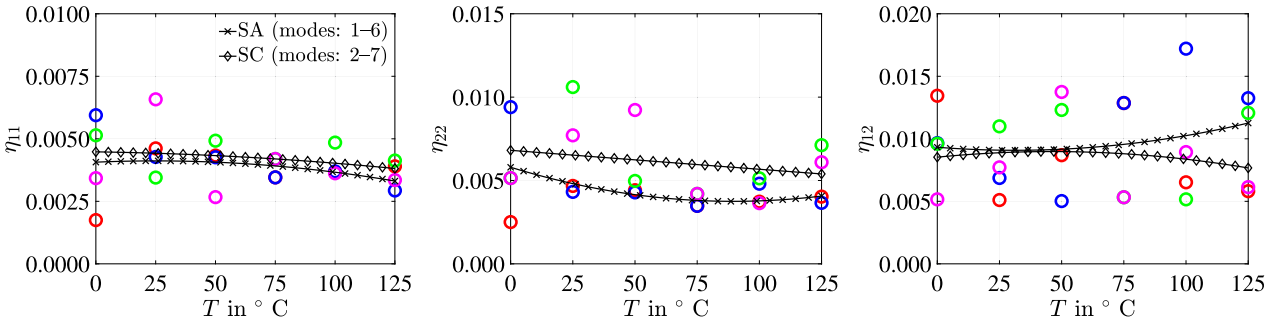

(g) Considered modes: 1–6 and 2–7
$\eta_{11,\mathrm{SA}} = 4.07\times10^{-3} + 4.04\times10^{-6}T - 8.07\times10^{-8}T^2$
$\eta_{11,\mathrm{SC}} = 4.48\times10^{-3} - 1.45\times10^{-6}T - 3.10\times10^{-8}T^2$

(h) Considered modes: 1–6 and 2–7
$\eta_{22,\mathrm{SA}} = 5.79\times10^{-3} - 4.56\times10^{-5}T + 2.54\times10^{-7}T^2$
$\eta_{22,\mathrm{SC}} = 6.81\times10^{-3} - 1.15\times10^{-5}T + 1.50\times10^{-9}T^2$

(i) Considered modes: 1–6 and 2–7
$\eta_{12,\mathrm{SA}} = 9.32\times10^{-3} - 1.55\times10^{-5}T + 2.48\times10^{-7}T^2$
$\eta_{12,\mathrm{SC}} = 8.53\times10^{-3} + 1.95\times10^{-5}T - 2.11\times10^{-7}T^2$

Fig. 12. Variation in the identified damping parameters (η_{11}, η_{22}, and η_{12}) for the plates SA2 ( ), SA10 ( ), SC5 ( ), and SC6 ( ) at different temperatures.

reliability in the extracted modal parameters and the identified material parameters. The identified shear modulus of the lamina exhibits a strong temperature dependency which decreases with increasing temperature. The identified damping parameters did not indicate a temperature-dependent pattern due to existence of an inherent uncertainty in the material properties. Furthermore, during identification of the material properties, consideration of the modal combination under which the structure's operating frequency exists is recommended. The implementation of the stochastic identification technique will represent the uncertainty in the evaluated temperature-dependent elastic and damping parameters, and has been identified as future scope of the study.

CRediT authorship contribution statement

S. Chandra: Conceptualization, Methodology, Conducting experiment, Programming, Software, Validation, Investigation, Result analysis, Data curation, Writing – original draft, Visualization, Writing – review & editing, Project administration. **M. Maeder:** Conceptualization, Methodology, Conducting experiment, Programming, Software, Validation, Investigation, Result analysis, Data curation, Writing – original draft, Writing – review & editing, Project administration. **J. Bienert:** Methodology, Programming, Software, Writing – review & editing. **H. Beinersdorf:** Conducting experiment, Writing – review & editing. **W. Jiang:** Methodology, Writing – review & editing. **V.A. Matsagar:** Conceptualization, Result analysis, Writing - review & editing, Supervision. **S. Marburg:** Resource, Result analysis, Writing – review & editing, Supervision.

Declaration of competing interest

The authors declare that they have no known competing financial interests or personal relationships that could have appeared to influence the work reported in this paper.

Data availability

Data will be made available on request.

Acknowledgments

The financial support extended by the Deutscher Akademischer Austauschdienst (DAAD), Germany under Research Grants - Doctoral Program in Germany, and the Alexander von Humboldt Foundation, Germany under Fellowship for Experienced Researcher to the first author and sixth author is greatly acknowledged.

Appendix A

Transformed reduced stiffness matrix of the k^{th} lamina in laminate coordinate (x, y, z) system:

$$\boldsymbol{Q}_{\text{k}} = \begin{bmatrix} Q_{11} & Q_{12} & Q_{16} & 0 & 0 \\ Q_{21} = Q_{12} & Q_{22} & Q_{26} & 0 & 0 \\ Q_{61} = Q_{16} & Q_{62} = Q_{26} & Q_{66} & 0 & 0 \\ 0 & 0 & 0 & Q_{44} & Q_{45} \\ 0 & 0 & 0 & Q_{54} = Q_{45} & Q_{55} \end{bmatrix}_{\text{k}}. \tag{A.1}$$

Stress–strain relationship matrix of the k^{th} lamina in lamina coordinate (1, 2, 3) system:

$$\boldsymbol{C}_{\text{k}} = \begin{bmatrix} C_{11} = \frac{E_{11}}{1-\nu_{12}\nu_{21}} & C_{12} = \frac{\nu_{12}E_{11}}{1-\nu_{12}\nu_{21}} & 0 & 0 & 0 \\ C_{21} = \frac{\nu_{12}E_{11}}{1-\nu_{12}\nu_{21}} & C_{22} = \frac{E_{22}}{1-\nu_{12}\nu_{21}} & 0 & 0 & 0 \\ 0 & 0 & C_{66} = G_{12} & 0 & 0 \\ 0 & 0 & 0 & C_{44} = G_{13} & 0 \\ 0 & 0 & 0 & 0 & C_{55} = G_{23} \end{bmatrix}_{\text{k}}. \tag{A.2}$$

Elemental stiffness matrix:

$$\boldsymbol{K}_{\mathbf{e}} = \int_{\text{A}_{\text{e}}} \boldsymbol{B}^{\text{T}} \boldsymbol{D}\, \boldsymbol{B} \text{d}A_{\text{e}}, \tag{A.3}$$

where $\boldsymbol{B}$ is the strain–displacement matrix [36].

Elemental geometric stiffness matrix:

$$\boldsymbol{K}_{\mathbf{Ge}} = \int_{\text{A}_{\text{e}}} \boldsymbol{G}^{\text{T}} \boldsymbol{S}_{\mathbf{r}} \boldsymbol{G} \text{d}A_{\text{e}}, \tag{A.4}$$

where $\boldsymbol{G}$ is the shape function matrix corresponding to the partial derivative of the displacement vector, $\boldsymbol{d}^*$, as

$$\boldsymbol{G} = \sum_{i=1}^{8} \begin{bmatrix} N_{\text{i,x}} & 0 & 0 & 0 & 0 \\ N_{\text{i,y}} & 0 & 0 & 0 & 0 \\ 0 & N_{\text{i,x}} & 0 & 0 & 0 \\ 0 & N_{\text{i,y}} & 0 & 0 & 0 \\ 0 & 0 & N_{\text{i,x}} & 0 & 0 \\ 0 & 0 & N_{\text{i,y}} & 0 & 0 \\ 0 & 0 & 0 & N_{\text{i,x}} & 0 \\ 0 & 0 & 0 & N_{\text{i,y}} & 0 \\ 0 & 0 & 0 & 0 & N_{\text{i,x}} \\ 0 & 0 & 0 & 0 & N_{\text{i,y}} \\ 0 & 0 & 0 & N_{\text{i}} & 0 \\ 0 & 0 & 0 & 0 & N_{\text{i}} \end{bmatrix}, \tag{A.5}$$

Table 2
Identified temperature-dependent elastic moduli (E_{11}, E_{22}, E_{12}) of a T700 carbon–epoxy lamina considering three different sets of modal contribution for the symmetric angle-ply, samples: SA2 and SA10, $(45°/-45°)_{7s}$ laminates and symmetric cross-ply, samples: SC5 and SC6, $(0°/90°)_{7s}$ laminates.

Considered modes	Temperature in °C	SA2			SA10		
		E_{11} in GPa	E_{22} in GPa	G_{12} in GPa	E_{11} in GPa	E_{22} in GPa	G_{12} in GPa
1 to 3	0	128.97	9.47	5.83	132.29	8.84	5.66
	25	130.07	8.60	5.54	133.22	8.45	5.44
	50	130.50	8.25	5.32	132.90	9.29	5.15
	75	130.53	8.13	5.08	132.42	9.74	4.93
	100	131.34	8.02	4.86	132.62	9.14	4.77
	125	131.07	7.90	4.56	133.63	8.65	4.5
4 to 6	0	129.27	8.92	5.70	132.29	8.84	5.66
	25	128.42	9.83	5.40	132.06	8.35	5.37
	50	128.67	9.28	5.10	128.95	9.55	5.34
	75	130.63	9.10	4.80	128.88	9.06	5.2
	100	131.66	8.20	4.54	130.51	8.23	4.8
	125	131.96	7.98	4.32	128.46	9.35	4.75
1 to 6	0	128.77	9.30	5.81	129.78	10.49	5.65
	25	127.67	10.26	5.52	131.99	8.54	5.44
	50	129.32	8.22	5.30	130.76	9.65	5.18
	75	130.30	7.76	5.07	132.61	8.52	4.95
	100	128.85	8.85	4.86	131.48	8.85	4.77
	125	130.31	8.16	4.54	132.62	8.31	4.51
		SC5			SC6		
2 to 4	0	126.34	10.53	5.60	129.08	8.98	5.78
	25	127.12	10.56	5.42	127.75	9.95	5.48
	50	130.29	8.37	5.10	129.81	8.1	5.27
	75	128.37	9.36	4.80	127.21	8.8	4.92
	100	129.68	9.27	4.64	130.16	7.96	4.71
	125	131.39	7.85	4.24	131.18	7.36	4.39
5 to 7	0	128.70	9.17	5.90	128.59	8.69	5.83
	25	127.34	10.02	5.66	126.32	8.87	5.92
	50	128.48	8.58	5.76	127.88	8.72	5.45
	75	128.86	8.59	5.37	129.42	7.94	5.07
	100	128.61	8.04	5.21	133.43	7.42	4.46
	125	128.76	9.40	4.70	132.46	7.61	4.17
2 to 7	0	127.98	9.38	5.79	128.73	8.96	5.78
	25	126.95	10.54	5.56	128.23	8.93	5.66
	50	128.67	9.52	5.43	129.00	8.42	5.36
	75	128.36	9.27	5.13	128.31	8.08	5.05
	100	128.95	9.40	4.87	131.43	7.80	4.58
	125	130.85	8.49	4.50	131.76	7.32	4.31

in which shape function for the 8-node isoparametric element is shown by N_{i} with $i = 1$ to 8, and $\boldsymbol{S}_{\mathbf{r}}$ is the resultant matrix obtained by integrating thermal residual stress [37] of individual lamina.

Elemental mass matrix:

$$\boldsymbol{M}_{\mathbf{e}} = \int_{\mathrm{A_e}} \boldsymbol{N}^{\mathrm{T}} \bar{\boldsymbol{M}} \boldsymbol{N} \mathrm{d}A_{\mathrm{e}}. \tag{A.6}$$

where, $\boldsymbol{N} = \sum_{i=1}^{8} N_{\mathrm{i}} \boldsymbol{I_5}$, $\boldsymbol{I_5}$ is a 5×5 identity matrix, and $\bar{\boldsymbol{M}}$ is the inertia matrix of the laminated composite plate which is shown as

$$\bar{\boldsymbol{M}} = \begin{bmatrix} \bar{p} & 0 & 0 & 0 & 0 \\ 0 & \bar{p} & 0 & 0 & 0 \\ 0 & 0 & \bar{p} & 0 & 0 \\ 0 & 0 & 0 & \bar{q} & 0 \\ 0 & 0 & 0 & 0 & \bar{q} \end{bmatrix}, \tag{A.7}$$

in which $(\bar{p}, \bar{q}) = \int_{-h/2}^{h/2} \rho(1, z^2) \mathrm{d}z$, and density of the plate is denoted by ρ.

Appendix B

See Tables 2 and 3.

Table 3
Identified temperature-dependent damping parameters (η_{11}, η_{22}, η_{12}) of a T700 carbon–epoxy lamina considering three different sets of modal contribution for the symmetric angle-ply, samples: SA2 and SA10, $(45°/-45°)_{7s}$ laminates and symmetric cross-ply, samples: SC5 and SC6, $(0°/90°)_{7s}$ laminates.

Considered modes	Temperature in °C	SA2			SA10		
		η_{11}	η_{22}	η_{12}	η_{11}	η_{22}	η_{12}
1 to 3	0	0.005736	0.012813	0.012955	0.005551	0.016573	0.0166
	25	0.005379	0.007276	0.007281	0.005248	0.011951	0.01573
	50	0.006814	0.01361	0.013949	0.003878	0.014583	0.015339
	75	0.002596	0.010118	0.017496	0.005063	0.005141	0.007163
	100	0.003613	0.004752	0.014058	0.003979	0.007613	0.01725
	125	0.00364	0.014302	0.015384	0.003293	0.003499	0.013675
4 to 6	0	0.001505	0.002506	0.012766	0.00575	0.00767	0.007958
	25	0.003561	0.003797	0.00638	0.003846	0.003909	0.005007
	50	0.004061	0.004131	0.005647	0.003534	0.003654	0.005037
	75	0.004401	0.004427	0.007906	0.00262	0.002776	0.014343
	100	0.003396	0.003462	0.005043	0.003415	0.003437	0.017486
	125	0.003417	0.003682	0.005007	0.002607	0.003959	0.012974
1 to 6	0	0.001749	0.002506	0.013443	0.005944	0.0094	0.009656
	25	0.004617	0.004673	0.005104	0.004274	0.004317	0.006868
	50	0.004329	0.004417	0.008688	0.004261	0.004286	0.005021
	75	0.003457	0.00348	0.012862	0.004229	0.004263	0.007845
	100	0.003667	0.003729	0.006521	0.003696	0.004808	0.017209
	125	0.003899	0.004032	0.005811	0.002933	0.003658	0.013249
		SC5			SC6		
2 to 4	0	0.005282	0.005689	0.01079	0.002419	0.004996	0.005037
	25	0.008011	0.005586	0.005017	0.006765	0.007934	0.007943
	50	0.004514	0.004531	0.013893	0.002862	0.018428	0.01845
	75	0.003382	0.003588	0.005033	0.00159	0.002506	0.005277
	100	0.004088	0.008199	0.008207	0.003315	0.00336	0.006134
	125	0.003815	0.00403	0.010572	0.00315	0.00341	0.005037
5 to 7	0	0.004819	0.004998	0.010023	0.005522	0.007781	0.007847
	25	0.002361	0.002802	0.017365	0.005745	0.009879	0.009987
	50	0.00614	0.008473	0.008825	0.00184	0.002527	0.016202
	75	0.006833	0.005987	0.005674	0.014998	0.029461	0.03
	100	0.00491	0.005247	0.005281	0.004693	0.01051	0.010511
	125	0.006806	0.010347	0.010475	0.004295	0.004339	0.011853
2 to 7	0	0.005141	0.005151	0.009609	0.003427	0.005144	0.005159
	25	0.00345	0.010604	0.010996	0.006579	0.007708	0.007718
	50	0.004925	0.004973	0.012306	0.002668	0.009228	0.013747
	75	0.004193	0.004195	0.005326	0.00159	0.002506	0.005277
	100	0.004848	0.005129	0.005159	0.003622	0.003641	0.008939
	125	0.004131	0.007119	0.012069	0.003351	0.006095	0.006136

Appendix C

Fig. 13 shows the mode shapes of the sample plate SA2, derived using identified elastic parameters at 25 °C temperature, considering the modal contribution 1–3. In the symmetric angle-ply laminates, the bending modes, i.e., 1st, 3rd, 4th, and 6th experimental eigenfrequencies decrease with the increment of temperature. In this laminate, fibers are oriented diagonally, therefore the bending modes are influenced by the degradation in the matrix-dominated elastic properties.

Fig. 14 shows the mode shapes of the sample plate SC5, derived by using identified elastic parameters at 25 °C temperature, considering the modal contribution 2–4. In symmetric cross-ply laminates, the non-bending modes, i.e., 3rd, 5th, and 6th experimental eigenfrequencies decrease with the increment of temperature. In this laminates, fibers are oriented along the longitudinal and transverse directions, therefore the non-bending modes are influenced by the degradation in the matrix-dominated elastic properties.

Appendix D. Supplementary data

It is suggested to read this paper along with the supplementary document.

Supplementary material related to this article can be found online at https://doi.org/10.1016/j.ymssp.2022.109945.

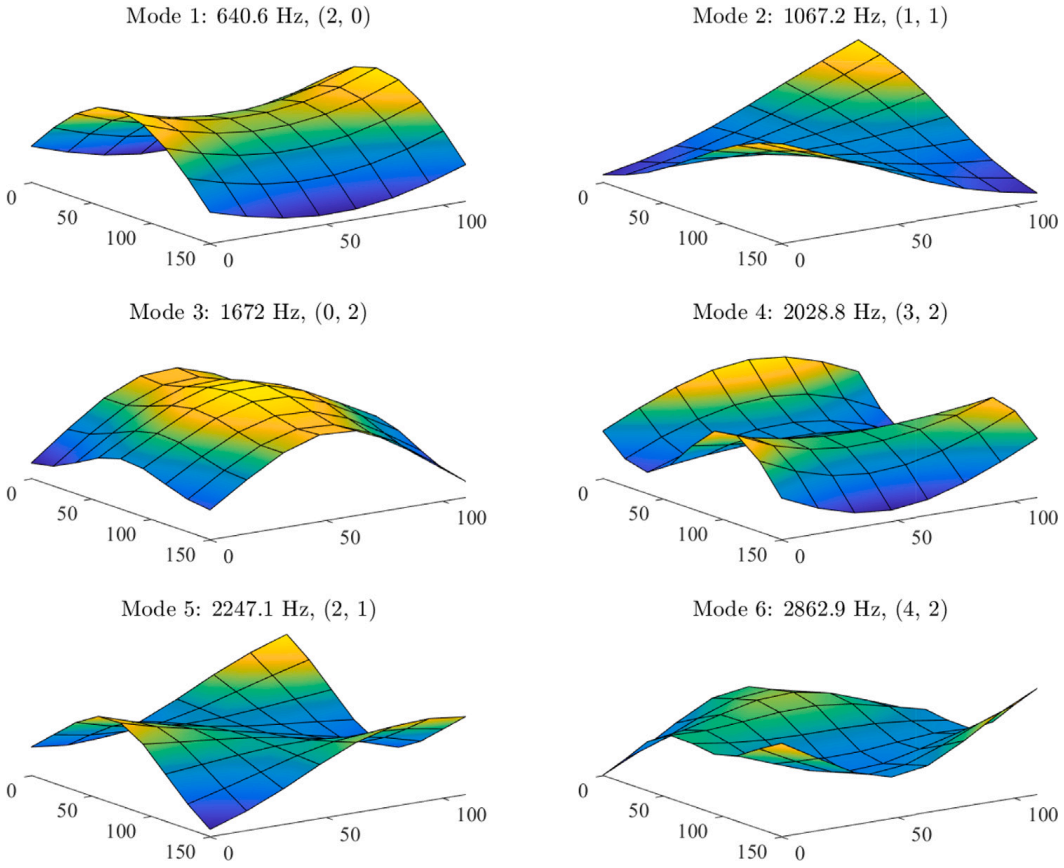

Fig. 13. Mode shapes of the sample plate SA2 using identified elastic parameters at 25 °C considering the modal contribution 1–3.

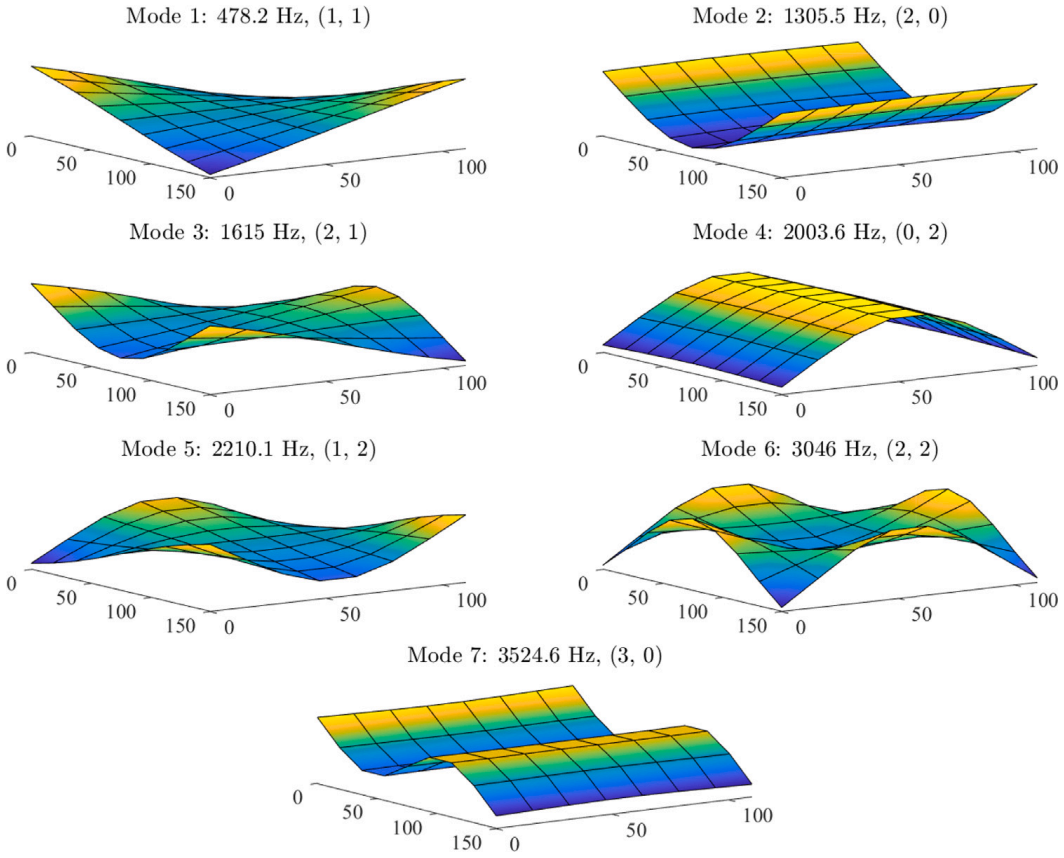

Fig. 14. Mode shapes of the sample plate SC5 using identified elastic parameters at 25 °C considering the modal contribution 2–4.

References

[1] D. Gay, Composite materials: Design and applications, third ed., CRC Press, Boca Raton, USA, 2014.
[2] D3039/D3039M, Standard test method for tensile properties of polymer matrix composite materials, Tech. rep., ASTM International, West Conshohocken, PA 19428-2959, U.S., 2017.
[3] D790-17, Standard test methods for flexural properties of unreinforced and reinforced plastics and electrical insulating materials, Tech. rep., ASTM International, West Conshohocken, PA 19428-2959, U.S., 2017.
[4] D3410/D3410M-16e1, Standard test method for compressive properties of polymer matrix composite materials with unsupported gage section by shear loading, Tech. rep., ASTM International, West Conshohocken, PA 19428-2959, U.S., 2021.
[5] D4255/D4255M, Standard test method for in-plane shear properties of polymer matrix composite materials by the rail shear method, Tech. rep., ASTM International, West Conshohocken, PA 19428-2959, U.S., 2020.
[6] D7078/D7078M-05, Standard test method for shear properties of composite materials by V-Notched rail shear method, Tech. rep., ASTM International, West Conshohocken, PA 19428-2959, U.S., 2012.
[7] V. Kodur, S. Venkatachari, V.A. Matsagar, S.B. Singh, Test methods for characterizing the properties of fiber-reinforced polymer composites at elevated temperatures, Polymers 14 (9) (2022).
[8] R. Adams, D. Bacon, Effect of fibre orientation and laminate geometry on the dynamic properties of CFRP, J. Compos. Mater. 7 (4) (1973) 402–428.
[9] R. Ni, R. Adams, The damping and dynamic moduli of symmetric laminated composite beams-theoretical and experimental results, J. Compos. Mater. 18 (2) (1984) 104–121.
[10] D.A. Saravanos, J.M. Pereira, Dynamic characteristics of specialty composite structures with embedded damping layers, J. Vib. Acoust. 117 (1) (1995) 62–69.
[11] D.A. Saravanos, C.C. Chamis, Unified micromechanics of damping for unidirectional fiber reinforced composites, Tech. rep., NASA, 1989, pp. 1–27.
[12] D. Saravanos, C. Chamis, Computational simulation of damping in composite structures, J. Reinf. Plast. Compos. 10 (3) (1991) 256–278.
[13] S.J. Hwang, R.F. Gibson, The use of strain energy-based finite element techniques in the analysis of various aspects of damping of composite materials and structures, J. Compos. Mater. 26 (17) (1992) 2585–2605.
[14] D.A. Saravanos, C.C. Chamis, Mechanics of damping for fiber composite laminates including hygro-thermal effects, AIAA J. 28 (10) (1990) 1813–1819.
[15] T. Brantseva, A. Antonov, Y.A.G.M. Kerber, Behaviour of polymer-fiber interface under various loading rates, in: Proceedings of the ICCM-12, (426) 1999.
[16] R. Gaertner, C. Gauthier, P. Franciosi, A. Khavandi, M. Shaterzadeh, Rheological and morphological influences on the viscoelastic behaviour of polymer composites, in: Proceedings of the ICCM-12, 1999.
[17] M. Tanaka, G. Dulikravich (Eds.), Inverse Problems in Engineering Mechanics, Elsevier Science Ltd, Oxford, U.K., 1998.
[18] J. Kaipio, E. Somersalo, Statistical and Computational Inverse Problems, Springer, New York, U.S.A., 2005,
[19] D. Lecompte, A. Smits, H. Sol, J. Vantomme, D. Van Hemelrijck, Mixed numerical-experimental technique for orthotropic parameter identification using biaxial tensile tests on cruciform specimens, Int. J. Solids Struct. 44 (5) (2007) 1643–1656.
[20] J. Wang, Y. Xiao, M. Kawai, Parameter identification problem in one-parameter plasticity model for fibrous composites, Adv. Compos. Mater. 28 (sup2) (2019) 29–51.
[21] Y. Mi, C. Zhu, X. Li, D. Wu, Acoustic emission study of effect of fiber weaving on properties of fiber-resin composite materials, Compos. Struct. 237 (2020) 111906.
[22] H. Sol, Identification of Anisotropic Plate Rigidities Using Free Vibration Data (Ph.D. thesis), Vrije Universiteit, Brussels, 1986.
[23] J.D. Visscher, Identification of the Complex Stiffness Matrix of Orthotropic Materials by a Mixed Numerical Experimental Method (Ph.D. thesis), Vrije Universiteit, Brussels, 1995.
[24] R.C. Aster, B. Borchers, C.H. Thurber (Eds.), Parameter Estimation and Inverse Problems, third ed., Elsevier, 2019.
[25] C. Soares, M. de Freitas, A. Araújo, P. Pedersen, Identification of material properties of composite plate specimens, Compos. Struct. 25 (1) (1993) 277–285.
[26] A. Bledzki, A. Kessler, R. Rikards, A. Chate, Determination of elastic constants of glass/epoxy unidirectional laminates by the vibration testing of plates, Compos. Sci. Technol. 59 (13) (1999) 2015–2024.
[27] R. Rikards, A. Chate, W. Steinchen, A. Kessler, A. Bledzki, Method for identification of elastic properties of laminates based on experiment design, Composites B 30 (3) (1999) 279–289.
[28] P.S. Frederiksen, Experimental procedure and results for the identification of elastic constants of thick orthotropic plates, J. Compos. Mater. 31 (4) (1997) 360–382.
[29] P.S. Frederiksen, Application of an improved model for the identification of material parameters, Mech. Compos. Mater. Struct. 4 (4) (1997) 297–316.
[30] P.S. Frederiksen, Parameter uncertainty and design of optimal experiments for the estimation of elastic constants, Int. J. Solids Struct. 35 (12) (1998) 1241–1260.
[31] T. Kant, Mallikarjuna, Non-linear dynamics of laminated plates with a higher-order theory and C^0 finite elements, Int. J. Non-Linear Mech. 26 (3) (1991) 335–343.
[32] T. Kant, C. Arora, J. Varaiya, Finite element transient analysis of composite and sandwich plates based on a refined theory and a mode superposition method, Compos. Struct. 22 (2) (1992) 109–120.
[33] J. Kommineni, T. Kant, Large deflection elastic and inelastic transient analyses of composite and sandwich plates with a refined theory, J. Reinf. Plast. Compos. 12 (11) (1993) 1150–1170.
[34] S. Kapuria, G. Achary, An efficient higher order zigzag theory for laminated plates subjected to thermal loading, Int. J. Solids Struct. 41 (16) (2004) 4661–4684.
[35] P. Dumir, J. Nath, P. Kumari, S. Kapuria, Improved efficient zigzag and third order theories for circular cylindrical shells under thermal loading, J. Thermal Stresses 31 (4) (2008) 343–367.
[36] S. Chandra, K. Sepahvand, V. Matsagar, S. Marburg, Dynamic response of stiffened laminated composite plate in thermal environment, Compos. Struct. (2022) 116049.
[37] S. Chandra, M. Maeder, K. Sepahvand, V. Matsagar, S. Marburg, Damping analysis of stiffened laminated composite plates in thermal environment, Compos. Struct. (2022) 116163.
[38] B.-G. Hu, M. Dokainish, Damped vibration of laminated composite plates-modeling and finite element analysis, Finite Elem. Anal. Des. 15 (2) (1993) 103–124.
[39] R.J. Mustafa, Temperature dependence of dynamic modulus and damping in continuous fiber-reinforced Al-(alloy) matrix composites at elevated temperatures, Jordan J. Mech. Ind. Eng. 2 (1) (2008) 15–21.
[40] Y. Sefrani, J.-M. Berthelot, Temperature effect on the damping properties of unidirectional glass fibre composites, Composites B 37 (4) (2006) 346–355.
[41] M. Klaerner, M. Wuehrl, L. Kroll, S. Marburg, Modelling and FEA-simulation of the anisotropic damping of thermoplastic composites, Adv. Airc. Spacecr. Sci. 3 (3) (2016) 331–349.
[42] S. Chandra, K. Sepahvand, V. Matsagar, S. Marburg, Stochastic modal damping analysis of stiffened laminated composite plate, in: S.K. Saha, M. Mukherjee (Eds.), Recent Advances in Computational Mechanics and Simulations, Springer Singapore, Singapore, 2021, pp. 635–650.

[43] O. Täger, M. Dannemann, W.A. Hufenbach, Analytical study of the structural-dynamics and sound radiation of anisotropic multilayered fibre-reinforced composites, J. Sound Vib. 342 (2015) 57–74.
[44] H. Sol, J.D. Visscher, W. Wild, Identification of the viscoelastic material properties of orthotropic plates using a mixed numerical/experimental technique, WIT Trans. Model. Simul. 5 (1993) 131–142.
[45] H. Sol, H. Rahier, J. Gu, Prediction and measurement of the damping ratios of laminated polymer composite plates, Materials 13 (15) (2020) 3370.
[46] J. De Visscher, H. Sol, W.P. De Wilde, J. Vantomme, Identification of the damping properties of orthotropic composite materials using a mixed numerical experimental method, Appl. Compos. Mater. 4 (1997) 13–33.
[47] J. De Visscher, H. Sol, W.P. De Wilde, J. Vantomme, Identification of the complex moduli of thin fibre reinforced polymer plates using measured modal parameters, in: Proceedings of the EUROMECH Colloquium Held in Kerkrade, the Netherlands, 7-9 April 1997, Kluwer Academic Publishers, 1997, pp. 1–10.
[48] M. Klaerner, M. Wuehrl, L. Kroll, S. Marburg, Metal-plastic composites with amplitude-dependent constraint layer damping, Proc. Inst. Mech. Eng. C 233 (18) (2019) 6425–6435.
[49] M. Klaerner, M. Wuehrl, L. Kroll, S. Marburg, Amplitude-dependent damping: Experimental determination and functional interpretation for metal-plastic composites, Int. J. Struct. Stab. Dyn. 19 (5) (2019) 1941001.
[50] H. Li, Y. Niu, C. Mu, B. Wen, Identification of loss factor of fiber-reinforced composite based on complex modulus method, Shock Vib. 2017 (2017) 6395739.
[51] K. Sepahvand, Stochastic finite element method for random harmonic analysis of composite plates with uncertain modal damping parameters, J. Sound Vib. 400 (2017) 1–12.
[52] K.K. Sepahvand, S. Marburg, Identification of composite uncertain material parameters from experimental modal data, Probab. Eng. Mech. 37 (2014) 148–153.
[53] S. Chandra, K. Sepahvand, C. Geweth, F. Saati, S. Marburg, Stochastic non-parametric identification in composite structures using experimental modal data, in: Proceedings of the 3rd International Conference on Uncertainty Quantification in Computational Sciences and Engineering (UNCECOMP 2019), Institute of Structural Analysis and Antiseismic Research School of Civil Engineering National Technical University of Athens (NTUA) Greece, 2019.
[54] S. Chandra, K. Sepahvand, C.A. Geweth, F. Saati, S. Marburg, Bayesian inference to damping identification of fiber-reinforced composites from experimental modal data, in: M. Ochmann (Ed.), Proceedings of the 23rd International Congress on Acoustics, Integrating 4th EAA Euroregio, DEGA, 2019.
[55] S. Chandra, K. Sepahvand, V. Matsagar, S. Marburg, Stochastic dynamic analysis of composite plate with random temperature increment, Compos. Struct. 226 (2019) 111159.
[56] J.D.D. Melo, D.W. Radford, Viscoelastic characterization of transversely isotropic composite laminae, J. Compos. Mater. 37 (2) (2003) 129–145.
[57] J.D.D. Melo, D.W. Radford, Time and temperature dependence of the viscoelastic properties of CFRP by dynamic mechanical analysis, Compos. Struct. 70 (2) (2005) 240–253.
[58] P.S. Frederiksen, Identification of temperature dependence for orthotropic material moduli, Mech. Mater. 13 (1) (1992) 79–90.
[59] P. Pedersen, P.S. Frederiksen, Identification of orthotropic material moduli by a combined experimental/numerical method, Measurement 10 (3) (1992) 113–118.
[60] H. Li, H. Wu, T. Zhang, B. Wen, Z. Guan, A nonlinear dynamic model of fiber-reinforced composite thin plate with temperature dependence in thermal environment, Composites B 162 (2019) 206–218.
[61] H. Li, T. Wu, Z. Gao, X. Wang, H. Ma, Q. Han, Z. Qin, An iterative method for identification of temperature and amplitude dependent material parameters of fiber-reinforced polymer composites, Int. J. Mech. Sci. 184 (2020) 105818.
[62] M. Maeder, S. Chandra, S. Marburg, Identification of temperature dependent material properties in composite plates utilizing experimental vibration data, in: H. Altenbach, M. Beitelschmidt, M. Kästner, K. Naumenko, T. Wallmersperger (Eds.), Material Modeling and Structural Mechanics, Springer International Publishing, Cham, 2022, pp. 115–134.
[63] C. Geweth, S. Baydoun, F. Saati, K. Sepahvand, S. Marburg, Effect of boundary conditions in the experimental determination of structural damping, Mech. Syst. Signal Process. 146 (2021) 107052.
[64] E. Orlowitz, A. Brandt, Comparison of experimental and operational modal analysis on a laboratory test plate, Measurement 102 (2017) 121–130.
[65] S. Das, A. Guha Niyogi, Free-vibration analysis of epoxy-based cross-ply laminated composite folded plates subjected to hygro-thermal loading, J. the Institution of Engineers (India): Series C 101 (3) (2020) 541–557.
[66] K.S. Ram, P. Sinha, Hygrothermal effects on the free vibration of laminated composite plates, J. Sound Vib. 158 (1) (1992) 133–148.
[67] R. Brincker, C.E. Ventura, Introduction To Operational Modal Analysis, John Wiley & Sons, Ltd, 2015.
[68] P. van Overschee, B.D. Moor, Subspace Identification for Linear Systems, Springer US, 1996.
[69] M. Aoki, State space modeling of time series, Springer Berlin Heidelberg, 1990.
[70] L. Ljung, System Identification - Theory for the User, Prentice Hall PTR, New Jersey, 1999.
[71] B. Sevim, A. Bayraktar, A.C. Altunişik, S. Adanur, M. Akköse, Modal parameter identification of a prototype arch dam using enhanced frequency domain decomposition and stochastic subspace identification techniques, J. Test. Eval. 38 (5) (2010) 1.
[72] M.D.A. Hasan, Z.A.B. Ahmad, M.S. Leong, L.M. Hee, Enhanced frequency domain decomposition algorithm: a review of a recent development for unbiased damping ratio estimates, J. Vibroengineering 20 (5) (2018) 1919–1936.
[73] A.G. Bendat, Random Data - Analysis and Measurement Procedures, John Wiley & Sons, New York, 2011.
[74] F. Magalhães, Á. Cunha, E. Caetano, R. Brincker, Damping estimation using free decays and ambient vibration tests, Mech. Syst. Signal Process. 24 (5) (2010) 1274–1290, Special Issue: Operational Modal Analysis.
[75] C. Tsai, I. Daniel, Determination of in-plane and out-of-plane shear moduli of composite materials, Exp. Mech. 30 (3) (1990) 295–299.
[76] M. Knight, Three-dimensional elastic moduli of graphite/epoxy composites, J. Compos. Mater. 16 (2) (1982) 153–159.
[77] J. Reddy, Mechanics of Laminated Composite Plates and Shells: Theory and Analysis, second ed., CRC Press, London, UK, 2001, pp. 109–112.
[78] TheMathWorks, Genetic algorithm and direct search toolbox: For use with MATLAB, 2004.
[79] M. Ozbek, D.J. Rixen, A new analysis methodology for estimating the eigenfrequencies of systems with high modal damping, J. Sound Vib. 361 (2016) 290–306.
[80] D.F. Giraldo, W. Song, S.J. Dyke, J.M. Caicedo, Modal identification through ambient vibration: Comparative study, J. Eng. Mech. 135 (8) (2009) 759–770.

Publication 4

Reference: S. Chandra, K. Sepahvand, V.A. Matsagar, S. Marburg, Stochastic dynamic analysis of composite plate with random temperature increment. *Composite Structures*, 226, 111159, 2019.

Composite Structures 226 (2019) 111159

Contents lists available at ScienceDirect

Composite Structures

journal homepage: www.elsevier.com/locate/compstruct

Stochastic dynamic analysis of composite plate with random temperature increment

S. Chandra[a,*], K. Sepahvand[a], V.A. Matsagar[b], S. Marburg[a]

[a] Chair of Vibroacoustics of Vehicles and Machines, Department of Mechanical Engineering, Technical University of Munich (TUM), 85748 Garching b. Munich, Germany.
[b] Department of Civil Engineering, Indian Institute of Technology (IIT) Delhi, Hauz Khas, New Delhi 110 016, India.

ARTICLE INFO

Keywords:
Stochastic finite element method (SFEM)
Graphite-epoxy composite
Random mean temperature
Generalized polynomial chaos (gPC)
Non-intrusive method.

ABSTRACT

During the service life, laminated composites may be subject to some random thermal environment. Quantification of the uncertainty in static and dynamic response of the composites under such condition is still a challenging issue. This work presents a stochastic dynamic response analysis of a graphite-epoxy composite plate using generalized polynomial chaos (gPC) expansion due to random mean temperature increment. A stochastic finite element method (SFEM) based on the first-order shear deformation theory (FSDT) is used to describe the free and forced vibration response of the graphite-epoxy composite plate under a uniform distribution of the temperature throughout the plate. Newmark's time integration scheme is used to predict the time-dependent displacement response under dynamic loading. The collocation-based non-intrusive gPC expansion method is used for stochastic dynamic analysis of the graphite-epoxy composite plate. The increment in the temperature is considered as an uncertain parameter and presented by the truncated gPC expansion. The stochastic system response of the plate is projected to the deterministic solver by using the stochastic Galerkin method. The statistical response of eigen frequencies and dynamic displacements of the composite plate at incremental random mean temperature are investigated, and are compared with the results of the Monte Carlo simulation. The numerical studies show a reduction in amplitude of the dynamic mean displacements with the increment in the time and it increases with the increment in the random mean temperature. The characteristics of loading have also significantly influenced the uncertainty in the time-dependent displacement response.

1. Introduction

Applicability of laminated composites in manufacturing important and critical components of the aircraft, rocket, space station, high-speed train, and racing car has widely increased nowadays for exploiting various inherent advantages from their material properties such as high strength-to-weight and high stiffness-to-weight ratios, long fatigue life, and dimensional stability during temperature change. The specific parts of the structures such as the nose and wings of the aircraft experience a wide range of temperature variation during the service life due to the movement at supersonic speeds. Similarly, due to the high speeds, the body of the racing car does also experience elevated temperatures. The increase in temperature is very random in nature depending upon various unpredictable influences. Due to high dimensional stability, low coefficient of thermal expansion (CTE), high strength, and high glass transition temperature graphite-epoxy composite is used to manufacture some of the critical components in the structures. Therefore, the variations in the temperature increment exhibit a significant range of uncertainties in the response of the graphite-epoxy composite structure. Moreover, adequate information on variability of the structural response is essential to design a thermally sensitive part of the structure using graphite-epoxy composite. On the other hand, structural strength of the composite plate is also random in nature. Stochastic studies of the graphite-epoxy plate under dynamic loading is essential to estimate the probability of failure in uncertain thermal environment. Thus, for the safe and reliable design of the structural components subjected to the uncertain temperature and different types of loading conditions instigate to study the stochastic dynamic response of the graphite-epoxy composite plate in the random thermal environment.

The analysis of fiber reinforced composite (FRC) plate in the thermal environment was initiated by Halpin [1], and was followed by Whitney and Ashton [2]. They had presented deterministic elastic response of the symmetric and anti-symmetric composite plates using generalized Duhamel-Neumann form of Hooke's law including the effect of moisture and thermal strain. Ram and Sinha [3] had presented a finite element (FE) method using first-order shear deformation theory

* Corresponding author.
E-mail address: sourav.chandra@tum.de (S. Chandra).

https://doi.org/10.1016/j.compstruct.2019.111159
Received 11 December 2018; Received in revised form 7 June 2019; Accepted 18 June 2019
Available online 22 June 2019
0263-8223/ © 2019 The Authors. Published by Elsevier Ltd. This is an open access article under the CC BY license (http://creativecommons.org/licenses/BY/4.0/).

(FSDT) to determine eigen frequency of the laminated composite plate with increasing uniform temperature and moisture concentration. They had shown that the eigen frequency of the composite plate decreases with increasing temperature and moisture concentration for symmetric and anti-symmetric angle-ply laminates with simply-supported and fixed boundary conditions. Rao and Sinha [4] had developed a three-dimensional FE model to represent the eigen frequency and transient response of the multidimensional composite plate using 20-node isoparametric quadratic elements at elevated temperature and moisture concentration. Mallikarjuna and Kant [5] and Kant and Mallikarjuna [6] had presented large deflection response of the composite plate using higher-order shear deformation theory (HSDT) with the application of C^0 isoparametric element. Rather extensive deterministic studies of the laminated plates and shells had appeared in the literature on the nonlinear transient response albeit without considering thermal and moisture effects [7–10]. Huang and Tauchert [11] had investigated temperature-induced large deflection behavior of the laminated composite plates and spherical panels. Patel et al. [12] had studied hygrothermal effects on thick laminated composite plate using higher-order theory. They had shown that eigen frequencies obtained from the application of the higher-order theory for thin laminated composite plate are comparable to those obtained from the FSDT in hygrothermal environment. Ganapathi et al. [13] had studied nonlinear dynamic response of the thick composite and sandwich plates subjected to thermal and mechanical loading using higher-order theory. Huang et al. [14] had studied the effects of deterministic nonlinear vibration and dynamic response of the FRC plate using the HSDT in the hygrothermal environment. They had obtained nonlinear frequencies and dynamic response of the composite plate by an improved perturbation technique. The nonlinear free vibration analysis and evaluation of transient response of a doubly-curved shell structure, by incorporating Green-Lagrange type nonlinear strain into the FSDT, using FE formulation was presented by Naidu and Sinha [15,16]. They had used Newmark's average acceleration method for the transient analysis conducted from the nonlinear governing equations of motion. Ribeiro and Jansen [17] had presented nonlinear transient response of the composite laminated shallow shells subjected to the simultaneous application of the thermal field and mechanical excitation. The FE model was based on the FSDT with hierarchical basis function. Mahapatra et al. [18,19] had investigated nonlinear frequency response of the singly- or doubly-curved laminated composite shell panels considering the HSDT and Green-Lagrange type nonlinearity. Nanda and Pradyumna [20] had presented nonlinear free vibration analysis and evaluation of transient response of the imperfect laminated composite shell in hygrothermal environment. The formulation was based on the FSDT and von Kármán-type nonlinear kinematics. Biswal et al. [21] had reported a numerical study of free vibration of woven fiber glass-epoxy laminated composite shallow shell under hygrothermal environment using the FSDT; wherein, the numerically simulated results were well supported by the experimental measurements. In all these studies, the elastic parameters had been considered as deterministic, and deterministic dynamic response of the structures was presented at various deterministic temperatures. However, in practical situations the temperature increment is not always deterministic necessarily, rather it is quite random in nature. Therefore, the probabilistic study of the dynamic response of the graphite-epoxy composite plate at elevated random temperature is deemed essential.

Uncertainty quantification in the system response of the FRC plate using the FE method has been investigated in the recent decade considering the aleatory uncertainties due to the randomness in the material properties of the composite. Stochastic static and dynamic analyses of the FRC plate using perturbation method were presented in details by Engelstad and Reddy [22], Park et al. [23], Salim et al. [24], Chen et al. [25], Singh et al. [26], Onkar and Yadav [27], and Lal et al. [28]. In perturbation method, the uncertain parameters are expanded by Taylor's series expansion about the mean value. However, the limitation of this method is, the deviation of the randomness cannot be too large with respect to the mean value of the parameters. The brute-force, Monte Carlo simulation (MCS) method is relatively simple and extensively applied to quantify the uncertainty in the static and dynamic response evaluation of the composite plates. Nevertheless, a large numbers of Monte Carlo (MC) realizations are required for achieving good accuracy in the simulation, which is time consuming and computationally inefficient. Application of the MC-based simulation for studying reliability of the laminated composite plate was shown by Zhang et al. [29]. To address the issue of computational efficiency, the spectrum-based generalized polynomial chaos (gPC) expansion method [30–35] has received a significant attention due to its computational efficiency with reasonable accuracy in the simulation over the sampling-based MCS. Sepahvand et al. [36–38] presented the application of the gPC expansion method to represent the uncertainty in the eigen frequencies and eigen modes of the FRC plates due to the uncertainty in the elastic moduli and fiber orientations. More details on the applications of the method can be found in [39,40].

In the recent past, some studies have been reported which address the uncertainty in the eigen frequency response of the composite plate in the thermal environment. Lal and Singh [41] had investigated the uncertainty in the first eigen frequency arising due to a small level of uncertainty in the individual system parameters of the composite plate at different temperatures. The system parameters included elastic moduli, Poisson's ratio, and thickness of the composite plate. They had used first-order perturbation technique (FOPT) in conjunction with the HSDT in the FE method for the composite plate. Singh and Verma [42] had studied the uncertainty in predicting the buckling load due to the uncertainty in the geometric and material properties of the composite plate at different moisture and temperature conditions using the HSDT and FOPT. They [41,42] had adopted simply-supported and fixed boundary conditions for the plates in the analysis. Kumar et al. [43] had studied stochastic free vibration response of the laminated composite plate resting on elastic foundation under hygrothermal environment using the HSDT. Dey et al. [44] had applied surrogate modeling approach to investigate the stochasticity in the first three natural frequencies of the laminated composite plate due to the uncertainty in the temperature, elastic moduli, and fiber angle/ orientations. They had considered cantilever laminated composite plate for the analysis. Kumar [45,46] had studied the mean and coefficient of variation (COV) of the first mode of linear and nonlinear eigen frequencies, respectively with the increment in the temperature and moisture content considering randomness in the elastic moduli, coefficient of thermal expansion, and moisture content using the FOPT. Nevertheless, the stochastic static and free vibration response of the composite plate due to the randomness in the material properties at various temperatures using the FOPT has been investigated in [45,46], considering limitation in the applicability of the COV equal to 0.1.

The perusal of the earlier works reveals that research is conducted on probabilistic study of the static response and eigen frequency response at higher temperatures due to the uncertainty in the system parameters using the FOPT. However, probabilistic dynamic analysis of the composite plate due to the random temperature increment is completely missing, though it is such an important consideration. Therefore, the present study intends to report the effect of random mean temperature increment on the eigen frequency and dynamic response of the composite plate with various stacking sequences using the gPC expansion method. Moreover, the application of the gPC expansion technique may be able to address the issue regarding consideration of the large uncertainty over the perturbation technique. The collocation-based non-intrusive gPC expansion method is applied to model the stochastic response of the eigen frequencies and the time-dependent displacement field. The stochastic response at each time step has been determined to describe the effect of the temperature uncertainty on the dynamic response of the composite plate. A deterministic FE model has been developed to realize the dynamic response considering the temperature-dependent elastic properties of the graphite-epoxy composite

plate. This FE model is developed to analyze the laminated composite plate in the thermal environment to evaluate the structural response from the non-intrusive stochastic model. The major contribution from this paper is, to study the effect of thermal stochasticity by using stochastic finite element method (SFEM) with the application of the gPC to evaluate the uncertainty in the eigen frequency and dynamic central displacement. Numerical dynamic analysis has been carried out with suddenly applied pulse and impulse loading to investigate the variation of uncertainty in the time domain for the cross-ply and angle-ply laminates.

The paper is organized as follows: development of the stochastic formulation of the graphite-epoxy composite laminated plate for the uncertainty in the temperature increment is presented in the next section. A step-by-step procedure for the numerical study is demonstrated in Section 3. Validation of the stochastic model and numerical results are given in Section 4, followed by conclusions in the last section of this paper.

2. Stochastic formulation for the random temperature increment

In the present study, a laminated composite plate of length L, width W, and uniform thickness h is considered consisting of n numbers of unidirectional lamina. It is assumed that each lamina of the composite plate is orthotropic, and bonded together with infinitely thin bonds to act as an integral part of the composite plate. The thickness of the composite plate is considered to be very small as compared to the in-plane dimensions, and shear deformation of the composite plate is constant throughout the thickness. Consequently, the FSDT is employed in the present study considering the desirable accuracy with improved computational efficiency [47]. A shear correction factor is applied here to account for the non-uniform distribution of the transverse shear strain along the thickness of the laminate.

2.1. Constitutive relationship of the composite plate

Mid-plane of the composite plate is considered as a reference plane to evaluate the displacement fields. According to the FSDT, normal to the mid-plane remains straight before and after deformation. The positive sign convention for the in-plane translations u and v, out-of-plane translation w, the rotations of the transverse normal θ_x and θ_y of the composite plate about y and x axes, respectively, and fiber orientations of the lamina are shown in Fig. 1. The generalized displacement vector $\{d\} = \{u \quad v \quad w \quad \theta_x \quad \theta_y\}^{\mathrm{T}}$ of the composite plate at a distance z from the mid-plane is expressed as

$$u = u_0 + z\theta_y, \; v = v_0 - z\theta_x, \; w = w_0. \tag{1}$$

Here, u_0, v_0, and w_0 are the mid-plane displacements along x, y, and z directions, respectively. Shear rotations φ_x and φ_y in $x-z$ and $y-z$ planes, respectively, are expressed as

$$\varphi_x = w_{,x} + \theta_y, \; \varphi_y = w_{,y} - \theta_x. \tag{2}$$

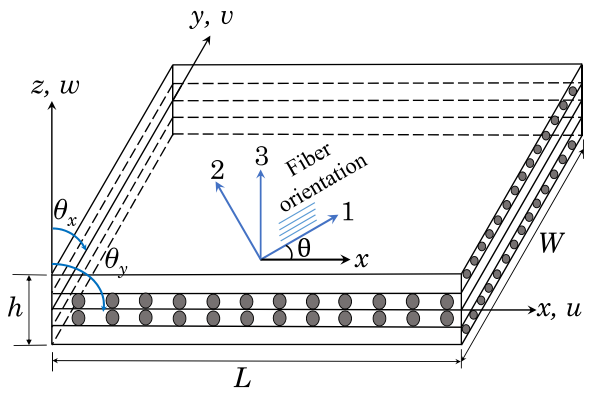

Fig. 1. Laminate geometry, and fiber angle orientations with respect to the global axes.

Components of linear strain vector $\{\varepsilon\}$ of the laminate at distance z from the mid-plane are derived from Eq. (1) as

$$\begin{aligned}
\varepsilon_x &= u_{0,x} + z\theta_{y,x},\\
\varepsilon_y &= v_{0,y} - z\theta_{x,y},\\
\varepsilon_{xy} &= u_{0,y} + v_{0,x} + z(\theta_{y,y} - \theta_{x,x}),\\
\varepsilon_{xz} &= \varphi_x,\\
\varepsilon_{yz} &= \varphi_y.
\end{aligned} \tag{3}$$

Linear strain terms are redefined as $\varepsilon_{0x} = u_{0,x}$, $\varepsilon_{0y} = v_{0,y}$, $\varepsilon_{0xy} = (u_{0,y} + v_{0,x})$, $\kappa_x = \theta_{y,x}$, $\kappa_y = -\theta_{x,y}$, and $\kappa_{xy} = (\theta_{y,y} - \theta_{x,x})$. When composite plate is subjected to the uniform distribution of the temperature, the stress-strain relationship for the k^{th} lamina with reference to the laminate axes (x, y, z) is written as

$$\{\sigma\}_k = [Q]_k[\{\varepsilon\}_k - \{\alpha\}_k\Delta T], \tag{4}$$

in which $\{\sigma\} = \{\sigma_x \quad \sigma_y \quad \sigma_{xy} \quad \sigma_{xz} \quad \sigma_{yz}\}^{\mathrm{T}}$ is stress vector, thermal expansion coefficient vector is written as $\{\alpha\} = \{\alpha_x \quad \alpha_y \quad \alpha_{xy} \quad 0 \quad 0\}^{\mathrm{T}}$ and ΔT is the increment in temperature over reference temperature. Here, $[Q]_k$ is the stress-strain relationship matrix for the k^{th} lamina with reference to the laminate axes, cf. [47,48] for further details. The force and moment resultant of the laminate are obtained by integrating Eq. (4) over the thickness and written as

$$\{F_r\} = [D][\{\varepsilon^*\} - \{e^*\}]. \tag{5}$$

In this equation, the resultant force and moment vector is

$$\{F_r\} = \{N_x \quad N_y \quad N_{xy} \quad M_x \quad M_y \quad M_{xy} \quad Q_x \quad Q_y\}^{\mathrm{T}}, \tag{6}$$

generalized mid-plain strain vector is

$$\{\varepsilon^*\} = \{\varepsilon_{0x} \quad \varepsilon_{0y} \quad \varepsilon_{0xy} \quad \kappa_x \quad \kappa_y \quad \kappa_{xy} \quad \varepsilon_{xz} \quad \varepsilon_{yz}\}^{\mathrm{T}}, \tag{7}$$

generalized thermal strain vector is

$$\{e^*\} = \{e_x \quad e_y \quad e_{xy} \quad 0 \quad 0 \quad 0 \quad 0 \quad 0\}^{\mathrm{T}}, \tag{8}$$

and $[D]$ is the load-strain relationship matrix of the laminated composite plate. Accordingly, Eq. (5) can be rewritten in a compact form as

$$\{F_r\} = [D]\{\varepsilon^*\} - \{F_N\}, \tag{9}$$

in which the thermal resultant force and moment vector are given by

$$\{F_N\} = \{N_x^N \quad N_y^N \quad N_{xy}^N \quad M_x^N \quad M_y^N \quad M_{xy}^N \quad 0 \quad 0\}^{\mathrm{T}}. \tag{10}$$

Initial strain $\{\varepsilon_{nt}\}$ due to thermal load is represented by the nonlinear portion [3,49] of the overall strain as

$$\begin{aligned}
\varepsilon_{xnt} &= \frac{1}{2}(u_{,x}^2 + v_{,x}^2 + w_{,x}^2),\\
\varepsilon_{ynt} &= \frac{1}{2}(u_{,y}^2 + v_{,y}^2 + w_{,y}^2),\\
\varepsilon_{xynt} &= (u_{,x}u_{,y} + v_{,x}v_{,y} + w_{,x}w_{,y}),\\
\varepsilon_{xznt} &= (u_{,x}u_{,z} + v_{,x}v_{,z}),\\
\varepsilon_{yznt} &= (u_{,y}u_{,z} + v_{,y}v_{,z}).
\end{aligned} \tag{11}$$

The Eq. (11) can be rewritten in a compact form with reference to the Eq. (1) as

$$\{\varepsilon_{nt}\} = \frac{1}{2}[R]\{d^*\}, \tag{12}$$

where $\{d^*\} = \{u_{0,x} \quad u_{0,y} \quad v_{0,x} \quad v_{0,y} \quad w_{,x} \quad w_{,y} \quad \theta_{x,x} \quad \theta_{x,y} \quad \theta_{y,x} \quad \theta_{y,y} \quad \theta_x \quad \theta_y\}^{\mathrm{T}}$, and $[R]$ is the strain-displacement relationship matrix of the nonlinear strain.

2.2. Equations of motion

The equations of motion of the laminated composite plate are presented here using the Hamilton variational principle [48], stated as

$$\int_{t_1}^{t_2} \delta\left(\mathbb{E} - \mathbb{K}\right)\mathrm{d}t = 0, \tag{13}$$

where $\mathbb{E}$ and $\mathbb{K}$ are total potential and kinetic energies, respectively, during the time interval (t_1, t_2). The total potential energy $\mathbb{E}$ can be written as $\mathbb{E} = \mathbb{U} - \mathbb{W}$, where $\mathbb{U}$ represents the strain energy of the plate, and $\mathbb{W}$ is the work done by the externally applied forces. The total potential energy $\mathbb{E}$ of the composite plate in the thermal environment is expressed as

$$\mathbb{E}=\left(\frac{1}{2}\int_{\mathrm{A}}\{\varepsilon^*\}^{\mathrm{T}}[D]\{\varepsilon^*\}\mathrm{d}A + \frac{1}{2}\int_{\mathrm{A}}\{d^*\}^{\mathrm{T}}[S_r]\{d^*\}\mathrm{d}A\right) - \left(\int_{\mathrm{A}}\{d\}^{\mathrm{T}}\{F\}\mathrm{d}A + \int_{\mathrm{A}}\{\varepsilon^*\}^{\mathrm{T}}\{F_N\}\mathrm{d}A\right), \tag{14}$$

in which $[S_r]$ is residual stress resultant matrix, see Appendix A.1; and $\{F\}$ is externally applied transverse load vector per unit area in the direction of the generalized displacement vector $\{d\}$. The kinetic energy $\mathbb{K}$ of the composite plate is presented as

$$\mathbb{K} = \frac{1}{2}\int_{\mathrm{A}}\{\dot{d}\}^{\mathrm{T}}[\overline{M}]\{\dot{d}\}\mathrm{d}A. \tag{15}$$

Here, $\{\dot{d}\}$ is a generalized velocity vector corresponding to $\{d\}$, and $[\overline{M}]$ is the distributed inertia matrix of the laminated composite plate. Accordingly, mathematical expression for the dynamic motions is formed by combining Eqs. (14) and (15) into the Hamilton variational principle, see Eq. (13), as

$$\delta\int_{t_1}^{t_2}\left[\frac{1}{2}\int_{\mathrm{A}}\{\varepsilon^*\}^{\mathrm{T}}[D]\{\varepsilon^*\}\mathrm{d}A + \frac{1}{2}\int_{\mathrm{A}}\{d^*\}^{\mathrm{T}}[S_r]\{d^*\}\mathrm{d}A - \int_{\mathrm{A}}\{d\}^{\mathrm{T}}\{F\}\mathrm{d}A - \int_{\mathrm{A}}\{\varepsilon^*\}^{\mathrm{T}}\{F_N\}\mathrm{d}A - \frac{1}{2}\int_{\mathrm{A}}\{\dot{d}\}^{\mathrm{T}}[\overline{M}]\{\dot{d}\}\mathrm{d}A\right]\mathrm{d}t = 0. \tag{16}$$

2.3. Stochastic modeling of uncertain parameters

Stochastic response of the dynamical system due to independent and identically distributed (iid) random parameters can be represented by generalized polynomial chaos (gPC) theory. The concept of application of the chaos theory to represent the stochastic response was first coined by Wiener [50]. A set of orthogonal polynomials is used to project the random variables onto the stochastic space. Consider a probability space represented by $(\Omega, \mathcal{F}, P)$, in which Ω is the random sample space, $\mathcal{F}$ is a σ-algebra on Ω, and P is a probability measure on the sample space. Any uncertain parameter $\mathcal{X}$: $\Omega \rightarrow \mathbb{R}$ with finite variance can be expressed as [32]

$$\mathcal{X} = \sum_{i_1=0}^{\infty} a_{i_1}\Psi_{i_1}(\xi). \tag{17}$$

This is the gPC expansion of the uncertain parameter $\mathcal{X}$ in a compact form. The random orthogonal polynomial Ψ_{i_1} is a multidimensional function of random variables, $\xi = \{\xi_i\}, \quad i = 1, 2, ..., n$ in the particular sample space. Selection of the orthogonal polynomial is dependent on the type of sample space of the random variables. It is convenient to use the truncated series for the expansion considering the accuracy and the sample space of the random variables. The unknown coefficients $\{a_{i_1}\}$ are determined by the Galerkin projection technique.

In the present study, uniform temperature increment of the composite plate is considered as a random variable. It is reported earlier that the elastic moduli of the graphite-epoxy composite plate varies with the variation in the temperature [51–53]. The elastic moduli of the graphite-epoxy composite is varied according to the random temperature increment, and consequently the dynamic response of the composite becomes stochastic in nature. Hence, uncertainty in the temperature increment can be represented by the truncated gPC expansion as

$$T(\xi) = \sum_{i_1=0}^{N_1} a_{i_1}\Psi_{i_1}(\xi) = \boldsymbol{a}^{\mathrm{T}}\boldsymbol{\Psi}, \tag{18}$$

in which $\boldsymbol{a} = \{a_{i_1}\}$ is the vector of deterministic unknown coefficients and N_1 is the finite number of terms of the gPC expansion of the random temperature. The orthogonality relation of the multidimensional polynomial functions, $\boldsymbol{\Psi} = \{\Psi_{i_1}(\xi)\}$ is written as

$$\mathbb{E}[\Psi_{i_1}, \Psi_{j_1}] = \mathbb{E}[\Psi_{i_1}^2]\delta_{i_1 j_1} = p_{i_1}^2\delta_{i_1 j_1}, \qquad i_1, j_1 = 0, 1, 2, ..., N_1, \tag{19}$$

in which $\delta_{i_1 j_1}$ and p_{i_1} represent Kronecker delta and the norm of the polynomials, respectively. The unknown coefficients $\{a_{i_1}\}$ are determined using Galerkin projection technique as

$$\{a_{i_1}\} = \frac{1}{\langle\Psi_{i_1}^2\rangle}\int_{\Omega}\left\{T(\xi)\right\}\left\{\Psi_{i_1}(\xi)\right\}\mathfrak{f}(\xi)\mathrm{d}\xi, \tag{20}$$

where $\langle\Psi_{i_1}^2\rangle$ denotes the inner products in the Hilbert space, and $\mathfrak{f}$ is the probability density function (PDF) of random variable ξ. Once $\{a_{i_1}\}$ are known, any statistical property of the random parameter can be calculated. For instance, the expected value μ_T and the variance σ_T^2 take the following forms

$$\mu_T = a_0, \quad \sigma_T^2 = \sum_{i_1=1}^{N_1} a_{i_1}^2 p_{i_1}^2. \tag{21}$$

Due to the increment in the random mean temperature, elastic properties of the composite are varied. The structural response of the composite also becomes uncertain. Accordingly, the random eigen frequency $f(\xi)$ and time-dependent random displacement $d(t, \xi)$ are approximated by truncated finite number of terms N_2 using the gPC expansions as

$$f(\xi) = \sum_{i_2=0}^{N_2} b_{i_2}\Psi_{i_2}(\xi) = \boldsymbol{b}^{\mathrm{T}}\boldsymbol{\Psi}, \tag{22}$$

$$d\left(t, \xi\right) = \sum_{i_2=0}^{N_2} c_{i_2}(t)\Psi_{i_2}(\xi) = \boldsymbol{c}^{\mathrm{T}}\boldsymbol{\Psi}. \tag{23}$$

Here, $\boldsymbol{b} = \{b_{i_2}\}$ and $\boldsymbol{c} = \{c_{i_2}(t)\}$ are the deterministic unknown coefficients for the random eigen frequency and random dynamic displacement at each time step, respectively, and $\boldsymbol{\Psi} = \{\Psi_{i_2}(\xi)\}$ is the orthogonal polynomial function.

2.4. Stochastic finite element modeling

Orthotropic composite plate is mathematically modeled by following finite element method (FEM), and the entire plate domain is discretized by eight-node C^0 isoparametric element with five degrees of freedom (DOF) per node. The stochastic element displacement vector $\{d(t, \xi)\}$ is expressed in terms of the stochastic nodal displacement vector $\{d_e(t, \xi)\}$ using elemental interpolation functions $[N]$, and is given by

$$\{d(t, \xi)\} = [N]\{d_e(t, \xi)\}. \tag{24}$$

Accordingly, the random mid-plain strain vector $\{\varepsilon^*(t, \xi)\}$ can be calculated from the stochastic nodal displacement vector $\{d_e(t, \xi)\}$ employing strain-nodal displacement matrix $[B]$, with reference to Eqs. (7) and (24) as

$$\{\varepsilon^*(t, \xi)\} = [B]\{d_e(t, \xi)\}. \tag{25}$$

The stochastic elemental strain energy for an element e is derived with reference to Eq. (16)

$$\int_{t_1}^{t_2}\Big[\int_{A_e}\delta\{d_e(t,\xi)\}^T[B]^T[D(T(\xi))][B]\{d_e(t,\xi)\}\,dA_e+\int_{A_e}\delta\{d_e(t,\xi)\}^T[G]^T[S_r(T(\xi))][G]\{d_e(t,\xi)\}\,dA_e-\int_{A_e}\delta\{d_e(t,\xi)\}^T[N]^T\{F(t)\}dA_e-\int_{A_e}\delta\{d_e(t,\xi)\}^T[B]^T[F_N(T(\xi))]dA_e+\int_{A_e}\delta\{d_e(t,\xi)\}^T[N]^T[\overline{M}][N]\{\ddot{d}(t,\xi)\}\Big]dt=0, \tag{26}$$

where $[G]$ is the matrix of shape functions given in Appendix A.2. Since, virtual displacement $\delta\{d_e(t,\xi)\}$ is arbitrary in nature, stochastic finite element model of the element e of the laminated composite plate can be presented as

$$\{[K_e(T(\xi))]+[K_{Ge}(T(\xi))]\}\{d_e(t,\xi)\}+[M_e]\{\ddot{d}_e(t,\xi)\}=\{P_e(t)\}+\{P_{N_e}(T(\xi))\}. \tag{27}$$

The stochastic elemental stiffness matrix $[K_e(T(\xi))]$, stochastic elemental geometric stiffness matrix $[K_{Ge}(T(\xi))]$, and stochastic elemental thermal load vector $\{P_{N_e}(T(\xi))\}$ are obtained as

$$\left[K_e\left(T(\xi)\right)\right]=\int_{A_e}[B]^T\left[D\left(T(\xi)\right)\right][B]dA_e, \tag{28}$$

$$\left[K_{Ge}\left(T(\xi)\right)\right]=\int_{A_e}[G]^T\left[S_r\left(T(\xi)\right)\right][G]dA_e, \tag{29}$$

$$\left\{P_{N_e}\left(T(\xi)\right)\right\}=\int_{A_e}[B]^T\left\{F_N\left(T(\xi)\right)\right\}dA_e. \tag{30}$$

The elemental mass matrix $[M_e]$ and elemental dynamic force vector $\{P_e(t)\}$ are given respectively by

$$[M_e]=\int_{A_e}[N]^T[\overline{M}][N]dA_e, \tag{31}$$

$$\left\{P_e(t)\right\}=\int_{A_e}[N]^T\left\{F(t)\right\}dA_e. \tag{32}$$

Elemental static load vector can be developed with reference to the Eq. (32) as

$$\{P_{Se}\}=\int_{A_e}[N]^T\{F\}dA_e, \tag{33}$$

and corresponding global static load vector $\{P_S\}$ is developed after proper assembling. The global stochastic FE model for the forced vibration can be obtained after assembling the element matrices in the following form

$$\{[K(T(\xi))]+[K_G(T(\xi))]\}\{d(t,\xi)\}+[M]\{\ddot{d}(t,\xi)\}=\{P(t)\}+\{P_N(T(\xi))\}. \tag{34}$$

It is stated earlier that elastic properties of the constituent materials of the composite are varied with the variation in the temperature [51–53,3]. Therefore, stiffness matrix, geometric stiffness matrix, and thermal force vector of the composite are expressed as functions of random matrices due to randomness in the temperature. The solution of the stochastic forced vibration problem is sought by Newmark's integration technique, and the randomness in the displacement at each time step is described. The homogeneous solution of Eq. (34) yields the stochasticity in the eigen frequency $f(\xi)$ of the composite plate for the specified boundary conditions. The stochastic representations, as discretized in Eqs. (18) and (23), using truncated gPC expansion method are substituted in Eq. (34), i.e.

$$\{[K(\boldsymbol{a}^T\boldsymbol{\Psi})]+[K_G(\boldsymbol{a}^T\boldsymbol{\Psi})]\}(\boldsymbol{c}^T\boldsymbol{\Psi})+[M](\ddot{\boldsymbol{c}}^T\boldsymbol{\Psi})=\{P(t)\}+\{P_N(\boldsymbol{a}^T\boldsymbol{\Psi})\}. \tag{35}$$

The unknown deterministic coefficients for the eigen frequencies $\boldsymbol{b}^T$ are estimated by minimization of the stochastic error $\{\epsilon_1(t,\xi)\}$ from the homogeneous solution of Eq. (35) as

$$\{\varepsilon_1(t,\xi)\}=\{[K(\boldsymbol{a}^T\boldsymbol{\Psi})]+[K_G(\boldsymbol{a}^T\boldsymbol{\Psi})]\}(\boldsymbol{c}^T\boldsymbol{\Psi})+[M](\ddot{\boldsymbol{c}}^T\boldsymbol{\Psi}). \tag{36}$$

Similarly, the solution of the unknown deterministic coefficients for time-dependent displacement field $\boldsymbol{c}^T$ are derived by minimization of the stochastic error $\{\epsilon_2(t,\xi)\}$ from

$$\{\varepsilon_2(t,\xi)\}=\{[K(\boldsymbol{a}^T\boldsymbol{\Psi})]+[K_G(\boldsymbol{a}^T\boldsymbol{\Psi})]\}(\boldsymbol{c}^T\boldsymbol{\Psi})+[M](\ddot{\boldsymbol{c}}^T\boldsymbol{\Psi})-\{P(t)\}-\{P_N(\boldsymbol{a}^T\boldsymbol{\Psi})\}. \tag{37}$$

The minimization of the stochastic error is carried out by calculating the deterministic response of the system at some specific collocation points, i.e. at the roots of the higher-order orthogonal polynomials, and minimizing the error between these response. The response is calculated by the gPC expansion using least-squares method [32]. The collocation-based non-intrusive method is implemented here to derive the unknown coefficient vectors. In this method, deterministic governing equations of motion are employed as a deterministic solver, and solutions are obtained at the specific collocation points. Selection of the collocation points depends on the choice of the order of the gPC expansion representing the randomness in the dynamical system, cf. [32] for more details.

3. Solution procedure

The solution of the non-intrusive gPC-based stochastic FE model is evaluated in two parts, i.e. the solution of the deterministic finite element model, and the solution of the stochastic model by determining the unknown coefficients while setting the random errors equal to zero at some predefined collocation points. The FE model developed for the laminated composite plate in the thermal environment is used as a deterministic solver, and runs of the deterministic FE model are repeated at the specified realizations of the selected random vector points. The detailed procedure of the numerical simulation, considering temperature uncertainty is summarized here in Algorithm 1 and Algorithm 2.

Algorithm 1: Deterministic analysis using FE model of the composite plate in thermal environment

1 Develop global matrices $[K]$ and $[M]$ as well as force vectors $\{P_S\}$, $\{P(t)\}$, and $\{P_N\}$ of the composite plate at the predefined temperature;
2 Calculate initial displacement $\{\delta_i\}$ from bending equation, $[K]\{\delta_i\}=\{P_S\}+\{P_N\}$;
3 Substitute initial displacement $\{\delta_i\}$ in Eqs. (25) and (9) to yield the residual stress resultants $\{F_r\}$;
4 Develop geometric stiffness matrix $[K_G]$;
5 Determine eigen frequencies and mode shapes of the laminated composite plate in the thermal environment from the homogeneous solution of Eq. (34);
6 Solve Eq. (34) for time-dependent forcing function $\{P(t)\}$ using Newmark's direct time integration method at each incremental time step to obtain the dynamic response.

Gauss quadrature rule is adopted here for integration over the elemental area for calculation of the element matrices. The 3-point Gauss quadrature rule is adopted to compute the bending stiffness matrix; whereas, 2-point Gauss quadrature rule is adopted to calculate the shear stiffness, mass matrix, and force vectors to avoid the shear locking phenomenon in the thin plate. The constant-average acceleration scheme is adopted to solve Newmark's direct time integration method for obtaining stable solution of the linear problem [54]. A deterministic MATLab® code has been developed to evaluate the eigen frequencies and transient response of the laminated composite plate in thermal environment, as stated in Algorithm 1.

Table 1
Elastic moduli of graphite-epoxy lamina at different temperatures, cf. [3]. $G_{13} = G_{12}$, $G_{23} = 0.5G_{12}$.

	Temperature, T (K)					
Elastic moduli (GPa)	300	325	350	375	400	425
E_{11}	130	130	130	130	130	130
E_{22}	9.5	8.5	8.0	7.5	7.0	6.75
G_{12}	6.0	6.0	5.5	5.0	4.75	4.5

Table 2
Mean μ_T and sd σ_T of the input random parameter.

Random parameter	Type of distribution	μ_T (K)	σ_T (K)
Temp. increment	Normal	25, 50, 75, 100	5, 10, 15, 20

Table 3
Geometric dimension, elastic parameters, density, coefficient of thermal expansion, lamina sequences of the graphite-epoxy laminated composite plate.

	Plate 1	Plate 2
Dimensions (mm)	$L = W = 100$, $h = 1$	$L = W = 100$, $h = 2$
Elastic moduli (GPa)	$E_{11} = 130$, $E_{22} = 9.5$, $G_{12} = 6.0$, $G_{13} = G_{12}$, $G_{23} = 0.5G_{12}$	See Table 1
Poisson's ratio	$\nu_{12} = 0.3$, $\nu_{21} = \nu_{12}\frac{E_{22}}{E_{11}}$	$\nu_{12} = 0.3$, $\nu_{21} = \nu_{12}\frac{E_{22}}{E_{11}}$
Density (kg/mm^3)	$\rho = 1.6 \times 10^{-6}$	$\rho = 1.6 \times 10^{-6}$
Coefficient of thermal expansion (\K)	$\beta_1 = -0.3 \times 10^{-6}$, $\beta_2 = 28.1 \times 10^{-6}$	$\beta_1 = -0.3 \times 10^{-6}$, $\beta_2 = 28.1 \times 10^{-6}$
Lamina sequence	For cross-ply laminate (0°/90°/90°/0°)	For cross-ply laminate (0°/90°/90°/0°), For angle-ply laminate (45°/−45°/−45°/45°)

Algorithm 2: Collocation-based SFEM for analysis of the composite plate due to thermal uncertainty

1 Define deterministic geometry of the model, elastic parameters, lamina sequence of the composite plate, as well as mean, standard deviation (sd), and probability space of the random temperature;
2 Represent the uncertainty in the temperature increment using the gPC expansion as $T(\xi)$, see Eq. (18);
3 Estimate the unknown coefficients a_{i_1} for the random temperature increment using Galerkin projection technique, see Eq. (20);
4 Select the type of orthogonal polynomial $\Psi_{i_2}(\xi)$ based on the random space of the input random variable, and the order of the polynomial function as N_2;
5 Construct the uncertainty in the structural response $f(\xi)$ and $d(t, \xi)$ using the truncated gPC expansion, see Eqs. (22) and (23);
6 Generate the collocation points from the roots of the higher-order polynomial function $\Psi_{i_2}(\xi)$. Number of collocation points should be at least equal to the number of unknown deterministic coefficients b_{i_2} and $c_{i_2}(t)$;
7 Generate the random temperature increment at the predefined collocation points;
8 Realize the structural response using the deterministic FE solver at the pre-generated random incremental temperature. Develop a set of equations from Eqs. (36) and (37) at the predefined collocation points;
9 Calculate the unknown coefficients b_{i_2} and $c_{i_2}(t)$ for the eigen frequency, and the time-dependent displacement, respectively from the above set of equations employing least-squares minimization technique;
10 Estimate the statistical parameters of the structural response, e.g. mean, sd, and corresponding PDF.

The selection of the orthogonal polynomial basis function depends on the type of variability in the random input parameters. For instance, Hermite polynomial is used for normally distributed input parameter, whereas Jacobi polynomial is used if the input random parameter is in Gamma distribution. Following Algorithm 2, a collocation-based SFEM code is developed in MATLab® environment to evaluate the unknown coefficients of the structural response in the gPC expansion method. Predefined deterministic FE solver is used to generate structural response at the collocation points.

Table 4
Suddenly applied transverse load.

	Pulse loading	Impulse loading
Loading (N/mm^2)	$q_0 = 0.001$	$q_0 = 0.001$
Time of excitation (s)	$t_p = 0.25$	$t_{ip} = 0.001$

4. Numerical study

Numerical study is conducted to evaluate uncertainty in the eigen frequency and dynamic response of the graphite-epoxy laminated composite plate due to random temperature increment using the gPC expansion method. The stochastic studies are conducted at the mean temperatures of 325 K, 350 K, 375 K, and 400 K. However, 300 K is considered as a reference temperature. The temperature-dependent elastic properties of the graphite-epoxy composite lamina are illustrated in Table 1. The mean μ_T and sd σ_T of the random temperature increment as input parameters are shown in Table 2. In the present study, elastic moduli, coefficient of thermal expansion, and Poisson's ratio of the composite plate are considered as deterministic. The geometric dimension, elastic properties, density, and stacking sequences of the composite plate considered here are shown in Table 3. The composite plates are subjected to the uniformly distributed transverse loads as given in Table 4.

The polynomial basis function is represented by Hermite polynomial for random input variable, which is normally distributed. The number of unknown coefficients are increased rapidly if the order of the polynomial is increased. Herein, one-dimensional 3rd order Hermite polynomial is used to approximate the stochastic response. Therefore, Hermite polynomial can be presented in term of the random variable ξ as $\Psi_0 = 1$, $\Psi_1 = \xi$, $\Psi_2 = (\xi^2 - 1)$, and $\Psi_3 = (\xi^3 - 3\xi)$. The eigen frequency f and the transverse central $(\frac{L}{2}, \frac{W}{2})$ displacement $d(t)$ of the composite plate are considered here to investigate the uncertainty in the dynamic response due to random mean temperature increment.

4.1. Validation of the FE model

The FE model of the laminated composite plate in thermal environment has been developed, and the frequencies extracted are compared with that reported in the literature. An ANSYS® parametric design language (APDL) code is employed to calculate the eigen frequencies of the composite plate considering the effect of thermal prestress during modal analysis. The eigen frequencies of the simply-supported graphite-epoxy laminated composite plate at the temperature of 300 K and 325 K are evaluated using the present formulation, and are compared with the frequencies reported by Ram and Sinha [3] and ANSYS® simulation to establish validity of the present deterministic formulation, cf. Table 5.

The parameters of Plate 1 (Table 3) are used for the validation analysis. The finite element mesh considered here is discretized as 4×4, based on mesh convergence procedure suggested in [55]. First four natural frequencies of the composite plate at temperatures of 300 K and 325 K represent a good agreement with the results reported by Ram and Sinha [3] and ANSYS® simulation (Table 5), which confirms validity of the in-house MATLab® code developed and used for further analysis. Furthermore, the dynamic response of the composite plate at a temperature of 300 K is compared with that reported by Kant et al. [48] and Niyogi et al. [56], and a good agreement is observed in the prediction of the results.

The convergence of the dynamic response, i.e. central displacement at different time steps of the (0°/90°/90°/0°) graphite-epoxy laminated

Table 5
Results of the free vibration analysis of the graphite-epoxy composite Plate 1 at $T = 300$ K and 325 K.

Mode Nos.	Temperature T (K)	Present Eigen freq. f (Hz)	Present NDF[1] λ	ANSYS® Eigen freq. f (Hz)	Ram and Sinha [3] NDF[1] λ
1	300	14.818	12.083	14.807	–
	325	9.929	8.097	9.917	8.088
2	300	29.434	24.001	29.330	–
	325	23.665	19.196	23.551	19.297
3	300	51.493	41.988	51.343	–
	325	48.428	39.324	48.276	39.324
4	300	62.050	50.600	61.780	–
	325	56.615	46.165	56.336	45.431

[1] Non-dimensional frequency, $\lambda = 2\pi f L^2 (\rho/E_{22}h^2)^{1/2}$

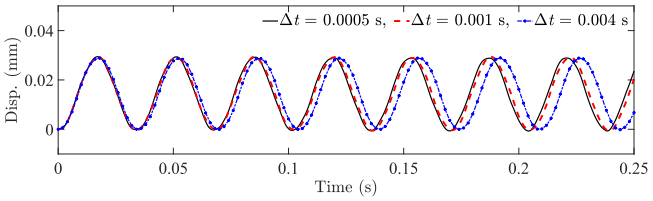

Fig. 2. Convergence studies of Newmark's integration method for a simply-supported (0°/90°/90°/0°) graphite-epoxy Plate 2 subjected to suddenly applied pulse loading, q_0 at $T = 325$ K.

composite plate, at a temperature of 325 K is shown in Fig. 2 for Plate 2. Newmark's time integration scheme is used for conducting transient analysis of the composite Plate 2. The converged value for time step $\triangle t = 0.001$ s is adopted in the present analysis. This FE model is subsequently used as a deterministic FE solver to evaluate the uncertainty in the eigen frequencies and the dynamic displacement of the graphite-epoxy laminated composite plate due to the random mean temperature increment.

4.2. Validation of the stochastic model

The gPC expansion method is a robust technique, which precisely predict randomness in the system response due to randomness in the input parameters. Effectiveness of the gPC expansion method is investigated here by comparing with the realizations generated from 10, 000 Monte Carlo simulations (MCS). Table 6 shows the mean μ_f and sd σ_f of the first three eigen frequencies derived using 3rd and 4th order gPC expansion method at a random mean temperature of 325 K, and are compared with the MC simulations of 10, 000 sample realizations.

A comparison of the PDFs for the first three eigen frequencies at the mean random temperature of 325 K for the composite Plate 2 is illustrated in Fig. 3. It is evident that, 3rd order gPC expansion is enough to represent the uncertain response of the composite plate due to random mean temperature increment.

The deterministic FE model of the laminated composite plate under uniform temperature is used to determine the unknown coefficients of 3rd order gPC expansion in Eqs. (22) and (23), at 25 sets of random temperatures using least-squares method. Deterministic dynamic response for each predefined temperature is calculated at every incremental time step using Newmark's step-by-step integration technique. The total time of study is kept as 0.25 s, and the time step considered is 0.001 s. Uncertainty in the time-dependent central displacement using 3rd order gPC expansion method, incorporating the Hermite polynomials, in Eq. (23) as represented in [57]

$$d(t, \xi) = c_0(t) + c_1(t)(\xi) + c_2(t)(\xi^2 - 1) + c_3(t)(\xi^3 - 3\xi). \tag{38}$$

The unknown coefficients $c_i(t)$ are derived by solving the stochastic Eq. (38) for a set of 25 collocation points generated from the roots of the 4th order Hermite polynomial at each incremental time step. Time history plots of the unknown coefficients for a simply-supported (0°/90°/90°/0°) graphite-epoxy laminate due to suddenly applied pulse and impulse loading are shown in Figs. 4 and 5, respectively at the mean temperatures of 325 K, 350 K, 375 K, and 400 K. The first coefficient c_0 indicates the mean response of the central displacement, and has dominating influence on both the types of loading conditions. On the other hand, the amplitude of the second coefficient c_1, which influences the sd of the response, is in increasing order with the increase in the random mean temperature. Moreover, the amplitude of c_1 is comparable with the mean response for the impulse loading at the random mean temperature of 400 K. It can be stated that, at the same level of uncertainty in temperature increment, the sensitivity of the dynamic response increases with the random mean temperature increment. Note that, the amplitude of c_0 is decreasing with the increment in time and is increasing with the increment of the random mean

Table 6
Comparison of the statistical results of first three eigen frequencies of the (0°/90°/90°/0°) laminate graphite-epoxy Plate 2 at a mean temperature, $T = 325$ K.

Method	1st eigen freq. (Hz)		2nd eigen freq. (Hz)		3rd eigen freq. (Hz)	
	μ_f	σ_f	μ_f	σ_f	μ_f	σ_f
MCS (10,000)	27.430	0.392	54.365	0.608	99.289	0.308
3rd order gPC	27.440	0.397	54.378	0.615	99.298	0.311
4th order gPC	27.435	0.397	54.375	0.616	99.291	0.313

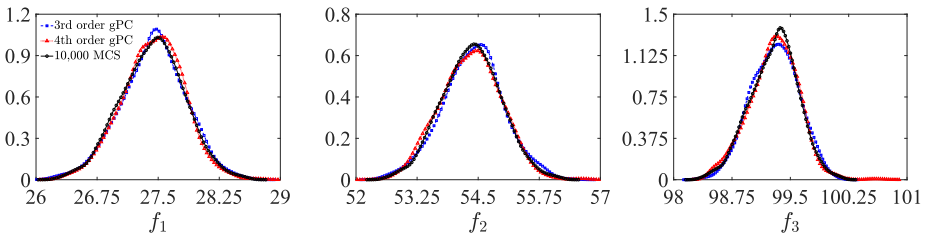

Fig. 3. PDFs of first three eigen frequencies (Hz) obtained using 3rd and 4th order gPC expansions compared with the MCS at mean random temperature of 325 K for Plate 2.

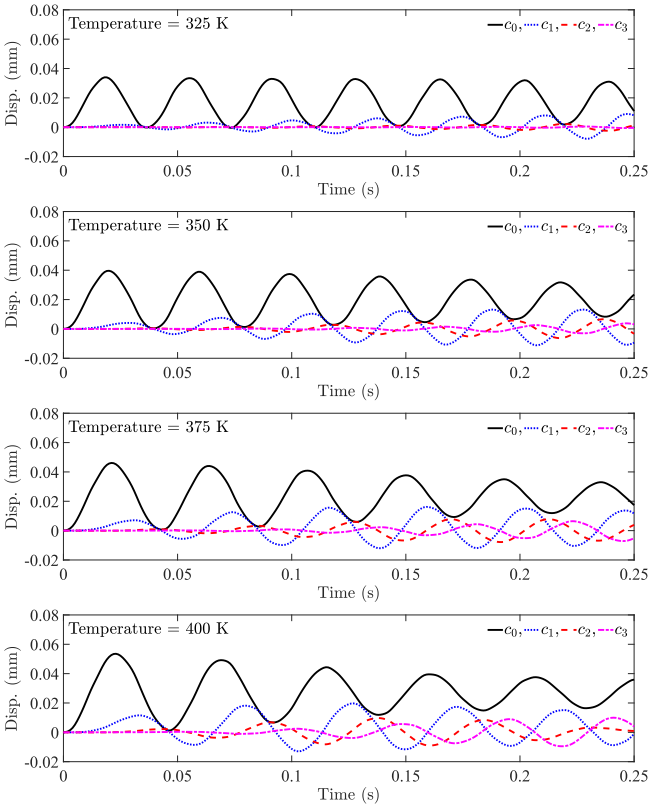

Fig. 4. ime history of the gPC expansion coefficients of central displacement for a simply-supported (0°/90°/90°/0°) laminate subjected to the pulse loading due to the randomness in temperature at 325 K, 350 K, 375 K, and 400 K, respectively for Plate 2.

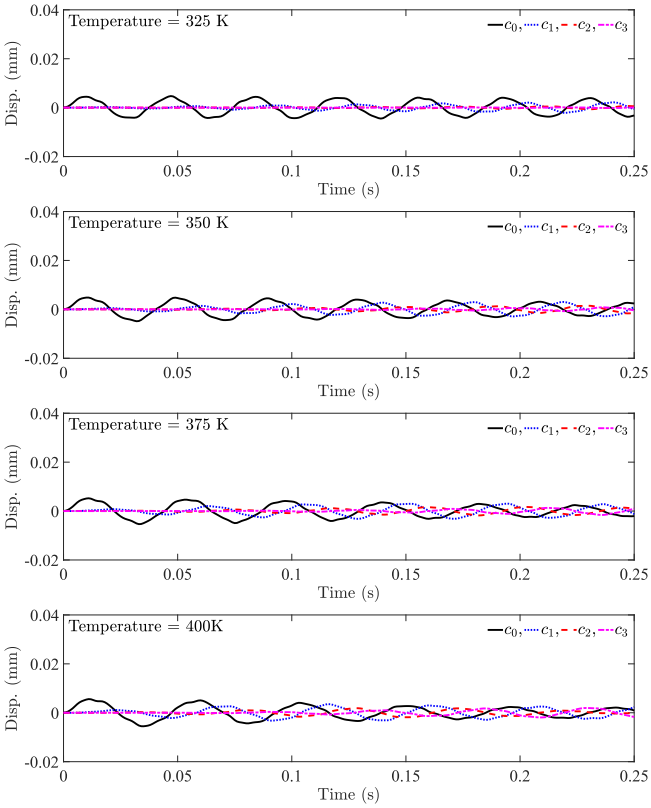

Fig. 5. Time history of the gPC expansion coefficients of central displacement for a simply-supported (0°/90°/90°/0°) laminate subjected to the impulse loading due to the randomness in temperature at 325 K, 350 K, 375 K, and 400 K, respectively for Plate 2.

temperature. The effectiveness of the gPC expansion method is established by the convergence of coefficients, c_1, c_2, and c_3.

4.3. PDF of the eigen frequencies

For safe design of the composite plate, and to estimate the factor of safety at elevated temperature the probabilistic analysis is necessary over the deterministic analysis. The mean and sd of the first three eigen frequencies of the symmetric cross-ply laminate at different random mean temperatures is presented in Table 7. Fig. 6 represents the PDF of the first three eigen frequencies at various random mean temperatures in increasing order and corresponding deterministic eigen frequencies at the mean temperature. It is observed from Table 7 and Fig. 6 that, deterministic values of the eigen frequencies lie near the maximum probability density. The sd, which represents the dispersion of the probability plot, is increased with the increase in the random mean temperature. The sd of the eigen frequencies at a temperature of 325 K is less in comparison with the higher random mean temperature. This indicates the fact that, the random mean temperature increment influences the variation in the elastic properties of the composite, and thereby increment in the level of uncertainty in the frequency response at the higher random temperature.

4.4. Stochastic dynamic response of laminated composite plates

The effect of uncertainty in the temperature increment on the time-dependent transverse central displacement for the symmetric cross-ply and angle-ply laminated composite plates for the suddenly applied pulse and impulse loading are investigated. The time-dependent deterministic and mean values of the central displacement for simply-supported cross-ply laminate under the suddenly applied pulse and impulse loading are plotted in Figs. 7 and 9, respectively. The ratio of the sd and mean values of transverse displacement at each time step is derived to measure the variation in the level of uncertainties in the dynamic response due to the random mean temperature increment for the symmetric cross-ply laminate in time domain, which are reported in Figs. 8 and 10 for the suddenly applied pulse and impulse loading, respectively. It is observed from Figs. 7 and 9 that deterministic and mean central displacements are in increasing order due to corresponding degradation in the material properties due to the increment in the random mean temperature under both types of loading. However, the mean central displacements are decaying with the time as compared to the deterministic values, and the decay is faster with the increment in the random mean temperature under both types of loading. This decay in the mean amplitude in time domain is due to the increasing randomness with the temperature increment [58]. The ratio of the sd and mean for the symmetric cross-ply laminate in Fig. 8 represents sudden peak at troughs of the corresponding time-dependent displacement plot for the pulse loading. The peak value is decreased with an increment in the random mean temperature. However, for the impulse loading in

Table 7
Statistics of the first three eigen frequencies (Hz) for a simply-supported (0°/90°/90°/0°) laminate due to the mean random temperature increment for Plate 2.

Temperature	1st mode		2nd mode		3rd mode	
	μ_f	σ_f	μ_f	σ_f	μ_f	σ_f
325 K	27.444	0.397	54.378	0.615	99.298	0.311
350 K	25.431	0.788	51.332	1.193	97.664	0.641
375 K	23.565	1.070	48.517	1.602	96.186	0.821
400 K	21.865	1.374	46.034	1.958	94.958	0.969

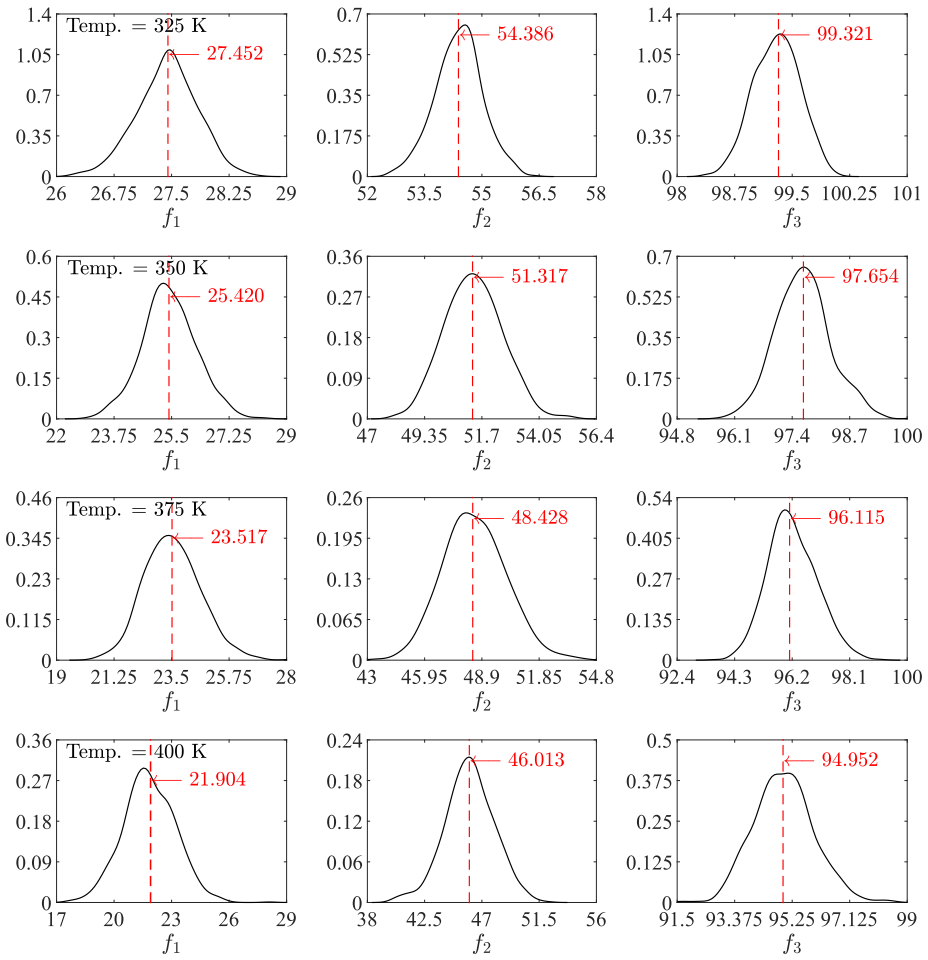

Fig. 6. PDF of first three natural frequencies (Hz) of a simply-supported (0°/90°/90°/0°) laminate due to the randomness in temperature at 325 K, 350 K, 375 K, and 400 K, respectively, and corresponding deterministic value (red dashed line) for Plate 2.

Fig. 10 sudden peak for sd/mean plot is observed in-between crests and troughs of the time-dependent displacement plot. The value of sd/mean is increased with the random mean temperature increment. It can be stated that characteristics of loading does influence the level of uncertainty in the dynamic displacement for uncertain temperature increment.

Figs. 11 and 13 present a comparison of the deterministic and the mean response of the central displacements for symmetric angle-ply laminate under pulse and impulse loading, respectively, and corresponding plots of sd/mean are shown in Figs. 12 and 14. When uncertainty in the response of the symmetric cross-ply and angle-ply laminates is compared, the rate of decay in the mean displacement with respect to time shows a comparable performance. The value of the sudden peak of sd/mean of corresponding time-dependent displacement for symmetric angle-ply laminate is more as compared to the symmetric cross-ply laminate.

Due to the suddenly applied impulse loading, the level of uncertainty in displacement is increased at delayed time domain response with an increment in the random mean temperature; whereas, the level of uncertainty is decreased at delayed time domain response of the central displacement under suddenly applied pulse loading with an increment in the random mean temperature. Thus, level of uncertainty in the dynamic displacement is significantly varied in time domain with the increment in the random mean temperature. Hence, prior to the engineering application, uncertainty quantification in the dynamic response of the composite plate with various anticipated loading conditions and lamina sequences subject to random temperature field is essential to ensure safety in its design.

It can be concluded from the earlier discussion in this section that, in case of the pulse loading the mean value and sd of the dynamic central displacement is decreasing at the delayed time domain due to the random mean temperature increment. However, in case of the impulse loading the amplitude of the mean central dynamic displacement is diminishing in time domain though the dispersion is increasing in time domain near the mean position of the amplitude along with the random mean temperature increment. Therefore, statistical parameters of the stochastic dynamic response due to the uncertain thermal parameters are also influenced by the characteristics of the applied loading. Application of four-layered symmetric cross-ply and angle-ply laminates does not have significant influence on the stochastic dynamic response characteristics.

4.5. PDF of peak displacement

The effect of temperature uncertainty on the peak dynamic displacement of the composite plate for the symmetric cross-ply and angle-ply laminates is demonstrated in Figs. 15 and 16, respectively with the applied pulse and impulse loading. The distribution of the peak central displacement due to 0.001 N/mm^2 pulse and impulse loading are plotted at various random mean temperatures in incremental order with the same level of uncertainty using the gPC expansion method. It is observed that the dispersion of the PDF increases with the increment in the random mean temperature, specifically under the pulse loading. Under the pulse loading, at a random mean temperature of 325 K the distributions are more symmetric, however at the higher random mean temperature the distribution became non-Gaussian and unsymmetric.

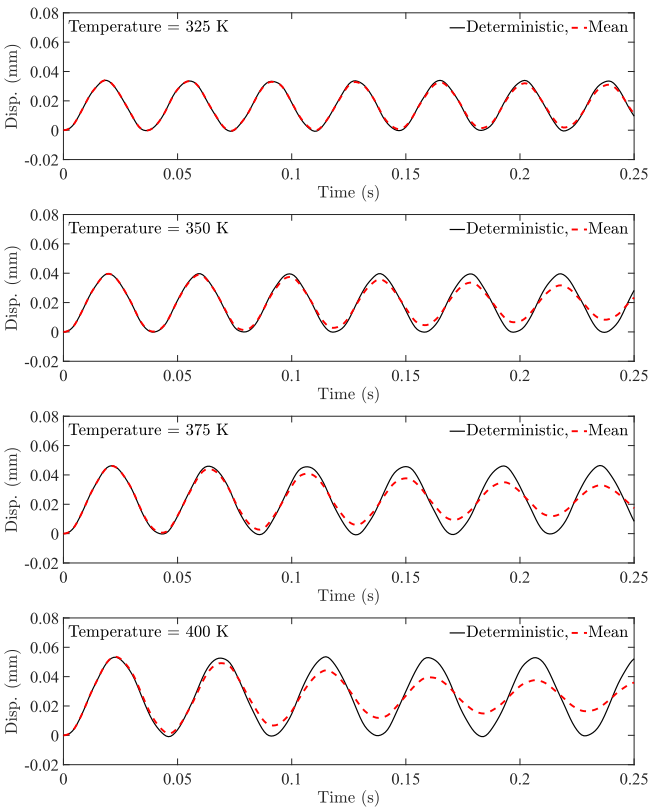

Fig. 7. Comparison of time history of the deterministic central displacement and mean of the central displacement for a simply-supported (0°/90°/90°/0°) laminate subjected to pulse loading due to the randomness in temperature at 325 K, 350 K, 375 K, and 400 K, respectively for Plate 2.

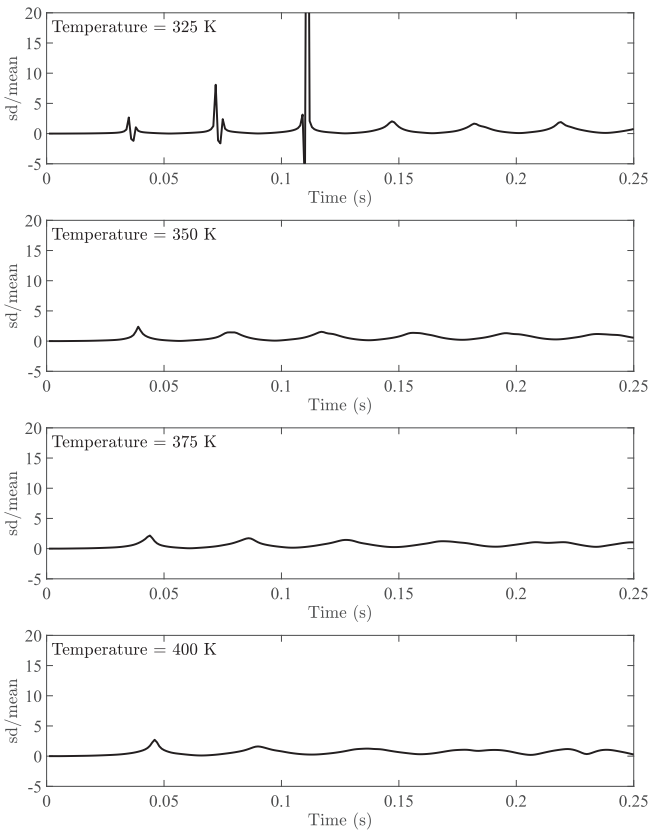

Fig. 8. Time history of sd/mean of the central displacement for a simply-supported (0°/90°/90°/0°) laminate subjected to pulse loading due to the randomness in temperature at 325 K, 350 K, 375 K, and 400 K, respectively for Plate 2.

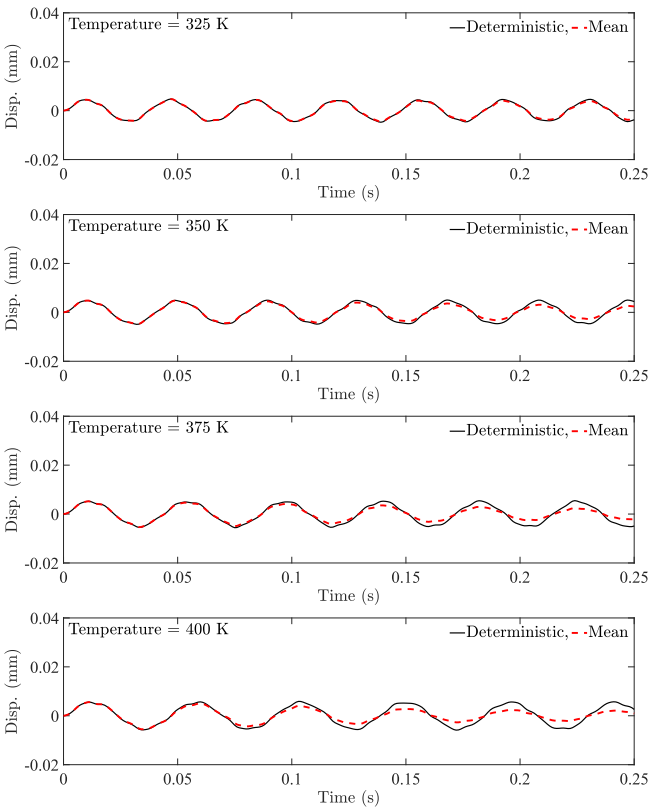

Fig. 9. Comparison of time history of the deterministic central displacement and mean of the central displacement for a simply-supported (0°/90°/90°/0°) laminate subjected to impulse loading due to the randomness in temperature at 325 K, 350 K, 375 K, and 400 K, respectively for Plate 2.

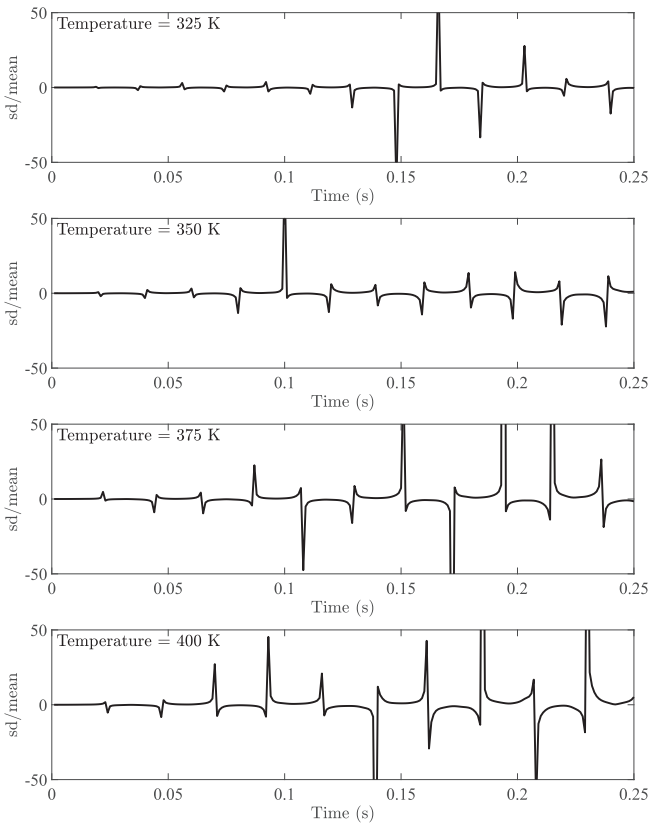

Fig. 10. Time history of sd/mean of the central displacement for a simply-supported (0°/90°/90°/0°) laminate subjected to impulse loading due to the randomness in temperature at 325 K, 350 K, 375 K, and 400 K, respectively for Plate 2.

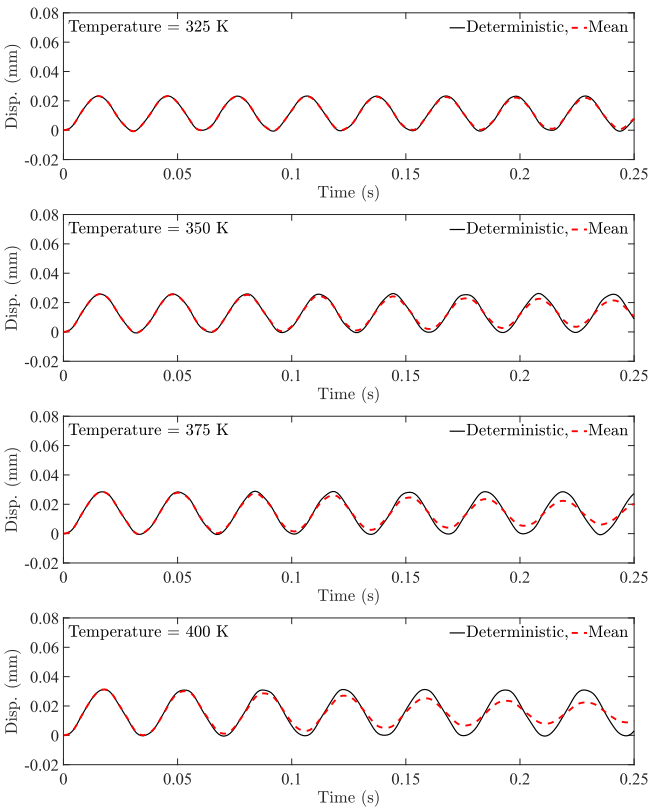

Fig. 11. Comparison of time history of the deterministic central displacement and mean of the central displacement for a simply-supported (45°/−45°/−45°/45°) laminate subjected to pulse loading due to the randomness in temperature at 325 K, 350 K, 375 K, and 400 K, respectively for Plate 2.

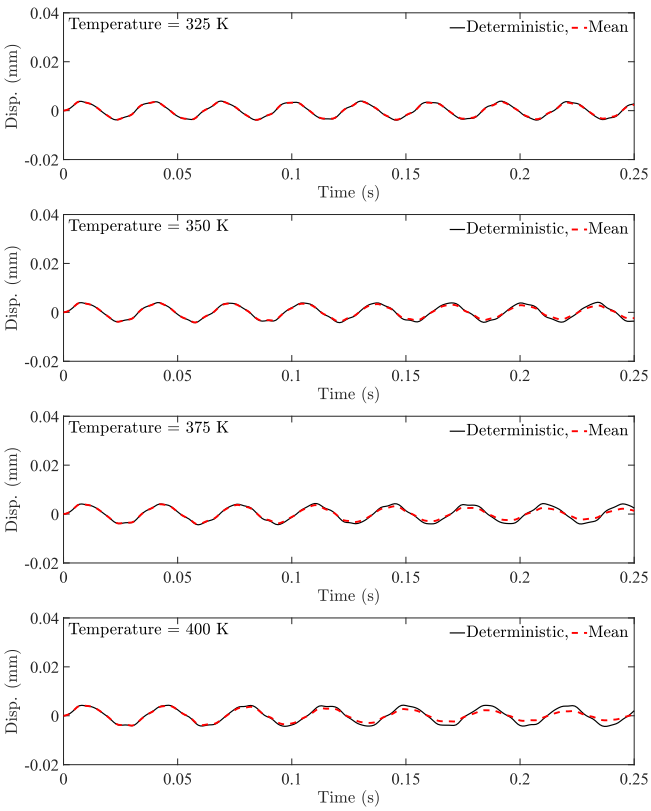

Fig. 13. Comparison of time history of the deterministic central displacement and mean of the central displacement for a simply-supported (45°/−45°/−45°/45°) laminate subjected to impulse loading due to the randomness in temperature at 325 K, 350 K, 375 K, and 400 K, respectively for Plate 2.

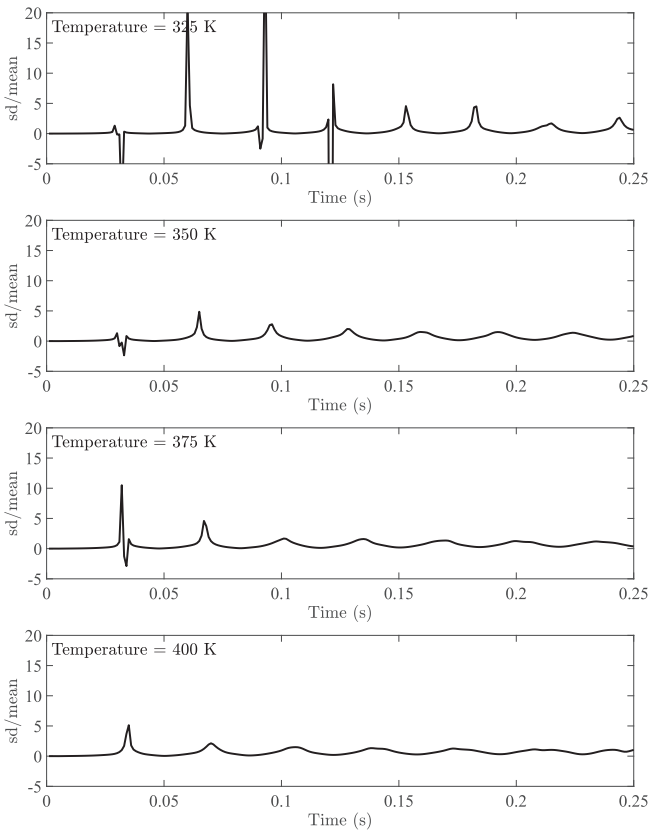

Fig. 12. Time history of sd/mean of the central displacement for a simply-supported (45°/−45°/−45°/45°) laminate subjected to pulse loading due to the randomness in temperature at 325 K, 350 K, 375 K, and 400 K, respectively for Plate 2.

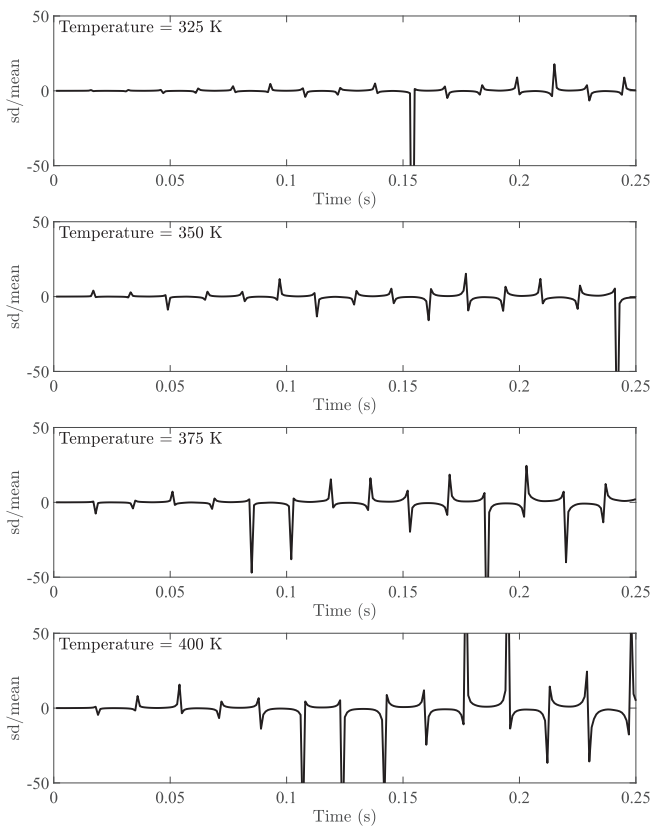

Fig. 14. Time history of sd/mean of the central displacement for a simply-supported (45°/−45°/−45°/45°) laminate subjected to impulse loading due to the randomness in temperature at 325 K, 350 K, 375 K, and 400 K, respectively for Plate 2.

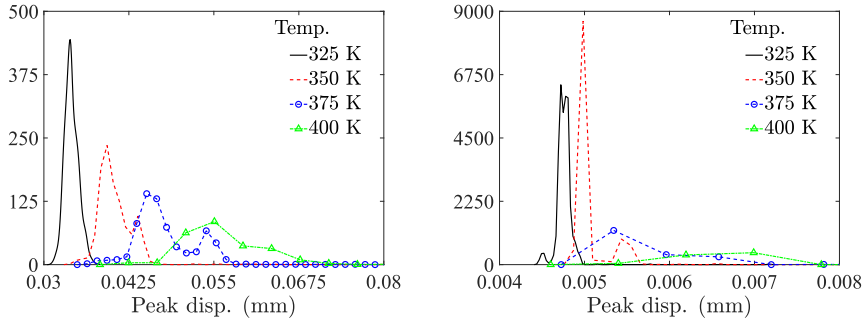

Fig. 15. PDF of peak central displacement for simply-supported (0°/90°/90°/0°) laminate subjected to pulse and impulse loading, respectively due to the randomness in temperature for Plate 2.

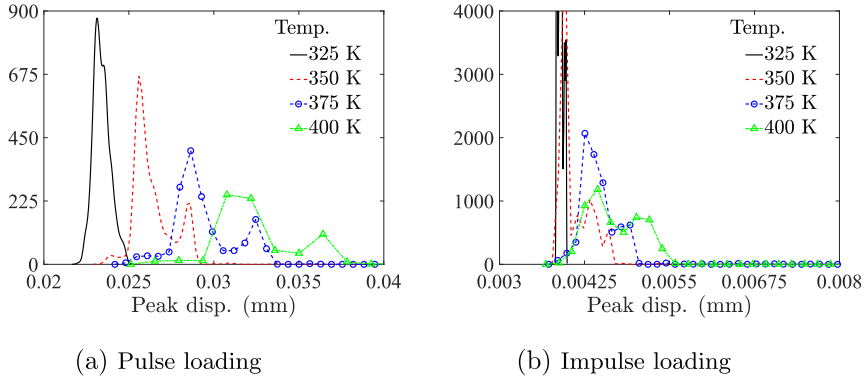

Fig. 16. PDF of peak central displacement for simply-supported (45°/−45°/−45°/45°) laminate subjected to pulse and impulse loading, respectively due to the randomness in temperature for Plate 2.

Under the impulse loading, the distributions are non-Gaussian, and larger part of the distributions overlap with each other at different random mean temperatures. Moreover, due to the impulse loading on the symmetric angle-ply laminate distributions of the peak central displacement are non-Gaussian, and noticeably unsymmetrical. Hence, appropriate evaluation of distribution of the peak displacement response is recommended for various lamina sequences with different loading conditions due to uncertainty in the temperature increment prior to real-field applications. Likewise, the peak failure stress induced in the composite plate is varied due to random mean temperature increment. A reliability analysis due to random thermal increment is necessary prior to application in the thermally sensitive part of the structure. This study has revealed the necessity of conducting further studies on the graphite-epoxy composite plates due to the random thermal environment.

5. Conclusions

The stochastic dynamic response of the graphite-epoxy composite plate under the applied pulse and impulse excitations, considering randomness in the incremental temperature is presented. The non-intrusive generalized polynomial chaos (gPC) expansion method is implemented for the stochastic simulations. The first-order shear deformation theory (FSDT) is adopted to analyze the thin composite plate under uniform temperature increment, and this deterministic finite element (FE) solver is used to generate the response at prescribed collocation points. The major advantage of the applicability of the gPC expansion method is to represent the mean and sd of the time-dependent dynamic response at each time step with reduced computational efforts. The convergence of the polynomial form of the dynamic response indicates the reduction in the error while representing the stochasticity in the temperature by using orthogonal polynomial. The computational accuracy of the gPC expansion method is well compared with the Monte Carlo simulations (MCS). Stochastic dynamic response of the composite plate due to thermal uncertainty is efficiently described here with the application of the gPC expansion method. The key findings from this study are summarized below.

1. The mean eigen frequency of the composite plate decreases with the increment in the random mean temperature, as elastic moduli of the composite plate decrease with the temperature.
2. The standard deviation (sd) of the eigen frequencies of the composite plate increases with the increment in the random mean temperature which imply an increment in the variation of the degraded elastic properties of the composite.
3. The stiffness of the composite plate decreases with the increment in the temperature, and subsequently amplitude of the dynamic displacement is increasing with the increment in the temperature. Moreover, the mean amplitude of the dynamic displacement of the composite plate decays gradually in the time domain with the random mean temperature increment.
4. The level of uncertainty in the dynamic response under impulse loading is higher due to higher rate of decay in corresponding mean transient response in time domain in comparison with the pulse loading.
5. The level of uncertainty in the dynamic displacement response in the delayed time domain is more under the suddenly applied impulse loading. Under the applied pulse loading, the level of

uncertainty in the dynamic displacement is decreasing in the delayed time domain. The PDF of the stochastic dynamic response in the random thermal environment should be studied for the various types of loading at several time steps before practical application.

6. The mean dynamic response is increasing with the increment in the random mean temperature due to the degradation in the material properties of the graphite-epoxy composite plate. Moreover, level of uncertainties are significantly varied in time and temperature domains. Thus, the stochastic studies of graphite-epoxy composite plate due to random thermal increment exhibited necessity over the deterministic analysis.
7. The distribution of the peak displacement at the lower random temperature is symmetrical, more evidently for the pulse loading. For the higher random temperature, the distribution became unsymmetric and non-Gaussian.
8. Statistical properties of the dynamic response are not much influenced by providing four layers of symmetric cross-ply and angle-ply laminates.

The presented methodology for quantifying uncertainty can be efficiently applied to complex structures. A deterministic FE model with complex geometry and advanced engineered materials can be developed in ANSYS® and corresponding modal analysis in thermal environment then can estimate the dynamic response efficiently. Non-intrusive gPC expansion can be efficiently used to estimate the stochastic parameters of the eigen frequencies and time-dependent dynamic response by limited numbers of realization of the deterministic FE model at predefined collocation points.

Declaration of Competing Interest

The authors declare that they have no conflicts of interest.

Acknowledgments

The first and third authors gratefully acknowledge the financial support extended by the Deutscher Akademischer Austauschdienst (DAAD) under Research Grants- Doctoral Programmes in Germany, and that by the Alexander von Humboldt Foundation under Fellowship for Experienced Researcher.

Appendix A

A.1. Appendix

$$[S_r] = \begin{bmatrix} N_x^r & N_{xy}^r & 0 & 0 & 0 & 0 & 0 & 0 & M_x^r & M_{xy}^r & 0 & Q_x^r \\ N_{xy}^r & N_y^r & 0 & 0 & 0 & 0 & 0 & 0 & M_{xy}^r & M_y^r & 0 & -Q_y^r \\ 0 & 0 & N_x^r & N_{xy}^r & 0 & 0 & -M_x^r & -M_{xy}^r & 0 & 0 & Q_x^r & 0 \\ 0 & 0 & N_{xy}^r & N_y^r & 0 & 0 & -M_{xy}^r & -M_y^r & 0 & 0 & -Q_y^r & 0 \\ 0 & 0 & 0 & 0 & N_x^r & N_{xy}^r & 0 & 0 & 0 & 0 & 0 & 0 \\ 0 & 0 & 0 & 0 & N_{xy}^r & N_y^r & 0 & 0 & 0 & 0 & 0 & 0 \\ 0 & 0 & -M_x^r & -M_{xy}^r & 0 & 0 & \frac{N_x^r h^2}{12} & \frac{N_{xy}^r h^2}{12} & 0 & 0 & 0 & 0 \\ 0 & 0 & -M_{xy}^r & -M_y^r & 0 & 0 & \frac{N_{xy}^r h^2}{12} & \frac{N_y^r h^2}{12} & 0 & 0 & 0 & 0 \\ M_x^r & M_{xy}^r & 0 & 0 & 0 & 0 & 0 & 0 & \frac{N_x^r h^2}{12} & \frac{N_{xy}^r h^2}{12} & 0 & 0 \\ M_{xy}^r & M_y^r & 0 & 0 & 0 & 0 & 0 & 0 & \frac{N_{xy}^r h^2}{12} & \frac{N_y^r h^2}{12} & 0 & 0 \\ 0 & 0 & Q_x^r & -Q_y^r & 0 & 0 & 0 & 0 & 0 & 0 & 0 & 0 \\ Q_x^r & -Q_y^r & 0 & 0 & 0 & 0 & 0 & 0 & 0 & 0 & 0 & 0 \end{bmatrix},$$

A.2. Appendix

$$[G] = \sum_{i=1}^{8} \begin{bmatrix} N_{i,x} & 0 & 0 & 0 & 0 \\ N_{i,y} & 0 & 0 & 0 & 0 \\ 0 & N_{i,x} & 0 & 0 & 0 \\ 0 & N_{i,y} & 0 & 0 & 0 \\ 0 & 0 & N_{i,x} & 0 & 0 \\ 0 & 0 & N_{i,y} & 0 & 0 \\ 0 & 0 & 0 & N_{i,x} & 0 \\ 0 & 0 & 0 & N_{i,y} & 0 \\ 0 & 0 & 0 & 0 & N_{i,x} \\ 0 & 0 & 0 & 0 & N_{i,y} \\ 0 & 0 & 0 & N_i & 0 \\ 0 & 0 & 0 & 0 & N_i \end{bmatrix}.$$

Appendix B. Supplementary data

Supplementary data associated with this article can be found, in the online version, at https://doi.org/10.1016/j.compstruct.2019.111159.

References

[1] Halpin J. Effect of environmental factors on composite materials [Technical Report AFML-TR-67-423]. 1969. p. 1–61.
[2] Whitney J, Ashton J. Effect of environment on the elastic response of layered composite plates. AIAA J 1971;9:1708–13.
[3] Ram KS, Sinha P. Hygrothermal effects on the free vibration of laminated composite plates. J Sound Vib 1992;158(1):133–48.
[4] Rao V, Sinha P. Dynamic response of multidirectional composites in hygrothermal environments. Compos Struct 2004;64(3):329–38.
[5] Mallikarjuna, Kant T. Dynamics of laminated composite plates with a higher-order theory and finite element discretization. J Sound Vib 1988;126(3):463–75.
[6] Kant T, Mallikarjuna. Non-linear dynamics of laminated plates with a higher-order theory and C^0 finite elements. Int J Non-Linear Mech 1991;26(3):335–43.
[7] Kant T, Arora C, Varaiya J. Finite element transient analysis of composite and sandwich plates based on a refined theory and a mode superposition method. Compos Struct 1992;22(2):109–20.
[8] Kommineni J, Kant T. Large deflection elastic and inelastic transient analyses of composite and sandwich plates with a refined theory. J Reinf Plast Compos 1993;12(11):1150–70.
[9] Kant T, Kommineni J. Geometrically non-linear transient analysis of laminated composite and sandwich shells with a refined theory and C^0 finite elements. J Comput Struct 1994;52(6):1243–59.
[10] Kant T, Kommineni JR. Large deflection inelastic pseudo-transient analysis of laminated composite plates. Int J Numer Methods Eng 1994;37(1):37–48.
[11] Huang N, Tauchert T. Large deflections of laminated cylindrical and doubly-curved panels under thermal loading. Comput Struct 1991;41(2):303–12.
[12] Patel B, Ganapathi M, Makhecha D. Hygrothermal effects on the structural behaviour of thick composite laminates using higher-order theory. Compos Struct 2002;56(1):25–34.
[13] Ganapathi M, Patel B, Makhecha D. Nonlinear dynamic analysis of thick composite/sandwich laminates using an accurate higher-order theory. Compos Part B: Eng 2004;35(4):345–55.
[14] Huang X-L, Shen H-S, Zheng J-J. Nonlinear vibration and dynamic response of shear deformable laminated plates in hygrothermal environments. Compos Sci Technol 2004;64(10):1419–35.
[15] Naidu NS, Sinha P. Nonlinear free vibration analysis of laminated composite shells in hygrothermal environments. Compos Struct 2007;77(4):475–83.
[16] Naidu NS, Sinha P. Nonlinear transient analysis of laminated composite shells in hygrothermal environments. Compos Struct 2006;72(3):280–8.
[17] Ribeiro P, Jansen E. Non-linear vibrations of laminated cylindrical shallow shells under thermomechanical loading. J Sound Vib 2008;315(3):626–40.
[18] Mahapatra T, Panda S, Kar V. Nonlinear hygro-thermo-elastic vibration analysis of doubly curved composite shell panel using finite element micromechanical model. Mech Adv Mater Struct 2016;23(11):1343–59.
[19] Mahapatra T, Kar V, Panda S. Nonlinear free vibration analysis of laminated composite doubly curved shell panel in hygrothermal environment. J Sandwich Struct Mater 2015;17(5):511–45.
[20] Nanda N, Pradyumna S. Nonlinear dynamic response of laminated shells with imperfections in hygrothermal environments. J Compos Mater 2011;45(20):2103–12.
[21] Biswal M, Sahu S, Asha A. Vibration of composite cylindrical shallow shells subjected to hygrothermal loading-experimental and numerical results. Compos Part B: Eng 2016;98:108–19.
[22] Engelstad S, Reddy J. Probabilistic nonlinear finite element analysis of composite structures. AIAA J 1993;31(2):362–9.
[23] Park J, Kim C, Hong C. Stochastic finite element method for laminated composite structures. J Reinf Plast Compos 1995;14(7):675–93.
[24] Salim S, Iyengar N, Yadav D. Natural frequency characteristics of composite plates with random properties. Struct Eng Mech 1998;6(6):659–71.
[25] Chen S-H, Qiu Z, Liu Z. Perturbation method for computing eigenvalue bounds in structural vibration systems with interval parameters. Commun Numer Methods Eng 1994;10(2):121–34.
[26] Singh B, Yadav D, Iyengar N. A C^0 element for free vibration of composite plates with uncertain material properties. Adv Compos Mater 2003;11(4):331–50.
[27] Onkar AK, Yadav D. Non-linear free vibration of laminated composite plate with random material properties. J Sound Vib 2004;272(3):627–41.
[28] Lal A, Singh B, Kumar R. Nonlinear free vibration of laminated composite plates on elastic foundation with random system properties. Int J Mech Sci 2008;50(7):1203–12.
[29] Zhang S, Zhang L, Wang Y, Tao J, Chen X. Effect of ply level thickness uncertainty on reliability of laminated composite panels. J Reinf Plast Compos 2016;35(19):1387–400.
[30] Ghanem R, Spanos P. Stochastic finite elements: a spectral approach. 1st ed. New York, USA: Springer-Verlag; 1991.
[31] Xiu D, Karniadakis G. The Wiener-Askey polynomial chaos for stochastic differential equations. J. Scientific Comput. 2002;24(2):619–44.
[32] Sepahvand K, Marburg S, Hardtke H-J. Uncertainty quantification in stochastic systems using polynomial chaos expansion. Int J Appl Mech 2010;02(02):305–53.
[33] Ghanem RG, Spanos PD. Spectral stochastic finite-element formulation for reliability analysis. J Eng Mech 1991;117(10):2351–72.
[34] Xiu D, Karniadakis GE. Modeling uncertainty in flow simulations via generalized polynomial chaos. J Comput Phys 2003;187(1):137–67.
[35] Soize C. A comprehensive overview of a non-parametric probabilistic approach of model uncertainties for predictive models in structural dynamics. J Sound Vib 2005;288(3):623–52.
[36] Sepahvand K, Marburg S, Hardtke H-J. Stochastic free vibration of orthotropic plates using generalized polynomial chaos expansion. J Sound Vib 2012;331(1):167–79.
[37] Sepahvand K, Scheffler M, Marburg S. Uncertainty quantification in natural frequencies and radiated acoustic power of composite plates: analytical and experimental investigation. Appl Acoust 2015;87:23–9.
[38] Sepahvand K. Spectral stochastic finite element vibration analysis of fiber-reinforced composites with random fiber orientation. Compos Struct 2016;145:119–28.
[39] Sepahvand K, Marburg S. Stochastic dynamic analysis of structures with spatially uncertain material parameters. Int J Struct Stab Dyn 2014;14(08):1440029.
[40] Sepahvand K, Marburg S. Random and stochastic structural acoustic analysis. New York, USA: John Wiley & Sons; 2016. Ch. 10, pp. 305–338.
[41] Lal A, Singh B. Stochastic free vibration of laminated composite plates in thermal environments. J Thermoplast Compos Mater 2010;23(1):57–77.
[42] Singh B, Verma V. Hygrothermal effects on the buckling of laminated composite plates with random geometric and material properties. J Reinf Plast Compos 2009;28(4):409–27.
[43] Kumar R, Patil H, Lal A. Hygrothermoelastic free vibration response of laminated composite plates resting on elastic foundations with random system properties: micromechanical model. J Thermoplast Compos Mater 2013;26(5):573–604.
[44] Dey S, Mukhopadhyay T, Sahu S, Li G, Rabitz H, Adhikari S. Thermal uncertainty quantification in frequency responses of laminated composite plates. Compos Part B: Eng 2015;80:186–97.
[45] Kumar R. Effects of hygrothermomechanical loading and uncertain system environments on flexural and free vibration response of shear deformable laminated plates: Stochastic finite element method micromechanical model investigation. J Front Aerospace Eng 2017;6(1):39–69.
[46] Kumar R. Hygrothermally induced nonlinear free vibration response of laminated composite plates with random system properties: stochastic finite element micromechanical model investigation. J Front Aerospace Eng 2017;6(2):116–45.
[47] Reddy J. Mechanics of laminated composite plates and shells: theory and analysis. 2nd ed. London, UK: CRC Press; 2001.
[48] Kant T, Varaiya J, Arora C. Finite element transient analysis of composite and sandwich plates based on a refined theory and implicit time integration schemes. Comput Struct 1990;36(3):401–20.
[49] Oden J. Mechanics of elastic structures. 1st ed. New York, USA: McGraw-Hill; 1967.
[50] Wiener N. The homogeneous chaos. Am J Math 1938;60(4):897–936.
[51] Chamis C, Sendeckyj G. Critique on theories predicting thermoelastic properties of fibrous composites. J Compos Mater 1968;2(3):332–58.
[52] Shen C-H, Springer G. Effects of moisture and temperature on the tensile strength of composite materials. J Compos Mater 1977;11(1):2–16.
[53] Gorji M, Mirzadeh F. Theoretical prediction of the thermoelastic properties and thermal stresses in unidirectional composites. J Reinf Plast Compos 1989;8(3):232–58.
[54] Hughes T. The finite element method: linear static and dynamic finite element analysis. Englewood Cliffs, New Jersey, USA: Prentice-Hall Inc; 1987.
[55] Rawat A, Matsagar V, Nagpal AK. Finite element analysis of thin circular cylindrical shells. Proc Indian Natl Sci Acad 2016;82(2):349–55.
[56] Niyogi A, Laha M, Sinha P. Finite element vibration analysis of laminated composite folded plate structures. Shock Vib 1999;6(5–6):273–83.
[57] Saha S, Sepahvand K, Matsagar V, Jain A, Marburg S. Stochastic analysis of base-isolated liquid storage tanks with uncertain isolator parameters under random excitation. Eng Struct 2013;57:465–74.
[58] Sepahvand K. Uncertainty quantification in stochastic forward and inverse vibration problems using generalized polynomial chaos expansion [Ph.D. thesis]. Germany: Technical University of Dresden; 2009.